Modulation of Hydroxyl Radical Reactivity and Radical Degradation of High Density Polyethylene

Susan M. Mitroka

Dissertation submitted to the faculty of the Virginia Polytechnic Institute and State University in partial fulfillment of the requirements for the degree of

Doctor of Philosophy

In

Chemistry

Dr. James M. Tanko, Chairman

Dr. Paul Carlier

Dr. Andrea Dietrich

Dr. Timothy E. Long

Dr. Diego Troya

June 25, 2010
Blacksburg, Virginia

Keywords: hydroxyl radical, hydrogen atom transfer, polarized transition state, oxidation, auto oxidation, high density polyethylene, accelerated aging

Modulation of Hydroxyl Radical Reactivity and Radical Degradation of High Density Polyethylene

Susan M. Mitroka

ABSTRACT

Oxidative processes are linked to a number of major disease states as well as the breakdown of many materials. Of particular importance are reactive oxygen species (ROS), as they are known to be endogenously produced in biological systems as well as exogenously produced through a variety of different means. In hopes of better understanding what controls the behavior of ROS, researchers have studied radical chemistry on a fundamental level. Fundamental knowledge of what contributes to oxidative processes can be extrapolated to more complex biological or macromolecular systems.

Fundamental concepts and applied data (i.e. interaction of ROS with polymers, biomolecules, etc.) are critical to understanding the reactivity of ROS. A detailed review of the literature, focusing primarily on the hydroxyl radical (HO•) and hydrogen atom (H•) abstraction reactions, is presented in Chapter 1. Also reviewed herein is the literature concerning high density polyethylene (HDPE) degradation. Exposure to treated water systems is known to greatly reduce the lifetime of HDPE pipe. While there is no consensus on what leads to HDPE breakdown, evidence suggests oxidative processes are at play.

The research which follows in Chapter 2 focuses on the reactivity of the hydroxyl radical and how it is controlled by its environment. The HO• has been thought to react instantaneously, approaching the diffusion controlled rate and showing little to no selectivity. Both experimental

and calculational evidence suggest that some of the previous assumptions regarding hydroxyl radical reactivity are wrong and that it is decidedly less reactive in an aprotic polar solvent than in aqueous solution. These findings are explained on the basis of a polarized transition state that can be stabilized via the hydrogen bonding afforded by water. Experimental and calculational evidence also suggest that the *degree* of polarization in the transition state will determine the magnitude of this solvent effect.

Chapter 3 discusses the results of HDPE degradation studies. While HDPE is an extremely stable polymer, exposure to chlorinated aqueous conditions severely reduces the lifetime of HDPE pipes. While much research exists detailing the mechanical breakdown and failure of these pipes under said conditions, a gap still exists in defining the species responsible or mechanism for this degradation. Experimental evidence put forth in this dissertation suggests that this is due to an auto-oxidative process initiated by free radicals in the chlorinated aqueous solution and propagated through singlet oxygen from the environment. A mechanism for HDPE degradation is proposed and discussed. Additionally two small molecules, 2,3-dichloro-2-methylbutane and 3-chloro-1,1-di-methylpropanol, have been suggested as HDPE byproducts. While the mechanism of formation for these products is still elusive, evidence concerning their identification and production in HDPE and PE oligomers is discussed.

Finally, Chapter 4 deals with concluding remarks of the aforementioned work. Future work needed to enhance and further the results published herein is also addressed.

Table of Contents

List of Figures

List of Schemes

List of Tables

List of Abbreviations

23DMB	2,3-dimethylbutane
ALS	Amyotrophic lateral sclerosis
BDE	bond dissociation energy
C	celcius
Cl•	chlorine radical
Cl_2	chlorine
ClO•	hypochlorite radical
cm	centimeter
cm^{-1}	wavenumber
DCMB	2,3-dichloro-2-methylbutane
DMCP	3-chloro-1,1-dimethylpropanol
DMPO	5,5-dimethyl-1-pyrroline-*N*-oxide
DMSO	dimethylsulfoxide
DNA	Deoxyribose nucleic acid
DOC	chlorine dioxide
e^-	electron
ESR	electron spin resonance
F	farenheit
F_C	correction factor
FT-IR	Fourier Transform-Infrared
GC	gas chromatography
H	enthlapy
H-atom	hydrogen atom
HDPE	high density polyethylene
HO•	hydroxyl Radical
HOO•	peroxyl radical
HRMS	high resolution mass spectroscopy
I	intensity
IR	infrared
JACS	J. Am. Chem. Soc.
K	Kelvin
kcal	kilocalories
KIE	kinetic isotope effect
l	liter
LDPE	low density polyethylene
LFP	laser flash photolysis
M	molarity (moles/liter)
MDPE	medium density polyethylene

mg	milligram
mm	millimeter
mM	millimolar (millimoles/liter)
Mol	moles
MS	mass spectroscopy
ms	millisecond
N	number of moles
$NCH_2C•$	acetonitrile radical
nm	nanometers
NMR	nuclear magnetic resonance
PE	polyethylene
ppm	parts per million
PSH	*N*-hydroxypyridine-2-thione
PyrS•	pyrithiyl radical (name)
PyrS—SPyr	pyrithiyldimer (name)
R	gas constant
R•	alkyl radical
RH	alkane
RNA	Ribonucleic Acid
RO•	alkoxyl radical
ROS	reactive oxygen species
RSH	thiol
S	entropy
T	temperature
T_g	glass-transition temperature
T_m	melting temperature
TS	trans-stilbene
t-SB	trans-stilbene
US	United States
UV/Vis	ultraviolet/visible
V	volume
XPS	X-ray photoelectron spectroscopy

Acknowledgements

I would like to start by thanking the Lord, not only for His divine intervention in my decision to come to Virginia Tech, or His strength and guidance in seeing me through this process, but also for the unending grace that he bestowed upon my advisor and committee in dealing with me for the last five years.

There are many, many, many people who have contributed love, advice, experience and sometimes name-calling for the sole purpose of seeing my fulfillment of a PhD. Of specific importance is my advisor, Dr. Jim Tanko. Dr. Tanko, without your help I never could have accomplished a graduate degree… And yet, even with your help I still managed to miss virtually all of my deadlines. I would also like to express my sincerest appreciation to the members of my committee both past and present; Dr. Paul Carlier for his extensive efforts in teaching me organic chemistry, as well as encouraging me to "talk to my inner chemist", Dr. Andrea Dietrich for not only teaching me the ropes as a water chemist, but also allowing me the pleasure of being a honorary member of her group, Dr. David Kingston for both his chemical and spiritual expertise, Dr. Tim Long for sharing his knowledge of polymer chemistry, encouraging me as a scientist and- most importantly- inspiring me to work hard at the gym, Dr. Craig Thatcher for serving on my committee during his tenure here- despite multiple and unending responsibilities, and Dr. Diego Troya for his direct contributions to my work, as well as graciously serving on my committee in the later stages of my PhD career. I'd like to especially thank Dr. Garth Wilkes for his very insightful consultations on polymer chemistry and direction in my research project. Additionally, a very special note of thanks goes out to Dr. Deck, who has been incredibly helpful in every step of my long and arduous graduating process.

Albeit not an “official” member of my committee, an enormous thank you goes out to my dear friend Andrew Whelton. Andy, I have appreciated your mentorship, advice and knowledge almost as much as I have appreciated your friendship.

I’d like to also thank the students and staff members who I have had the pleasure of working with during my time here at Virginia Tech: Michelle Grimm, Jared Spencer, Akiko Nakamura, Shraddha Patil-Patwardhan, Tyler Horseman, Jun Yin, Liang Chen, Hayati Celik, Stephanie Zimmeck, Angie Miller, Kay Castagnoli, Claire Santos, Tom Bell, Bill Bebout and all of Analytical Services for their time and efforts in helping me succeed.

Most importantly are the people for whom I could always count on for emotional support and guidance- my friends and family. Amber Nicole Hancock, I do not even know which is of greater value to me, your friendship or my PhD. Fortunately, I get them both. I cannot express how much your friendship and loyalty has meant to me over the past five years. All I can do is promise not to wake you up at two in the morning to try to explain how much your friendship and loyalty has meant to me over the past five years. Barbara Macri (as well as Richard and Stephen), you have been and continue to be my family and I am ever so lucky to have met you. Nipa Deora Alvares and Sampada Karkare, I do not know where I would be without you. Had you two not taken me under your wing and taught me even the very basics of chemistry (i.e. “What is C2 symmetry?”) I do not know that I would be here today. And to the Tanko group as a whole, my unending thanks and appreciation for all the help, guidance and education that you have bestowed upon me.

I also feel the intense need to thank those who have spent the past five years entertaining me. So John, Paul, Ringo and George- thanks guys. You made working in lab much more

enjoyable. And to Jon Stewart and Stephen Colbert, thanks not only for the entertainment, but also for putting your respective shows in a time slot where I could actually enjoy them.

And to my wonderful family, Mom, Dad, Chris, Jenny, Angie, Damon, Matthew and Morgan, and of course baby Lilly, I will never be able to fully express how much you all mean to me, but I will try. You have all been my rock and inspiration throughout the past five years. When things were rough, I could always look forward to seeing you guys and it would put a smile on my face (and it always will). Thank you so much for your love and encouragement- I certainly could not have done this without you.

To all who I have missed, I am greatly sorry… but I will try to do better in the acknowledgements of my next 200 page document so be watching!

Finally, I would like to once again thank Jim Tanko. Dr. Tanko your encouragement and faith in me can never be repaid, but please rest assured I will spend the rest of my life being grateful for it.

Lovingly Dedicated to Felix & Lillian Restuccia and George & Margaret Mitroka

Chapter 1 Radical Chemistry: Methods, Reactivities, and Degradation Processes

1.1 Introduction

It has been well established that oxidative damage is responsible, at least in part, for many degradative processes. Reactive oxygen species (ROS) are increasingly being explored as the etiology of many diseases. Conditions such as cancer,[1, 2] ALS and Parkinson's disease[3, 4] are believed to be the result of oxidative stress to the body. ROS are also known to be of great significance in environmental chemistry and materials science. These highly reactive species are known to play a major part in the breakdown of many materials. Because of this fact, there is an increasing interest in exploring the chemistry of reactive oxygen species on a fundamental level. The hydroxyl radical (HO•) can be formed through a variety of different means that allow it to be studied in various environments (i.e. gas phase, aqueous solution, etc.) The complexity of the pathways through which these processes occur requires that the molecular mechanisms be first examined in a smaller, more controlled environment. Once an understanding of the production and activity of these radicals has been established, the model of such a mechanism can be extrapolated to the more complicated systems.

1.2 Photochemistry and Chemical Kinetics--Theory

In pulse radiolysis, a sample is exposed to a high energy pulse of monochromatic light. This sudden flash of light causes immediate photo-excitation of the sample, which then leads to the chemical events that are to be monitored.[5] The energy provided is sufficiently intense to create very reactive species, such as radicals. Generally, the pulse should be able to produce a

measurable change in the system, typically an amount of product in the range of 10^{-5} to 10^{-2} M , which is desirable for UV/Vis detection.[5]

Once the radical of interest has been generated, it can react with its intended substrate. There are several methods which may be used to monitor the progress of the reaction, the most common of which is optical absorption. Common optical detectors span wavelengths of approximately 3-0.2 micrometers.[6] The response time of the system is generally very rapid, usually on the order of a few nanoseconds.[6] The absorption of a species is monitored as a function of time to deduce the rate of the reaction.

The rate of bimolecular reactions is often determined under pseudo-first order conditions. Given a reaction:

$$A + B \longrightarrow C + D \qquad \textbf{(1-1)}$$

The rate of the reaction can be expressed as $\frac{-d[A]}{dt} = k[A][B]$. If the concentration of species B were inflated to the point that it stayed approximately constant throughout the reaction (at least 10 times the concentration of A), then the expression could be reduced to $\frac{-d[A]}{dt} = k_{obs}[B]$, where $k_{obs} = k[B]_0$, and $[B]_0$ represents the initial concentration of *B*. Combining like terms and integrating over all time, the expression further reduces to:

$$[A]_t = [A]_0 e^{-k_{obs}t} \qquad \textbf{(1-2)}$$

nd expressed in term of optical absorbance:

$$\ln\left(\frac{A_t - A_\infty}{A_o - A_\infty}\right) = -k_{obs}t \qquad \textbf{(1-3)}$$

Once k_{obs} has been established, the absolute rate constant can be determined by varying the concentration of species *B*. This determination is also done via linear regression where:

$$k_{obs} = k[B]_0 \qquad \textbf{(1-4)}$$

where the absolute rate constant is a slope of the graph of $[B]_0$ vs. k_{obs}.

In a system involving very reactive species, such as a ROS, more than one reaction may be taking place. For example, reactive species A may react not only with B but also with one or more other species in the system (such as the solvent, C):

$$A + B \xrightarrow{k_1} D \qquad \textbf{(1-5)}$$

$$A + C \xrightarrow{k_2} E \qquad \textbf{(1-6)}$$

The rate of the reaction *v*, will be:

$$v = k_{obs}[A] \qquad \textbf{(1-7)}$$

where k_{obs} is equal to the sum of all of the micro rate constants for reactions that A undergoes.[7] Parallel first- or pseudo-first order reactions provide the basis for a technique known as the probe method. The intermediate is reacted with a substrate that produces an observable product- alone and in the presence of the substrate of interest. The difference in activity allows a reaction with no detectable product or intermediate to be kinetically monitored, as illustrated in Scheme 1-1.

Scheme 1-1: Probe method

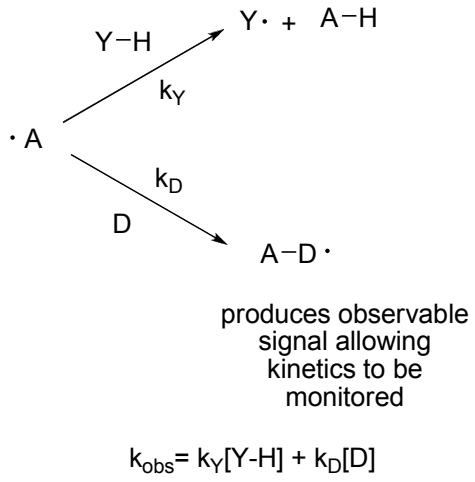

The HO•, as well alkoxyl radicals RO• in general, are highly reactive and very short lived. They are naturally produced in a variety of ways; in biological systems they are not only produced by exogenous sources, such as radiation, but they are also the result of normal processes such as the redox reactions of enzymes.[8] In the atmosphere, hydrogen peroxide serves as a precursor to the formation of the HO•, which reacts with a class of pollutants known as polycyclic aromatic hydrocarbons, as well as other volatile organic compounds.[9, 10] A variety of methods exist for experimentally creating the HO• to study its reactions. One of the most common methods is through the Fenton reaction, which involves the reduction of H_2O_2 with a metal.[11] The ferrous agent combined with hydrogen peroxide is a well established method of producing the HO•:

$$Fe^{2+} + H_2O_2 \longrightarrow Fe^{3+} + HO^- + HO\cdot \qquad \textbf{(1-8)}$$

The rate constant for this reaction is measured at approximately 60 L mol^{-1} s^{-1}.

In laser flash photolysis, hydroxyl and alkoxyl radicals are often formed when a suitable precursor is hit with a photon of light. One example is the direct photolysis of water at 184 nm.

Although this is an inexpensive and convenient method for production of the HO•, there are several other products that are formed from the ionization of water:[11]

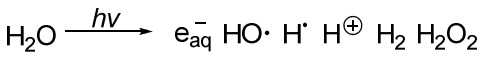

(1-9)

By adding N_2O, the yield of HO• is greatly increased:[11]

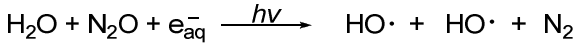

(1-10)

Although this increases the yield of hydroxyl to 90%, there are still other side products that may contribute to the reaction being monitored. In addition, many organic compounds absorb light in the < 200 nm region. This makes it impossible to cleanly generate the HO• to study its kinetics with organic substrates.

Another HO• precursor is *N*-hydroxy-pyridine-2(1*H*)-thione.[9, 12, 13] Photolysis of this compound produces the HO• and the 2-pyridylthyl radical (by-product) via homolytic cleavage of the N-O bond:[13]

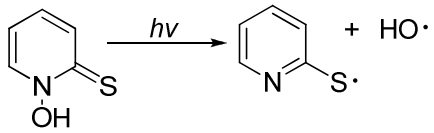

(1-11)

This reaction is somewhat complicated. Tautomerization of the starting material is pH dependant, and at neutral pH, the anionic form of the structure is present leading to a proton and hydrated electron:[13]

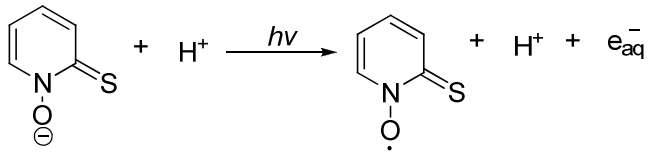

(1-12)

The formation of the 2-pyridylthyil radical further complicates the usage of *N*-hydroxy-pyridine-2(1*H*)-thione as a HO• source. This radical is not optically transparent, and reacts to form

dimers. Absorption from the resulting dimers may interfere with monitoring the desired reaction.[14]

Additional methods for developing a clean source for HO• are currently being investigated. One such method uses the structurally similar *N*-hydroxy-2(1*H*)-pyridone.[13] The HO• is produced similarly through homolytic N-O bond cleavage. However, as opposed to *N*-hydroxy-pyridine-2(1*H*)-thione, in neutral solution the keto tautomer is the dominant species, leading primarily to the formation of the HO•. The 2-pyridyloxyl radical is also much less reactive than its sulfur analog. If used in a biological system,[13] this would ensure that the relative rate of reaction is due solely to the actions of the HO•:[13]

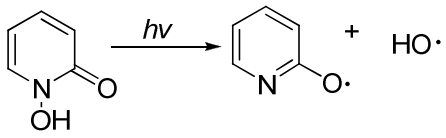

(1-13)

1.3 HO• Reactions: Methods and Rates of Hydrogen Abstraction

The oxidation of alkanes with the HO• play a central role in combustion and atmospheric chemistry.[15, 16] Because of this, many of the reported kinetic have been performed in the gas phase, using a variety of different conditions and methods. Bayes et al. studied the rates of hydrogen abstraction from several alkanes and cycloalkanes[15] via competition experiments with ethane, whose rate constant for reaction with HO• is well-established. [15, 16]

The method involved measuring the fractional loss of the alkane of interest and the reference compound (ethane) then determining the rate constant ratio using the mathematical equation:

$$\frac{k_{\text{reactant}}}{k_{\text{reference}}} = \frac{\ln(DF)_{\text{reactant}}}{\ln(DF)_{\text{reference}}} \qquad \textbf{(1-14)}$$

where DF is the ratio of the initial concentration of said species to the final concentration. Rate constants were determined over a temperature range from 230 to 430 K. At 298 K the results were in good agreement with published data, however at temperatures below 270 K, several reactants showed little of the curvature previously reported and attributed to nonlinear Arrhenius behavior. Bayes suggests this detail to a systematic error; while absolute measurements (from literature) *did* show non-linear Arrhenius behavior, these results were not replicated when using relative rate data (as employed by Bayes) at low temperatures. He suggests that what is occurring is loss of the hydroxyl radical to impurities which would effectively interfere with absolute measurements, but not relative measurements. Thus, Bayes favors his method of using relative measurements rather than absolute data for obtaining rate constants at lower temperatures. He does concede that at temperatures above 270 K, relative and absolute measurements are essentially the same (within 5%).

Anderson et al. performed similar studies of the HO• reactions with ten different alkanes over a temperature range of 300 to 400 K.[16] These reactions were carried out in the gas phase using a high pressure flow system. By observing the kinetics of the hydrogen abstraction reaction over a wide range of temperatures, Anderson was able to determine the Arrhenius parameters specific to each alkane, by using a modified form of the Arrhenius equation consistent with transition state theory:[16]

$$k(T) = \frac{Be^{\frac{-E_a}{T}}}{T\left(1-e^{\frac{-1.44v1}{T}}\right)^2\left(1-e^{\frac{-1.44v2}{T}}\right)} \qquad \textbf{(1-15)}$$

In this equation v_1 is the degeneracy of the C-H-O bend, v_2 is the H-O-H bend frequency, and B is the pre-exponential factor. This equation assumes a late transition state in which the intermediate resembles the products. The C-H-O (hydrogen abstraction from the alkane) axis is

almost linear and the H-O-H axis (formation of water from abstraction) is bent, similar to the structure of the water produced.[16]

Anderson and coworkers also used a less established technique to determine the same rate constants. Gas phase techniques, such as those previously employed by the group, show strong non-Arrhenius behavior at low temperatures when the reaction has a the loose transition state with no well-defined free energy maximum, such as those typical for these radical reactions.[16, 17] This is due to the plug-flow approximation that is employed in traditional flow techniques. The flow tube is operated at lower pressures to ensure mixing of the reactants in the tube via diffusion and to allow reaction distances to be converted into reaction time.[18] The continuity of flow in this method is determined using the equation:

$$v(r)\frac{\partial C}{\partial z} = D\left(\frac{\partial^2 C}{\partial z^2} + \frac{\partial^2 C}{\partial r^2} + \left(\frac{1}{r}\frac{\partial C}{\partial r}\right)\right) + k_1 C \qquad \textbf{(1-16)}$$

where r is the radial coordinate, z is the axial coordinate, $v(r)$ is the bulk velocity, D is the molecular diffusion coefficient, C is the concentration of the limiting reagent and k_1 is the first order rate constant.[17] The new high pressure system employed by Anderson does not require this approximation. Instead radial profile and the radical concentration profiles are used simultaneously to determine the continuity for a rate constant.[17] Anderson used this method to determine several rate constants, all of which were similar to those previously determined.

Droege and Tully examined the rate constant for reaction of HO• with cyclohexane and cyclopentane, as well as their deuterated counterparts.[19] Experiments were again performed in the gas phase via laser photolysis, using time resolved HO• profiles to determine the loss of HO•. The concentration of the HO• was monitored using laser-induced fluorescence near 307 nm. In

all of the experiments performed, the concentration of the cycloalkane was much greater than that of the HO•, allowing for a pseudo-first order reaction to occur:

$$[OH]_t = [OH]_0^{-(k_i[cycloalkane]+k_d)t} = [OH]_0^{-k't} \qquad \textbf{(1-17)}$$

where *k'* is the measured pseudo first order rate constant, k_i is the bimolecular rate coefficient for the reaction and k_d is the rate of hydroxyl reactivity in the absence of any added cycloalkane.[19] In their studies the authors noted that the rate of either hydrogen or deuterium abstraction for a single methylene group is faster for cyclohexane than cyclopentane, with rate coefficients per methylene sites of 1.19 x 10^{-12} and 1.00 x 10^{-12} cm^3 $molecule^{-1}$ s^{-1}, respectively. [19] The authors attribute this to the stabilizing contributions from neighboring methylene sites, as reported bond dissociation energies (BDEs) are nearly equivalent (cyclopentane: 94.5 (±1.0) and cyclohexane: 95.5 (±1.0) kcal mol^{-1}).[20] While experimental values of cyclopentane and cyclohexane C—H BDEs indicate that both values are very similar, recent calculational work suggests there is a noticeable disparity between the two values. Using G3 and W1 calculations, Kass et al. determined the BDE of cyclohexane to be larger than reported, by as much as 4 kcal mol^{-1}.[21] While this is somewhat unexpected in light of Tully's results, Kass argues that a lower BDE for cyclopentane is to be expected, as hydrogen atom abstraction would relieve cyclopentane of four eclipsing interactions.

Another important class of compounds that has been investigated in terms of HO• oxidation is alcohols. In their experiments, Paraskevopoulos et al. studied the rates of hydrogen abstraction from a series of alcohols in the gas phase.[22] Monitoring the concentration of the HO• via time resolved attenuation of its resonance radiation, Paraskevopoulos et al. developed a scheme for determining the rate of hydrogen abstraction from the alcohol. They suggested that the following set of reactions is likely to occur:

Scheme 1-2: Reactions occurring upon pulse radiolysis of water

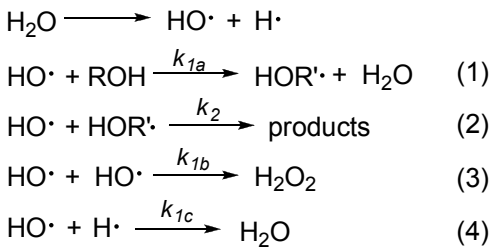

where HOR'• is the result of the hydrogen abstraction reaction by the HO•. While the authors don't specifically comment on whether abstraction at the OH site of the alcohol take place, they do comment that the expected product is a carbon-centered radical, indicating the only C—H abstraction would occur. By setting up a pseudo first order system in which the concentration of the alcohol is much greater than that of the HO•, the authors were able to establish the rate of hydrogen abstraction (Equation 2, Scheme 1-2) using a set of two equations[22]:

$$\frac{-d[\bullet OH]}{dt} = k_1[\bullet OH] + k_2[\bullet OH][\bullet R'OH] \qquad \textbf{(1-18)}$$

$$\frac{-d[\bullet R'OH]}{dt} = k_1[\bullet OH] - k_2[\bullet OH][\bullet R'OH] \qquad \textbf{(1-19)}$$

The authors used these equations as a means of differentiating between HO• loss via hydrogen atom abstraction and HO• loss via addition to carbon-centered radicals. The term k_1 is the overall rate constant of HO• decay (which is being monitored, and is the sum of k_{1a}, k_{1b}, k_{1c} and k_2 in Scheme 1-3). The term k_2 is assigned a value of 2×10^{14} cm^3 mol^{-1} s^{-1} (the collision rate). The authors then numerically integrated these equations and determined a corrected value for k_1, which was then used to determine the rate constant of the HO• reacting with an alcohol:[22]

$$k_1 = \alpha + k_{1\alpha}[ROH] \qquad \textbf{(1-20)}$$

Although the authors went through great lengths to correct for any additional loss of hydroxyl radical (other than reacting with the alcohol), their rate constants showed no significant difference from previously reported data.

To further probe where the primary site of hydrogen abstraction may be, several studies involving isotopic labeling have been conducted. Hess and Tully examined the deuterium isotope effects on the rate of abstraction from methanol over the temperature range of 293-866 K.[23] Using a three parameter expression the authors were able to establish the absolute rate constants:[23]

$$CH_3OH: \quad k(T) = 5.89\times10^{-20} T^{2.65} e^{883cal/molRT} \qquad \textbf{(1-21)}$$

$$CD_3OH: \quad k(T) = 1.28\times10^{-22} T^{23482.65} e^{1275cal/molRT} \qquad \textbf{(1-22)}$$

Abstraction is slower for the deuterated form of methanol over the entire temperature range examined. However the difference in rate between the two varies with increasing temperature. The authors suggest that the overall abstraction rate is the combination of two processes:

$$k_{overall} = k_{CH_3 \diagup CD_3} + k_{OH} \qquad \textbf{(1-23)}$$

At lower temperatures, the overall rate is dominated by hydrogen abstraction from the methyl group, due to the large kinetic isotope effect seen. At higher temperatures, the KIE decreases indicating the increasing importance of the OH hydrogen abstraction[23].

While gas phase reactions are imperative to understanding the HO• reactivity in many environmental processes, equally- if not more important- is the study of the HO• in aqueous solution. Similar alcohol studies were conducted by Janata et al., who used pulse radiolysis to monitor reaction of alcohols .[24] Like Paraskevopoulos, a series of equations to describe all possible processes that might occur in the system was derived:

Scheme 1-3: Reactions occurring in pulse radiolysis of alcohols

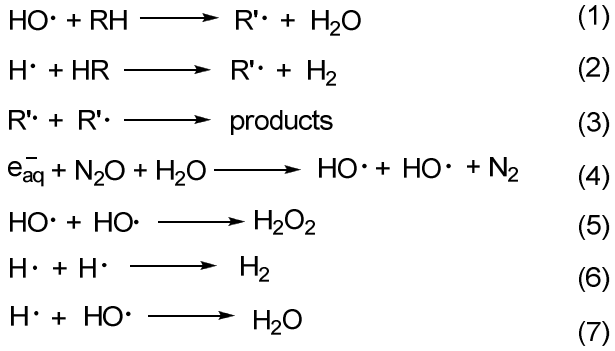

To determine the rate constant for the desired reaction (Equation 1, Scheme 1-3), computer simulations (using previously determined rate constants for reactions 2-7) were employed.[25] The values obtained by Janata were congruent with previously obtained values for this set of reactions.

Another important class of compounds that undergo this type of hydrogen abstraction is amines. Pramanick and Bhattacharyya have studied the rates of abstraction for several amines using entrapping mechanisms for polymer end groups.[26] Using Fenton chemistry to create the HO•, the authors studied several different amines via the reactions outlined in Scheme 1-4:[26]

Scheme 1-4: HO• trapping by polymer end groups

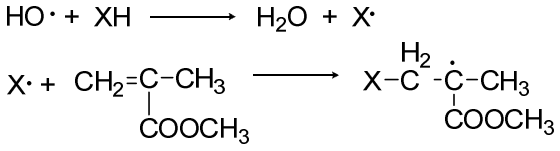

where the amine (X) is now trapped as a polymer end group and can be examined via a dye partitioning technique.[26] In this process, polymer samples were taken at different time intervals, and carefully washed and dried. The rate of abstraction was the slope of the plot of the degree of polymerization against time. Through this method, the authors were able to establish the rate constants for hydrogen abstraction (from carbon) for several different amines. In addition they also examined the rate of reactivity for different classes of amines. The reactivity order revealed that secondary amines were the most reactive, with tertiary amines being only slightly less reactive and primary compounds being the least reactive.[26] This trend is a combination of both steric effects and activation of the methylene group from which abstraction is occurring. The neighboring alkyl substituents increase reactivity for both secondary and tertiary amines. However the steric bulk of the tertiary amines negates part of this activation, decreasing the rate of abstraction relative to secondary amines.

Other classes of organic compounds have also been widely studied. Thomas examined the rate of the HO• with several alcohols, as well as diethyl ether and acetone via competition kinetics with the iodide ion (I^-).[27] Scheme 1-5 illustrates the mechanics of this: the ·OH radical was generated via pulse radiolysis with the iodide reaction product (I_2^-) used as a probe.

Scheme 1-5: HO•/I_2^- probe

$$HO^{\cdot} + I^- \longrightarrow HO^- + I$$

$$I + I^- \longrightarrow I_2^-$$

$$\lambda_{max} = 400 \text{ nm}$$

Although the reaction of HO• and diethyl ether is clearly hydrogen abstraction, the author did not comment on whether the reaction with acetone was hydrogen abstraction or addition to the carbonyl carbon. However, Walling and co-workers had later reported a significant isotope effect between acetone and d_6-acetone (k_H/k_D= 3.54), indicating hydrogen abstraction as the

likely pathway.[28] Neta et al. used similar methods, gamma radiolysis and competition kinetics, to determine the HO• reactivity with several compounds, including both chloroform and acetonitrile.[29] Rate constants were found to be remarkably lower for these two compounds than for other aliphatic compounds examined. The authors determined the relative substituent effects on a series of substituted methanes (Figure 1-1):

Figure 1-1. Relative reactivity of HO• towards substituted methanes (CH_3—X)

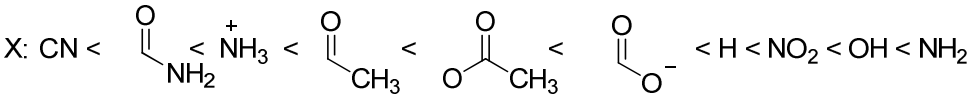

wherein presence of a cyano group greatly decreases the reactivity of methane, and presence of an amine causes a significant increase in reactivity.

The HO• is known to play a role in the oxidation of polymer based pipes, and is also believed to interact with drinking water contaminants.[30, 31] Haag and Yao studied the reaction of the HO• with 25 potential drinking water contaminants, including dichloromethane, bromoform and chloroform.[31] Several different methods were used to create the HO• in aqueous media, including the photo Fenton method and ozone decomposition, depending on the light stability of the compound being examined. All reactions were monitored via competition kinetics using the equation:

$$k_{\bullet OH}^{M} = \frac{\ln [M]_0 / [M]_\infty}{\ln [C]_0 / [C]_\infty} = k_{\bullet OH}^{C} \qquad \textbf{(1-24)}$$

Where M is the substrate and C is the reference compound. As seen in Neta's work, compounds containing halogen substituents, namely dichloromethane, chloroform and bromoform, all

proved to have rate constants significantly lower (1 to 2 orders of magnitude) than reported values given for hydrocarbons or alcohols.

1.4 HO• Additions

When reacting with conjugated systems, the HO• generally undergoes an addition reaction preferentially to the hydrogen abstraction reaction. This is of extreme importance in areas such as environmental science, where polyaromatic systems are commonly produced as byproducts of burning fuels. Platz et al. studied the reactivity of the HO• with a series of conjugated hydrocarbons in acetonitrile.[9] Using several deuterated compounds, the kinetic isotope effects were also established. The authors determined that the primary pathway for each of the aromatic systems studied was, in fact, the addition reaction. The authors also noticed that the rate constants for addition reaction were smaller in acetonitrile than those that had been established for the same reaction in water. This was attributed to a stabilization of the transition state compared to reactants by hydrogen bonding with water (Figure 1-2). [9]

Figure 1-2. Stabilization of transition state in HO• addition reaction

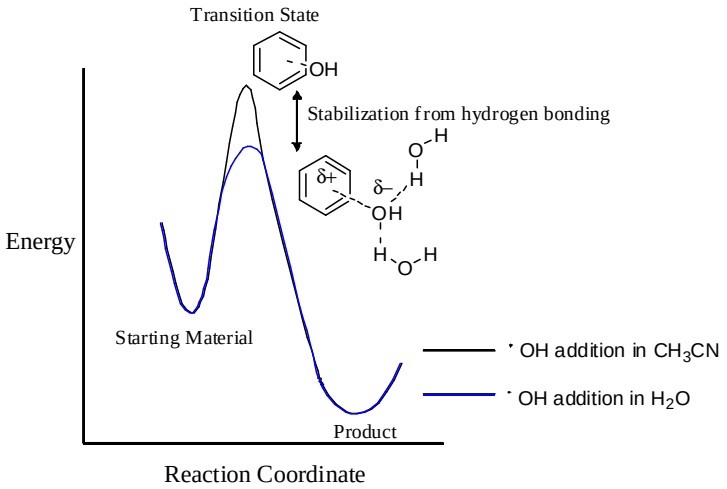

In a similar study, Albarran and Schuler examined the effects of substituents on the addition of the HO• to aromatic rings.[32] The strong electrophilic character of the HO• leads it to add to the most electron rich sites. For the meta substituted cresol, the ortho- and para- products predicted by the Hamett equation were observed. In the case of para-cresol, only two products are expected but four were determined to be present. For ortho-cresol, five products are expected, and seven were determined to be present. The additional products were determined to be both the ipso product as well as the corresponding para- and ortho- dienones (Figure 3). For each of these compounds, both the hydroxyl and methyl substituents belonging to cresol effect the electrophilic addition reaction of the HO•.[32] The methyl substitution clearly has a much more profound effect on the addition to ortho- and para- cresol than when substituted in the meta- position, as shown in Figure 1-3.

Figure 1-3. HO• addition products to cresols

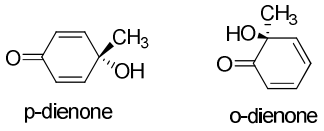

p-dienone o-dienone

1.5 Alkoxyl Radical Reactions.

Although the HO• is the most aggressive of the reactive oxygen species, alkoxyl radicals are also very powerful oxidizing agents. One of the most widely studied alkoxyl radicals is the tert-butoxyl radical. Tanko et al. have studied the reactivity of this radical oxygen species as a model for C-H bond cleavage for several enzyme catalyzed reactions.[33] This radical shows similar reactivity to the P-450 enzyme and is a useful model for biological systems.[34] The tert-butoxyl radical shows mild selectivity, as expected for alkanes, however, the trend of increasing hydrogen atom abstraction rate with decreasing bond strength is not seen in tertiary amines, or

for substrates with bond dissociation energies below 92 kcal/mol.[35] The fact that this reaction does not follow the typical structure/reactivity relationships is due to the reaction being entropy controlled, rather than the more common enthalpy controlled reaction. The tert-butoxyl radical is so reactive that the rate of hydrogen abstraction is based more upon accessibility of the radical to the hydrogen, rather than by the strength of the C-H bond. Since the tert-butoxyl radical is rather sterically bulky, the ability of the radical to properly orient itself in a fashion necessary for hydrogen abstraction is more difficult than for smaller alkoxyl radicals. This suggests that the tert-butoxyl radical may not be a representative prototype for the reactivity of oxygen-centered radicals[35].

1.6 Biological Implications of HO• Oxidation

As oxidation reactions are a contributing factor to many degenerative diseases, several studies have used fundamental organic chemistry to investigate the reactions that are believed to be involved in the onset of such diseases. Free radicals are formed in biological systems either by endogenous processes (metabolism of food, exercise) or by exposure to exogenous factors (smoke, radiation). These extremely reactive free radicals will target many biomolecules, including DNA, proteins, lipids and carbohydrates. Davies et al. studied the effects of radicals on proteins.[8] Radical attack on proteins can destroy the protein or alter it drastically. Some of the products formed from the radical attack on proteins, namely hydroperoxides, have oxidizing properties which, in the presence of metal ions and UV light, decompose to ROS which can further act as oxidizing agents. The reaction scheme for the formation of hydroperoxides on the protein backbone and side chain is believed to be (Scheme 1-6):

Scheme 1-6: Chain reaction of HO• production

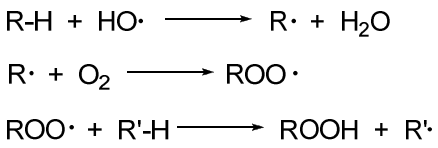

Incubation of hydroperoxide with Fe(II)-EDTA in the presence of 3,6-dimethyl-2,5-piperazinedione allowed for the identification of the HO• and alkoxyl radical as decomposition products by EPR spectroscopy:

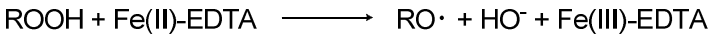

(1-25)

These series of reactions, which are initiated by hydroxyl and alkoxyl radicals lead to the fragmentation of the protein backbone (Scheme 1-7):

Scheme 1-7: Oxidative degradation of protein backbone

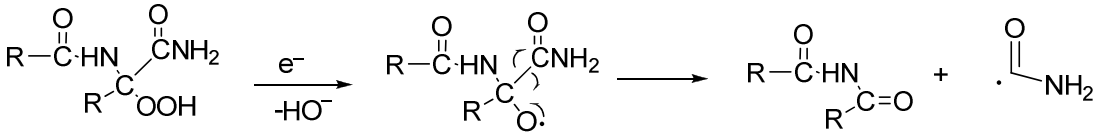

Saha-Moller et al. investigated the effects of the HO• on mouse lymphoma cells using the *N*-tert-butoxypyridine-2-thione HO• precursor.[36] The photo-cytotoxicity and photo-genotoxicity of the mouse lymphoma cell line L5178 was examined and showed a time dependant decrease in relative cell growth and increase in membrane damaged cells.[36] When a radical scavenger was employed the photo-cytotoxicity of the compound was greatly diminished, indicating that it is the alkoxyl radical responsible for this type of toxicity, (although the thiyl radical is believed to induce the genotoxicity).

A similar set of experiments was carried out by this group using super-coiled pBR322 DNA[37]. The tert-butoxyl, benzoyloxyl and iso-propoxyl radicals were generated from the

corresponding N-alkoxypyridine-2-thione in the presence of this DNA which was then analyzed via gel electropheresis for strand breakage. The alkoxyl radicals all induced strand breakage. Once again, when a radical scavenger was employed, the amount of open-circular DNA was greatly reduced.

DNA base damage is what is specifically believed to be responsible for the strand breakage of the double helix. Of the four bases found in DNA, the purine base deoxyguanine appears to be the most susceptible to this oxidative attack, although the reasons for this are not apparent.[38] Scheirer et al. did a similar experiment involving the photolysis of a photo-Fenton reagent which produces the tert-butoxyl radical.[39] This radical undergoes beta cleavage to produce a methyl radical, which may subsequently react with molecular oxygen to form methylperoxyl radical, $CH_3OO\cdot$. The methyl and methyl-peroxyl radicals cause damage to the deoxyguanine base of DNA which leads to subsequent strand breakage. Car et. al found that the specific mechanism of hydroxyl attack on each base is different.[38] The use of static and dynamic ab initio methods was employed in order to elucidate the mechanism of hydroxyl attack on the thymine and guanine bases found in DNA. For thymine, the HO• reaction of dehydrogenation is most favorable with the C-5 methyl group, being exothermic to -108.6 kJ/mol in gas phase and -112.2 kJ/mol in aqueous solution. The second most favorable site is at N1 which gives values of -86.7/-84.7 kJ/mol. For the hydroxylation reaction the most favorable site is the C-6 position followed by the C-5 position. These values are in agreement with the experimentally determined products that arise from the dehydrogenation and hydroxylation reactions.

Singlet oxygen is also a large contributor to DNA base damage seen in cells. Box et al. studied the specific damage done by singlet oxygen to the guanine base.[1] After exposing a tetramer of DNA composed of each base to UVA light in solution containing methylene blue,

HPLC analysis confirmed the presence of three unharmed bases. The only resonance not accounted for was guanine, which was confirmed to have been oxidized into 8-oxo-7,8-dihydro-guanine (Figure 1-4, I) and spiroiminodihydantoin(Figure 1-4, II).

Figure 1-4. Guanine oxidation products

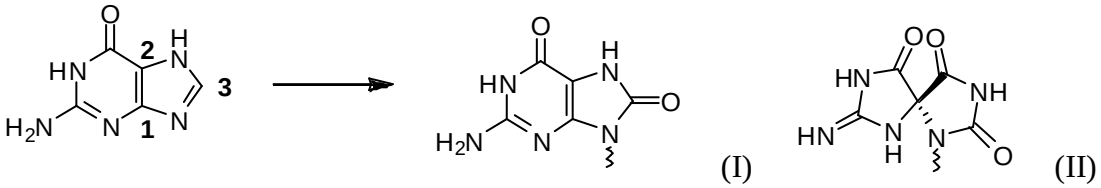

The product are the result of an oxidative addition to the N-C3 bond to form product I or to the C1-C2 double bond, which subsequently breaks to form the two five membered rings in product II.

1.7 Accelerated Aging of Polyethylene Potable Water Material

Polyethylene (PE) pipes, and specifically high density polyethylene (HDPE) pipes, are becoming increasingly popular as a means of water transport for industrial and residential applications. The relative low cost of the material, combined with its projected 50 to 100 year service life, makes HDPE and ideal material for water distribution. Both medium density polyethylene (MDPE) and HDPE are currently approved for applications of 25°C or less, and in 2004, PE water pipe comprised a third of the world's plastic pipe demand.[30]

HDPE pipes are generally enhanced with additives such as UV stabilizers, antioxidants, and phosphites that provide the material with a tremendous resistance to oxidative stress. However, long term exposure to chlorinated water is known to have a deleterious effect on both mechanical strength, as well as chemical composition of the pipe. Chlorine is used as a disinfectant in the US, as well as other parts of the world, to help prevent the spread of infectious disease. In the US, the chlorine content can be very high, reaching greater than 1 part per million

in some areas. Repeated exposure of pipes to such high levels of chlorine causes early deterioration of the material.

While it is widely established and accepted that chlorinated water increases degradation of PE pipes, the exact circumstances of how this occurs remain somewhat controversial. Several researchers have reported that the initial stage of PE pipe degradations involves the loss of anti-oxidants from the material. Dear and Mason looked at the differences between chlorinated water and unchlorinated water on the properties of MDPE pipe.[40] The loss of antioxidant was found to be much greater for a wall surface of MDPE exposed to chlorinated water than a wall surface exposed to unchlorinated water. In fact, the authors suggest that the chlorinated water need only penetrate the first millimeter of wall thickness before superficial environmental stress cracking starts to occur. This initial stress cracking is the cause of mechanical failure, and is increased with increasing chlorine content. The authors note that while these PE pipes may have an expected lifetime of several decades in dry air, exposure to chlorinated water may decrease their lifetime to less than ten years.

Gedde and coworkers examined the effects of chlorinated water and elevated temperatures on the degradation of HDPE pipes.[41] Using differential scanning calorimetry (DSC) to measure oxidation induction time (OIT), Gedde measured the amount of effective antioxidant after chlorine exposure at different temperatures in different areas of the pipe (taking a cross-section from the inner wall, which was immediately exposed to the chlorinated water, to the outer wall which was unexposed). Gedde found that approximately 80% of stabilizer was lost through chemical consumption stemming from exposure to hot chlorinated water. In pipe exposed simply to hot water, antioxidant consumption was negligible indicating that chlorine in the water sample is clearly responsible for loss of antioxidants within HDPE. The researchers

also found that chlorine exposed pipe produced a highly degraded inner wall. This inner wall was examined via infrared spectroscopy, which confirmed the presence of a newly formed absorption band at 1700 cm^{-1}. However, what was extremely fascinating was that the area immediately beneath this porous layer was completely unoxidized. The oxidized layer also proved to have significantly higher mass crystallinity content than other cross-sections of the same pipe. From these conclusions, Gedde suggests that the species responsible for antioxidant loss is not very reactive with the pipe material; the species responsible for pipe degradation must, however, be extremely reactive and/or insoluble in the polymer itself, as only the immediate surface is oxidized.

Insight into the degradation of the PE material itself is helpful to understanding what might be behind this accelerated aging in chlorinated water solutions. Pinheiro et al. found that, during processing, oxygen content played a significant role in the degree and content of degradation of HDPE.[42] Macroradicals are formed during processing which can either react with each other (giving an unsaturated site such as a vinyl group or transvinylene group), or which can react with dioxygen, forming a peroxyl radical. Hydrogen abstraction by this newly formed radical and subsequent beta-scission leads to the formation of a carbonyl end group (thus breaking the chain) and formation of another highly reactive radical, HO•.

Pinheiro focused on two different HDPE resins: Phillips and Ziegler-Natta. Samples of each resin were processed in a totally filled (TF) chamber, where 100% of the container was filled with resin, or a partially filled (PF) container containing only 70% resin. Carbonyl content was increased for both sets of resin in the PF chamber due to the higher volume of oxygen. Significant differences were seen in the vinyl index; While Zieglar-Natta HDPE resin showed a minimal amount of vinyl group consumption for both TF and PF chambers, there was a

significant difference between vinyl group consumption in the Phillips HDPE resin (with the PF chamber showing significantly more consumption than the TF chamber). The difference in behavior among the resins can be attributed to the much greater initial concentration of vinyl groups found in the Phillips HDPE compared to the Zieglar-Natta. Looking at molecular weight distribution the trends in reactivity became clear: In the presence of oxygen, both HDPE resins are likely to react, resulting in the formation of carbonyl groups. Zieglar-Natta HDPE is likely to undergo chain scission, as molecular weight distribution curves shift towards lower molecular weights. Phillips HDPE- which contains a much greater amount of initial vinyl groups- is likely to undergo chain branching, as molecular weight distribution curves shift towards higher molecular weights.

The most thorough investigation to date regarding the accelerated aging of HDPE pipes was conducted by Dietrich et al. There has been great variation in techniques, conditions and reporting of accelerated aging studies. While there are several different viable methods for conducting such research, variations in pH, chlorine concentration, and alkalinity (used as an acid neutralizer) can greatly alter the chemistry behind this polymeric breakdown. In their work, Dietrich and co-workers determined appropriate accelerated aging conditions that minimized variation in water chemistry as well as water sorption.[30] The authors set to identify a set of conditions that would mimic potable water systems commonly found in the US, as well as control chlorine speciation (Scheme 1-8):

Scheme 1-8: Chlorine speciation

$$\text{Free available chlorine} = [HOCl] + [OCl^-] + [Cl_2] \quad (1)$$

$$HOCl \longrightarrow OCl^- + H^+ \quad pK_a = 7.5 \text{ at } 25°C \quad (2)$$

$$Cl_2 + H_2O \longrightarrow HOCl + Cl^- + H^+ \quad pK_a < 2.0 \text{ at } 25°C \quad (3)$$

HDPE samples were immersed in one of nine aging solutions with varying chlorine (Cl_2) levels (0, 45, and 250 ppm Cl_2) and varying temperature (23°, 37° and 70°C) and stored in the dark. Samples were rinsed and immersed in a new solution every three days, at which point each solution was measured for changes in pH, Cl_2 and alkalinity levels. Of the six Cl_2 solutions tested, solutions of 45 ppm Cl_2 at 23°C and 37°C were found to be the most stable, with no significant changes to pH, Cl_2 concentration or alkalinity over a three day time period. Pipes that had been aged in the 45 ppm Cl_2 at 37°C showed a characteristic carbonyl formation near 1710 and 1730 cm^{-1}. The formation of this functionality was detected as early as 720 h- with increasing intensity up to 3884 h- well before oxidation induction time levels had gone to zero, indicating the pipe was oxidized while antioxidants were still present.

Like Dietrich, Bourgine et al. wanted to see the effects of another common disinfectant, chlorine dioxide (DOC), on the process of accelerated aging.[43] Much interest in exists in examining the effects of DOC on polyethylene pipe, as a massive HDPE breakdown in the south of France occurred after only a few years of exposure to this disinfectant. Similar to Dietrich, the authors maintained constant solution conditions, periodically titrating the water samples and readjusting to initial conditions. The authors tested over a range of 1 to 100 ppm DOC at either 20° or 40°C over a twenty week period. As expected, the authors found that antioxidant consumption was greatest among single concentrations with increasing time, and increased with increasing DOC concentration. Again, the formation of carbonyls were seen, however the authors did note that the presence of these functional groups was superficial, extending only a few hundred micrometers of the 4.5 mm sample. The authors speculate that a likely mechanism behind the formation of the carbonyl is breakdown of hydroperoxides, forming an alkoxyl radical

that undergoes beta-scission producing a carbonyl, and thus breaking the PE chain. While this seems highly plausible, the authors did also note that the number of chain scission was not proportional to the number of carbonyls, in fact there were approximately four times as many carbonyls than chain scissions, indicating a chemical event that produced a carbonyl without breaking the PE chain.

Though research has clearly indicated that addition of chlorine to water aids in the consumption of anti-oxidants as well as the breakdown of the polymer chains, the exact species involved in these mechanisms are still up for debate. Bradley and co-workers suggest that chlorine is not in fact that culprit, but rather the addition of chlorine to form hypochlorous acid leads to the formation of activated oxygen, which is responsible for the oxidation of the carbon chain (Scheme 1-9):[44]

Scheme 1-9: Production of activated oxygen via chlorinated water

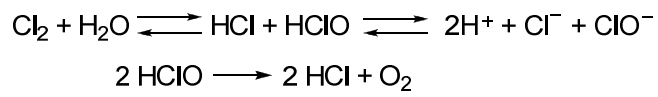

Bradley suggests that oxidation reduction potential is a better predictor of environmental stress on polyalkene pipes than chlorine concentration alone. While at every pH the oxidation reduction potential increased with increasing chlorine concentration, this phenomenon did not occur in a linear fashion. As such, free chlorine concentration, pH and trace metal concentration should all be taken into consideration when studying an aqueous solution, rather than simply chlorine content.

While HDPE oxidation serves as good evidence to suggest that free radicals are present in chlorinated water, several studies have been conducted on chlorinated water solutions to detect conclusively for the presence- and identification- of said free radicals. Using the spin trapping reagent 5,5-Dimethyl-1-pyrroline-N-oxide (DMPO), Hamada et al. was able to detect the

presence of free radicals in chlorinated solutions via electron spin resonance (ESR).[45] Using DMPO, highly reactive, unstable radicals can be converted to a more stable radical and identified.

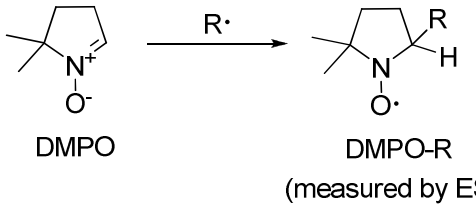

(1-26)

The authors found that the presence of free radicals in aqueous solution was strongly dependant on the chlorine concentration. The most abundant free radical that was identified was the hydroxyl radical, being present in chlorinated solutions as low as 2mg/L chlorine. To further confirm that the hydroxyl radical was indeed present, dimethyl sulfoxide (DMSO), a known hydroxyl radical scavenger was added to the chlorinated solutions. The addition of this scavenger notably decreased the DMPH-OH signal. At higher concentrations, several other DMPO adducts were detected, all of which the authors suggest the hydroxyl radical contributes too (Scheme 1-10).

Scheme 1-10: DMPO- hydroxyl radical products

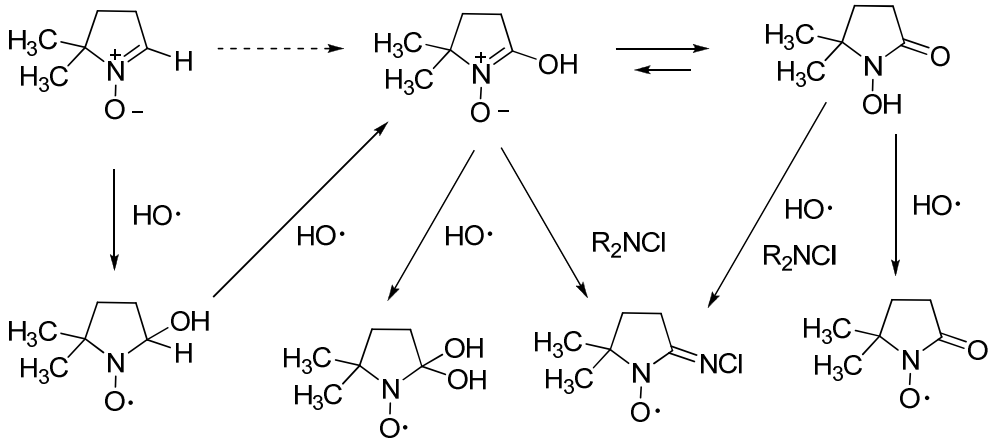

While several studies have pointed to the fact that anti-oxidants and stabilizers are consumed prior to polymer degradation,[46-49] few studies have used neat PE as a probe to elucidate its degradation. Pukanszky and co-workers studied the relative effects of a 1-year soaking period of distilled water on both stabilized and neat Phillips PE.[50] The overall properties of stabilized PE samples did not significantly change during the one year soaking in distilled water- a marked difference from the results of Dietrich who found significant changes to PE samples subjected to chlorinated water over a 144-day period. They did find that not only were there significant changes to neat polyethylene, but that these changes varied based on the number of extrusions each sample went, and were not consistent. For example, all samples showed a change in color over the soaking period (increase in a yellowish tint), however samples extruded only once showed a bell curve in yellowish tint, maxing out at 9 months and then decreasing, whereas samples extracted 3 and 6 times produced a steady increase in yellowish tint. Similar trends were seen in terms of mechanical properties; once extruded pipes showed a significant decrease in tensile strength between 3 and 9 months, however "bounced back" to its pre-treatment value at 12 months, while 3 and 6 time extruded samples stayed consistent throughout the entire 12 month period. The authors provided two possible explanations to these unusual and unpredictable trends: 1) sample-to-sample variability, in which samples extruded only once are more susceptible to extremes, however samples with a longer processing history are more consistent in their behavior, and thus likely more consistent in chemical structure; or 2) During the first processing of the PE, weak sites are formed (namely oxygen containing groups), which decompose in water leading to chain extension, and thus a stronger polymer over time. More severe processing history destroys weak sites prior to storage, so this trend is not seen.

While processing clearly plays a significant role in the degradation of any PE sample, the authors did note that all samples showed a strong correlation in all functional groups formed. Although no correlation between soaking time and carbonyl content could be seen, there was a near perfect correlation between vinyl concentration and relative carbonyl concentration (namely, as vinyl concentration decreases, carbonyl concentration increases), and that the amount of oxygen in the system determines the direction of the proceeding reactions. While the authors conclude that these two functionalities are related to each other, exactly how they were related could not be explained. They suggest a possible mechanism that fits with their results (decrease in unsaturation, increase in carbonyl content and increase in methyl content), however admit it is unlikely due to the formation of an unstable epoxy group (Scheme 1-11).

Scheme 1-11: Proposed mechanism of PE oxidation in distilled water

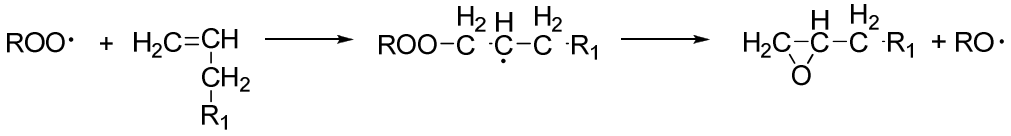

While PE pipe failure is clearly linked to oxidation, a direct mechanism for this failure has yet to be discovered. Clearly, chlorine disinfectants increase the likelihood and time frame of this failure, however a clear pathway of how this occurs must be formulated in order to better prevent against premature PE pipe failure. Systematic accelerated aging studies that address the species, conditions and mechanisms responsible for this failure are still necessary in order to get a complete picture of PE pipe degradation.

Table 1-1. Summary of literature rate constants for gas phase HO• reactions

Substrate	Notes	Phase	k (L mol^{-1} s^{-1})	Ref.
propane	298K	gas	6.68 $x10^{9}$	15
n-butane	298K	gas	1.43 $x10^{10}$	15
n-pentane	298K	gas	2.23 $x10^{10}$	15
n-hexane	298K	gas	3.12 $x10^{10}$	15
cyclopropane	298K	gas	4.60 $x10^{8}$	15
cyclobutane	298K	gas	1.25 $x10^{10}$	15
cyclopentane	298K	gas	2.91 $x10^{10}$	15
cyclohexane	298K	gas	4.03 $x10^{10}$	15
dimethyl ether	298K	gas	1.61 $x10^{10}$	15
ethane	300K	gas	1.56 $x10^{9}$	16
propane	300K	gas	5.67 $x10^{9}$	16
n-butane	300K	gas	1.46 $x10^{10}$	16
2-methylpropane	300K	gas	1.26 $x10^{10}$	16
n-pentane	300K	gas	2.40 $x10^{10}$	16
n-hexane	300K	gas	3.28 $x10^{10}$	16
cyclopentane	300K	gas	3.55 $x10^{10}$	16
cyclohexane	300K	gas	4.61 $x10^{10}$	16
cycloheptane	300K	gas	7.23 $x10^{10}$	16
cyclooctane	300K	gas	8.03 $x10^{10}$	16
ethane	297K	gas	1.43 $x10^{9}$	17
propane	297K	gas	7.29 $x10^{9}$	17
n-butane	297K	gas	1.36 $x10^{10}$	17
n-pentane	297K	gas	2.54 $x10^{10}$	17
cyclopentane	295K	gas	3.02 $x10^{10}$	19
d_{10}-cyclopentane	292K	gas	1.10 $x10^{10}$	19
cyclohexane	295K	gas	4.30 $x10^{10}$	19
d_{12}-cyclohexane	292K	gas	1.66 $x10^{10}$	19
methanol	294K	gas	5.60 x 10^{9}	23
d-methanol	293K	gas	2.62 x 10^{9}	23

Substrate	Notes	Phase	k (L mol^{-1} s^{-1})	Ref.
methanol	293K	aqueous	9.0×10^8	24
ethanol	293K	aqueous	2.2×10^9	24
Iso-propanol	293K	aqueous	2.0×10^9	24
tert-butanol	293K	aqueous	6.2×10^8	24
methanol	293K	aqueous	9.7×10^8	25
ethanol	293K	aqueous	1.9×10^9	25
iso-propanol	293K	aqueous	1.9×10^9	25
1-propanol	293K	aqueous	2.8×10^9	25
n-butyl amine	293K	aqueous	1.00×10^{10}	26
n-hexyl amine	293K	aqueous	1.31×10^{10}	26
n-octyl amine	293K	aqueous	1.46×10^{10}	26
di-butyl amine	293K	aqueous	1.81×10^{10}	26
tri-butyl amine	293K	aqueous	1.67×10^{10}	26
diethyl ether	293K	aqueous	3.9×10^9	27
acetone	293K	aqueous	7.7×10^7	27
methanol	293K	aqueous	4.7×10^8	27
ethanol	293K	aqueous	7.2×10^8	27
isopropyl alcohol	293K	aqueous	1.74 x109	27
acetone	293, pH=1	aqueous	8.85×10^7	28
d_6-acetone	293, pH=1	aqueous	2.50×10^7	28
dimethoxymethane	293K	aqueous	8.10×10^8	29
diethoxymethane	293K	aqueous	9.20×10^8	29
chloroform	293K	aqueous	8.50×10^6	29
acetonitrile	293K	aqueous	2.12×10^6	29
methane	293K	aqueous	1.43×10^8	29
ethylene	293K	aqueous	4.1×10^9	51
propylene	293K	aqueous	6.5×10^9	51
1-butene	293K	aqueous	6.5×10^9	51
isobutylene	293K	aqueous	5.0×10^9	51
butadiene	293K	aqueous	6.5×10^9	51

References

1. DeFederics, H.-C.; Patrzye, M. J.; Rajecki, E. E.; Budzinski, H. I.; Dawidzik, J. B.; Evans, M. S.; Grenne, K. F.; Box, H. C., Singlet Oxygen-Induced DNA Damage. *Radiation Research* **2006,** 165, 445-451.
2. Headlam, H. A.; Davies, M. J., Beta-Scission of Side-Chain Alkoxyl Radicals on Peptides and Proteins Results in the loss of Side-Chains as Aldehydes and Keytones. *Free Radical Biology and Medicine* **2002,** 32, (11), 1171-1184.
3. Plato, C. C.; Galasko, D.; Garruto, R. M.; Plato, M.; Gamst, A.; Craig, U. K.; Torres, J. M.; Wiederholt, W., ALS and PDC of Guam Forty Year Follow-up. *Neuruology* **2002,** 58, 765-773.
4. Suleman, N. K.; Flores, J.; Tanko, J. M.; Isin, E. M.; Castagnoli Jr, N., The Hydrogen Atom Abstraction Reactions of the Parkinsonian Inducing Proneurotoxin 1-Methyl-4-phenyl-1,2,3,6-tetrahydropyridine (MPTP) and selected tertairy Amines with tert-Butoxy Radical. In Virginia Polytechnic and State University: Blacksburg, Va, 2001; pp 1-15.
5. Baxendale, J. H.; Rodgers, M. A. J. *Contributions of Pulse Radiolysis to Chemistry*; Manchester University Center for Fast Kinetic Research, University of Texas-Austin Manchester, England; Austin, Texas, 1976; pp 235-263.
6. Baxendale, J. H.; Bell, C.; Mayer, J., Some solid state photodetectors used in pulse radiolysis studies; operational details and performance *International Journal for Radiation Physics and Chemistry* **1974,** 6, (2), 117-128.
7. Espenson, J. H., *Chemical Kinetics and Reaction Mechanisms Second Edition*. Second ed.; McGraw Hill: 2002; p 281.

8. Davies, M. J., Protein and Peptide Alkoxyl Radicals Can Give Rise to C-Terminal Decarboxylation and Backbone Cleavage. *Archives of Biochemistry and Biophysics* **1996,** 336, (1), 163-172.

9. Poole, J. S.; Shi, X.; Hadad, C. M.; Platz, M. S., Reaction of Hydroxyl Radical with Aromatic Hydrocarbons in NonAqueous Solutions: A Laser Flash Photolysis Study in Acetonitrile. *J. Phys. Chem. A* **2005,** 109, 2547-2551.

10. Vereecken, L.; Peeters, J., H-atom abstraction by OH-radicals from (biogenic) (poly)alkanes: C-H bonds strengths and abstraction rates. *Chemical Physical Letters* **2000,** 333, 162-168.

11. Theruvathu, J. A.; Aravindakumar, C. T.; Flyunt, R.; von Sonntag, J.; von Sonntag, C., Fenton Chemistry of 1,3-Dimethyluracil. *J. Am. Chem. Soc.* **2001,** 123, (37), 9007-9014.

12. Arnone, M.; Hartung, J.; Engels, B., On the Homolytic Cleavage of the N,O Bond in N-(Methoxy)pyridine-2(1H)-thione and N-(Methoxy)thiazole-2(3H)-thione in Thermally and Photochemically Induced Reactions: A Theoretical Study. *J. Phys. Chem. A* **2005,** 109, (26), 5943-5950.

13. Aveline, B. M.; Kochevar, I. E.; Redmond, R. W., Photochemistry of N-Hydroxy-2(1H)-pyridone, a More Selective Source of Hydroxyl Radicals Than N-Hydroxypyridine-2(1H)-thione. *J. Am. Chem. Soc.* **1996,** 118, 10124-10133.

14. DeMatteo, M. P.; Poole, J. S.; Shi, X.; Sachdeva, R.; Hatcher, P. D.; Hadad, C. M.; Platz, M. S., On the Electrophilicity of Hydroxyl Radical: A Laser Flash Photolysis and Computational Study. *J. Am. Chem. Soc.* **2005,** 127, 7094-7109.

15. DeMore, W. B.; Bayes, K. D., Rate Constants for Reactions with Several Alkanes, Cycloalkanes, and Dimethyl Ether. *J. Phys. Chem. A* **1999,** 103, 2649-2654.

16. Donahue, N. M.; Anderson, J. G., New Rate Constants for Ten OH Alkane Reactions from 300 to 400 K: An Assessment of Accuracy. *J. Phys. Chem. A* **1998,** 102, 3121-3126.

17. Abbatt, J. P. D.; Demerjian, K. L.; Anderson, J. G., A New Approach to Free Radical Kinetics: Radially and Axially Resolved High-Pressure Discharge Flow with Results for ·OH + (C_2H_6, C_3H_8, n-C_4H_{10}, n-C_5H_{12})-> Products at 297K. *J. Phys. Chem.* **1990,** 94, 4566-4575.

18. Howard, C. J., *J. Phys. Chem.*, **1979,** 83, (3).

19. Droege, A. T.; Tully, F. P., Hydrogen-Atom Abstraction from Alkanes by OH. 6. Cyclopentane and Cyclohexane. *J. Phys. Chem.* **1987,** 91, (5), 1222-1225.

20. McMillen, D. F.; Golden, D. M., *Annu. Rev. Phys. Chem.* **1982,** 33, 493-532.

21. Tian, Z.; Fattahi, A.; Lis, L.; Kass, S., Cycloalkane and Cycloalkene C-H Bond Dissociation Energies. *J. Am. Chem. Soc.* **2006,** 128, 17087-17092.

22. Overend, R.; Paraskevopoulos, G., Rates of OH Reactions. 4. Reactions with Methanol, Ethanol, 1-Propanol and 2-Propanol at 296 K. *J. Phys. Chem.* **1978,** 82, (12), 1329-1333.

23. Hess, W. P.; Tully, F. P., Hydrogen-Atom Abstraction from Methanol by OH. *J. Phys. Chem.* **1989,** 93, 1944-1947.

24. Alam, M. S.; Rao, B. S. M.; Janata, E., Hydroxyl radical reactions with aliphatic alcohols:evaluation of kinetics by direct optical absorption measurement. A pulse radiolysis study. *Radiation Physics and Chemistry* **2003,** 67, (6), 723-728.

25. Buxton, G. V.; Greenstock, C. L.; Helman, W. P.; Ross, A. B., Critical Review of Rate Constants for reactions of hydrated electrons and hydroxyl radicals in aqueous solution. *J. Phys. Chem. Reference Data* **1988,** 17, (2).

26. Pramanick, D.; Bhattacharyya, R., Studies on Some Radical Transfer Reactions by Entrapping the Radicals as Polymer End Groups. I. Reaction of Hydroxyl Radicals with Amines. *Journal of Polymer Science: Part A: Polymer Chemistry* **1986,** 24, 2401-2414.

27. Thomas, J. K., *Trans. Faraday Soc.* **1965,** 61, 702-707.

28. Walling, C.; El-Tailiawi, G. M., Fenton's Reagent. II. Reactions of Carbonyl Compounds and alpha,beta-Unstaurated Acids. *J. Am. Chem. Soc.* **1972,** 95, (3), 844-847.

29. Anbar, M.; Meyerstein, D.; Neta, P., Reactivity of Aliphatic Compounds towards Hydroxyl Radicals. *Journal of the Chemical Society B: Physical Organic* **1966**, 742-747.

30. Whelton, A. J.; Dietrich, A., Critical considerations for the accelerated ageing of high-density polyethylene potable water systems. *Polymer Stability and Degradation* **2009,** 94, 1163-1175.

31. Haag, W. R.; Yao, C. C., Rate constants for reaction of hydroxyl radicals with several drinking water contaminants. *Environ. Sci. Technol.* **1992,** 26, (5), 1005-1013.

32. Albarran, G.; Schuler, R. H., Concerted Effects of Substituents in the Reaction of Hydroxyl Radicals with Aromatics: The Cresols. *J. Phys. Chem. A* **2005,** 109, (41), 9363-9370.

33. Tanko, J. M.; Friedline, R.; Suleman, N. K.; Castagnoli Jr, N., tert-Butoxyl as a Model for Radicals in Biological Systems: Caveat Emptor *J. Am. Chem. Soc.* **2001,** 123, (24), 5808-5809.

34. Dinnocenzo, J. P.; Karki, S. B.; Jones, J. P., On isotope effects for the cytochrome P-450 oxidation of substituted N,N-dimethylanilines *J. Am. Chem. Soc.* **1993,** 115, (16), 7111-7116.

35. Finn, M.; Friedline, R.; Suleman, N. K.; Wohl, C.; Tanko, J. M., Chemistry of the t-Butoxy Radical: Evidence that Most Hydrogen Abstraction from Carbon are Entropy-Controlled. *J. Am. Chem. Soc.* **2004,** 126, (24), 7578-7584.

36. Moller, M.; Adam, W.; Marquardt, S.; Saha-Moller, C.; Stopper, H., Cytotoxicity and Genotoxicity induced by the photochemical alkoxyl radical source N-tert-butoxypyridine-2-thione in L5178Y mouse lymphoma cells under UVA radiation. *Free Radical Biology and Medicine* **2005,** 39, 473-482.

37. Adam, W.; Grimm, G. N.; Saha-Moller, C., DNA Cleavage Induced by Alkoxyl Radicals Generated in the Photolysis on N-Alkoxypyridinethiones. *Free Radical Biology and Medicine* **1998,** 24, (2), 234-238.

38. Wu, V.; Mundy, C. J.; Cobin, M. E.; Car, R., On the Mechanism of OH Radical Induced DNA-Base Damage: A Comparitive Quantum Chemical and Car- Parrinello Molecular Dynamics Study. *J. Phys. Chem. A* **2004,** 108, 2922-2929.

39. Adam, W.; Marquardt, S.; Kemmer, D.; Saha-Moller, C.; Schreier, P., 2'-Deoxyguanosine (DG) Oxidation and Strand-Break Formation in DNA by the Radicals Released in the Photolysis of N-tert-Butoxy-2-pyridone. Are tert-Buroxy or Methyl Radicals Responsible for the Photooxidative Damage in Aqueous Media. *Organic Letters* **2001,** 4, (2), 225-228.

40. Dear, J. P.; Mason, N. S., The Effects of Chlorine Depletion of Antioxidants in Polyethylene. *Polymers and Polymer Composites* **2001,** 9, (1), 1-13.

41. Hassinen, J.; Lundback, M.; Ifwarson, M.; Gedde, U. W., Deterioration of polyethylene pipes exposed to chlorinated water. *Polymer Degradation and Stability* **2004,** 84, 261-267.

42. Canevarolo, S. V.; Chinelatto, M. A.; Pinheiro, L. A., Evaluation of Phillips and Ziegler-Natta high-density polyethylene degradation during processing in an internal mixer using the chain scission and branching distribution function analysis. *Polymer Degradation and Stability* **2006,** 91, 2324-2332.

43. Colin, X.; Audoin, L.; Verdu, J.; Rozental-Evesque, M.; Rabaud, B.; Martin, F.; Bourgine, F., Aging of Polyethylene Pipes Transporting Drinking Water Disinfected by Chlorine Dioxide. Part II- Lifetime Prediction. *Polymer Engineering and Science* **2009,** 49, 1642-1652.

44. Gill, T. S.; Knapp, R. J.; Bradley, S. W.; Bradley, W. L., Long term durability of crosslinked polyethylene tubing used in chlorinated hot water systems. *Plastics, Rubber and Composites* **1999,** 28, (6), 309-313.

45. Utsumi, H.; Hakoda, M.; Shimbara, S.; Nagaoka, H.; Chung, Y.; Hamada, A., Active Oxygen Species Generated During Chlorination and Ozonation. *Water Science and Technology* **1995,** 30, (9), 91-99.

46. Karlsson, K.; Eriksson, P.; Hedenqvist, M.; Ifwarson, M.; Smith, G.; Gedde, U. W., Molecular structure, morphology and antioxidant consumption in poly-butene-1 pipes in hot water applications. *Polymer Engineering and Science* **1993,** 33, (5), 303-310.

47. Smith, G.; Karlsson, K.; Gedde, U. W., Modeling of anti-oxidant loss from polyolefins in hot water applications. I: model and application of medium-density polyenthylene pipes. *Polymer Engineering and Science* **1992,** 32, (10), 658-667.

48. Viebke, J.; Gedde, U. W., Anti-oxidant diffussion in polyethylene hot water pipes. *Polymer Engineering and Science* **1997,** 37, (5), 896-911.

49. Viebke, J.; Hedenqvist, M.; Gedde, U. W., Anti-oxidant efficiency and loss by precipitation and diffussion to surrounding media in polyethylene hot-water pipes. *Polymer Engineering and Science* **1996,** 36, (24), 2894-2904.

50. Kriston, I.; Foldes, E.; Staniek, P.; Pukanszky, B., Dominating reactions in the degradation of HDPE during long term aging in water. *Polymer Degradation and Stability* **2008,** 93, 1715-1722.

51. Thomas, J. K., Pulse radiolysis of aqueous solutions of methyl iodide and methyl bromide. The reactions of iodine atoms and methyl radicals in water. *The J. Phys. Chem.* **1967,** 71, (6), 1919-1925.

Chapter 2 How Hydroxyl Radical Reactivity is Modulated by Solvent

Contributions

This chapter represents a modified version and expansion of a published article centering on hydroxyl radical reactivity in a non-aqueous solution.[1] Contributions from co-authors of the article are described as follows: Dr. Susan Mitroka, author of this dissertation, performed the great majority of the experimental work and contributed significantly to the writing and editing of the manuscript. Selected experiments were either performed or repeated by Ms. Stephanie Zimmeck. Preparation for publication and selected calculations were done by Dr. James Tanko, chair of the thesis committee and principal author of the manuscript. Finally Dr. Diego Troya (a member of the thesis committee) performed a large basis of calculations as described in the text, and provided significant intellectual contributions for this work.

1. Mitroka, S.; Zimmeck, S.; Troya, D.; Tanko, J. M. How Solvent Modulates Hydroxyl Radical Reactivity in Hydrogen Atom Abstractions. *J. Am. Chem. Soc.* **2010,** 132, (9), 2907-2913.

Abstract: The hydroxyl radical (HO•) is a highly reactive oxygen-centered radical whose bimolecular rate constants for reaction with organic compounds (hydrogen atom abstraction) approach the diffusion-controlled limit in aqueous solution. The results reported herein show that hydroxyl radical is considerably *less reactive* in dipolar, aprotic solvents such as acetonitrile. This diminished reactivity is explained on the basis of a polarized transition state for hydrogen abstraction, in which the oxygen of the hydroxyl radical becomes highly negative, and can serve as a hydrogen bond acceptor. Because acetonitrile cannot participate as a hydrogen bond donor, the transition state cannot be stabilized by hydrogen bonding, and the reaction rate is lower—the opposite is true when water is the solvent. This hypothesis explains hydroxyl radical reactivity both in solution and in the gas phase, and may be the basis for a "containment strategy" used by nature when hydroxyl radical is produced endogenously.

2.1 Introduction

The hydroxyl radical (HO•) is recognized as the most reactive of the so-called reactive oxygen species (ROS). In biology, HO• not only plays a role in disease but is also a vital part of the body's natural defense mechanisms. ROS are produced endogenously as a means of destroying foreign antigens or abnormal cells. It is often stated that in biological systems, HO• reacts with the first molecule it encounters.

The hydroxyl radical is also important in atmospheric chemistry because of its ability to oxidize volatile organic pollutants, and has been referred to as the atmosphere's "detergent."[1] Recently, Vohringer-Martinez *et al.* examined the role of water in the gas-phase reaction of the hydroxyl radical with acetaldehyde, reporting that a water concentration of 3% led to an increase in the rate of hydrogen abstraction (abstraction taking place from the aldehydic hydrogen).[2] Their hypothesis that hydrogen bonding to water in the transition state lowered the reaction barrier, raises several intriguing questions: Why is hydrogen bonding to water is more important in the transition state as compared to reactants? Is this stabilization unique to substrates with functional groups that are capable of hydrogen bonding (such as the carbonyl group in acetalaldehyde)? Is this stabilization also important for reactions of hydroxyl radical in solution? In short, how general is this phenomenon, and can we understand it on molecular level?

Solvent polarity can have a huge effect on the kinetics of reactions involving, or forming, charged species in solution. In contrast, reactions of neutral radicals are much less sensitive to solvent polarity effects—mainly because charged species are not involved, and there is not a significant change in dipole moment in the progression from reactants to transition state. Because of this, other, more subtle solvent properties such as viscosity or internal pressure can influence

the rate of certain radical reactions; such solvent effects are much more difficult to detect in polar reactions because they are masked by the overwhelming effect of solvent polarity.[3]

For example, solvent viscosity can affect the rate and product distribution when radical caged-pairs (geminate or diffusive) are involved. Internal pressure can influence rate if there is a difference in the volume of the reactants compared to the transition state ($\Delta V_{act} \neq 0$), and can influence the relative rate of some radical reactions. However, these solvent effects are generally small, with changes in rate or product distribution not much greater than an order of magnitude.[3] Consequently, instances where solvent *dramatically* affects the rate or selectivity of reactions involving neutral radicals are rare, and noteworthy.

The classic example of a significant solvent effect in a radical reaction involves free radical chlorinations of alkanes conducted in benzene solvent. The chain-carrying chlorine atom forms a complex with benzene, lowering its reactivity and increasing its selectivity (by nearly two orders of magnitude) in hydrogen atom abstractions.[3, 4] A more recent example of a significant solvent effect was reported by Ingold and co-workers, who found that rate constants for hydrogen atom abstractions from phenols were reduced in solvents where the phenol was stabilized by hydrogen bonding.[5] In this case, it was the reactivity of the substrate, not the radical, which was diminished as a result of a solute/solvent interaction.

Until recently, pulse radiolysis was one of a few means of generating HO• in solution for the determination of absolute reaction rates. Because this technique, by definition, involves the radiolysis of water, solution phase studies of hydroxyl radical kinetics have largely been conducted in water.[6] As a result, relatively little is known about the reactivity of HO• in other solvents. Recent developments have made it possible to study HO• in a non-aqueous environment through the use of photolabile hydroxyl radical precursors. *N*-hydroxypyridine-2-

thione (PSH), developed by Zard *et al.*,[7] is one such precursor that, when photolyzed at 355 nm, cleanly produces HO•.

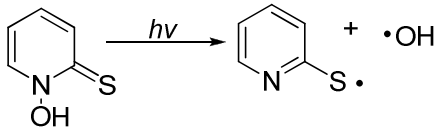

(2-1)

Because the radical by-product (pyrithyl radical) is relatively stable, decaying on a microsecond timescale, this precursor is an ideal candidate for studying the hydroxyl radical kinetics in solution via laser flash photolysis (LFP).[8-10]

Platz, *et al.*[9, 10] developed a method for "visualizing" the hydroxyl radical, which does not have a convenient absorption in the UV-Vis: Hydroxyl radical addition to the ortho and para positions of *trans*-stilbene produces an adduct with an absorption at 392 nm, allowing *trans*-stilbene to act as a viable spectroscopic probe for monitoring HO• kinetics. These workers also noted a solvent effect on HO• reactivity: The rate constant for addition to aromatics (*trans*-stilbene, benzene) was observed to be lower in acetonitrile compared to water. Continued work from this group, using trans-stilbene as a probe, gave similar results for a wide variety of aromatic compounds.[10] Molecular orbital calculations supported the notion that this was due to a polarized transition state, reminiscent of the polar effect introduced by Russell,[11] Walling,[12] and others[13] for hydrogen atom abstraction reactions (*vide infra*). Other studies reporting Hammett parameters for HO• addition reactions to aromatic compounds have given negative ρ+ values, consistent with the buildup of negative charge on the hydroxyl moiety in the transition state.[14, 15] The strong dipole that is formed in the transition state has the ability to be stabilized by the surrounding solvent.

Very little is known about the kinetics of hydrogen abstractions by HO• in non-aqueous solvents. The observations reported herein provide answers to all of the questions posed above

and a comprehensive understanding of HO• reactivity in solution and the gas phase, correcting what we now believe to be some of the misconceptions pertaining to the chemistry of HO• in solution.

2.2 Results

The results of Platz *et al*. were initially verified in order to assess the validity and reproducibility of the proposed methods. The rate constant for the reaction of HO• with trans-stilbene was determined by direct measurement using pseudo-first order kinetics as described in Chapter 1. The rate constant was determined over a 12-fold concentration range of trans-stilbene and found to be congruent with the published results. In addition to the trans-stilbene rate constant, the rate constant for the reaction of the hydroxyl radical with acetonitrile can be estimated from the intercept of the line. The upper limit of rate constant was approximated by Platz to be 1.0×10^6 M^{-1} s^{-1}, indicative of an extremely unreactive solvent.[9]

For trans-stilbene to be a viable probe, a concentration was needed that yielded a sufficient signal in a suitable time frame. The observed rate constant is the sum of all the rates within the system (Chapter 1); Thus a higher concentration of trans-stilbene might produce a better signal, however adding a substrate (and thus increasing the rate) would bring the reaction out of the time scale that can be monitored by laser flash photolysis. The concentration of trans-stilbene that gave optimal results in terms of both signal and rate was determined to be 1.5 mM and was held constant for all reactions.

Platz noted an interesting phenomenon regarding this system: the signal at 392 nm increased at the *microsecond* time scale- a time far too long to be attributable to HO• . Simultaneously, a transient produced at 470 nm, ostensibly due to formation of the pyrithiyl

radical, decreased. Platz attributed the increase in the 392 nm signal to the formation of a pyrithiyl dimer, a theory initially proposed by Aveline et al.[8]:

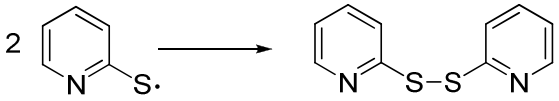

(2-2)

While the production of another species that absorbs at the 392 nm has a great potential to interfere with the kinetics being monitored, the pyrithiyl radical is a rather stable radical- unlikely to react anywhere near as rapidly as the hydroxyl radical. However to confirm that the kinetics of the pyrithiyl radical produced do not interfere with HO• kinetics, an authentic sample of the commercially available disulfide dimer, 2,2-dithiodipyridine, was used to determine the apparent rate of decay for the pyrithiyl radical (monitored at 470 nm) as well as the apparent rate of re-formation of the disulfide dimer (392 nm). Again, the results were consistent with the previously reported data, with both the apparent rate of decay and rate of dimer formation being on the microsecond time scale. As expected, the rate of formation of the dimer was identical to the rate of decay for the pyrithiyl radical. Additionally, the rate of pyrithiyl radical decay was measured in the presence of trans-stilbene. The rate of decay was analogous the rate of decay with no trans-stilbene, indicating no observable interaction between trans-stilbene and the pyrithiyl radical on the monitored time scale (Table 2-1).

Table 2-1. k_{app} for pyrithiyl radical (PyrS•) disappearance and 2,2-dithiodipyridine (PyrS—SPyr) formation

	$k_{app} \times 10^{-6}$(no trans-stilbene), s^{-1}	**$k_{app} \times 10^{-6}$ (15 mM trans-stilbene present), s^{-1}**
PyrS• decay (470 nm)	3.73	2.10
PyrS—SPyr formation (392 nm)	2.96	N/A

Rate constants for the reaction of HO• with a variety of substrates in acetonitrile are summarized in Table 2. Compared to *t*-butoxyl radical,[16] rate constants for hydrogen abstraction by hydroxyl radical are generally two to three orders of magnitude greater. The high reactivity of HO• is accompanied by low selectivity. For aliphatic hydrogens, the per-hydrogen reactivity is approximately tertiary (13.9) > secondary (1.4) > primary (1.0), based upon a multiple regression analysis of the results (assuming the global rate constant to be the sum of contributions from each type of hydrogen). For the alcohols, the hydrogen of the hydroxyl group is about 3x more reactive than a primary, aliphatic hydrogen.

Table 2-2 also summarizes rate constants for reactions of HO• in water obtained from the literature. In cases where more than one value was available, these were averaged and reported with 95% confidence limits. For hydrocarbons, the rate constants for hydrogen abstraction by HO• are nearly two orders of magnitude *lower* in acetonitrile than in water solvent. When the substrate possesses an electronegative substituent (halogen, carbonyl, *etc*.), this difference diminishes to much less than an order of magnitude. However, the solvent effect is restored—the rate constants in water are again, about two orders of magnitude greater than in acetonitrile, when the substrate bears an electron donating group such as alkoxyl or hydroxyl.

Table 2-2. Rate constants for hydrogen abstraction by HO• from various organic substrates in CH_3CN and H_2O[a]

Substrate	$k_H(CH_3CN) \times 10^{-7}$ ($M^{-1}s^{-1}$)	$k_H(H_2O) \times 10^{-7}$ ($M^{-1}s^{-1}$)	$k_H(H_2O)/k_H(CH_3CN)$
$(CH_3)_3CC(CH_3)_3$	5.83 (± 0.61)	-	
$CH_3(CH_2)_4CH_3$	4.48 (± 0.79)	660[b]	147
$CH_3(CH_2)_5CH_3$	6.24 (± 0.88)	770[b]	123
c-C_6H_{11}-CH_3	4.22 (± 0.28)	710[b]	168
c-C_6H_{12}	6.72 (± 0.99)	610[b]	90
$(CH_3)_2CHCH(CH_3)_2$	12.0 (± 3.90)	-	-
$CH_3(CH_2)_3OH$	4.20 (± 0.98)	420 (± 33.4)[c-f]	100
CH_3CH_2OH	8.28 (± 3.20)	193(± 10.4)[c-e,g-j,l-p,ee]	23
$(CH_3)_2CHOH$	7.19 (± 1.72)	200(± 24.0)[c-d,g,I,q-s]	28
CH_3OH	5.90 (± 0.67)	95(±4.4)[c-g,I,k,m-n]	16
$(CH_3)_3COH$	3.62 (± 0.03)	-	
$(CH_3CH_2)_2O$	4.56 (± 1.00)	355(± 127)[s-t]	78
$CH_3OC(CH_3)_3$	4.35 (± 0.35)	160[t]	37
$CH_3CH_2OC(CH_3)_3$	1.78 (± 0.63)	225(±88)[u-v]	126
C_4H_8O (THF)	3.50 (± 0.65)	410[t]	117
CH_2Cl_2	7.63 (± 0.89)	8.8(±1.8)[w-y]	1.2
$(CH_3)_2CO$	3.21 (± 1.16)	11.3(± 2.7) [d,f,I,s]	3.5
$CHBr_3$	8.41 (± 2.32)	10.5(± 0.97)[w,z]	1
$CHCl_3$	4.85 (± 0.92)	1.74(± 1.4)[w, aa-dd]	0.35
$ClCH_2CO_2H$	5.09 (± 0.96)	4.3[f]	0.85

[a]The rate constants in water were obtained from the Notre Dame Radiation Laboratory database (http://www.rcdc.nd.edu/index.html); these values were verified by consulting the original papers. [b]Reference [17]; [c]Reference [18]; [d]Reference [19]; [e]Reference [20]; [f]Reference [21]; [g]Reference [22]; [h]Reference [23]; [i]Reference [24]; [j]Reference [25]; [k]Reference [26]; [l]Reference [27]; [m]Reference [28]; [n]Reference [29]; [o]Reference [30]; [p]Reference [31]; [q]Reference [32]; [r]Reference [33]; [s]Reference [34]; [t]Reference [35]; [u]Reference [36]; [v]Reference [37]; [w]Reference [38]; [x]Reference [39]; [y]Reference [40]; [z]Reference [41]; [aa]Reference [42]; [bb]Reference [43]; [cc]Reference [44]; [dd]Reference [45]; [ee]Reference [46].

The results in Table 2-3 extend these observations: In going from neat acetonitrile to a 90% acetonitrile/water co-solvent, the rate constants increase by about a factor of two for the hydrocarbons, but remain virtually unchanged for substrates with electronegative substituents. (Higher proportions of water could not be used because of solubility problems).

Table 2-3. Rate constants for hydrogen abstraction by HO• from various organic substrates in 90% CH_3CN:H_2O and 100% CH_3CN

Substrate	**k_H (CH_3CN/H_2O) x 10^{-7} ($M^{-1}s^{-1}$)**	**k_H(CH_3CN) x 10^{-7} ($M^{-1}s^{-1}$)**	**k_H (CH_3CN/H_2O)/ k_H(CH_3CN)**
$CH_3(CH)_4CH_3$	11.3 (± 1.04)	4.48 (± 0.79)	2.5
c-C_6H_{10}	15.2 (± 0.68)	6.72 (± 0.99)	2.3
$(CH_3)_2CHCH(CH_3)_2$	16.8 (± 0.81)	12.0 (± 3.90)	1.4
CH_3CH_2OH	11.1 (± 0.80)	8.28 (± 3.20)	1.3
$CHBr_3$	8.33 (± 0.84)	8.41 (± 2.32)	1.0
$CHCl_3$	4.26 (± 1.06)	4.85 (± 0.92)	0.9

Preparative-scale experiments were performed in acetonitrile, using cyclohexane and 2,3-dimethylbutane as substrates. The photo-initiated (350 nm) reaction of PSH with alkanes yields

the corresponding sulfides in good yield, presumably via the chain mechanism depicted in Scheme 2-1.[7]

Scheme 2-1: Chain reaction of PSH

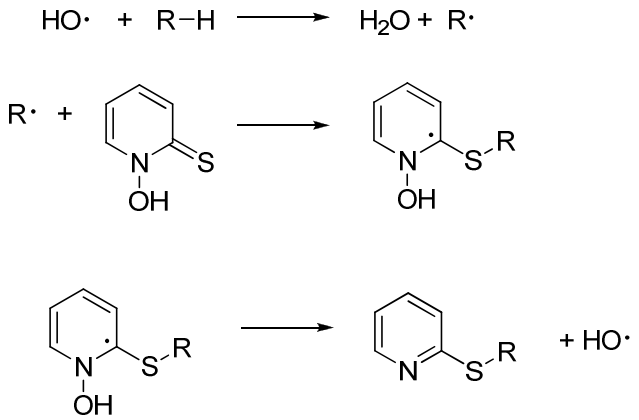

To ascertain relative reactivities of primary, secondary and tertiary hydrogens, competition experiments were conducted using 2,3-dimethylbutane as the source for primary and tertiary hydrogens, and cyclohexane as the source for secondary hydrogens. Rather than being present in mM concentrations as with the laser flash experiments, the hydrocarbon substrates were used in equimolar amounts as co-solvents. The derived relative reactivities in acetonitrile, 3^o (15.2) > 2^o (3.9) > 1^o (1.0) compare favorably to the values estimated. The resulting products from the reaction of PSH with these alkanes included the corresponding sulfides (Figure 2-1: 1 – 3) , as well as the pyrithiyl dimer (Figure 2-1: 4). Percent yields were determined to be 81.5% and 83.5% for cyclohexane and dimethylbutane, respectively.

Figure 2-1. Isolated products from the reaction of PSH and cyclohexane or 2,3-dimethylbutane

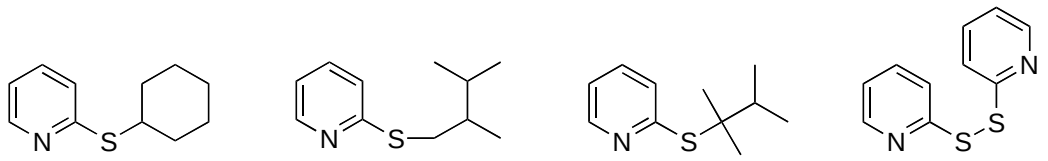

1 **2** **3** **4**

Laser flash experiments were repeated using a solvent devoid of abstractable hydrogens, specifically Freon 113 (1,1,2-trichlorotrifluoroethane). In this solvent, the rate constants for hydrogen abstraction from cyclohexane and methanol were 7.3 (±0.5) x 10^7 and 9.2 (±1.1) x 10^7 $M^{-1}s^{-1}$, respectively, nearly identical to those measured in acetonitrile. Competition experiments were also run in Freon-113, yielding relative reactivities of 3^o (18.9) > 2^o (1.9) > 1^o (1.0). Again, these results are consistent with what was attained using acetonitrile as a solvent.

2.3 Discussion

2.3.1 Identity of the Hydroxyl Radical

In the aqueous phase, the hydroxyl radical reacts almost instantaneously with a substrate, showing little to no selectivity. While such drastic differences in rate constants can and will be explained in the context of a solvent effect, it is important that we establish that we are considering the hydroxyl radical in these reactions and not a byproduct, namely either PyrS• or the resulting radical from solvent hydrogen atom abstraction, NCH_2C•. To provide new evidence that eliminates NCH_2C• or PyrS• from consideration as a hydrogen atom abstractors

under these conditions, extensive experiments and research were conducted to- as much as possible- eliminate these species as a possible contenders for hydrogen atom abstraction.

Several arguments based on both experimental and theoretical evidence can be made as to why the hydroxyl radical must be responsible for this reactivity:

2.3.1.1 The transient generated via photolysis of PSH reacts <u>both</u> with the *trans*-stilbene (probe) and added substrates (RH).

Let X• represent the radical produced from PSH. If X• reacts with both t-SB and RH (Scheme 2), two phenomena should be observed as this is a parallel (pseudo) first order reaction: a) The observed rate constant (k_{obs}) should increase with increasing [RH] (constant [t-SB]), and b) the intensity of the absorption arising from X•/t-SB should decrease with increasing [RH] (because less of it is formed when RH is present). This is illustrated in Scheme 2-2.

Scheme 2-2: Parallel (pseudo) first order kinetics of X•

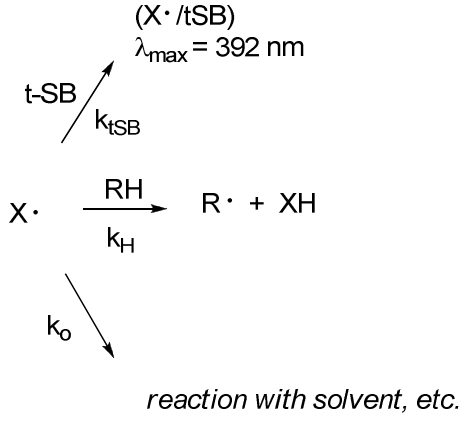

$$k_{obs} = k_o + k_{tSB}[tSB] + k_H[RH]$$

The results for RH = 2,3-dimethylbutane (23DMB) are shown below in Figure 2-2. The value of k_{obs} increases with increasing [23DMB]; the slope of this line yields $k_H = 1.2 \times 10^8$ M

Figure 2-2. Plot of k_{obs} (x) and signal intensity (□) *vs*. [2,3-dimethylbutane]

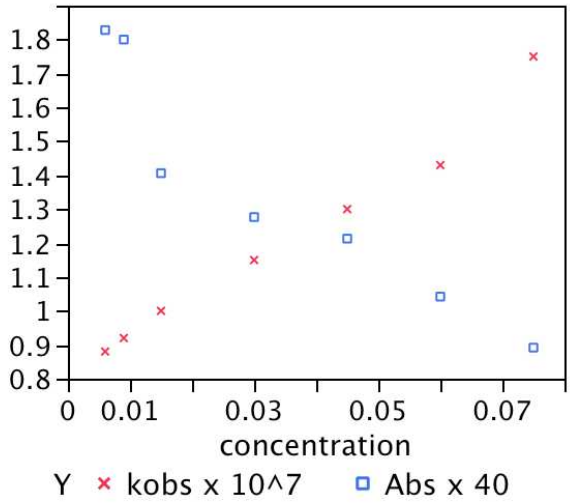

In addition, the intensity of the absorption at 392 nm decreases with increasing [23DMB]—as expected. This data can also be used (crudely) to estimate k_H because

$$\frac{1}{I} = \frac{1}{I_o}\frac{k_H}{k_{SB}[t-SB]}[RH] + \frac{1}{I_o} \qquad \textbf{(2-3)}$$

where I and I_o is the intensity of the 392 nm absorption in the presence and absence of RH ([t-SB] held constant). From the slope and intercept of the I^{-1} *vs*. [RH] plot ($k_{SB} = 6.1 \times 10^9$ $M^{-1}s^{-1}$, courtesy of Platz; [t-SB] = 0.0015 M), the derived value of k_H is 1.3×10^8 $M^{-1}s^{-1}$, in nearly perfect agreement with the value obtained from the variation of k_{obs}.

(Note: Though the data for 23DMB is presented, the observations are similar for every substrate

examined: k_{obs} *vs*. concentration plots are linear; signal intensity decreases as substrate is added.)

2.3.1.2 X• cannot be NCH_2C• or PyrS•

a) The same transient is formed (at nearly the same rate) when the solvent is changed to CCl_4 (originally reported by Platz, confirmed by us) effectively ruling out NCH_2C•. Moreover, it is highly unlikely that the rate constant for reaction of NCH_2C• with t-SB would be 6 x 10^9 $M^{-1}s^{-1}$ (The rate constant assigned by Platz for addition of HO• to t-SB).

However, to unambiguously demonstrate that NCH_2C• was neither responsible for the transient signal, nor the active hydrogen atom abstractor when substrates were added, the rate constants for cyclohexane and methanol were also measured in Freon 113 (1,1,2-trichlorotrifluoroethane). As observed for CH_3CN solvent, k_{obs} increased with increasing substrate concentration, allowing the rate constant for hydrogen abstraction to be determined from the slope of k_{obs} *vs*. [substrate].

Table 2-4. Rate constant for hydrogen abstraction by HO• in CH_3CN and Freon-113

	$k \times 10^{-7}$(CH_3CN), $M^{-1}s^{-1}$	**$k \times 10^{-7}$(Freon-113), $M^{-1}s^{-1}$**
c-C_6H_{12}	6.72 (± 0.99)	7.3 (±0.5)
CH_3OH	5.90 (± 0.67)	9.2 (±1.1)

The rate constants obtained in CH_3CN and Freon 113 were nearly identical, consistent with HO• as the (common) hydrogen abstractor. Accordingly, X• cannot be NCH_2C•.

b) The reaction between NCH_2C• and RH is expected to be too slow to be observed on the nanosecond time scale, The C-H bond strength in the product (acetonitrile) is 85 kcal/mol, while for a hydrocarbon it is 96 - 100 kcal/mol (depending on whether the hydrogen is primary, secondary or tertiary). The energy of activation must be greater than or equal to the difference in

bond strengths (≥ 11 kcal/mol), and allowing a generous pre-exponential factor of 10^{10} $M^{-1}s^{-1}$ for a bimolecular reaction in solution means that the rate constant for this hypothetical process would be less than 100 $M^{-1}s^{-1}$ (best case scenario). At the concentrations used in this study, this process would occur in the millisecond (or longer) time regime. The aforementioned reactions occur on the nanosecond time scale. (Moreover, because this process is so unfavorable, one would expect $NCH_2C•$ high selectivity in H-atom abstractions. The timescale & low-selectivity suggest a much more reactive species, namely HO•)

To further substantiate the difference in reactivity between HO• and $NCH_2C•$ with common alkanes and quantify the activation energies mentioned above, barriers for hydrogen abstraction from methane by these two radicals were calculated by Diego Troya using high-level quantum-mechanical methods. Highly-accurate CCSD(T)/aug-cc-pVDZ calculations indicate that while the barrier for the $HO•+CH_4$ $H_2O+H_3C•$ reaction is relatively low (5.04 kcal/mol, Table 3), the barrier for the $NCH_2C•+CH_4$ $CH_3CN+ H_3C•$ reaction is much higher (18.58 kcal/mol). The large difference in the barriers leads to a difference in the rates for hydrogen abstraction for HO• and $NCH_2C•$ of almost 10 orders of magnitude at room temperature. Therefore, we strongly believe that virtually none of the reactive events observed are due to hydrogen abstraction by the $NCH_2C•$ radical.further showing that X• cannot be $NCH_2C•$.

c) PyrS•, generated by 355 nm irradiation of the corresponding disulfide, absorbs at 470 nm. The buildup of the 392 nm transient (X•/t-SB adduct) occurs *much more rapidly* than the decay of the 470 nm transient (PyrS•). The reaction is dimerization, not addition to t-SB, as reported by Platz[9] and earlier by Aveline.[8] We also confirm this result and interpretation examining the disulfide kinetics alone and in the presence of trans-stilbene.

Clearly, PyrS• does not react with t-SB in the time frame of these experiments, but

rather, undergoes dimerization. Not only does PyrS• not act as a hydrogen atom abstractor, the reverse reaction is preferred as thiols (RSH) are good hydrogen atom donors to alkyl radicals. (There are reports that RS• can abstract hydrogen from reactive substrates, *e.g.*, the a-C-H bond of peptides;[47] However, the rate constants are much lower than anything reported herein). X• cannot be PyrS•.

d) Though addition of NCH_2C• or PyrS• to t-SB can in principle occur, most likely addition occurs to the C=C as opposed to the aromatic ring. The resulting benzyl radical will have λ_{max} = 315 nm, not 392 nm. The only way to explain a 392 nm absorption is the addition of a highly reactive (presumably HO•) to the aromatic ring (generating a highly conjugated radical), as was discussed in depth by Platz in his *JACS* paper (Figure 2-3).

Figure 2-3. Absorptions from radical additions

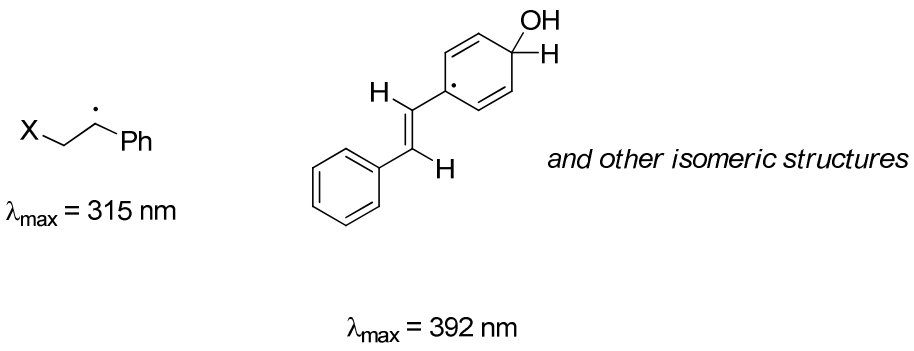

e) Experiments performed on a preparative scale, under conditions of substantially higher substrate concentrations indicate an extremely reactive, unselective species. The observed selectivities ($3^o > 2^o > 1^o$) for H-abstraction from alkanes are very low (suggestive of a highly reactive oxygen-centered radical) and completely consistent with the values derived from the

LFP studies:

Preparative scale (acetonitrile): 3^o (15) > 2^o (4) > 1^o (1.0)

LFP: 3^o (14) > 2^o (1.4) > 1^o (1.0)

This selectivity data suggests that the same intermediate is involved in both the preparative scale and LFP experiments, namely HO•. When PSH is photolyzed in CH_3CN without added hydrocarbon, no products are detected that can be attributed to any reaction of NCH_2C•. (Presumably this species either dimerizes or disproportionates). Again, the only detected product is the disulfide, arising from decomposition of PSH.

Unfortunately, these experiments and arguments do not *prove* that the observed chemistry is attributable to hydroxyl radical. Rather, they only eliminate other reasonable alternative explanations. In addition to the aforementioned *trans*-stilbene adducts with PyrS• and NCH_2C•, Platz and coworkers also considered, and eliminated, triplet stilbene and stilbene radical cation as species giving rise to the 392 nm transient.

Computational studies provided no evidence for HO•/CH_3CN complexes to explain the diminished reactivity of hydroxyl radical in acetonitrile—our results in Freon 113 add additional support this conclusion. Based upon the laser flash results and the accompanying product studies, hydroxyl radical emerges as the most likely explanation for the observed chemistry.

2.3.2 Discussion of Polarized Transition State

Walling,[12] Russell,[4] and others[13] have argued for the importance of a polar transition state for hydrogen atom abstraction reactions. These results can be explained by taking their ideas one step further (Figure 2-4): Because oxygen is more electronegative than carbon and hydrogen, in the transition state for hydrogen abstraction, electron density is pulled towards the oxygen of the

hydroxyl radical giving it a partial negative charge, and a partial positive charge on the RH portion of the transition state. This development of negative charge on the oxygen of the hydroxyl radical affords the opportunity for the solvent (H_2O) to stabilize the transition state through its polarity and/or ability to participate in hydrogen bonding. Table 2-3 shows that for hydrocarbons, even 10% addition of water has a significant effect on the rate because the transition state is so highly polarized. In contrast, when the substrate possesses electronegative substituents (*e.g.*, halogen, carbonyl), the transition state is less polarized because the substituent competes for electron density; there is less transfer of negative charge to the oxygen of the hydroxyl radical—hydrogen bonding interactions are expected to be weaker, thus explaining why there is little to no rate enhancement in going from acetonitrile to water for these substrates. It should be noted that the hydrogen on the hydroxyl radical (not involved in the reaction) bears substantial positive charge in the reactant, transition state, and product. Although this hydrogen can also participate in hydrogen bonding, this interaction does not affect the relative energies because the charge on this hydrogen remains constant in the progression from reactant to transition state to product.

Figure 2-4. Formation of a polarized transition state for hydrogen atom abstraction from a hydrocarbon by hydroxyl radical.

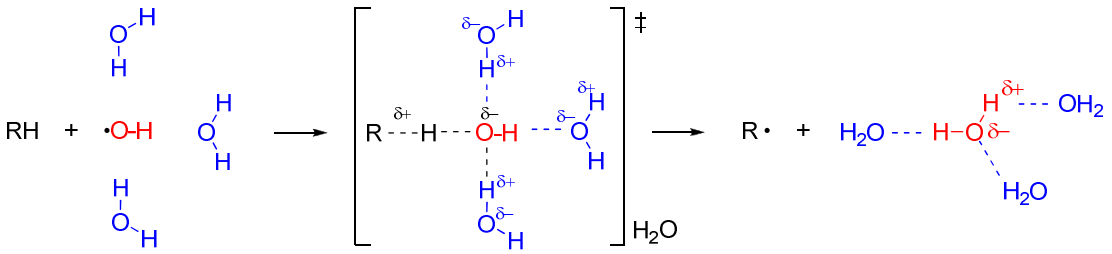

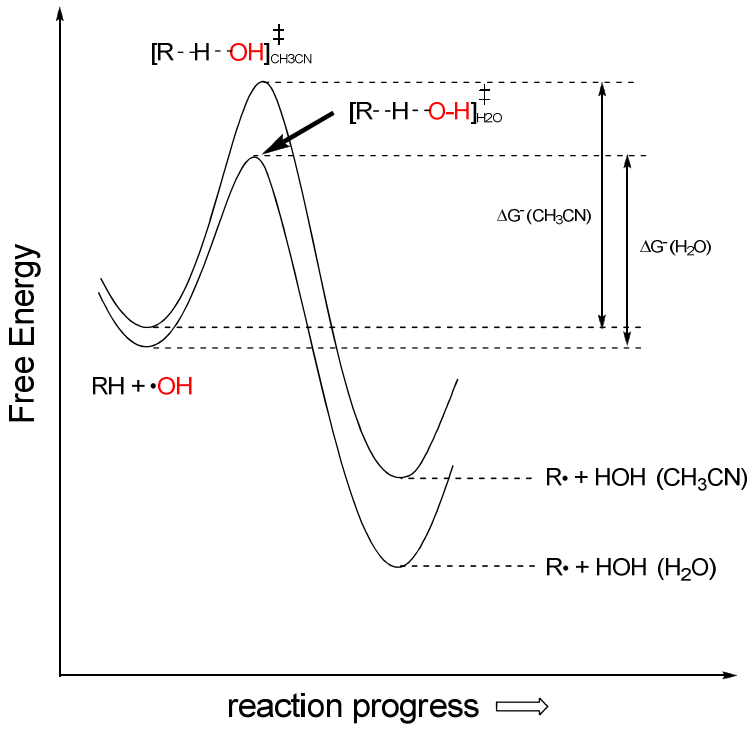

For alcohols and ethers, where H-abstraction also occurs at the α-carbon, we hypothesize that the electron-withdrawing properties of oxygen in the substrate (manifested through an

inductive effect), are offset by the resonance stabilization afforded by the lone pair of electrons (Scheme 2-3). This resonance effect would thus allow the oxygen of the hydroxyl radical to become highly negative so that hydrogen bonding interactions would again become important. Presumably the effect of oxygen diminishes with distance so that the β-hydrogens (and beyond) are aliphatic in nature, and the solvent effect on their reactivity is similar to the alkanes.

Scheme 2-3: Electron donation from oxygen in alcohols

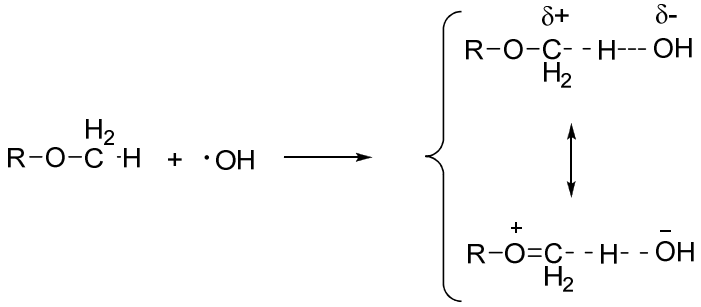

In order to test these hypotheses, and assess how atomic charges on individual atoms vary in the progression from reactants transition state product, molecular orbital calculations were performed by James Tanko on the pertinent species for the reactions a) CH_4 + HO• CH_3• + H_2O, and b) Cl_3CH + HO• Cl_3C• + H_2O, and c) $HOCH_3$ + HO• $HOCH_2$• + H_2O at various levels of theory.[48] In Figure 2-5, the charges obtained from a natural population analysis at the MP2(full)/aug-cc-pVQZ//UHF/6-311G* levels are reported. It should be noted that every level of theory (AM1, B3LYP/6-311G*, UHF/6-311G*) employed gave virtually the same qualitative results. As the reactants approach the transition state, the hydrogen being transferred becomes substantially more positive, and the oxygen, more negative, consistent with the notion of a polarized transition state. However, the *degree* of polarization is far greater for CH_4 and CH_3OH compared to $CHCl_3$, as expected based upon the preceding discussion. The

negative charge on the oxygen of hydroxyl radical in the transition state means that this oxygen can be a hydrogen bond acceptor.

Figure 2-5. Atomic charges for the reaction of hydroxyl radical with CH_4, CH_3OH and $CHCl_3$ obtained from natural population analysis of the reactants, transition states, and products at the MP2(full)/aug-cc-pVQZ//UHF/6-311G* levels

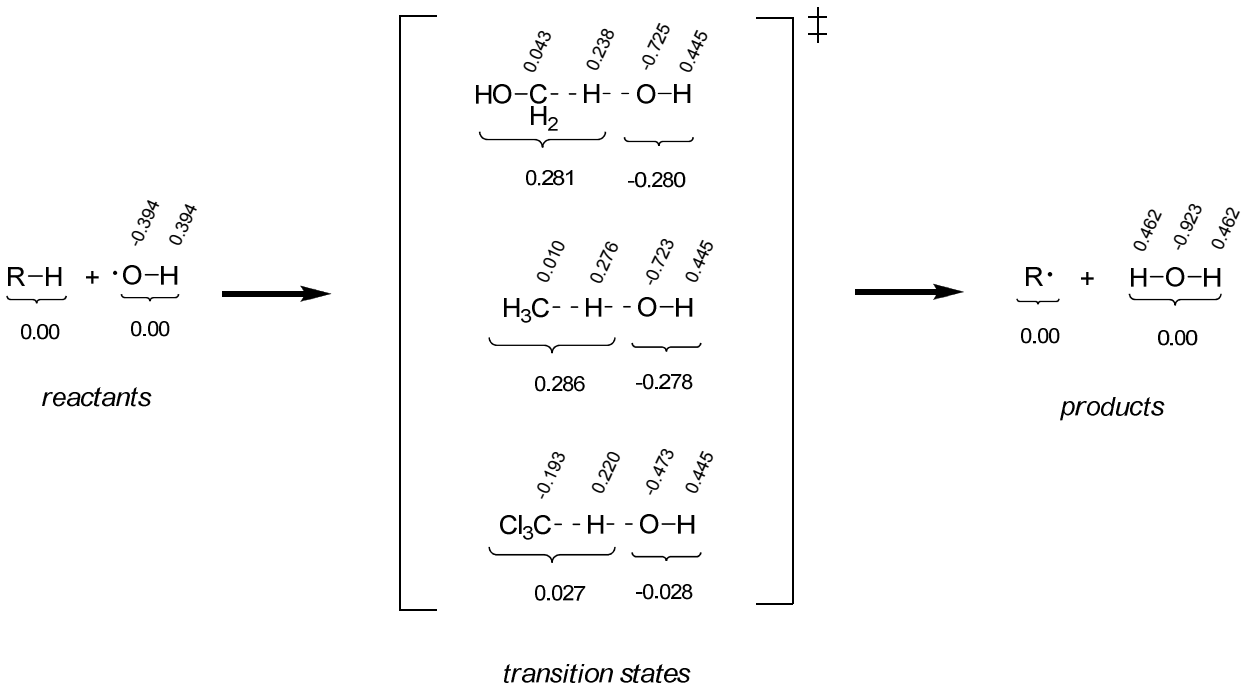

As noted, there are in principle, two contributors to the observed solvent effect. In addition to hydrogen bonding, it is also possible that solvent polarity plays a role in stabilizing the transition state (relative to the reactants). However, the following analysis strongly suggests that hydrogen bonding interactions in the transition state, rather than a simple solvent polarity effect, is the etiology of the effect.

The free energy of solvation of a polar molecule in a polar solvent can be estimated by the Kirkwood equation, and applied to the reaction between two polar molecules A + B transition state (ts) via activated complex theory.[49] The magnitude of the solvent effect depends on the dipole moment (μ) and radius (r) of the transition state relative to reactants, and the dielectric constant (ε) of the solvent as expressed in Eq. 2-2, where $\ln(k_o)$ refers to the rate constant in a solvent of dielectric constant of unity; ε_o is the permittivity of vacuum, and N, π, R and T have their usual meanings.

$$\ln k = \ln k_o + \frac{1}{4\pi\varepsilon_o}\frac{N}{RT}\left(\frac{\mu_{ts}^2}{r_{ts}^3} - \frac{\mu_A^2}{r_A^3} - \frac{\mu_B^2}{r_B^3}\right)\left(\frac{\varepsilon - 1}{2\varepsilon + 1}\right) \qquad \textbf{(2-4)}$$

Using the dipole moments and radii for CH_4, HO•, and $(CH_4/HO•)^{\neq}$ obtained from CCSD(T)/aug-cc-pVDZ calculations based on MP2/aug-cc-pVDZ geometries (*vide infra*), the rate is actually predicted to be slightly *greater* in acetonitrile than water (k_{CH3CN}/k_{H20} = 1.01).[48] This result makes sense because one of the reactants (hydroxyl radical) possesses a significant dipole moment; the transition state has a slightly lower dipole moment, and a larger radius. The increased rate in water thus cannot arise simply because it is a more polar solvent than acetonitrile, but rather because it is able to stabilize the developing negative charge on the hydroxyl radical in the transition state by acting as a hydrogen bond donor. It should also be noted that the results obtained in Freon 113 add further support to this hypothesis because a) the

rate constants are the same as in acetonitrile, and b) Freon 113 has a substantially lower dielectric constant than acetonitrile.

To further assess the contribution of dipolar interactions to the observed rate enhancement in water, electronic-structure calculations of the $HO\bullet + CH_4 \rightarrow H_2O + CH_3\bullet$ reaction barrier were performed by Diego Troya using implicit solvation models. CCSD(T)/aug-cc-pVDZ calculations with the polarized continuum model (PCM) using geometries and frequencies calculated at the MP2/aug-cc-pVDZ level indicate that the reaction in water should be *slower* than in acetonitrile or the gas phase.[48] In effect, the barrier for the PCM calculations using water as a solvent in the PCM model (6.76 kcal/mol) is larger than the barrier when using acetonitrile as a solvent (5.86 kcal/mol). Both barriers are larger than the gas-phase barrier at that level (5.03 kcal/mol). These predictions (based upon the PCM model, which does not account for explicit hydrogen bonding) are in stark contrast with the experimental results in water solvent. This "disparity" is easily reconciled if the transition state for hydrogen atom abstraction is stabilized by hydrogen bonding in water solvent.

As a final confirmation of this interpretation, the effect of solvent water molecules on the minimum-energy reaction path of the $HO\bullet + CH_4 \rightarrow H_2O + CH_3\bullet$ reaction was calculated.[48] Geometry optimizations and frequency calculations were conducted at the MP2/aug-cc-pVDZ level, and energies were refined at the CCSD(T)/aug-cc-pVDZ level. Qualitatively, when water molecules were added to the calculations for the $HO\bullet/CH_4$ reaction, the resulting transition state clearly shows that the water molecules properly align so as to stabilize the developing charges as hypothesized. Quantitatively, the magnitude of the stabilization is consistent with the magnitude of the observed kinetic solvent effect.

Table 2-5 shows the calculated barriers and calculated relative rate constants for HO• + CH_4 H_2O + CH_3• with various water molecules hydrogen bonding to different sites of the HO•/CH_4 system either as donors or acceptors. One water molecule acting as hydrogen-bond donor to the OH radical reduces the barrier by 1.52 kcal mol^{-1}. On the other hand, if the solvating water molecule acts as hydrogen-bond acceptor, the barrier increases by 0.32 kcal mol^{-1}. If one water molecule acts as hydrogen-bond donor and another one as hydrogen-bond acceptor, the barrier decreases by 1.14 kcal mol^{-1}. This decrease is almost a perfect balance between the 1.52 kcal mol^{-1} decrease and 0.32 kcal mol^{-1} increase in the barriers of the transition states with only one molecule acting as donor or acceptor, respectively, suggesting that the effect of individual water molecules might be additive. Attempts to study the reaction in which two water molecules act as hydrogen-bond donors failed to locate the appropriate reagents conformation. In effect, even though a transition state in which two water molecules are acting as hydrogen-bond donors was located, optimizations of the OH radical with two water molecules acting as hydrogen-bond donors always led to the isomer in which one water molecule acts as hydrogen-bond donor and the other is an acceptor.

Table 2-5. Barriers of the HO• + CH_4 H_2O + CH_3• reaction with various levels of solvation[a]

	# of waters	# of HB acceptors	# of HB donors	Barrier (kcal/mol)	k_{rel}
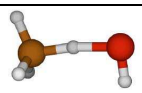	0	0	0	5.04	1.0
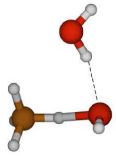	1	0	1	3.48	13.9
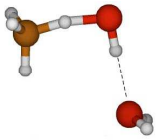	1	1	0	5.25	0.7
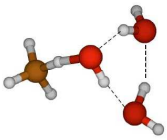	2	1	1	3.90	6.8
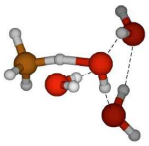	3	1	2	2.37	90.2

[a]Energies calculated at the CCSD(T)/aug-cc-pVDZ level using geometries and harmonic frequencies obtained at the MP2/aug-cc-pVDZ level. The barriers correspond to enthalpies of activation at 0 K.

Finally, the barrier of the HO• + CH_4 H_2O + CH_3• reaction with two water molecules acting as hydrogen bond donors, and one water molecule acting as hydrogen bond acceptor was calculated.[48] The decrease in the barrier for this solvation level with respect to the unsolvated system is 2.37 kcal/mol^{-1}, with a relative rate enhancement consistent with experimental results. Various attempts to include additional water molecules that are in direct contact with the OH radical at the transition state led to solvation of any of the three water molecules forming the first solvation sphere, as expected.

2.4 Conclusions

The hypothesis that the hydroxyl radical reacts through a polar transition state is fully supported by the experimental and theoretical data obtained in this study. As a consequence of this polarization, hydrogen bonding to water stabilizes the transition state resulting in larger rate constants when water is the solvent. This explanation also predicts that the *magnitude* of the solvent effect will decrease when electronegative substituents are present on the α-carbon of the substrate. The solvent effect is also significant when the substrate possesses electron-donating substituents, presumably because of competing inductive (electron withdrawing) and resonance (electron donating) effects.

These results extend the observations of Platz, and coworkers,[9, 10] who argued for a highly polarized transition state for the addition of HO• to aromatic substrates to explain a nearly two order of magnitude diminution in rate in acetonitrile compared to water. For these additions, calculations suggested that the hydroxyl moiety was nearly anionic in the transition state, providing a clear opportunity for water stabilization via hydrogen bonding. The effect water has on modulating HO• reactivity has enormous implications. In biological systems, this means that HO• may be less reactive in the hydrophobic regions of a cell than previously believed, *i.e.*, hydroxyl radical does not necessarily react with the first molecule it encounters. Indeed, Nature may use this as a containment strategy when hydroxyl radical is produced naturally within cells.

Based upon rate measurements in water, reactions of HO• were generally thought to be diffusion-controlled. Consequently, it has been assumed that attempts to protect against the damaging effects of HO• through the use of antioxidants are doomed to failure because a successful defense strategy requires a degree of selectivity to be demonstrated by the reactive radical. The radical must react preferentially with antioxidant, rather than the molecule or

materials which one is trying to protect, in order for any defense system to be effective. Our results demonstrate that such selectivity might be attainable in a hydrophobic environment.

Finally, it should be stressed that the ideas presented herein provide a molecular-level understanding of hydroxyl radical reactivity both in solution and the gas phase.

2.5 Experimental

2.5.1 Materials. All of the solvents and fine chemicals used in this study were obtained from Sigma-Aldrich. Liquid substrates were distilled and *N*-hydroxypyridine-2-thione was recrystallized prior to use.

2.5.2 Apparatus. Steady-state UV-vis spectra were recorded on a Hewlett-Packard diode array UV-vis spectrophotometer (HP 8452A). Laser flash photolysis experiments were conducted using an Applied Photophysic LKS.60 spectrometer using the third harmonic of a Continuum Surelite I-10 Nd:YAG laser (4-6 ns pulse, 355 nm). Transient signals were monitored by a Hewlett-Packard Infinium digital oscilloscope and analyzed with the Applied Photophysics SpectraKinetic Workstation software package (v. 4.59).

2.5.3 Laser Flash Photolysis (LFP). Substrates were prepared in acetonitrile, carbon tetrachloride, Freon-113 or an acetonitrile:water co-solvent, and deoxygenated prior to photolysis. (Steady-state UV-vis spectra were recorded to verify that *N*-hydroxypyridine-2-thione was the only species absorbing at the excitation wavelength). In all LFP experiments, a fixed concentration of *trans*-stilbene (0.0015M) was utilized as a spectroscopic probe, monitoring the signal buildup at 392 nm. Low laser power (*ca*. 10 – 20 mJ) was used in all experiments to eliminate any laser power dependency to the observed rate constants thereby, minimizing the contributions of radical-radical reactions to the observed rate constant. Substrate concentrations were varied over a factor of at least 10 over five to seven separate experiments.

Rate constants were averaged and determined with 95% confidence limits. R-squared values were ≥0.90 for all concentration profiles. A sample transient and concentration gradient is demonstrated in Figure 2-6.

Figure 2-6. Hydrogen abstraction from tetramethylbutane by HO•

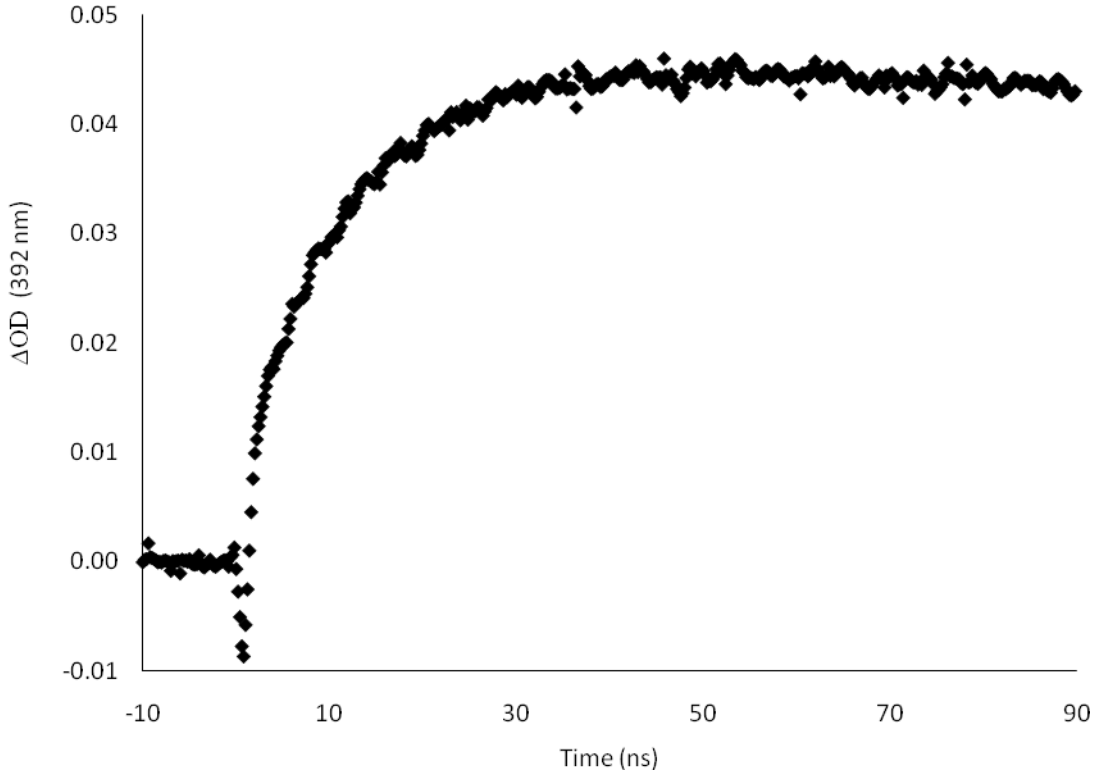

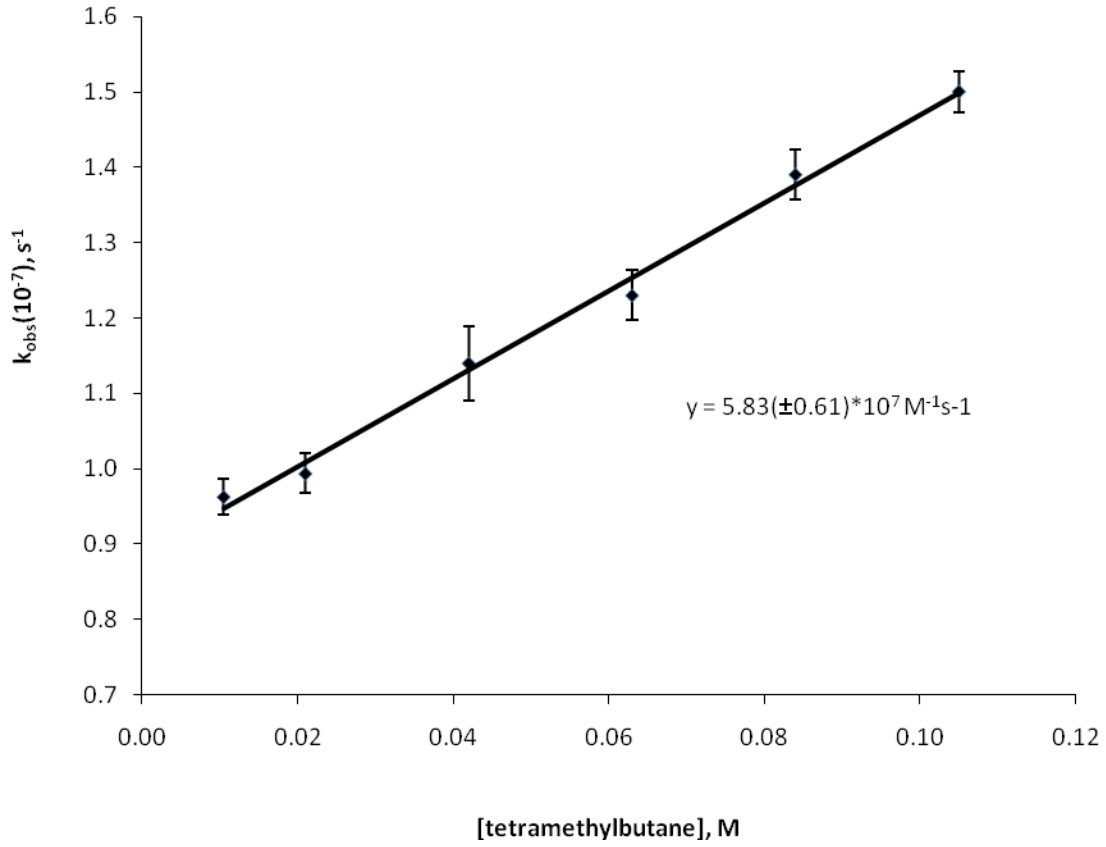

[tetramethylbutane], M	$k_{obs}(10^{-7})$, s^{-1}	Standard Deviation(10^{-7})
0.011	0.96	0.024
0.021	0.99	0.027
0.042	1.14	0.049
0.063	1.23	0.033
0.084	1.39	0.033
0.105	1.50	0.028

2.5.4 Calculations. Electronic structure calculations were performed using either the Spartan 04[50] molecular modeling software or Gaussian 03.[50]

2.5.5 Competition Experiments. Products used in competition experiments were synthesized, isolated and characterized using NMR, IR, GC/MS and High Resolution GC/MS (HRMS). Equal

molar amounts (153 mM) of 2,3 dimethylbutane and cyclohexane were irradiated at 350 nM with 4.7 mM *N*-hydroxypyridinethione in acetonitrile for 30 minutes.

2.5.5.1 Product Isolation/Characterization. To isolate products from the reaction mixtures, column chromatography was performed using Sigma-Aldrich neutral aluminum oxide, Brockmann I, standard grade (~150 mesh, 58 angstrom). TLC analyses were performed on commercial aluminum sheets. All chemicals were purchased from Aldrich without further purification unless otherwise noted.

Infrared Spectroscopy was conducted using a Perkin Elmer Spectrum One Fourier Transform Infrared spectrometer (Waltham, MA) in Attenuated Transform Reflectance (ATR) mode with a ZnSe crystal at 4 cm^{-1} resolution. Background was determined using 50 scans from 4000 to 600 cm^{-1}, and 25 scans were conducted for each sample also over this range. ^{1}HNMR spectra were taken on a Varian Inova 400 MHz spectrometer. All chemical shifts were given in δ value with tetramethylsilane as an internal standard. Gas chromatographic/mass spectral analyses were obtained on a HP MSD low-resolution GCMS. High resolution mass spectra were obtained on an Agilent LC-ESI-TOF under FAB conditions. Gas chromatographic analyses were performed on a Hewlett-Packard HP 5890 A instrument equipped with an FID detector and an HP 3393A reporting integrator using a 30 m SE-54 capillary column (0.25 mm diameter).

2-(cyclohexylthio)pyridine (**Figure 2-1:1**) was prepared following the general procedure. The compound was isolated using a neutral alumina column with a 1:1 diethyl ether:hexane system. The compound is a yellow liquid and has previously been synthesized an characterized:[51] IR (CH_2Cl_2) 2929/2852, 1450/1413, 1338, 1263, 1115 cm^{-1}; ^{1}H NMR ($CDCl_3$) δ 1.2-1.8 (m, 8H), 2.0-2.2 (m, 2H), 3.7-3.9 (m, 1H), 6.9 (m, 1H), 7.1 (m, 1H), 7.4 (m, 1H), 8.4 (m, 1H) MS, m/e

(relative intensity): 193 (M+, 27.4), 111 (100); Exact Mass (HRMS): 193.093, Exact Mass (calculated): 193.093

2-(2,3-dimethylbutylthio)pyridine (**Figure 2-1:2**) and 2-(2,3-dimethylbutan-2-ylthio)pyridine (**Figure 2-1:3**) were prepared following the general procedure. The compounds were isolated using a neutral alumina column with a 1:3 diethyl ether:hexane system, but could not be separated from each other. (The ratio of isomers was determined by ^{1}HNMR, and confirmed by GC). The compounds are a yellow liquid.

IR (CH_2Cl_2) 2962/2875, 1450/1413, 1377, 1265/1277, 1087 cm^{-1}.; NMR ($CDCl_3$) δ 0.9-1.8 (overlay of several multiplets), 2.10-2.2 (septuplet, 3H), 2.9-3.0 (q, 1H), 3.25-3.35 (q, 1H), 7.1 (m, 1H), 7.4 (m, 4H), 7.7 (m, 4H), 8.3 (m, 4H)

2-(2,3-dimethylbutylthio)pyridine: MS, m/e (relative intensity): 193 (M+, 9.1), 111 (100); Exact Mass (HRMS): 195.1904, Exact Mass (calculated): 195.1082

2-(2,3-dimethylbutan-2-ylthio)pyridine: MS, m/e (relative intensity): 195 (M+, 0.6), 111 (100), Exact Mass (HRMS): 195.1904, Exact Mass (calculated): 195.1082

Acknowledgements. This work was supported by the National Science Foundation (CHE-0548129, CHE-0547543) and in part by the Macromolecular Interfaces with Life Sciences (MILES) Integrative Graduate Education and Research Traineeship (IGERT) of the National Science Foundation under Agreement No. DGE-0333378 in the form of fellowships to S.M. and S.Z. D.T. is a Cottrell Scholar of Research Corporation. We thank Profs. T. Daniel Crawford and Naushadalli K. Suleman for helpful discussions.

Supporting Information Available. Representative transient traces, k_{obs} *vs*. concentration plots, the absolute energies and optimized geometries of all calculated structures, and the complete Gaussian 03 citation is available online and in Appendix A of this dissertation.

References

1. Li, S.; Matthews, J.; Sinha, A., *Science* **2008,** 319, 1657 - 1660.
2. Vöhringer-Martinez, E.; Hansmann, B.; Hernandez-Soto, H.; Francisco, J. S.; Troe, J.; Abel, B., *Science* **2007,** 315, 497 - 501.
3. Tanko, J. M.; Suleman, N. K., Solvent Effects in the Reactions of Neutral Free Radicals. In *Energetics of Organic Free Radicals*, Simões, J. A. M.; Greenberg, A.; Liebman, J., Eds. Chapman & Hall: New York, 1996; pp 224 - 293.
4. Russell, G. A., *J. Am. Chem. Soc.* **1958,** 80, 4987 - 4996.
5. Litwinienko, G.; Ingold, K. U., *Acc. Chem. Res.* **2007,** 40, 222 - 230.
6. Xu, G.; Chance, M. R., *Chem. Rev.* **2007,** 107, (8), 3514 - 3543.
7. Boivin, J.; Crépon, E.; Zard, S. Z., *Tetrahedron Lett.* **1990,** 47, 6869 - 6872.
8. Aveline, B. M.; Kochevar, I. E.; Redmond, R. W., *J. Am. Chem. Soc.* **1995,** 117, 9699 - 9708.
9. DeMatteo, M. P.; Poole, J. S.; Shi, X.; Sachdeva, R.; Hatcher, P. G.; Hadad, C. M.; Platz, M. S., *J. Am. Chem. Soc.* **2005,** 127, 7094 - 7109.
10. Poole, J. S.; Shi, X.; Hadad, C. M.; Platz, M. S., *J. Phys. Chem. A.* **2005,** 109, 2547 - 2551.
11. Russell, G. A., Reactivity, Selectivity, and Polar Effects in Hydrogen Atom Transfer Reactions. In *Free Radicals, Vol. I*, Kochi, J. K., Ed. John Wiley & Sons, Inc.: New York 1973; pp 275 - 331.
12. Walling, C., *Free Radicals in Solution*. John Wiley & Sons, Inc.: New York, 1957.
13. Roberts, B. P., *Chem. Soc. Rev.* **1999,** 28, 25 - 35.
14. Merga, G.; Rao, B. S. M.; Mohan, H.; Mittal, J. P., *J. Phys. Chem* **1994,** 98, 9158 - 9164.

15. Anbar, M.; Meyerstein, D.; Neta, P., *J. Phys. Chem* **1966,** 70, 2660 - 2662.

16. Finn, M.; Friedline, R.; Suleman, N. K.; Wohl, C. J.; Tanko, J. M., *J. Am. Chem. Soc.* **2004,** 126, 7578 – 7584.

17. Rudakov, E. S.; Volkova, L. K.; Tret'yakov, V. P., *React. Kinet. Catal. Lett.* **1981,** 16, 333 - 337.

18. Buxton, G. V.; Greenstock, C. L.; Helman, W. P.; Ross, A. B., *J. Phys. Chem. Ref. Data* **1988,** 17, 513 - 886.

19. Willson, R. L.; Greenstock, C. L.; Adams, G. E.; Wageman, R.; Dorfman, L. M., *Int. J. Radiat. Phys. Chem.* **1971**, 211 - 220.

20. Adams, G. E.; Boag, J. W.; Michael, B. D., *Trans. Faraday Soc.* **1965,** 61, 1417 - 1424.

21. Adams, G. E.; Boag, J. W.; Currant, J.; Michael, B. D., In *Pulse Radiolysis*, Ebert, M.; Keene, J. P.; Swallow, A. J.; Baxendale, J. H., Eds. Academic Press: New York, 1965; pp 131 - 143.

22. Motohashi, N.; Saito, Y., *Chem. Pharm. Bull.* **1993,** 41, 1842 - 1845.

23. Park, H.-R.; Getoff, N., *Z. Naturforsch., A. Phys. Sci* **1992,** 47A, 985 - 991.

24. Wolfenden, B. S.; Willson, R. L., *J. Chem. Soc., Perkin Trans.* **1982**, 805 - 812.

25. Matheson, M. S.; Mamou, A.; Silverman, J.; Rabani, J., *J. Phys. Chem.* **1973,** 77, 2420 - 2424.

26. Elliot, A. J.; McCraken, D. R., *Radiat. Phys. Chem* **1989,** 33, 69 - 74.

27. Buxton, G. V., *Trans. Faraday Soc.* **1970,** 66, 1656 - 1660.

28. Baxendale, J. H.; Khan, A. A., *Int. J. Radiat. Phys. Chem.* **1969,** 1, 11 - 24.

29. Neta, P.; Dorfman, L. M., *Adv. Chem. Ser* **1968,** 81, 222 - 230.

30. Heckel, E.; Henglein, A.; Beck, G., *Ber. Bunsenges. Phys. Chem.* **1966,** 70, 149 - 154.

31. Matthews, R. W.; Sangster, D. F., *J. Phys. Chem* **1965,** 69, 1938 - 1946.

32. Elliot, A. J.; Simsons, A. S., *Radiat. Phys. Chem* **1984,** 24, 229 - 231.

33. Greenstock, C. L.; Ng, M.; Hunt, J. W., *Adv. Chem. Ser.* **1968,** 81, 397 - 417.

34. Thomas, J. K., *Trans. Faraday Soc.* **1965,** 61, 702 - 707.

35. Eibenberger, J. Vienna Univ., Vienna, Austria, 1980.

36. Karpel Vel Leitner, N.; Papailhou, A.-L.; Croue, J.-P.; Peyrot, J.; Dore, M., *Ozone Sci. Eng.* **1994,** 16, 41 - 54.

37. Mezyk, S. P.; Cooper, W. J.; Bartels, D. M.; O'Shea, K. E.; Wu, T., *J. Phys. Chem. A* **2001,** 105, 3521 - 3526.

38. Haag, W. R.; Yao, C. C. D., *Environ. Sci. Technol.* **1992,** 26, 1005 - 1013.

39. Getoff, N., *Radiat. Phys. Chem.* **1991,** 37, 673 - 680.

40. Emmi, S. S.; Beggiato, G.; Casalbore-Miceli, G.; Fuochi, P. G., *J. Radioanal. Nucl. Chem., Lett.* **1985,** 93, 189 - 197.

41. Lal, M.; Mahal, H. S., *Radiat. Phys. Chem.* **1992,** 40, 23 - 26.

42. Rezansoff, B. J.; McCallum, K. J.; Woods, R. J., *Can. J. Chem.* **1970,** 48, 271 - 276.

43. Anbar, M.; Meyerstein, D.; Neta, P., *J. Chem. Soc. B* **1966**, 742 - 747.

44. Chutny, B., *Collect. Czech. Chem. Commun.* **1966,** 31, 358 - 361.

45. Bednar, J.; Teply, J., *Collect. Czech. Chem. Commun.* **1960,** 25, 842 - 851.

46. Adams, G. E.; Boag, J. W.; Michael, B. D., *Trans. Faraday Soc.* **1965,** 61, 492 - 505.

47. Bobrowski, K.; Hug, G. L.; Pogocki, D.; Marciniak, B.; Schaneich, C., Stabilization of Sulfide Radical Cations through Complexation with the Peptide Bond: Mechanisms Relevant to Oxidation of Proteins Containing Multiple Methionine Residues. *The J. Phys. Chem. B* **2007,** 111, (32), 9608-9620.

48. Mitroka, S.; Zimmeck, S.; Troya, D.; Tanko, J. M., How Solvent Modulates Hydroxyl Radical Reactivity in Hydrogen Atom Abstractions. . *Journal of the American Chemical Society* **2010,** 132, (9), 2907-2913.

49. Reichardt, C., *Solvents and Solvent Effects in Organic Chemistry*. 2nd ed.; VCH: Weinheim, 1990.

50. Frisch, M. J.; Trucks, G. W.; Schlegel, H. B.; Scuseria, G. E.; Robb, M. A.; Cheeseman, J. R.; Montgomery, J., J. A.; Vreven, T.; Kudin, K. N.; Burant, J. C.; Millam, J. M.; Iyengar, S. S.; Tomasi, J.; Barone, V.; Mennucci, B.; Cossi, M.; Scalmani, G.; Rega, N.; Petersson, G. A.; Nakatsuji, H.; Hada, M.; Ehara, M.; Toyota, K.; Fukuda, R.; Hasegawa, J.; Ishida, M.; Nakajima, T.; Honda, Y.; Kitao, O.; Nakai, H.; Klene, M.; Li, X.; Knox, J. E.; Hratchian, H. P.; Cross, J. B.; Bakken, V.; Adamo, C.; Jaramillo, J.; Gomperts, R.; Stratmann, R. E.; Yazyev, O.; Austin, A. J.; Cammi, R.; Pomelli, C.; Ochterski, J. W.; Ayala, P. Y.; Morokuma, K.; Voth, G. A.; Salvador, P.; Dannenberg, J. J.; Zakrzewski, V. G.; Dapprich, S.; Daniels, A. D.; Strain, M. C.; Farkas, O.; Malick, D. K.; Rabuck, A. D.; Raghavachari, K.; Foresman, J. B.; Ortiz, J. V.; Cui, Q.; Baboul, A. G.; Clifford, S.; Cioslowski, J.; Stefanov, B. B.; Liu, G.; Liashenko, A.; Piskorz, P.; Komaromi, I.; Martin, R. L.; Fox, D. J.; Keith, T.; Al-Laham, M. A.; Peng, C. Y.; Nanayakkara, A.; Challacombe, M.; Gill, P. M. W.; Johnson, B.; Chen, W.; Wong, M. W.; Gonzalez, C.; Pople, J. A. *Gaussian 03, Revision C.02*, Gaussian, Inc.: Wallingford CT, 2004.

51. Barton, D. H. R. C.-Y., C.; Jaszberenyi, J. C. , *Tetrahedron Letters* **1992,** 33, 5013-5016.

Chapter 3 Mechanistic Degradation of High Density Polyethylene Potable Water Materials

Contributions

This chapter represents an extension and continuation of studies previously performed in the Dietrich laboratory, with whom this work was a collaborative effort.[1] Ms. Susan Mitroka was primary author of the resulting manuscript and performed the majority of experimental procedures. Mr. Timothy Smiley performed all pipe extraction and HDPE pipe liquid/liquid extraction experiments. Dr. Andrew Whelton (former member of the Dietrich lab) contributed significantly to the experimental design of several aging experiments performed. Dr. James Tanko and Dr. Andrea Dietrich (member of the thesis committee) contributed significantly to the experimental design of the project, as well as the intellectual merit of the manuscript.

1. Whelton, A. J.; Dietrich, A., Critical considerations for the accelerated ageing of high-density polyethylene potable water systems. *Polymer Stability and Degradation* **2009,** 94, 1163-1175.

Abstract: Accelerated aging conditions with chlorinated water solutions that minimize variations in solution chemistry were used in 160 - 190 day (3840 - 4560 h) immersion studies of high density polyethylene (HDPE) pipe and anti-oxidant (AO) free HDPE resin. Samples were periodically characterized for changes in visual appearance and surface chemistry using infrared spectroscopy. Formation of surface carbonyl bonds were detected for both HDPE pipe and AO free HDPE resin samples. Isotopic $^{18}O_2$ gas was then used to assess the source (or one of the sources) of the carbonyl oxygen. Liquid/liquid extractions from the water of both HDPE pipe and AO free HDPE resin samples indicated the formation of novel HDPE breakdown products which can leach into water. From this data, species involved in the breakdown of HDPE pipe have been identified, and a possible mechanism for the polyalkene breakdown is proposed.

3.1 Introduction

Polyethylene (PE) pipes are becoming increasingly popular as a means of water transport for industrial and residential applications. PE pipes compose a third of the world's plastic pipe demand, with their low cost and durability making them an attractive option for transport of disinfected drinking water.[1] Currently, medium density polyethylene (MDPE) and high density polyethylene (HDPE) resins are commonly used and approved for cold water applications at about 25 ºC or less, well above their glass-transition temperature (T_g) and comfortably below their reported melting temperatures (T_m). These pipes are known to have a high degree of flexibility and unusually tough resistance to stress; HDPE pipes survived a tremendous earthquake in Kobe Japan, which led to massive destruction and fatalities due to ruptured gas lines. All damage was reportedly due to steel pipe failure, with no indication of HDPE pipes failing.[2, 3]

While these pipes have projected 50 to 100 year service life, chlorinated water exposure greatly decreases this value,[1, 4-7] with studies indicating that the actual usage time under severe conditions being less than ten years.[7] Additives such as phosphate, hindered phenol antioxidants, carbon black, and UV stabilizers provide a great amount of oxidative resistance, yet over repeated exposure to chlorinated water, these stabilizers are expended, leaving the polyalkene open to oxidative attack.[4, 5, 8, 9]

Long-term exposure to water containing free available chlorine is known to have a damaging effect on PE pipe mechanical, surface, and morphological characteristics, however the exact mechanism behind these processes remains a bit of a mystery.[1, 4, 5, 9, 10] PE pipe failure depends on a variety of different factors, including chemical structure of the polymer (e.g., the presence of reactive unsaturated sites), temperature, water pH, free available chlorine

concentration, and exposure time. At low stresses (as is generally the case in water transport) the failure one of these pipes is due to the slow and consistent growth of a crack,[2] generally initiated at the surface of the pipe exposed to the water.[4, 6] It is generally reported that PE oxidation does not occur until antioxidants have been depleted- at least from the surface of the pipe exposed to chlorinated water,[4, 5, 9] which is then susceptible to oxidative attack. Although many of these studies were performed under extreme conditions not representative of disinfected drinking water (such as temperature up to 105°C and aqueous chlorine concentrations exceeding 100,000 mg/L), it would be expected that the same phenomena would occur under drinking water conditions but over longer periods of time.

The proposed first major stage of PE pressure pipe degradation is chlorinated water attack on the pipe surface, resulting in characteristic functional groups of oxygen, chlorine, hydroxyl, and vinyl components that can be detected by FTIR. Previous work from this group and others have established that when HDPE pipe samples are subjected to constant chlorinated accelerated aging conditions, the first functionality to appear is a carbonyl stretch at 1715 cm^{-1}.[1, 10] These carbonyls on the inner diameter of the pipe are precursors to the formation of microcracks, eventually evolving into macrocracks, leading to pipe failure.[10] While these components are characteristic of most HDPE accelerated aging studies involving chlorinated water, there is no consensus of either what species are involved in this process, or what the mechanism leading to these changes might be. This initial fracturing of the alkane structure is what eventually leads to microcracks, which propagate through the pipe wall until the water pressure exceeds the pipe's mechanical strength, leading to pipe rupture.[2, 4]

Species involved in chlorine water degradation of HDPE pipe are still evasive, and yet knowledge of these species is fundamental to understanding the mechanistic breakdown of these

pipes. Chorine speciation depends on the pH, which directly affects the degree of polymer oxidation. For typical drinking waters in the US, where the pH of water is near 7.0, HOCl is the dominant species. Besides the chlorine radical itself, evidence has been reported that indicates reactive oxygen species are present in chlorinated aqueous solutions.[11] Molecular oxygen has been linked to the degradation of other polyethylenes and may be a contributing factor. Bradley reported that chlorinated water oxidation is not a function of direct interactions between the polymer and chlorine, rather the presence of HOCl results in the formation of activated oxygen, which is responsible for polyalkene pipe degradation (Scheme 3-1).[7]

Scheme 3-1: HOCl degradation to HCl and O_2

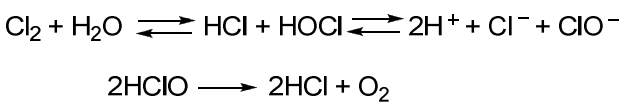

The research goal was to identify the species and mechanism(s) behind the oxidative breakdown of HDPE under accelerated aging conditions that more closely resemble conditions of potable drinking water. Our specific objectives were to: (1) differentiate between oxidation of HDPE pipe (containing additives) and anti-oxidant (AO) free HDPE resin (2) decipher the source of oxygen leading to the carbonyl peak and deduce any additional HDPE degradation products and (3) provide a mechanism for HDPE degradation.

3.2 Experimental Methods

3.2.1 Materials and Polymer Preparation.

AO free HDPE resin, CPChem HDPE, was obtained from Chevron-Phillips with a reported density of 0.955 g/cm^3, M_w= 317.48 kg/mol, and M_n= 9.37 kg/mol. AO free HDPE resin was obtained as a powder and melt pressed under argon into 0.58 mm sheets (5.0 cm x 5.0 cm) at

135°C for approximately 3 minutes. HDPE potable water pipe 19 mm in diameter, standard inner diameter dimension ratio of 9 mm, and reported density of 0.954 g/cm^3 was commercially obtained. Dog-bone shaped samples were cut from both the HDPE pipe and AO free AO free HDPE resin using a microtensile die Dewes Gumbs Die Company, Inc. (Long Island City, NY). All samples were then thrice rinsed in distilled water and were dried at room temperature for 48 h. All samples were 2.0 cm in length; AO free HDPE resin samples had a thickness of 0.58 mm and HDPE pipe samples had a thickness of 2.6 mm.

3.2.2 Water Quality Measurements and Accelerated Aging Methods.

Aging solutions were prepared with reagent water from a Barnstead (Dubuque, IA) Nanopure® ultrapure water system, 6.5% sodium hypochlorite, and sodium bicarbonate. Water pH was adjusted with hydrochloric acid, and pH was measured using a bench-top Accumet™ pH Meter 910 with probe. Alkalinity was measured by titration with 0.025 N sulfuric acid to an end-point pH of 4.5 in accordance with Standard Method 2320(B).[12] Free chlorine concentration was measured by titrating test solutions with added potassium iodide and glacial acetic acid using 0.025 N sodium thiosulfate according to Standard Method 4500-Cl(B).[12]

Fifty die-cut dog-bone shaped AO free HDPE resin or HDPE pipe samples were placed in separate 500 mL glass bottles with polypropylene caps. 500 mL aqueous solution of two chlorine concentrations were used for each set of samples: for HDPE pipe, 500 mg/L and 50 mg/L aqueous chlorine concentrations were used; for AO free HDPE resin, 250 mg/L and 50 mg/L aqueous chlorine concentrations were used. All solutions initially contained 50 mg/L alkalinity (added as sodium bicarbonate) at pH 6.5 and the aging solution was changed every 3 days. At each 3 day time point, water pH, free available chlorine, and alkalinity were measured and samples were rinsed thrice with reagent water before being placed in new aging solutions. A

smaller scale experiment was also employed for each set of samples at each chlorine concentration. This involved taking individual samples, which were initially assessed by Fourier Transform – Infrared (FT-IR) for any signs of oxidation prior to accelerated aging- and housing them in smaller, individual glass volatile organic analyses (VOA) vials with approximately 10 mL of the appropriate aqueous solution. These samples were then re-assessed by FT-IR spectroscopy and visual observation analyses in an effort to detect signs of oxidation/aging. The aging experiments were stopped at 190 days (4560 hs) for the HDPE pipe samples and 160 days (3840 hs) for AO free HDPE resin samples. All experiments were conducted in the dark with no agitation to the system at a constant temperature of 37°C.

Additionally, controls to assess the role of the polymer in the aging solution were conducted using 50 mg/L, 250 mg/L and 500 mg/L aqueous chlorine solutions devoid of HDPE samples. Water was evaluated for changes in pH, alkalinity and chlorine concentration as previously described.

3.2.3 Polymer Characterization

Application of Characterization Techniques.

HDPE pipe and AO free HDPE resin samples from each concentration were periodically assessed for oxidative damage through visual assessment and FT-IR spectroscopy. HDPE pipe data is reported for days 45, 90 and 160. AO free HDPE resin data is reported for days 21, 90 and 160.

Surface Characteristics.

Surface chemistry was characterized using a Perkin Elmer Spectrum One Fourier Transform Infrared spectrometer (Waltham, MA) in Attenuated Transform Reflectance (ATR) mode with a ZnSe crystal at 4 cm^{-1} resolution. Background was determined using 100 scans from

3500 to 600 cm^{-1}, and 25 scans were conducted for each sample also over this range. Select bond indices were calculated based on IR data (relative to C—H bend frequency at 1462 cm^{-1}). These include: carbonyl ($\sigma_{1715}/ \sigma_{1462}$ and $\sigma_{1742}/ \sigma_{1462}$), vinyl ($\sigma_{908}/ \sigma_{1462}$), peroxide ($\sigma_{1030}/ \sigma_{1462}$), and chlorine ($\sigma_{660}/ \sigma_{1462}$). The peak at 1462 cm^{-1} is used as a relative internal standard and assumes that the amount of new bonds formed is small relative to the amount of unreacted C—H bonds. Although this method does not provide an exact measure of new species formed, it does offer a valid comparison for overall degradation over time. FT-IR spectra were taken at the surface of each sample, probing approximately 2-3 microns into the polymer. Samples were also visually assessed for changes in color.

3.2.3.1 Methylene Chloride Extractions

Liquid/Solid Extraction: Antioxidant Extraction and Aging In order to extract additives from the HDPE pipe, a Kontes liquid/liquid, heavier than water micro scale apparatus was used as a micro scale soxhlet extraction apparatus. Twelve samples of pipe were used for each extraction and the weight was taken to the nearest 0.001 grams. A boiling chip and 75mL of methylene chloride were placed in a 100 mL, 14/20 round bottom flask. Methylene chloride was chosen as the solvent for the extraction, as it is able to dissolve many organic compounds and can be refluxed at a low temperature (boiling point = 40°C) to reduce degradation of extracted materials. The solvent/HDPE pipe system was refluxed for 12 h at 40°C. The extract was then concentrated to 5 mL and kept for further evaluation. 50 samples of methylene chloride extracted HDPE pipe and 50 samples of non-extracted HDPE pipe were separately aged in 500 mL of 250 mg/L aqueous solution previously described. Water was changed and monitored every three days (Section 2.2).

Liquid/Liquid Extraction. Liquid/liquid extractions were performed on three sets of HDPE aging solutions: AO free HDPE resin, HDPE pipe, and methylene chloride extracted HDPE pipe.

190 mL of each aging solution (AO free HDPE resin, HDPE pipe and methylene chloride extracted HDPE pipe) were treated with 20 mL of methylene chloride, mixed, and allowed to separate. This was performed in triplicate for each sample and methylene chloride was then concentrated using the method mentioned earlier.

Liquid/liquid extractions were performed at Day 3, 9, 12, 15 and 18 for HDPE pipe and methylene chloride extracted HDPE pipe aging solutions. Extractions were performed at Day 60 and 66 for AO free HDPE resin aging solutions.

Acetone Rinse. To ensure that antioxidants, antioxidant degradation products, and other additives in HDPE pipe samples were not interfering with the monitoring of HDPE degradation, HDPE pipe samples were rinsed with acetone prior to FT-IR calculation of bond indices.

3.2.4 Oxygen-18 labeled O_2 Experiments.

Addition of $^{18}O_2$ gas to Chlorinated Water Samples.

250 mg/L aqueous chlorine solutions were prepared as previously described. Each experimental set-up consisted of one AO free HDPE resin dogbone sample and 10 mL 250 mg/L aqueous chlorine solution in a high pressure vacuum tube. The HDPE-aqueous chlorine sample underwent triplicate freeze- pump- thaw procedures on a high pressure vacuum line (in triplicate) in order to remove any $^{16}O_2$ from the water and atmosphere. $^{18}O_2$ gas was first added to the vacuum line (at 25 mT pressure), then transferred to the vacuum tube. Approximately 8 to 12 mL of $^{18}O_2$ gas (0.33 to 0.50 mmol) was added to each sample (the calculated density of $^{18}O_2$ is 1.47 g/L at 1 atm and 25°C).

Four AO free HDPE resin samples were individually contacted with 250 mg/L aqueous chlorine. These samples were housed in the dark with no agitation to the system at a constant temperature of 37°C for 3 weeks without water changing. One AO free HDPE resin sample was kept at these conditions for three weeks, in which every three days the water was changed and the above procedure was repeated. As a control, one AO free HDPE resin sample underwent the same freeze, pump, thaw process, but was then exposed to an air environment. The control sample was housed in the dark with no agitation to the system at a constant temperature of 37°C for 3 weeks without water changing.

Addition of $^{18}O_2$: Effect on Surface Characteristics.

Surface chemistry was characterized using a Perkin Elmer Spectrum One Fourier Transform Infrared as previously described. Select bond indices were calculated based on IR data. Functional groups detected include: ^{16}O carbonyl ($\sigma_{1742 \text{ and } 1715} / \sigma_{1462}$), ^{18}O carbonyl ($\sigma_{1648}/ \sigma_{1462}$), vinyl ($\sigma_{908}/ \sigma_{1462}$), ^{16}O peroxide ($\sigma_{1115}/ \sigma_{1462}$), ^{18}O peroxide ($\sigma_{1030}/ \sigma_{1462}$), and chlorine ($\sigma_{660}/ \sigma_{1462}$).

3.3 Results

3.3.1 Accelerated Aging: HDPE Pipe

Stability of Oxidant Solution During Aging. During the 190 day exposure period of HDPE pipe samples with water changes every 72 h (3 days), free available chlorine levels for the 50 mg/L aqueous chlorine solution control and solutions containing HDPE pipe samples stayed consistent, showing no measurable decrease in chlorine concentration, pH or alkalinity. Conversely, the 500 mg/L aqueous chlorine solution showed consistent decreases in pH from pH 6.5 to about pH 6.0, decreases in alkalinity from 100 to 70 mg/L as sodium bicarbonate, and decreases in chlorine concentration from 500 mg/L to 250-300 mg/L in the presence or absence

of HDPE pipe samples. All three of these parameters were found to be significantly different ($p<0.05$) after the three day period. The changes in both 500 mg/L aqueous chlorine solutions are attributed to the decomposition of HOCl as outlined in Scheme 1, and the presence of bicarbonate to provide buffer capacity and resist pH change.

Pipe Surface Chemistry Oxidation During Aging.

HDPE pipe surface oxidation occurred under both aging conditions as indicated by IR spectroscopy data from Day 0, 45, 90 and 160. Detectable changes in absorbance were found at each exposure time and both aqueous chlorine concentrations. Primarily, a broad carbonyl band, likely representing a compilation of both an aldehyde and ketone carbonyl species[13] was detected with a maxima at 1742 and 1715 cm^{-1} respectively, and gradually increased in intensity under both aging conditions (Table 3-1).

Table 3-1. Relative intensities of carbonyl peaks in HDPE pipe accelerated aging studies. % relative to C—H bend at 1462 cm^{-1}.

Time	**50 mg/L Cl_2**		**500 mg/L Cl_2**	
	1715 cm^{-1}	1742 cm^{-1}	1715 cm^{-1}	1742 cm^{-1}
Day 0	0	0	0	0
Day 45	18.1	17.2	22.3	17.6
Day 90	22.3	13.8	23.0	16.0
Day 160	36.5	34.7	40.2	23.5

Despite a ten-fold difference in chlorine concentration, each samples from each time interval showed similar carbonyl intensities. Another interesting phenomenon was seen at around day 90, in both the 50 mg/L and 500 mg/L chlorine aging conditions. The intensities of the carbonyl absorbances were greatly increased, and multiple new bands (3300, 1690, 1298, 1174, 1050 cm^{-1}; Figure 3-1) appeared. However after each sample was washed with acetone, only characteristic carbonyl bands (1742 and 1715 cm^{-1}) remained. These absorbances are believed to be due to degraded antioxidants that were present or migrated to the surface, and which were removed with acetone. Many of the Irganox® antioxidants contain carbonyls which may have contributed to the activity in the 1550 cm^{-1} to 1800 cm^{-1} region.

Figure 3-1. a) IR of HDPE pipe sample after 90 days (2160 h) of accelerated aging at 500 mg/L Cl2. Multiple bands are present (3300, 1690, 1298,1742, 1715, 1174, 1050 cm-1). **b)** IR of sample after 2 minute wash with acetone.

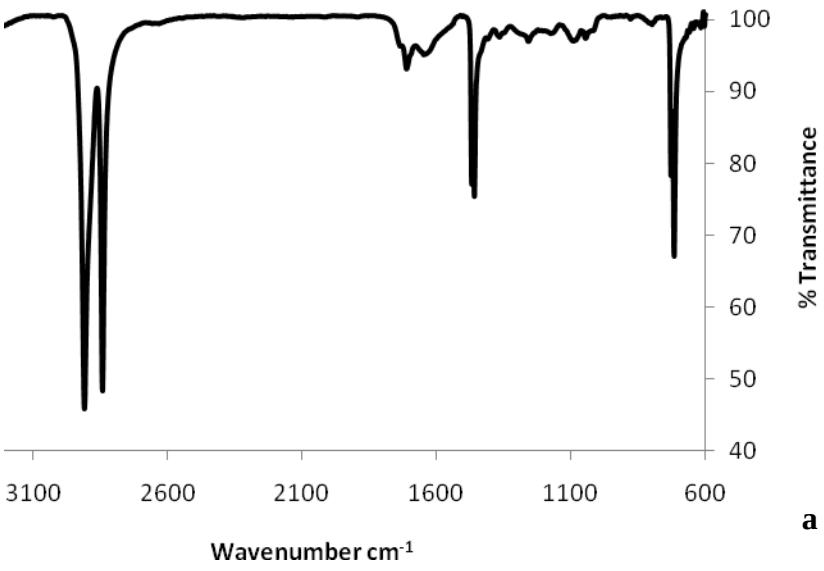

a

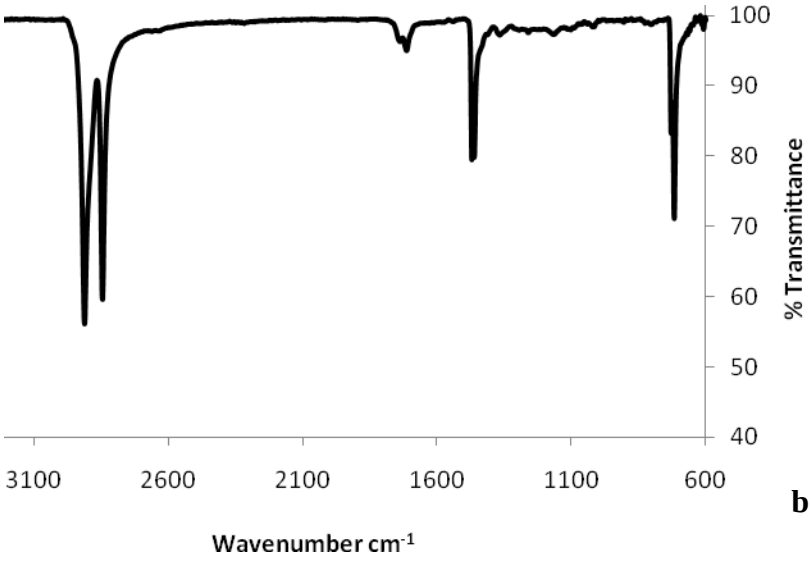

b

3.3.2 Accelerated Aging: AO free HDPE resin

Stability of Oxidant Solution During Aging. During the 160 day exposure period with water changes every 72 h (3 days), free available chlorine levels for the 50 mg/L aqueous chlorine solutions (control and solution containing AO free HDPE resin samples) stayed fairly

consistent, showing no measurable decrease in chlorine concentration or alkalinity, however pH did show a significant increase from 6.5 to about 6.9 ($p<0.05$). Conversely, the 250 mg/L aqueous chlorine solutions (control and solution containing AO free HDPE resin samples) exhibited no change in pH, yet did show a decreases in alkalinity from 100 to 80-90 mg/L as sodium bicarbonate, and slight decreases in chlorine concentration from 250 mg/L to 200-250 mg/L, both of which were determined to be statistically significant ($p<0.05$).

Resin Oxidation During Aging.

Both 50 and 250 mg/L aqueous chlorine conditions resulted in AO free HDPE resin surface oxidation (Table 3-2). Detectable changes in absorbance were found for at each exposure time. Primarily, a broad carbonyl band, likely representing a compilation of both an aldehyde and ketone carbonyl species was detected at 1742 and 1715 cm^{-1} respectively and gradually increased in intensity for both aging conditions. Again, in spite of significant differences in aqueous chlorine concentration, each time point sample showed very similar carbonyl intensities. No bands that had been detected and attributed to antioxidant decomposition in HDPE pipe samples were present at any time point during the AO free HDPE resin aging.

Table 3-2. Relative intensities of carbonyl peaks in AO free HDPE resin accelerated aging studies. Numbers reported as a percent of 1462 cm-1 peak (C—H stretch).

Time	**50 mg/L Cl_2**		**250 mg/L Cl_2**	
	1715 cm^{-1}	1742 cm^{-1}	1715 cm^{-1}	1742 cm^{-1}
Day 0	0	0	0	0
Day 21	0	10.1	0	18
Day 90	6.0	8.0	12.0	9.4
Day 160	36.6	34.7	24.2	18.7

3.3.3 Accelerated Aging: $^{18}O_2$ gas

Aged samples exposed to $^{18}O_2$ gas showed the presence of two carbonyl peaks,: one at 1715 cm^{-1}, which would be expected for a typical saturated ketone containing molecular oxygen, and another peak at 1648 cm^{-1}, which is believed to be the result of a carbonyl with ^{18}O incorporation (Figures 3-2).

Figure 3-2. a) IR of AO free HDPE resin sample after 21 days (504 h) of accelerated aging at 250 mg/L aqueous chlorine in the presence of $^{18}O_2$. $C^{16}O$ stretch (ketone): 1715 cm^{-1} *;* $C^{18}O$ stretch (ketone): 1648 cm^{-1}; Relative intensities (measured to C—H bend at 1462 cm^{-1}): 9.1% (1742cm^{-1}) and 7.5% (1648 cm^{-1}) **b)** Comparison of an $^{18}O_2$ treated HDPE sample (black, 21 days) with normal aging sample (blue, 42 days).

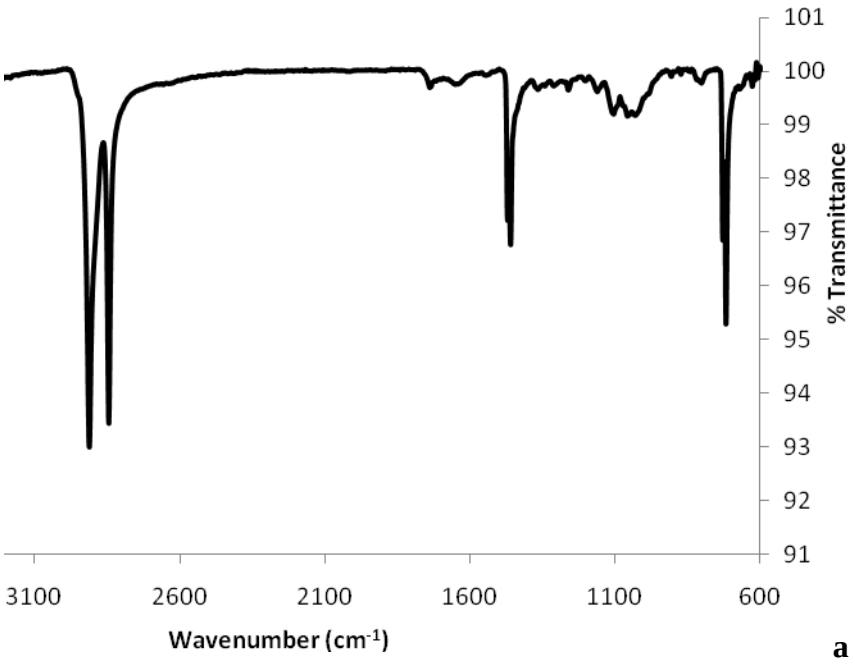

a

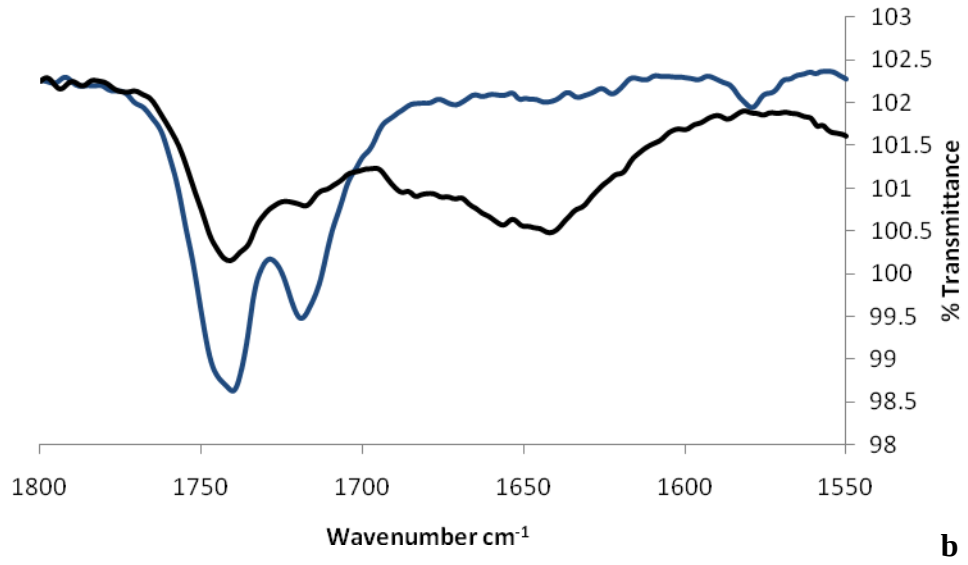

b

The shift in carbonyl intensity can be estimated using a variation of Hooke's law. Using this approximation, the bond is thought of as two masses (the atoms) joined by a spring (the bond). The bond between the two atoms is capable of oscillation; the frequency of this oscillation is related to the force constant of the bond, as well as the masses of both atoms:

$$v = \frac{1}{2\pi c}\left[\frac{f}{M_x M_y / M_x + M_y}\right]^{1/2} \qquad \textbf{(3-1)}$$

In this approximation, M_x is the molecular weight of carbon, M_y is the molecular weight of oxygen, f is the force constant of the bond, and c is the speed of light. To determine the shift, the equation was back calculated using the value of v= 1715 cm^{-1} for the carbonyl bond containing molecular oxygen to obtain the value of f. The derived result predicts a carbonyl shift at 1668 cm^{-1}. This shift to a lower frequency would be expected with an atom of higher atomic weight (^{18}O as opposed to ^{16}O), since the frequency is inversely proportional to the molecular weight of an atom for a given force constant. The calculated value for the shift is slightly higher than the measured value (1648 cm^{-1}). However it should be noted that this is a mathematical

approximation, and some degree of variance is to be expected. The shift in carbonyl peak appeared in all resin samples exposed to the $^{18}O_2$ environment, and was absent in all resin samples not exposed to $^{18}O_2$.

Nucleophilic Substitution Reaction To assess the other source of carbonyl oxygen from the $^{18}O_2$ studies, samples containing both peaks (1715 cm^{-1} and 1648 cm^{-1}) were immersed in a slightly acidic aqueous solution to determine whether nucleophilic substitution was occurring, leading to an exchange of oxygen. Nanopure® water solutions were adjusted to a pH of 6.5 with sodium bicarbonate and hydrochloric acid. Samples were housed individually in 10 mL of water at 37°C.

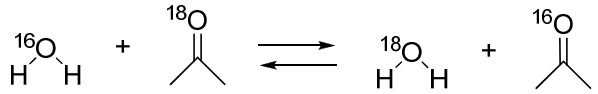

(3-2)

After three weeks of being immersed in the water system, a noticeable shift took place in the relative intensities of each carbonyl peak (Figure 3-3). The 1742 cm^{-1} band increased, with a simultaneous decrease in the intensity of the 1648 cm-1 peak.

Figure 3-3. a) AO free HDPE resin sample with both ^{16}O (1742 cm^{-1}) and 18O (1648 cm^{-1}) carbonyl bands present. Relative intensities (measured to C—H bend at 1462 cm^{-1}): 9.1% (1742cm^{-1}) and 7.5% (1648 cm^{-1}). **b)** Sample after 3 week immersion in slightly acidic aqueous solution (pH= 6.5). Relative intensities (measured to 1462 cm^{-1}): 18.3% (1742 cm^{-1}) and 6.0% (1648 cm^{-1}).

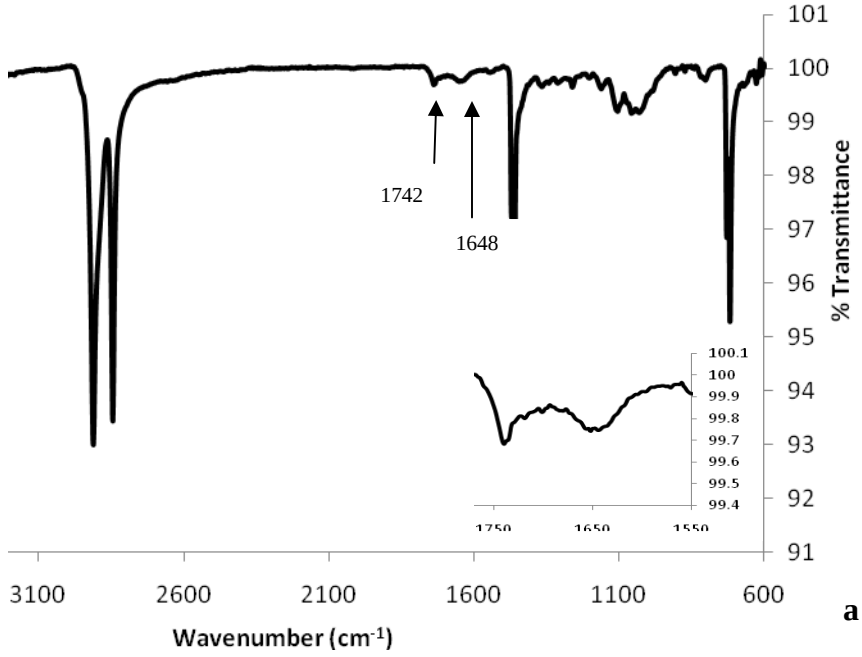
1742
1648
% Transmittance
Wavenumber (cm-1)
3100
2600
2100
1600
1100
600

a

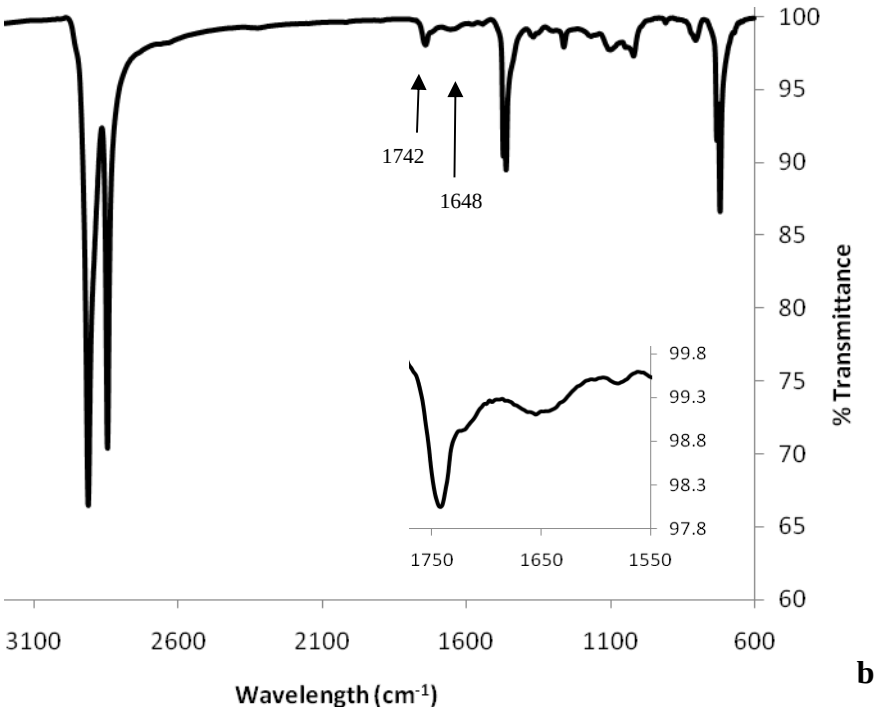
1742
1648
% Transmittance
Wavelength (cm-1)
3100
2600
2100
1600
1100
600

b

3.3.4 Liquid/Liquid Extraction

Extracted and Non-Extracted HDPE Pipe GC/MS data was analyzed by dividing the peak area of interest by the peak area of the internal standard with the closest retention time. Two unexpected compounds were found, 3-chloro-1,1-di-methylpropanol (DMCP) and 2,3-dichloro-2-methylbutane (DCMB) (Figure 3-4). Both compounds were identified through library search matches of the mass spectra; while authentic samples were not available for comparison, each compound from the liquid/liquid extraction showed a 90% or greater correlation to the library match spectra.

Figure 3-4: Compounds obtained from liquid/liquid extraction of HDPE pipe

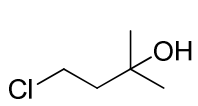

3-chloro-1,1-dimethylpropanol (DMCP)

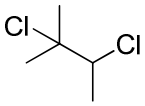

2,3-dichloro-2-methylbutane (DCMB)

Figure 3-5 shows a summary of the production of these compounds over time. As it can be seen in these figures, both extracted and new pipe showed an increase in each of the chlorinated product over time. The extracted pipe showed slightly less of these products at later time points than new pipe, perhaps due to the removal of small alkane chains during the extraction process.

Figure 3-5. Graphs showing the relative abundance of **a)** DCMB and **b)** DMCP from new and extracted HDPE pipes.

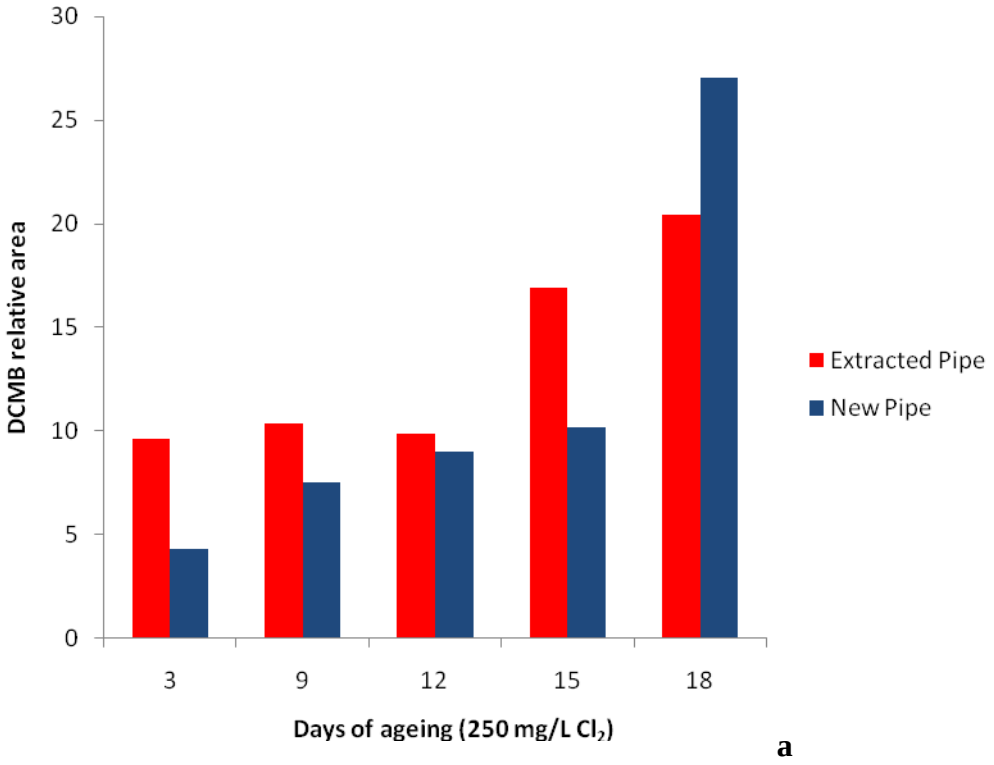

a

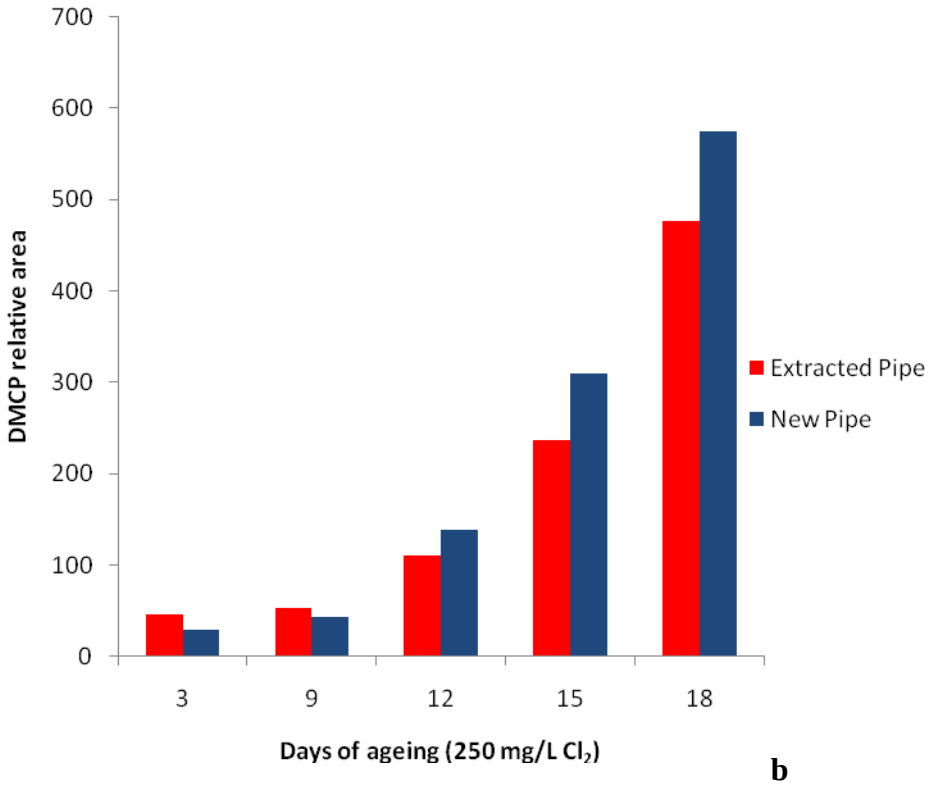

b

AO free HDPE resin To better ascertain if the two isolated products (DCMP and DCMB) were derived from an antioxidant or the HDPE polymer, a liquid/liquid extraction was performed on Day 60 and Day 66 water solutions of the AO free HDPE resin aging experiment. Both products obtained from the liquid/liquid extraction of the HDPE pipe were also obtained from the AO free HDPE resin water extraction. The amount of product was related to the amount of chlorine present in the aging solution, with about 3 to 4 times more products obtained from the 250 mg/L chlorinated water than the 50 mg/L chlorinated solution.

Competition Experiments Several researchers have indicated that a variety of radicals, including the hydroxyl radical (HO•), chlorine radical (Cl•), O_2 and the hypochlorite radical (ClO•) may be present in chlorinated aqueous solutions,[1, 4, 10, 11] however the chemical

contributions of these radicals are not expected to be the same. To identify the potential hydrogen atom abstraction that initiates HDPE degradation, competition experiments were conducted using 2,3-dimethylbutane as the source for primary and tertiary hydrogens, and cyclohexane as the source for secondary hydrogens. While extremely reactive radicals, such as the hydroxyl radical (HO•) or the chlorine radical (Cl•) would be expected to show little to no selectivity, less reactive radicals (i.e. the peroxyl radical HOO•, hypochlorite radical ClO•, or singlet O_2)[14-16] would favor abstraction of tertiary hydrogen, with lesser reactivity towards secondary and primary hydrogen. Equimolar amounts (92 mmol) of each substrate were added to 1 L of 250 mg/L aqueous chlorine and mixed in the dark for 6 h at room temperature. Relative amounts of the chlorinated products were used to determine relative reactivities of the hydrogen. The relative amounts of product were determined using GC/MS analysis, as discussed in Chapter 2. 2-chloro-2,3-dimethylbutane and 1-chloro-2,3-dimethylbutane had previously been synthesized and characterized by the group with correction factors (F) determined to be 0.974 for each product. Chlorocyclohexane was commercially available, with a correction factor determined to be 0.953 (Figure 3-6)

Figure 3-6. Products and GC correction factors for small molecule chlorination study.

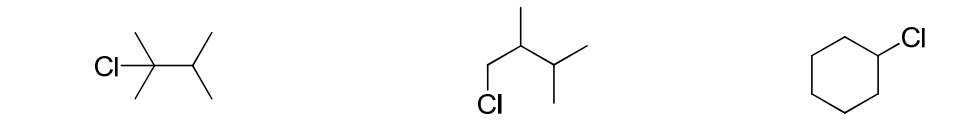

2-chloro-2,3-dimethylbutane F= 0.974

1-chloro-2,3-dimethylbutane F=0.974

chlorocyclohexane F= 0.953

The derived relative reactivities were, 3^o (4.5) > 2^o (2) > 1^o (1.0). These results closely match the reactivities expected from the chlorine radical. However, this is a rather crude estimate, as

we would expect the formation of far more products that simply the chlorinated species. Clearly, the non-selective behavior indicates a highly reactive specie (or species) involved in the first step of hydrogen atom abstraction.

3.4 Discussion

Several key findings can be noted from this work. One interesting note can be made about the amount of chlorine in the accelerated aging study and the subsequent polymer degradation. While HDPE pipe and AO free HDPE resin samples show an increase in carbonyl intensity over time, there are not significant differences at any given point between aqueous chlorine concentrations. As seen in Figure 3-7, the carbonyl bands from the HDPE pipe day 90 samples overlap nearly perfectly. Despite the distinct loss of chlorine in the 500 mg/L aqueous chlorine solution, carbonyl formation remains similar to the 50 mg/L Cl_2 solution samples.

Figure 3-7. Overlap of day 90 HDPE pipe carbonyl peaks (blue= 500 mg/L Cl_2 aging conditions; red= 50 mg/L Cl_2 aging conditions.

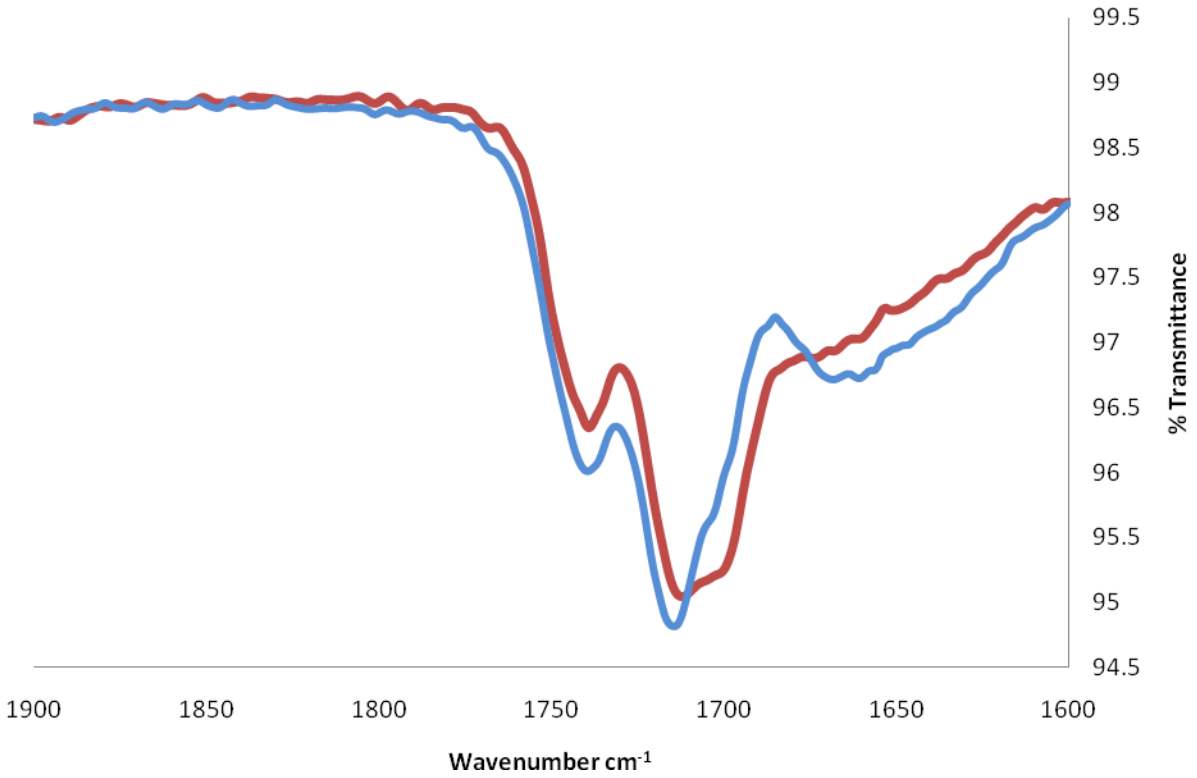

This chlorine decrease is also seen when no polymer samples are present, indicating that the loss of chlorine is not due to interaction with the HDPE pipe or antioxidants.

This of course raises the question of what is causing this chlorine depletion, and if/how this phenomenon affects the degradation of the polymer. The likely reason for the chlorine loss is degradation into hydrochloric acid and oxygen gas.[7] $^{18}O_2$ studies play a significant role in helping to determine where this carbonyl oxygen is coming from; In the AO free HDPE resin sample, the presence of $^{18}O_2$ causes both the appearance of a new carbonyl peak; however the analogous peak that corresponds to ^{16}O is still present. Several different hypotheses could be used to explain this: 1) not all molecular oxygen was removed, or molecular oxygen seeped in

through a leak in the vacuum system, 2) molecular oxygen from water and/or hypochlorous acid is involved in this process, or 3) molecular oxygen is produced through another means, namely HOCl decomposition.[7] Changes in aqueous chlorine concentration and alkalinity indicate that perhaps some molecular oxygen is produced (Scheme 3-1), which may react directly with the polymer in an auto-oxidative process. However, this instance would have to be relatively minor; the amount of molecular oxygen produced due to the decomposition of HOCL would be significantly less than the amount of $^{18}O_2$ added- at most only about one third (or 0.15 mmol based on loss of free available chlorine).

Nucleophilic substitution reactions indicate that substitution of the carbonyl ^{18}O is certainly a plausible explanation for the continued presence of a 1715 cm^{-1} peak. This is not surprising given the slightly acidic environment and relative amounts of ^{18}O and ^{16}O atoms present in the aging conditions. At a maximum, 0.50 mmol of $^{18}O_2$ was added to a sample- corresponding to approximately 6.1×10^{20} atoms of ^{18}O, or 3.05×10^{20} molecules of $^{18}O_2$ capable of interacting with the polymer. Conversely, there are approximately 3.23×10^{23} atoms of ^{16}O present - a 1000-fold excess compared to ^{18}O. The large amount of ^{16}O present would make it quite probable that some molecular oxygen be incorporated into the polymer, most likely via both of the aforementioned processes.

All experimental results obtained in this study clearly indicate that O_2 is directly involved in the oxidation of HDPE. From the data obtained we propose the following mechanism for degradation as highlighted in Scheme 3-2: hydrogen atom abstraction by a highly reactive radical (eg Cl• or HO•) occurs from the alkane chain, producing a carbon centered radical, that reacts with aqueous triplet oxygen. This produces a peroxyl on the polyalkane chain. Several possibilities exist for peroxyl decomposition: 1) beta-cleavage to form an aldehyde or ketone,

and a subsequent hydroxyl radical 2) a similar beta-cleavage aided by another radical in the system[18] or 3) breaking of the weak oxygen-oxygen bond leading to a carbon centered radical and hydroxyl radical. It is believed that all of these mechanisms play a role in ketone/aldehyde formation on the polyalkane chain.

Scheme 3-2: Mechanisms of HDPE Autooxidation. Several mechanisms are believed to contribute to the formation of carbonyls: 1) beta-cleavage of the peroxyl 2) beta-cleavage aided by another radical in the system 3) breaking of the weak oxygen-oxygen bond leading to the additional formation of a carbon centered radical. The initiating radical (·X) may be one of several different species.

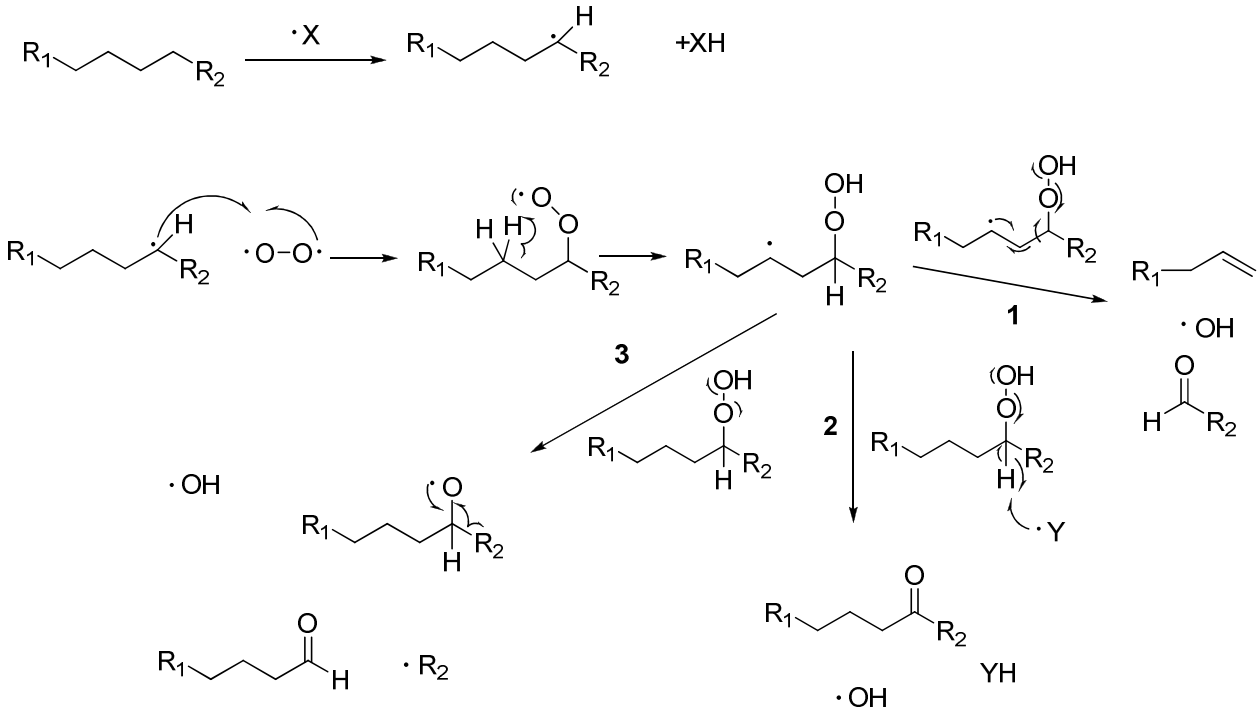

Similar autooxidative processes have been seen in macromolecules such as DNA, proteins and lipids.[18-22] While singlet oxygen is far less reactive (in terms of hydrogen atom abstraction) than HO• and Cl•, its involvement in reproducing such highly reactive radicals makes it a major contributor to polymer degradation.

Finally, we detect the presence of two novel HDPE degradation products via liquid/liquid extraction with water solutions, 3-chloro-1,1-di-methylpropanol and 2,3-dichloro-2-methylbutane. AO free HDPE resin- containing no antioxidants- showed the formation of both products after exposure to chlorinated water, indicating formation via decomposition of the polymer as opposed to an antioxidant. Non-extracted and methylene chloride extracted HDPE pipe samples also showed formation of these products when exposed to chlorinated water. Of interest to note, is that upon continued exposure to chlorinated water, new HDPE pipe samples actually showed greater formation of these products compared to samples from which antioxidants were extracted. This suggests that antioxidants may not provide significant defense against the reactive radicals involved in DCMB and DMCP formation.

The mechanism of formation of these products is believed to be directly linked to the auto-oxidation process previously described (Scheme 3-2). Again, it is the formation of low molecular weight alkanes that contribute to the production of the two chlorinated species (Scheme 3-3).

Scheme 3-3: Possible mechanism of formation of DCMB and DMCP during auto-oxidation.

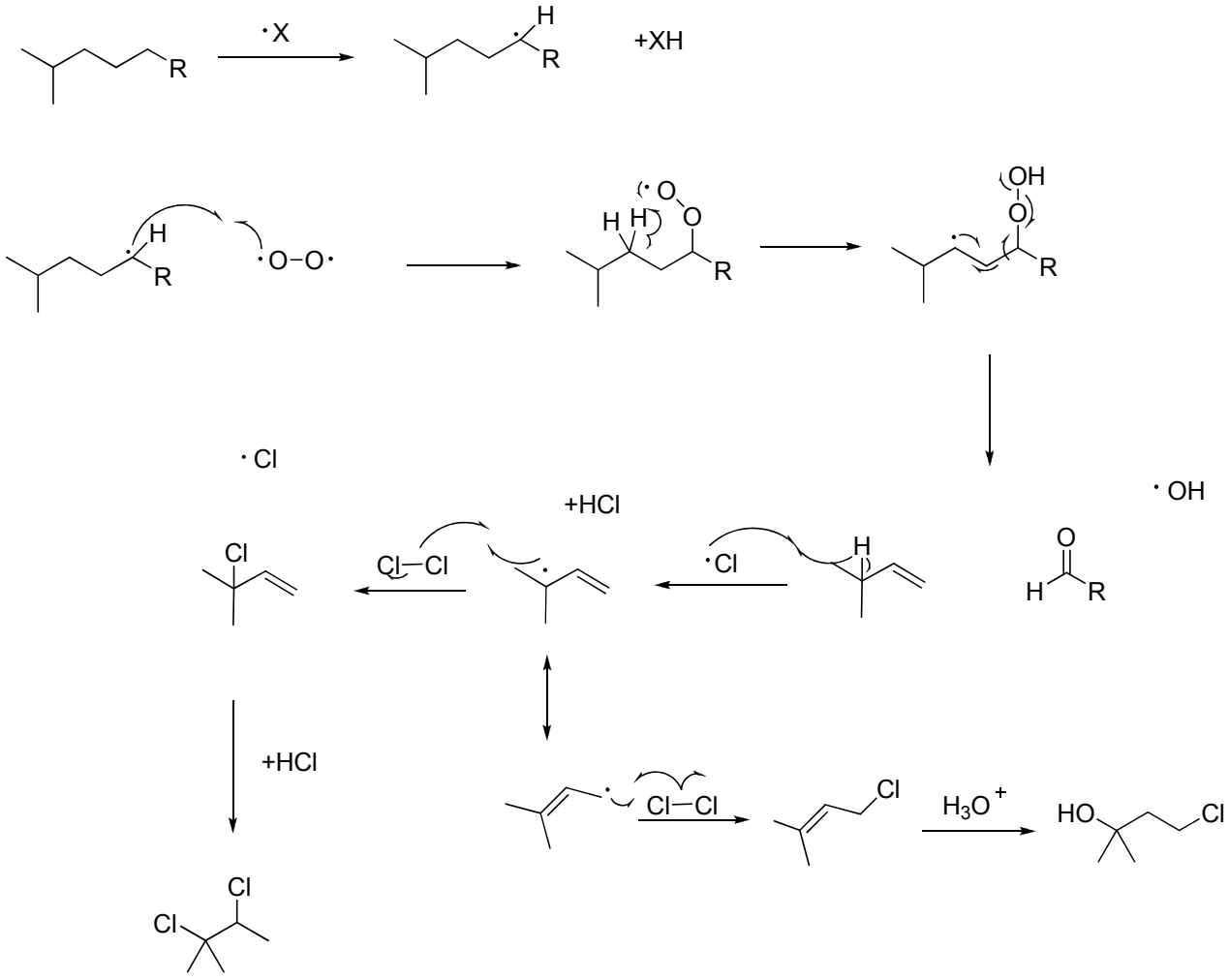

While DCMB has not been thoroughly investigated for toxicological effects, DMCP is known to be only slightly toxic by ingestion, with an LD 50 in rats of 110 mg/kg (oral exposure), which is approximately two thirds of the LD 50 for caffeine (192 mg/kg, oral exposure). While the toxicological effects of these byproducts appear to be minimal, their influence on taste or odor properties of water may be more substantial.

3.5 Conclusions

Carbonyl formation is the first observable step in HDPE degradation. Using AO free HDPE resin devoid of antioxidants demonstrates that 1) the carbonyl functionality is the first visible sign (via IR) of degradation and 2) the presence of this species is the direct result of oxidation to the polymer, and not a decomposed antioxidant. The oxygen found in the carbonyl is the result of autooxidation to the polymer; While it is likely that there is some nucleophilic exchange with the aqueous environment, this only occurs after the initial oxidative process outlined in Scheme 3-2.

Of interest to note is the lack of a detectable carbon chlorine bond present on the polymer. While there is more than a ten-fold excess of chlorine (250 mg/L aqueous chlorine = 3.5 mmol) in the systems as compared to dissolved oxygen (which, at 37°C is approximately 0.2 mmol),[23] no C-Cl bond is detected by IR. This is believed to be due primarily to the fact that a C-Cl bond is simply more difficult to detect via IR- not that such a bond is absent. It's clearly known through the identification of other HDPE degradation products that Cl• can and does interact with the alkane. Although not detectable, it is believed that chlorine does add to the carbon centered radicals of the polymer in a similar fashion as the low molecular weight alkanes shown in Scheme 3-3.

While visual characteristics of HDPE pipe are different between a 50 mg/L and 500 mg/L Cl_2 accelerated aging study, formation of the carbonyl moiety is unaffected by chlorine concentration. AO free HDPE resin shows similar results, indicating the formation of the carbonyl band is decidedly due to polymer oxidation, and is not an artifact of antioxidant decomposition. Only a small amount of aqueous chlorine is necessary to initiate the ensuing chain reaction, capable of producing more radicals that can react with the polymer surface.

We have also discovered two novel HDPE degradation products, 3-chloro-1,1-di-methylpropanol and 2,3-dichloro-2-methylbutane. Concentration of these products is both related to chlorine concentration of the aqueous solution. These products are believed to be formed from the reaction of smaller alkyl chains with chlorine and other reactive species in the water. Production of these compounds may serve as another means of monitoring HDPE polymer degradation in accelerated aging studies.

Supporting Information. Representative IR spectra of aged HDPE pipe and AO free HDPE resin samples are available online and in Appendix B of this dissertation.

Acknowledgements

We gratefully acknowledge funding provided by the AWWA Research Foundation and USA National Science Foundation (Awards CBET-0755342 and DGE-0333378). Opinions, findings, conclusions, and recommendations expressed in this material are those of the authors and do not necessarily reflect the views of either funding agencies. We also thank the following people at Virginia Tech for their assistance and insights: Dr. Garth L. Wilkes, Dr. Timothy Long, Dr. Herve' Marand, Dr. Robert Moore, Dr. Andrew Whelton, Dr. James McGrath, as well as Jody Smiley, Geno Appodoca, Claudia Brodkin, and Victoria Long.

References

1. Whelton, A. J.; Dietrich, A., Critical considerations for the accelerated aging of high-density polyethylene potable water systems. *Polymer Stability and Degradation* **2009,** 94, 1163-1175.
2. Krishnaswamy, R. K., Analysis of ductile and brittle failures from creep rupture testing of high-density polyethylene (HDPE) pipes. *Polymer* **2005,** 46, 11664-11672.
3. Nishimura, H., Maeba, H. In Proceedings of the 10th international plastics pipes conference, Gotenbur, Sweden, 1998; Gotenbur, Sweden, 1998.
4. Hassinen, J.; Lundback, M.; Ifwarson, M.; Gedde, U. W., Deterioration of polyethylene pipes exposed to chlorinated water. *Polymer Degradation and Stability* **2004,** 84, 261-267.
5. Viebke, J.; Hedenqvist, M.; Gedde, U. W., Anti-oxidant efficiency and loss by precipitation and diffussion to surrounding media in polyethylene hot-water pipes. *Polymer Engineering and Science* **1996,** 36, (24), 2894-2904.
6. Dear, J. P.; Mason, N. S., The Effects of Chlorine Depletion of Antioxidants in Polyethylene. *Polymers and Polymer Composites* **2001,** 9, (1), 1-13.
7. Gill, T. S.; Knapp, R. J.; Bradley, S. W.; Bradley, W. L., Long term durability of crosslinked polyethylene tubing used in chlorinated hot water systems. *Plastics, Rubber and Composites* **1999,** 28, (6), 309-313.
8. Karlsson, K.; Eriksson, P.; Hedenqvist, M.; Ifwarson, M.; Smith, G.; Gedde, U. W., Molecular structure, morphology and antioxidant consumption in poly-butene-1 pipes in hot water applications. *Polymer Engineering and Science* **1993,** 33, (5), 303-310.

9. Viebke, J.; Gedde, U. W., Anti-oxidant diffussion in polyethylene hot water pipes. *Polymer Engineering and Science* **1997,** 37, (5), 896-911.

10. Colin, X.; Audoin, L.; Verdu, J.; Rozental-Evesque, M.; Rabaud, B.; Martin, F.; Bourgine, F., Aging of Polyethylene Pipes Transporting Drinking Water Disinfected by Chlorine Dioxide. Part II- Lifetime Prediction. *Polymer Engineering and Science* **2009,** 49, 1642-1652.

11. Utsumi, H.; Hakoda, M.; Shimbara, S.; Nagaoka, H.; Chung, Y.; Hamada, A., Active Oxygen Species Generated During Chlorination and Ozonation. *Water Science and Technology* **1995,** 30, (9), 91-99.

12. American Public Health Association (APHA), A. W. W. A. A., Water Environment Federation (WEF). , Standard Methods for the Examination of Water and Wastewater, 22nd ed. . In 2000.

13. . Silverstein RM, W. F., Kiemle D. , *Spectrometric Identification of Organic Compounds.* . John Wiley and Sons, Inc. : New York, NY, 2005.

14. Neta, P.; Mosseri, S.; Alfassi, Z. B., Reactivities of Chlorine Atoms and Peroxyl Radicals Formed in the Radiolysis of Dichloromethane. *J. Phys. Chem* **1988,** 93, 1380-1385.

15. Jovanovic, S. V. J., I.; Josimovic, L. , *J. Am. Chem. Soc.* **1992,** 114, 9018-9021.

16. Monroe, B. M., *J. Phys. Chem* **1977,** 81, 1861-1864.

17. Smith, G.; Karlsson, K.; Gedde, U. W., Modeling of anti-oxidant loss from polyolefins in hot water applications. I: model and application of medium-density polyenthylene pipes. *Polymer Engineering and Science* **1992,** 32, (10), 658-667.

18. Frenette, M.; Scaiano, J., Evidence for Hydroxyl Radical Generation During Lipid (Linoleate) Peroxidation. *J. Am. Chem. Soc.* **2008,** 130, 9634-9635.

19. Davies, M. J., Protein and Peptide Alkoxyl Radicals Can Give Rise to C-Terminal Decarboxylation and Backbone Cleavage. *Archives of Biochemistry and Biophysics* **1996,** 336, (1), 163-172.

20. Headlam, H. A.; Davies, M. J., Beta-Scission of Side-Chain Alkoxyl Radicals on Peptides and Proteins Results in the loss of Side-Chains as Aldehydes and Ketones. *Free Radical Biology and Medicine* **2002,** 32, (11), 1171-1184.

21. Aust, A.; Eveleigh, J., Mechanisms of DNA Oxidation. *Pub. Soc. Exp. Bio. and Med.* **1999,** 222, 246-252.

22. DeFederics, H.-C.; Patrzye, M. J.; Rajecki, E. E.; Budzinski, H. I.; Dawidzik, J. B.; Evans, M. S.; Grenne, K. F.; Box, H. C., Singlet Oxygen-Induced DNA Damage. *Radiation Research* **2006,** 165, 445-451.

23. Tromans, D., Modeling Oxygen Solubility in Water and Electrolyte Solutions. *Ind. Eng. Chem. Res.* **2000,** 39, 805-812.

Chapter 3 Addendum

Two novel HDPE degradation products, 3-chloro-1,1-di-methylpropanol and 2,3-dichloro-2-methylbutane, were identified during accelerated aging studies with AO free HDPE resin. The proposed mechanism of formation in Chapter 3 (Scheme 3-3) considers a branch point as a necessary component to create these compounds. However subsequent investigation suggests that this branch point is not necessary in the creation of either molecule.

Accelerated aging studies using an oligomer of polyethylene containing no tertiary hydrogen (identified by 1HNMR: ∂0.92 (1H), ∂1.20 (8H)) were carried out in a 50 mg/L aqueous chlorine solution. After 3 days, a methylene chloride liquid/liquid extraction confirmed the presence of both 3-chloro-1,1-di-methylpropanol and 2,3-dichloro-2-methylbutane. Production of both compounds suggests that a tertiary carbon need not be initially present in order to form the tertiary halide or tertiary alcohol.

While the exact mechanism of formation for these products is unknown, some key findings can be reported from these studies:

1) GC/MS data strongly indicates the products to be a tertiary alcohol (m/z= 59 (100%)) and tertiary chlorinated compound (m/z= 77 (100%); 79 (31%)). Thus while a tertiary carbon need not be initially present for product formation, a tertiary structure is formed.

2) While products are consistently present in AO free HDPE resin and HDPE pipe aging solutions, they are not present in control solutions including: AO free HDPE resin in 0mg/L Cl_2 aqueous solution, 50 mg/L Cl_2 solution (no polymer), and CH_2Cl_2 blank

3) Authentic samples of 3-chloro-1,1-di-methylpropanol and 2,3-dichloro-2-methylbutane are necessary to confirm identification of each product

Chapter 4 Summary and Future Work

4.1 Introduction

Radical chemistry is a foundational component of atmospheric, synthetic, polymer and biological sciences. While much attention has been paid over the years to how radical reactions occur, many anomalies have not been fully addressed. Factors such as solvent effect are proving to have much more of an impact on radical chemistry than previously believed. Additionally, the high reactivity and low selectivity of radicals can have severe undesired consequences. Both the hydroxyl radical and the chlorine radical are known to be extremely reactive and unselective species. This aggressive behavior often has particularly damaging effects, making it important to understand- and when possible, protect against- undesired aspects of their reactivity. If a "slowing down" of their reactivity could be achieved, radical trapping (via anti-oxidants) might pose as a reasonable protection strategy against oxidation.

This preceding research aims to address such questions in order to get a better understanding of how radicals react. Through direct examination of radical reactions, as well as radical effects on a polymer, we can further recognize the processes taking place.

4.2 Solvent Effect and Polarized Transition state

One of the most significant contributions to solvent effects on radical chemistry was established by Russell,[1] who found that in the presence of an aromatic solvent, the photo-initiated chlorination of 2,3-dimethylbutane yielded far different results than the same reaction in an aliphatic solvent. The chlorine radical shows a marked increase in selectivity when reacting with 2,3-dimethylbutane, in an aromatic solvent, with yields of the 2-isomer reaching up to 95% :

Simply changing the solvent system from cyclohexane to benzene increases the yield of the 2-isomer by nearly a factor of two under analogous conditions, and even further selectivity can be obtained with increasing concentration of aromatic solvent (Table 1):

Table 4-1. Percent yield of 2-chloro-2,3-dimethylbutane

Solvent (55°C)	% Yield 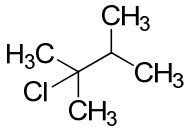
Cyclohexane (4.0 M)	37.5
Benzene (4.0 M)	70.9
Benzene (8.0 M)	84.2

Russell explains this increased selectivity on the basis of a π-complex that is formed between the free chlorine radical and the π electrons of the aromatic solvent. This complexed radical is less reactive than the free chlorine radical, and therefore exhibits greater selectivity.

The question of what causes this increased stability can be found by looking at the nature of the free chlorine radical. Chlorine is an extremely electrophilic radical. Any electron contribution that the radical can receive from a solvent will provide a degree of stabilization, thus increasing its selectivity (Figure 4-1):

Figure 4-1. π- complex stabilization of chlorine radical

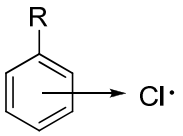

Electrophilic radicals, such as the chlorine radical or bromine radical, are also known to develop a negative charge in their transition state during hydrogen atom abstraction reactions. Similarly, the hydroxyl radical, which is also electron deficient, develops a charged transition state relative to reactants and products. The charge build-up makes solvent a contributing factor to the rate of the reaction; Similar to how the chlorine radical (reactant) is stabilized by an aromatic solvent, the transition state- which is polarized- can be stabilized by its environment.

The notion of a polarized transition state is not limited to radical addition or abstraction; Analogous trends can also be seen in homolysis reactions when there is an electronegativity gap between the dissociating atoms. Goldberg, et al. reported that during the dissociation of a H_3C—X bond (where X is an atom more electronegative than CH_3), ionization occurs, in which there is an initial charge build-up during which decreases to zero as products are formed.[2] Looking at the homolytic dissociation of the C—OH bond in methanol, the authors calculated an increase in ionization up to 1.8 angstroms, at which point ionization begins to decrease eventually leading to neutral products. Ab initio calculations showed a direct correlation between the maximum radius for ionization and bond dissociation energy; As bond dissociation energy decreases, the corrected maximum distance for ionization decreases linearly. These radical reactions illustrate that the transition state, whether early or late, may have characteristics different from both reactants and products (which remain neutral).[2]

4.3 Auto-oxidation and Chain Reactions.

The hydroxyl and chlorine radicals are extremely destructive radicals. Additionally, both have been known to be involved in chain reactions in which the reactive species is reproduced. Examples of both auto-oxidation and a chain reaction in which the radicals are reproduced are demonstrated in the degradation of HDPE (Chapter 3, Scheme 3-2 and Scheme 3-3).

Many polyethylenes are known to be susceptible to auto-oxidation. Evidence suggests that low density polyethylene will degrade in an auto-oxidative fashion when exposed to UV radiation.[3] Even cyclohexane, a small molecule of polyethylene, reacts with oxygen to undergo an auto-oxidative process.[4] In fact, auto-oxidation has been linked to the degradation of many macromolecules. Almost all biological macromolecules are susceptible to oxidative processes that create new radicals. Lipids, DNA (Chapter 4, Scheme 4-1) and proteins (Chapter 1, Scheme 1-7) all undergo similar auto-oxidative processes. It is the continuous generation of radicals that contributes to the severity of oxidative disease and macromolecule deterioration.[5-7] HDPE studies show that an aqueous solution containing 50 mg/L Cl_2 (9 mM) will start to oxidize HDPE in simply a matter of weeks. Such powerful oxidants can have devastating effects in very small doses due to their ability to propagate.

4.4 Selectivity

Clearly, both the hydroxyl and chlorine radicals are extremely aggressive. Their electrophilic nature and lack of steric hindrance cause the species to exhibit nearly no selectivity. For biomolecules such as DNA, the hydroxyl radical can extract a hydrogen from any of the five carbons of the deoxyribose sugar, and will react immediately at the location where it is formed.[8] This extreme reactivity leads not only to DNA breakdown, but the formation of additional radicals:

Scheme 4-1: Hydroxyl induced DNA oxidation. Hydroxyl attack on the C-5 carbon of the dexoyribose sugar leads to strand breakage and the formation of an aldehyde. The hydroxyl radical is reproduced in a chain reaction under aerobic conditions.

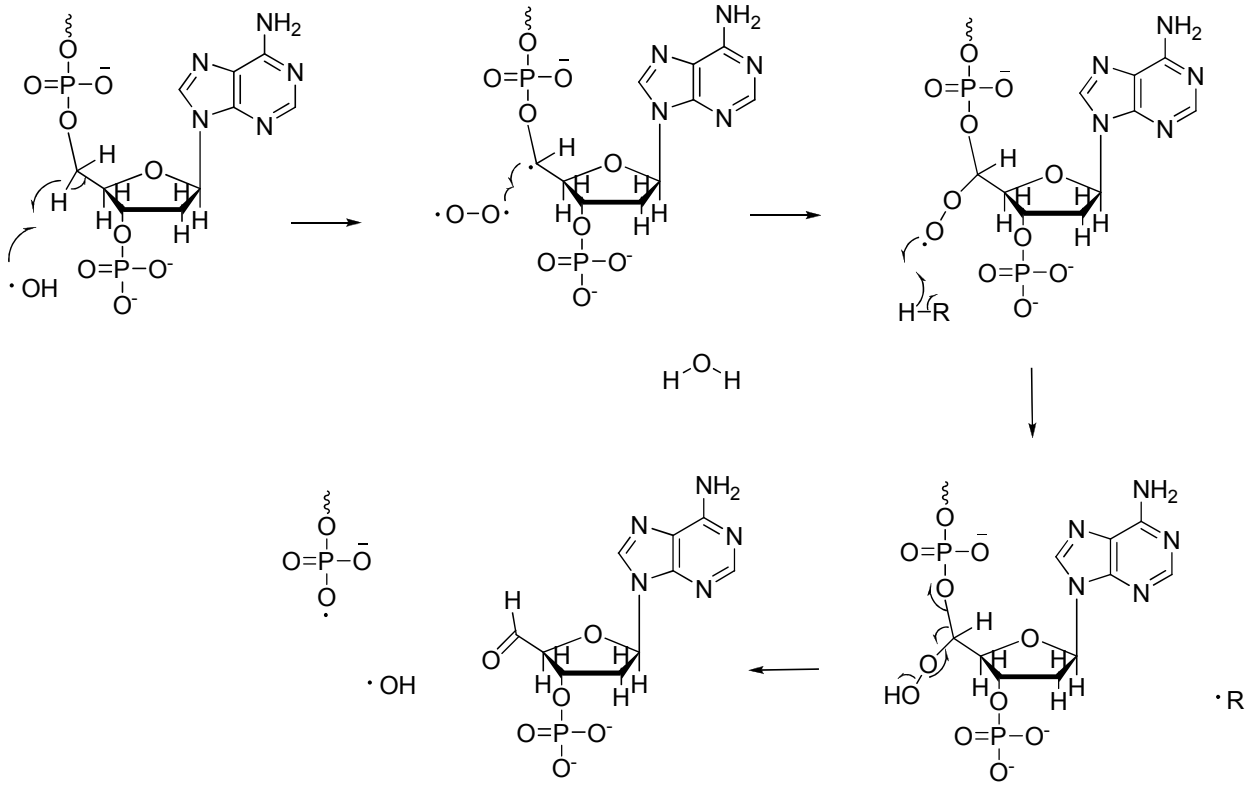

A similar lack of selectivity is seen in hyaluronan. The biomolecules, that are found in the synovial fluid of the joints, are also susceptible to non-selective hydroxyl radical attack.[9, 10] Again, under aerobic conditions the polymer degrades in an auto-oxidative type fashion, reproducing the hydroxyl radical in a chain mechanism.

The chlorine radical's reactivity is also known to be instantaneous, with relative rates for hydrogen abstraction of 3.5 to 1 for tertiary and primary hydrogens and reaction rate constants at near the diffussion-controlled limit.[11] As such, both of these radicals have the ability to be

extremely destructive. The lack of selectivity exhibited by these radicals makes trapping nearly impossible. In order to make any kind of anti-oxidant defense useful, a degree of selectivity must be obtained.

The results of Russell, as well as the results from this work, indicate that obtaining a certain degree of selectivity might be possible, even for these extremely reactive radicals.
If radicals can be trapped, the results would be quite significant; In addition to reducing the immediate damage from the radical, the continuous production of these species would be eliminated.

4.5 Future Work

4.5.1 Oxygen Centered Radicals

While it is likely that the transition state polarization exhibited by the hydroxyl radical would be a characteristic of all hydrogen atom abstraction reactions from alkoxyl radicals, the extent to which this would occur may differ. Whether an alkyl group would affect the degree of transition state polarization is unknown. With the exception of the tert-butoxyl radical, there is very little kinetic data for the reactivity of alkoxyl radicals in solution. It's also been recognized that the tert-butoxyl radical behaves differently from other alkoxyl radicals; The large tert-butyl group forces substantially increases the entropic factor of these reactions. Rather than hydrogen cleavage based on enthalpic factors (bond dissociation energies), steric effects play a large role in controlling relative reactivities of these radicals.[12, 13] Smaller alkoxyl radicals (perhaps methoxyl or ethoxyl) might also be subject to the same stabilization effects as the hydroxyl experiences.

To assess the degree of polarization of alkoxyl radicals, as well as the *relative* entropic effects, several other alkoxyl radicals need to be examined, both experimentally and

calculationally. The methoxyl, ethoxyl and isopropoxyl radicals will give insight into both the degree of polarization across alkoxyl radicals during hydrogen abstraction reactions, as well as a better understanding of how sterics effect the relative contributions of enthalpy and entropy in these reactions.

Arrhenius studies to determine the activation energies of these reactions are also needed to better qualitatively understand the degree of polarization in the transition state. It would be expected that a hydrogen abstraction reaction in acetonitrile would have a larger activation energy than the analogous reaction in water, in which the transition state is stabilized. The degree of this stabilization can be better assessed through comparison of activation energies for each reaction. Also, variable temperature experiments would enable us to test the hypothesis that the tert-butoxyl radical is entropy controlled (this hypothesis, which was developed from previous work in the Tanko lab, is based upon experiments conducted at room temperature). The experimental evidence at room temperature indicates $\Delta H^{\ddagger} < T\Delta S^{\ddagger}$. Since most of the tert-butoxyl radical is aliphatic bulk, it is thought that the transition state for H-atom abstraction is more ordered. A smaller radical may have more flexibility in terms of trajectory attack, and thus a lower $\Delta S^{\ddagger}$

Finally, the issue of hydroxyl radical reactivity with various biomolecules should be accessed directly. The fact that the hydroxyl radical proceeds through a polarized transition state indicates that perhaps it is less reactive in hydrophobic regions of the body, in which there would be no hydrogen bonding stabilization. This would suggest that anti-oxidant defense systems might be better targeted towards these regions, as the radical might be easier to trap and not continue with the auto-oxidative process. Directly monitoring a biomolecule in both an aqueous

and non-aqueous environment would be an excellent way to establish if- and how -this difference in reactivity could be used to better halt the propagating radical chain.

4.5.2 High and Low Density Polyethylenes.

Oxygen is a main contributor to the oxidation of many macromolecules, including HDPE. Though several of the species involved in the mechanistic breakdown of HDPE have been determined and a mechanism has been proposed, other reactions also occur after the initial oxidative process, leading to the presence of other functional groups such as vinylic, alcohol and chlorine sites. These oxidative markers are more difficult to detect through IR spectroscopy; As such, higher level techniques such as X-ray photoelectron spectroscopy (XPS), which can provide a better assessment of polymer surface degradation, need to be utilized.

HDPE is not conducive to other spectroscopic techniques (NMR, EPR, etc.) due to its extremely low solubility. To utilize these techniques, and better assess the complexity of the auto-oxidative process, low density polyethylene studies need to be conducted under analogous circumstances. Using a lower molecular weight polymer will allow the use of other techniques to decipher the presentation of other functionalities that may not be detectable by IR spectroscopy, and help elucidate functionalities that may be ambiguous.

References

1. Russell, G. A., *J. Am. Chem. Soc.* **1958,** 80, 4987 - 4996.
2. Hoz, S.; Basch, H.; Goldberg, M., Charge oscillation in the homolysis of MeX derivatives. *J. Am. Chem. Soc.* **1992,** 114, (11), 4364-4366.
3. Utsumi, H.; Hakoda, M.; Shimbara, S.; Nagaoka, H.; Chung, Y.; Hamada, A., Active Oxygen Species Generated During Chlorination and Ozonation. *Water Science and Technology* **1995,** 30, (9), 91-99.
4. Walling, C., Free Radicals in Solution. In Jon Wiley & Sons, Inc: New York, 1957.
5. Ihara, Y.; Chuda, M.; Kuoda, S.; Hayabara, T., Hydroxyl radical and superoxide dismutase in blood of patients with Parkinson's disease: relationship to clinical data. *Journal of Neurological Sciences* **1999,** 170, 90-95.
6. Jenner, P., Oxidative Stress in Parkinson's Disease. *Ann Neurol* **2003,** 53, (3), S26-S38.
7. Li, S. W.; Lin, T.-S.; Minteer, S.; Burke, W., 3,4-Dihydroxyphenylacetaldehyde and hydrogen peroxide generate a hydroxyl radical: possible role in Parkinson's Disease pathogenesis. *Molecular Brain Research* **2001,** 93, 1-7.
8. Aust, A.; Eveleigh, J., Mechanisms of DNA Oxidation. *Pub. Soc. Exp. Bio. and Med.* **1999,** 222, 246-252.
9. Kvam, B. J.; Fragonas, E.; Degrassi, A.; Kvam, C.; Matulova, M.; Pollesello, P.; Zanetti, F.; Vittur, F., Oxygen-Derived Free Radical (ODFR) Action on Hyaluronan (HA), on Two HA Ester Derivatives, and on the Metabolism of Articular Chondrocytes. *Experimental Cell Research* **1995,** 218, 79-86.

10. Soltes, L.; Mendichi, R.; Kogan, G.; Schiller, J.; Stankovska, M.; Arnhold, J., Degredative Action of Reactive Oxygen Species on Hyaluronan. *Biomacrocolecules* **2005,** 7, (3), 659-668.

11. Russel, G. A.; Brown, H. C., The Liquid Phase Photochlorination and Sulfuryl Chloride Chlorination of Branchedchain Hydrocarbons; the Effect of Structure on the Relative Reactivities of Tertiary Hydrogen in Free Radical Chlorinations. *J. Am. Chem. Soc.* **1955,** 77, (15), 4031-4035.

12. Finn, M.; Friedline, R.; Suleman, N. K.; Wohl, C.; Tanko, J. M., Chemistry of the t-Butoxy Radical: Evidence that Most Hydrogen Abstraction from Carbon are Entropy-Controlled. *J. Am. Chem. Soc.* **2004,** 126, (24), 7578-7584.

13. Tanko, J. M.; Friedline, R.; Suleman, N. K.; Castagnoli Jr, N., tert-Butoxyl as a Model for Radicals in Biological Systems: Caveat Emptor *J. Am. Chem. Soc.* **2001,** 123, (24), 5808-5809.

Appendix A: Supporting Material for Chapter 2 How Solvent Modulates Hydroxyl Radical Reactivity in Hydrogen Atom Abstractions

The following represents the supporting information for Chapter 2, and includes representative transient traces for each substrate examined, k_{obs} *vs*. concentration plots, the absolute energies and optimized geometries of all calculated structures, and the complete Gaussian 03 citation.

Figure 2-7. Transient signal for the buildup of **HO-TS•** at 392 nm in the presence of 0.0105 M tetramethylbutane in acetonitrile generated by laser flash photolysis of 0.65 mM PSH.

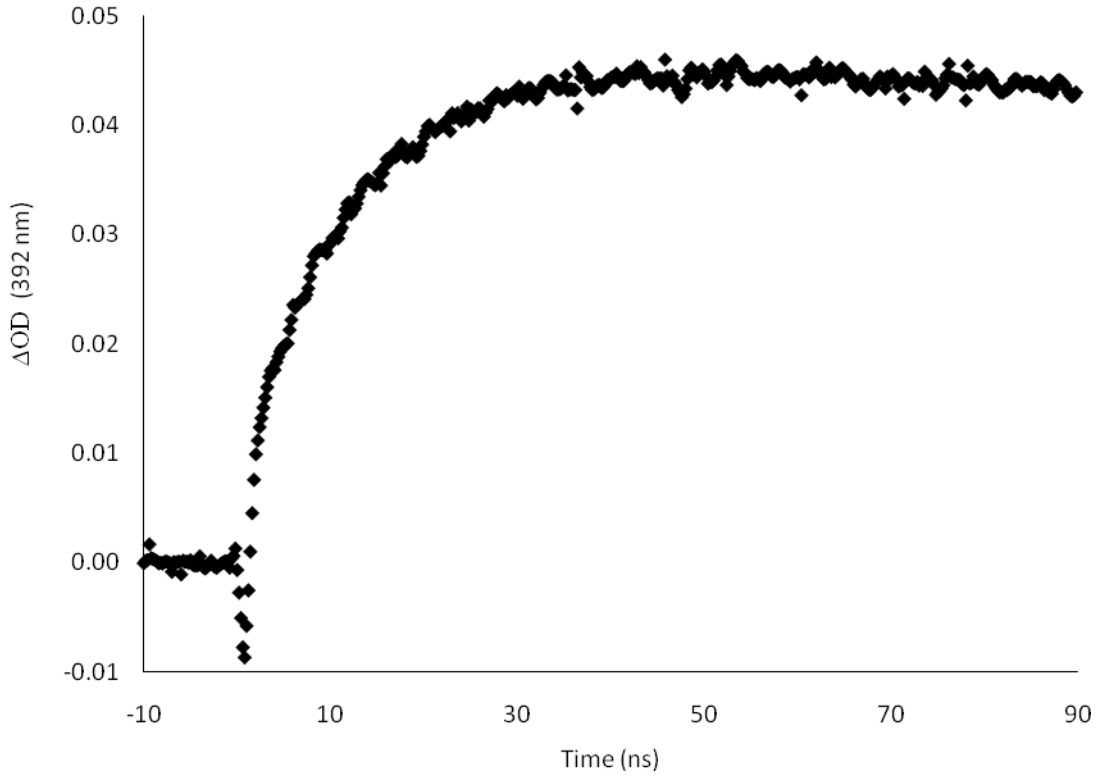

Figure 2-8. Transient signal for the buildup of **HO-TS•** at 392 nm in the presence of 0.015 M hexane in acetonitrile generated by laser flash photolysis of 0.65 mM PSH.

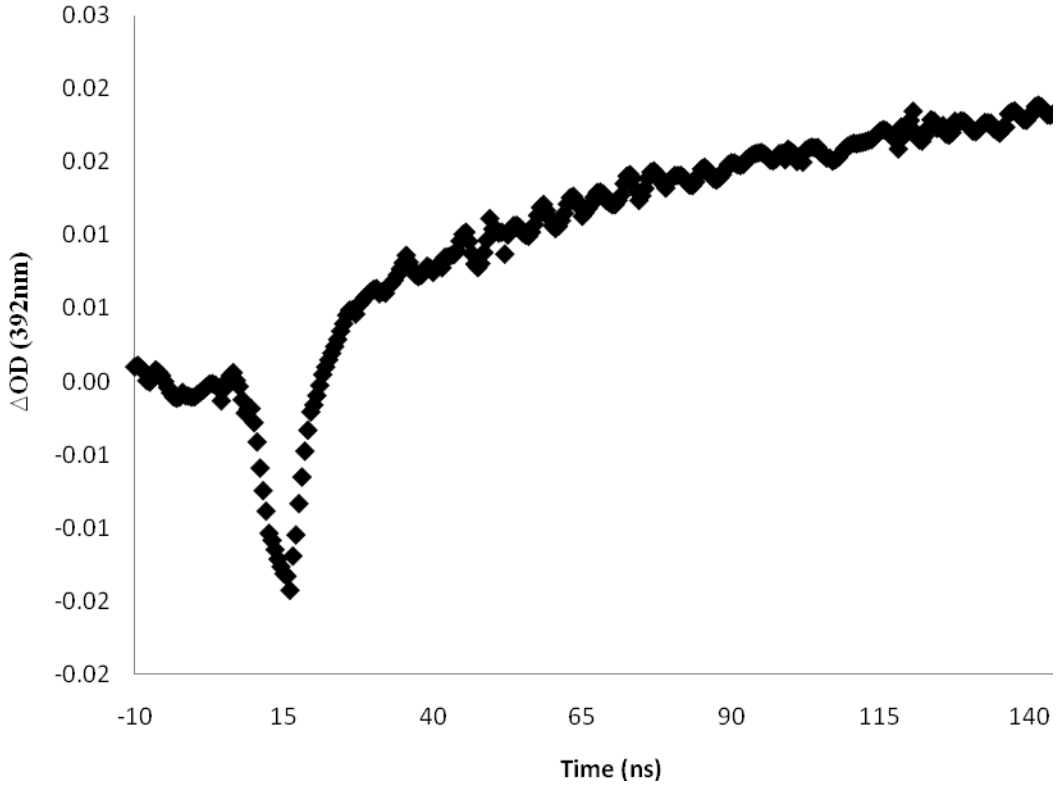

Figure 2-9. Transient signal for the buildup of **HO-TS•** at 392 nm in the presence of 0.021 M heptane in acetonitrile generated by laser flash photolysis of 0.65 mM PSH.

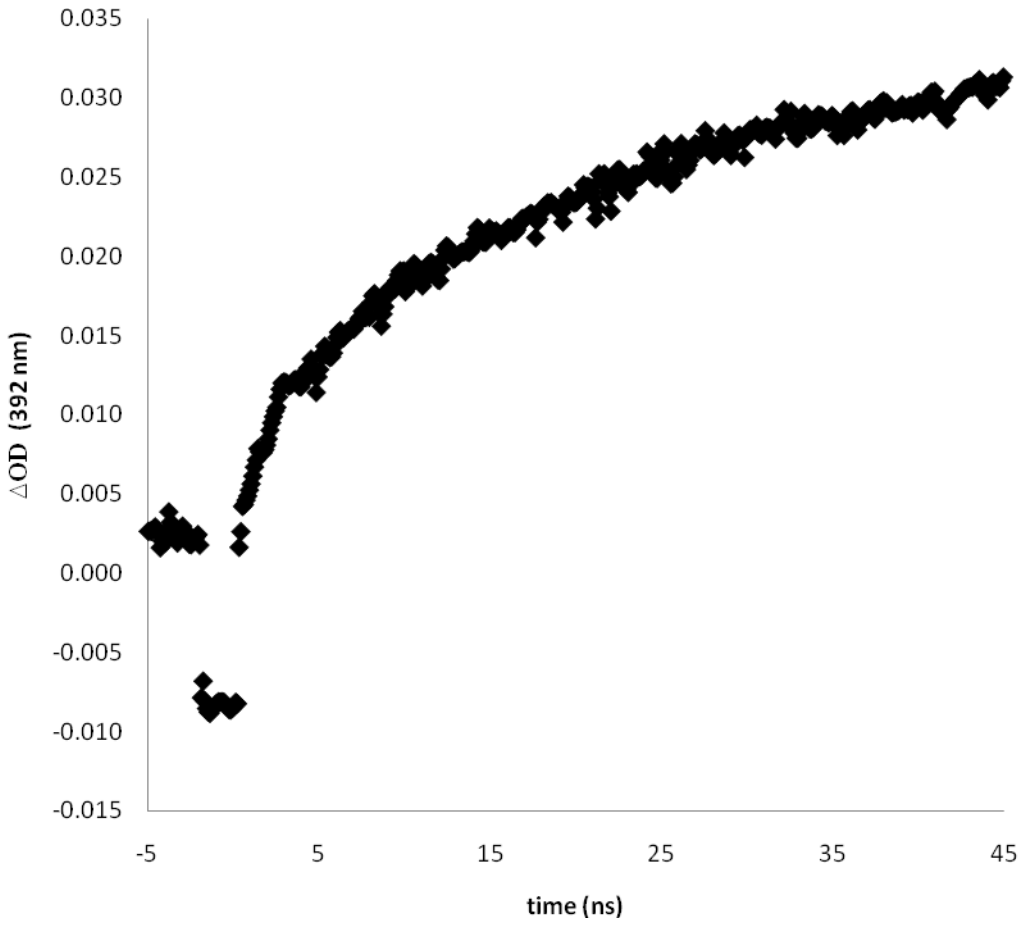

Figure 2-10. Transient signal for the buildup of **HO-TS•** at 392 nm in the presence of 0.100 M methylcyclohexane in acetonitrile generated by laser flash photolysis of 0.65 mM PSH.

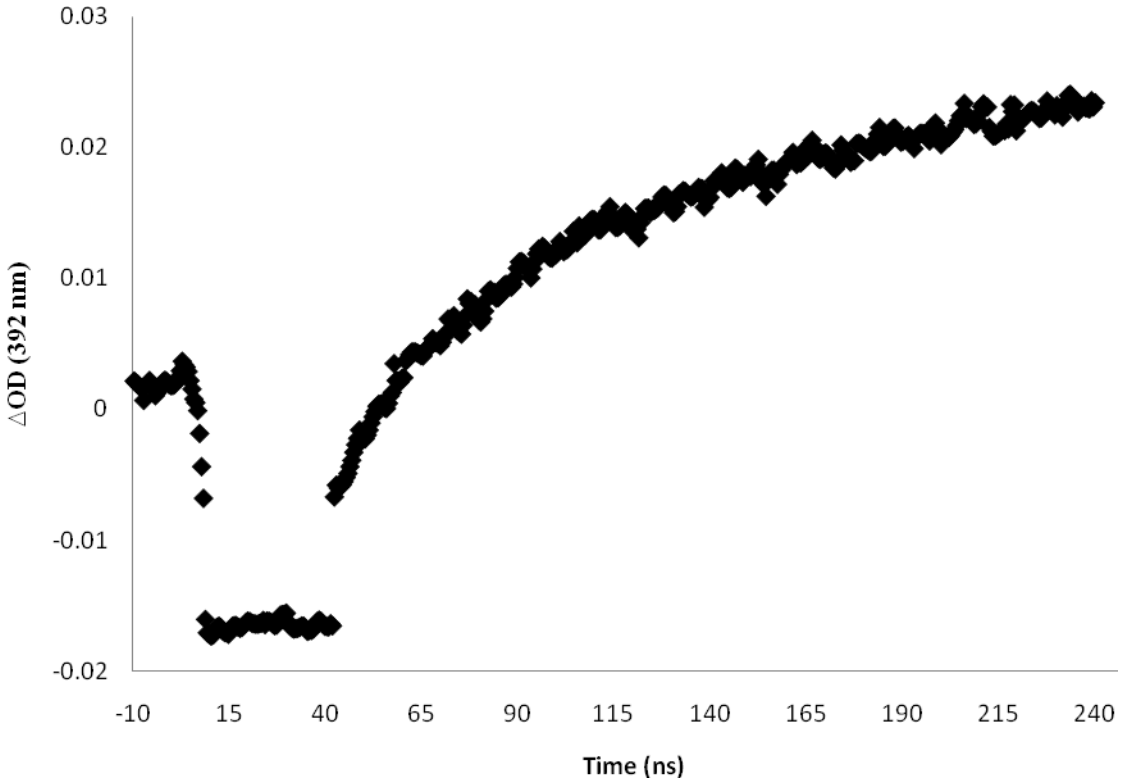

Figure 2-11. Transient signal for the buildup of **HO-TS•** at 392 nm in the presence of 0.030 M cyclohexane in acetonitrile generated by laser flash photolysis of 0.65 mM PSH.

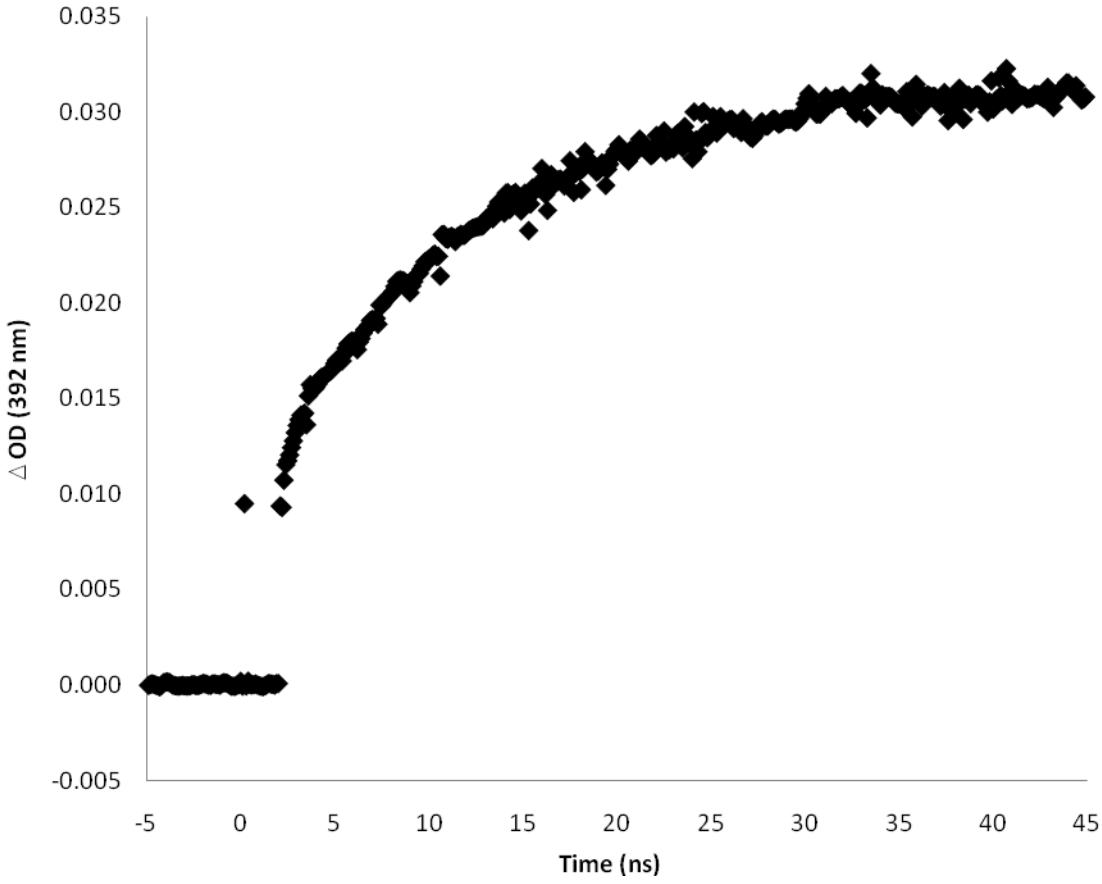

Figure 2-12. Transient signal for the buildup of **HO-TS•** at 392 nm in the presence of 0.015 M dimethylbutane in acetonitrile generated by laser flash photolysis of 0.65 mM PSH.

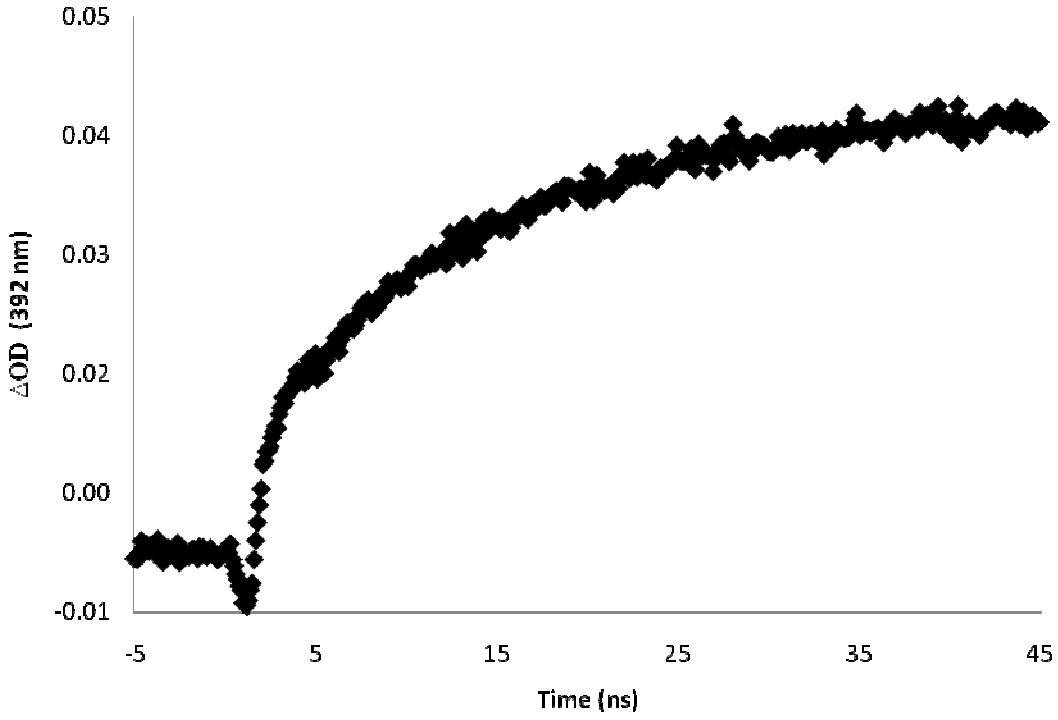

Figure 2-13. Transient signal for the buildup of **HO-TS•** at 392 nm in the presence of 0.016 M 1-butanol in acetonitrile generated by laser flash photolysis of 0.65 mM PSH.

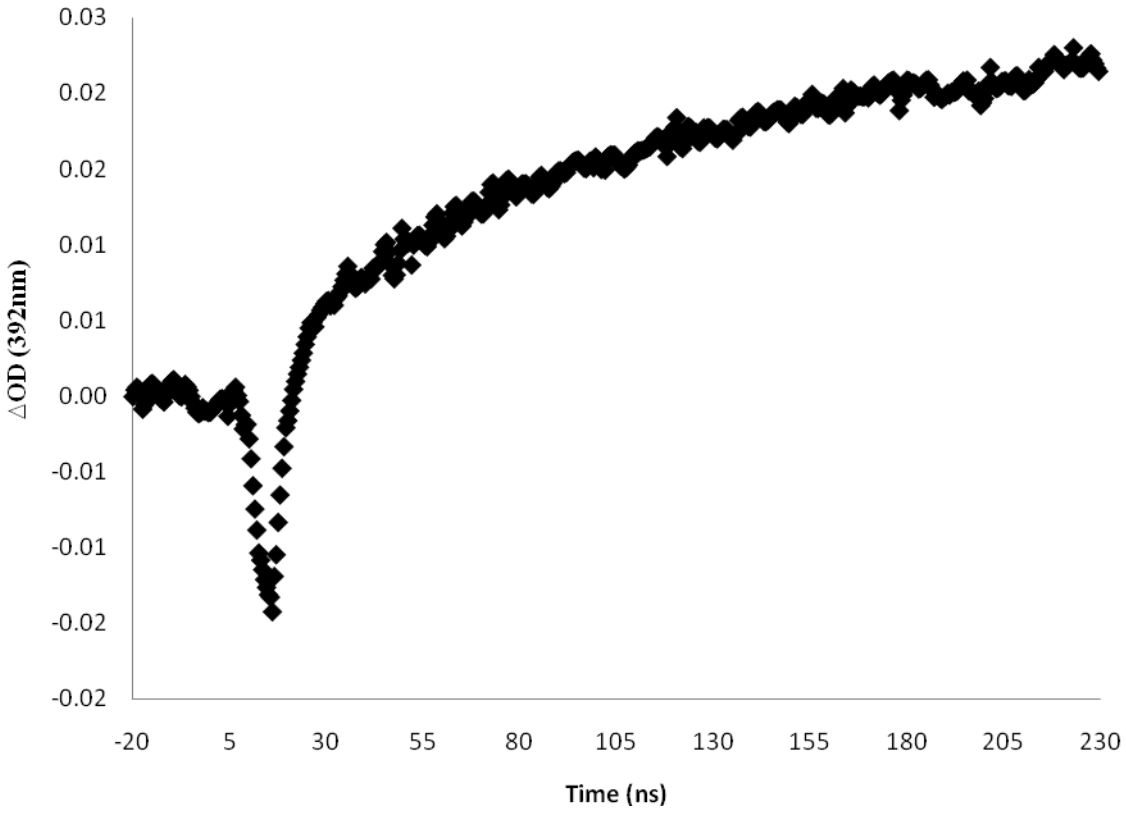

Figure 2-14. Transient signal for the buildup of **HO-TS•** at 392 nm in the presence of 0.015 M ethanol in acetonitrile generated by laser flash photolysis of 0.65 mM PSH.

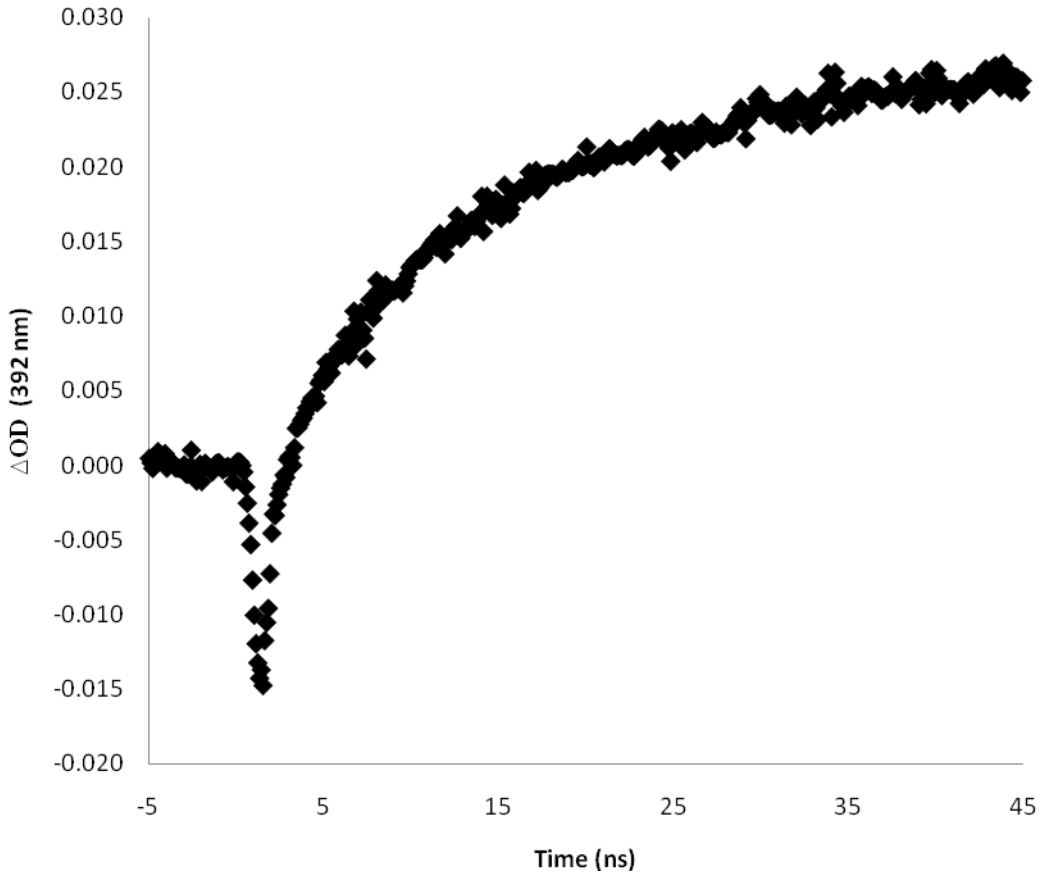

Figure 2-15. Transient signal for the buildup of **HO-TS•** at 392 nm in the presence of 0.090 M isopropanol in acetonitrile generated by laser flash photolysis of 0.65 mM PSH.

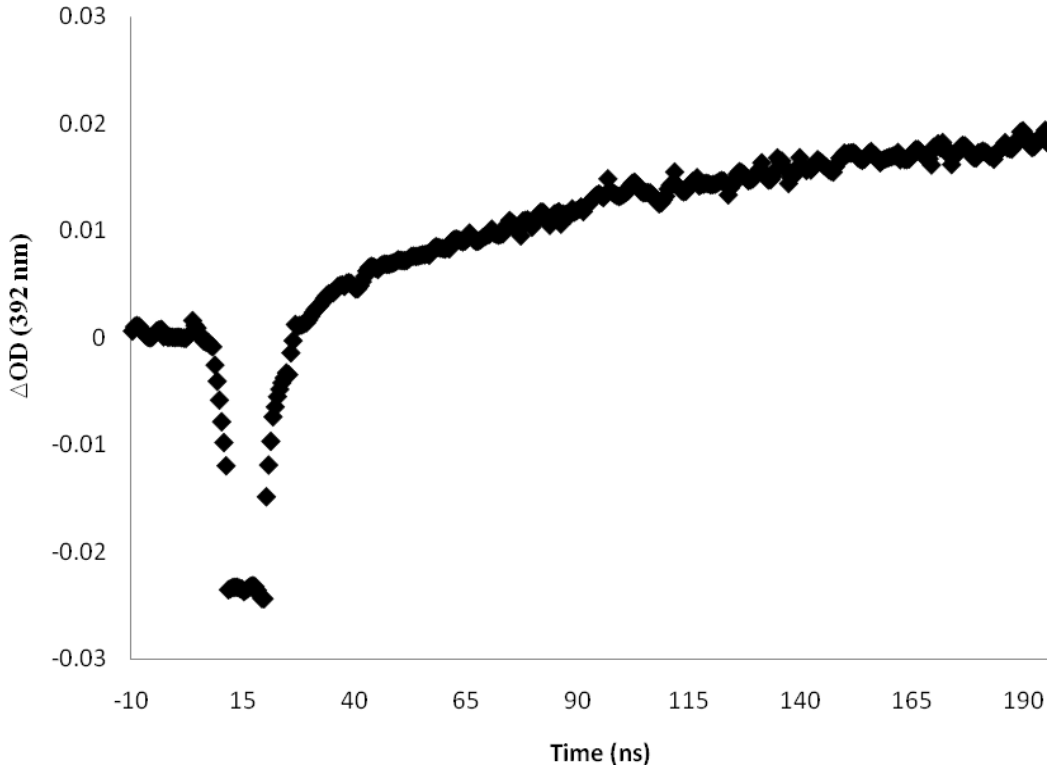

Figure 2-16. Transient signal for the buildup of **HO-TS•** at 392 nm in the presence of 0.070 M methanol in acetonitrile generated by laser flash photolysis of 0.65 mM PSH.

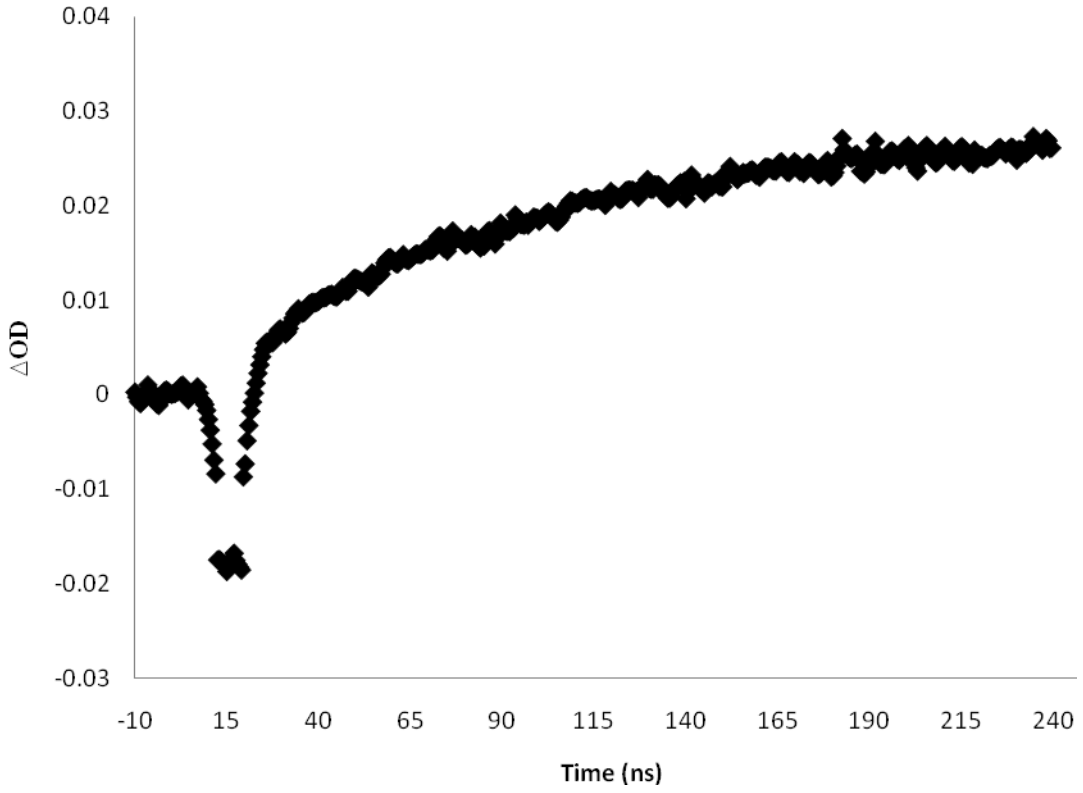

Figure 2-17. Transient signal for the buildup of **HO-TS•** at 392 nm in the presence of 0.100 M tert-butanol in acetonitrile generated by laser flash photolysis of 0.65 mM PSH.

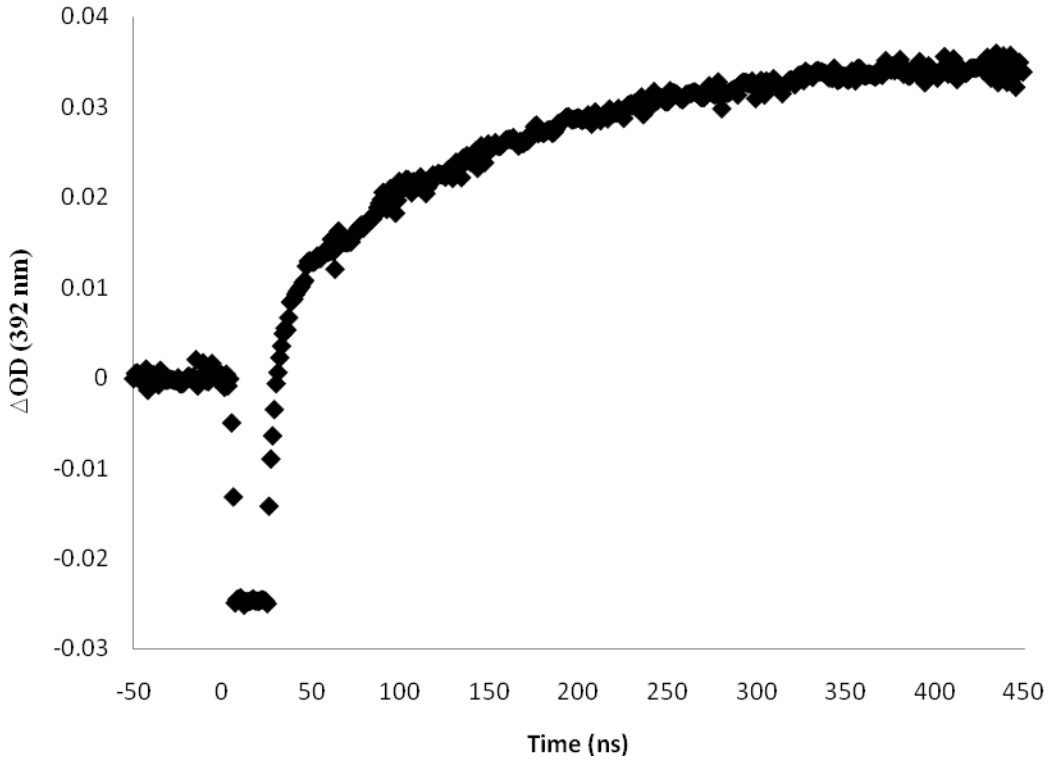

Figure 2-18. Transient signal for the buildup of **HO-TS•** at 392 nm in the presence of 0.015 M diethyl ether in acetonitrile generated by laser flash photolysis of 0.65 mM PSH.

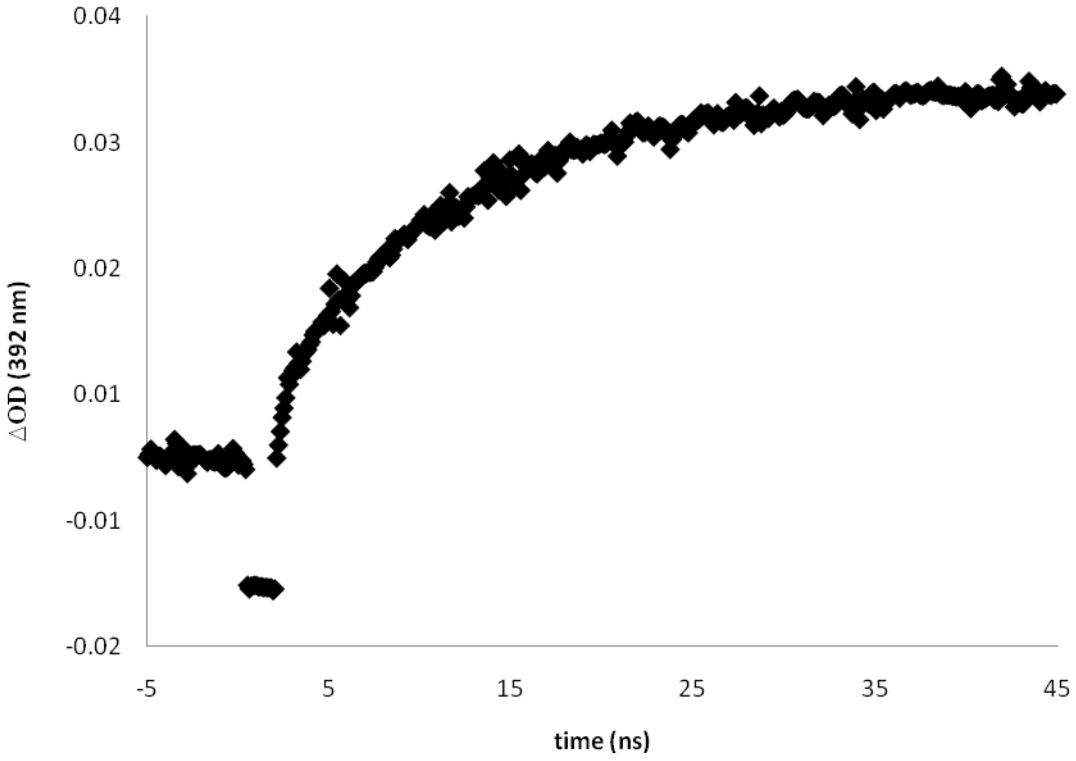

Figure 2-19. Transient signal for the buildup of **HO-TS•** at 392 nm in the presence of 0.120 M tert-butyl methyl ether in acetonitrile generated by laser flash photolysis of 0.65 mM PSH.

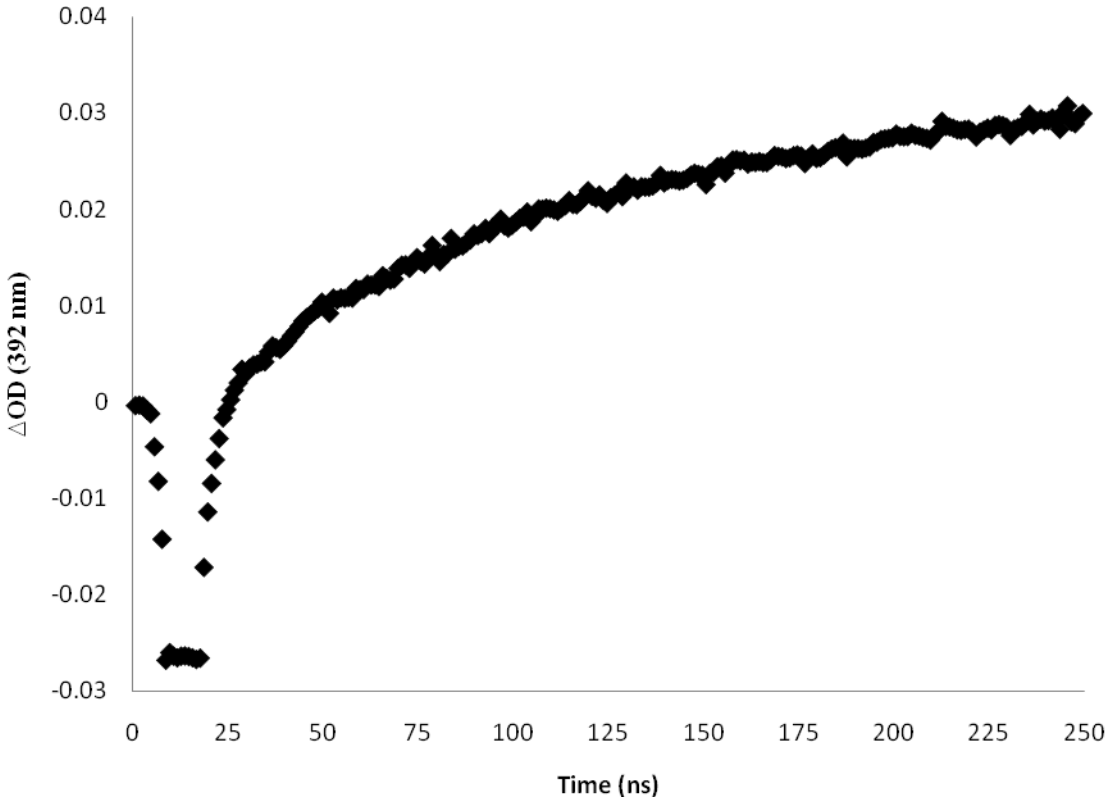

Figure 2-20. Transient signal for the buildup of **HO-TS•** at 392 nm in the presence of 0.070 M tert-butyl ethyl ether in acetonitrile generated by laser flash photolysis of 0.65 mM PSH.

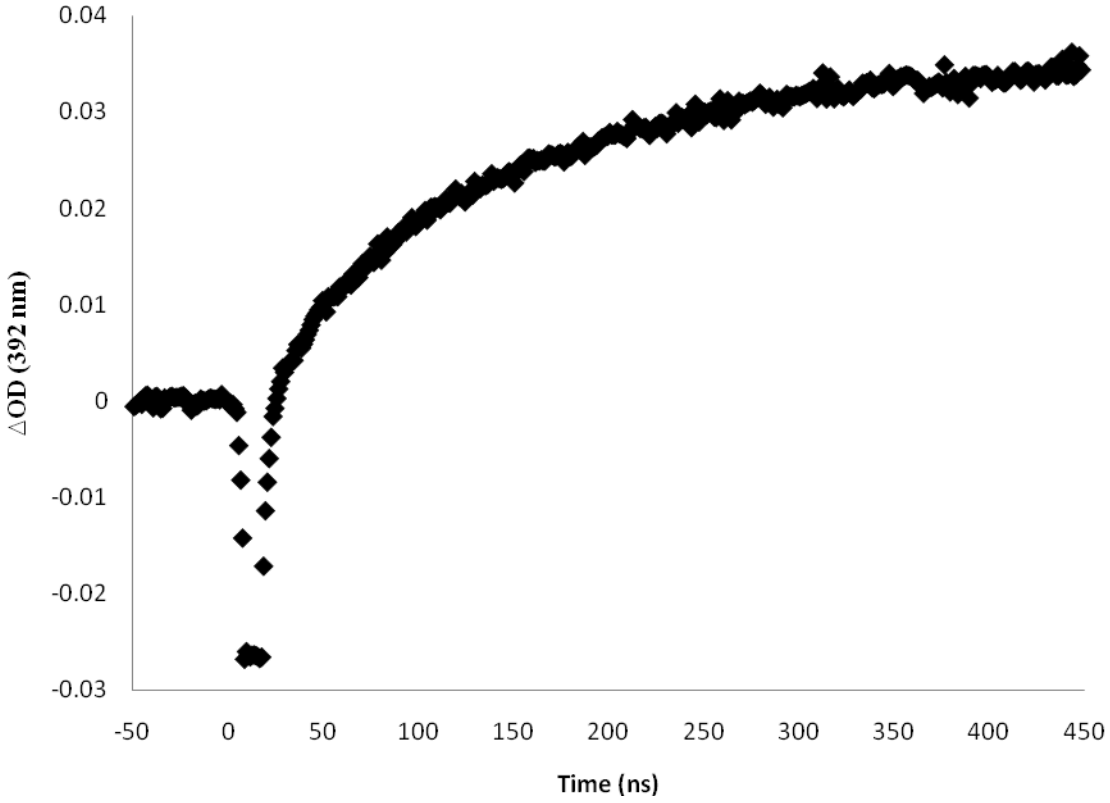

Figure 2-21. Transient signal for the buildup of **HO-TS•** at 392 nm in the presence of 0.100 M tetrahydrofuran in acetonitrile generated by laser flash photolysis of 0.65 mM PSH.

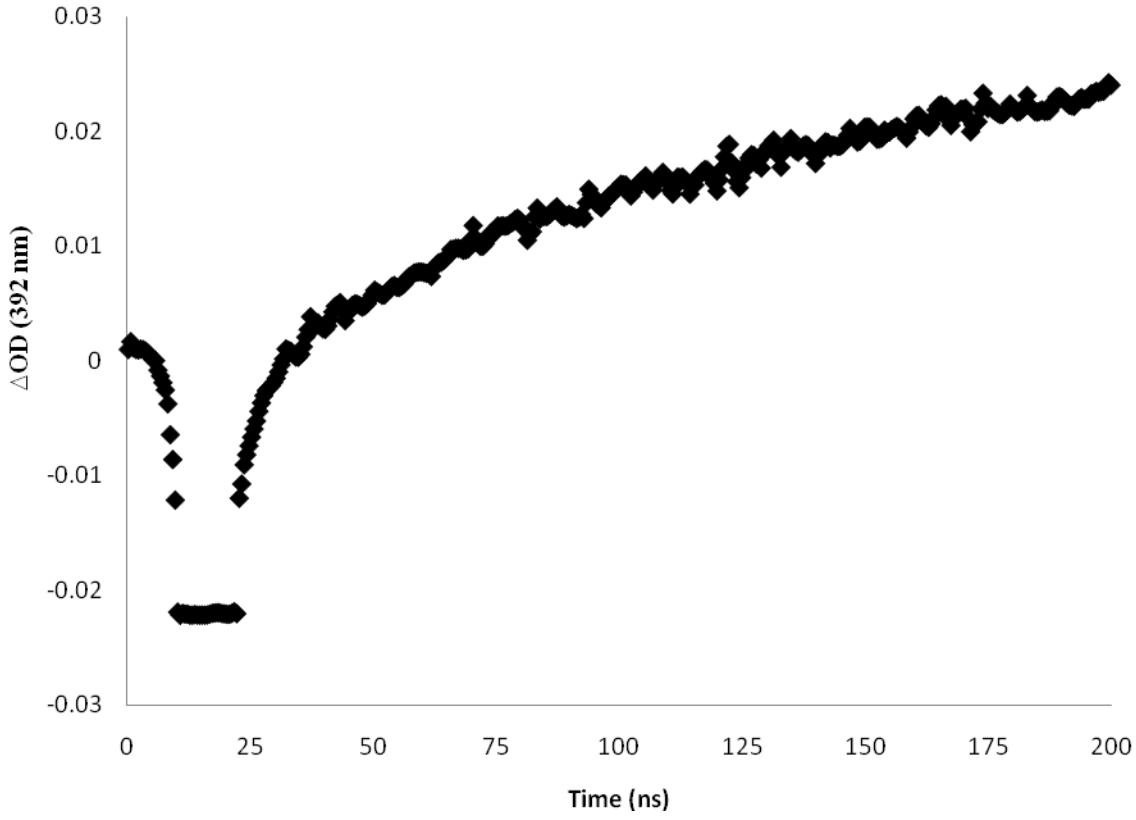

Figure 2-22. Transient signal for the buildup of **HO-TS•** at 392 nm in the presence of 0.020 M methylene chloride in acetonitrile generated by laser flash photolysis of 0.65 mM PSH.

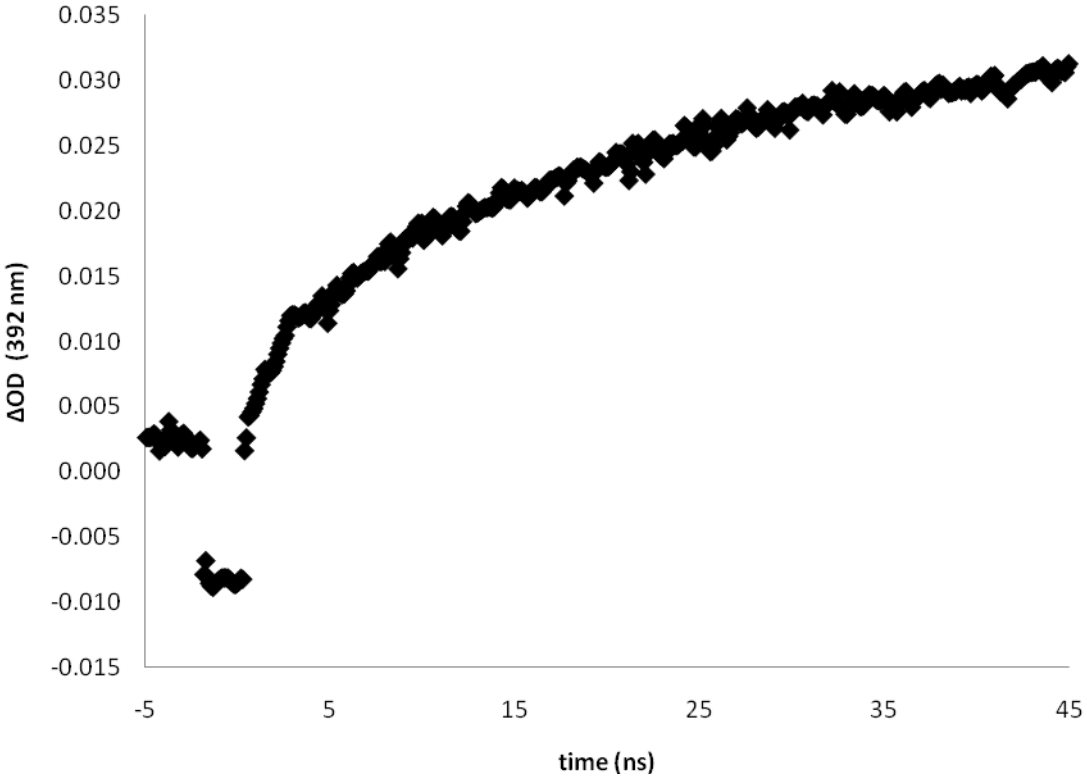

Figure 2-23. Transient signal for the buildup of **HO-TS•** at 392 nm in the presence of 0.050 M acetone in acetonitrile generated by laser flash photolysis of 0.65 mM PSH.

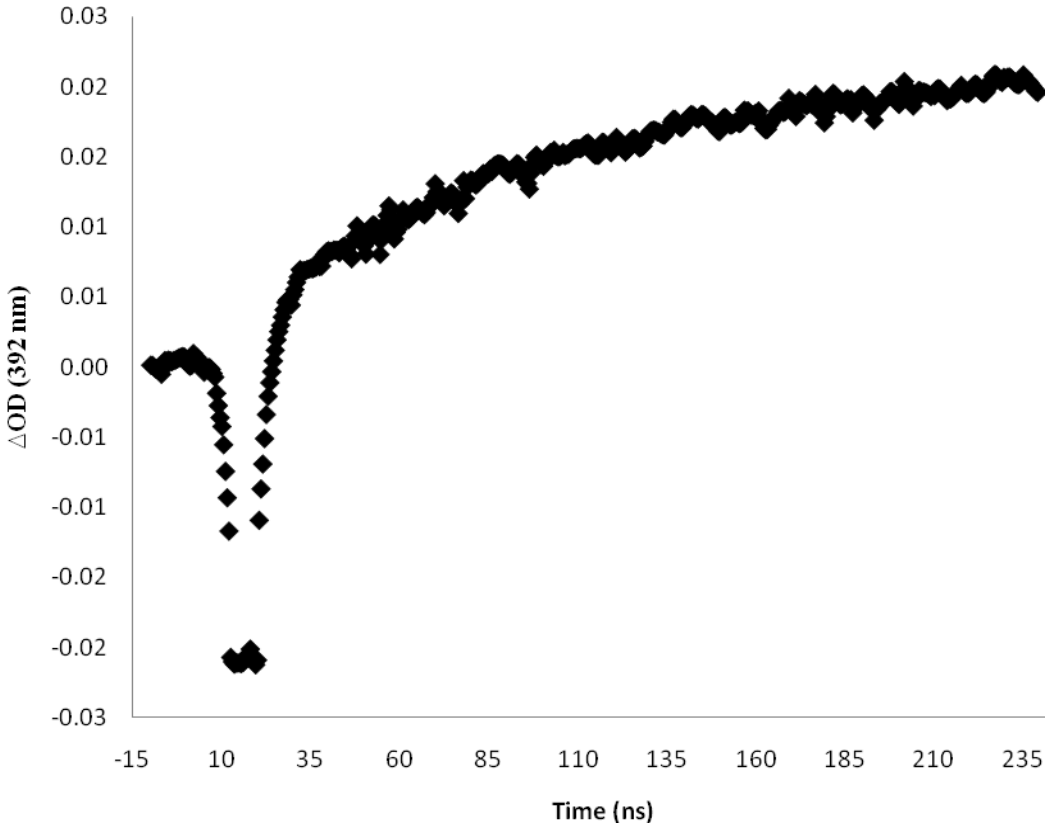

Figure 2-24. Transient signal for the buildup of **HO-TS•** at 392 nm in the presence of 0.045 M bromoform in acetonitrile generated by laser flash photolysis of 0.65 mM PSH.

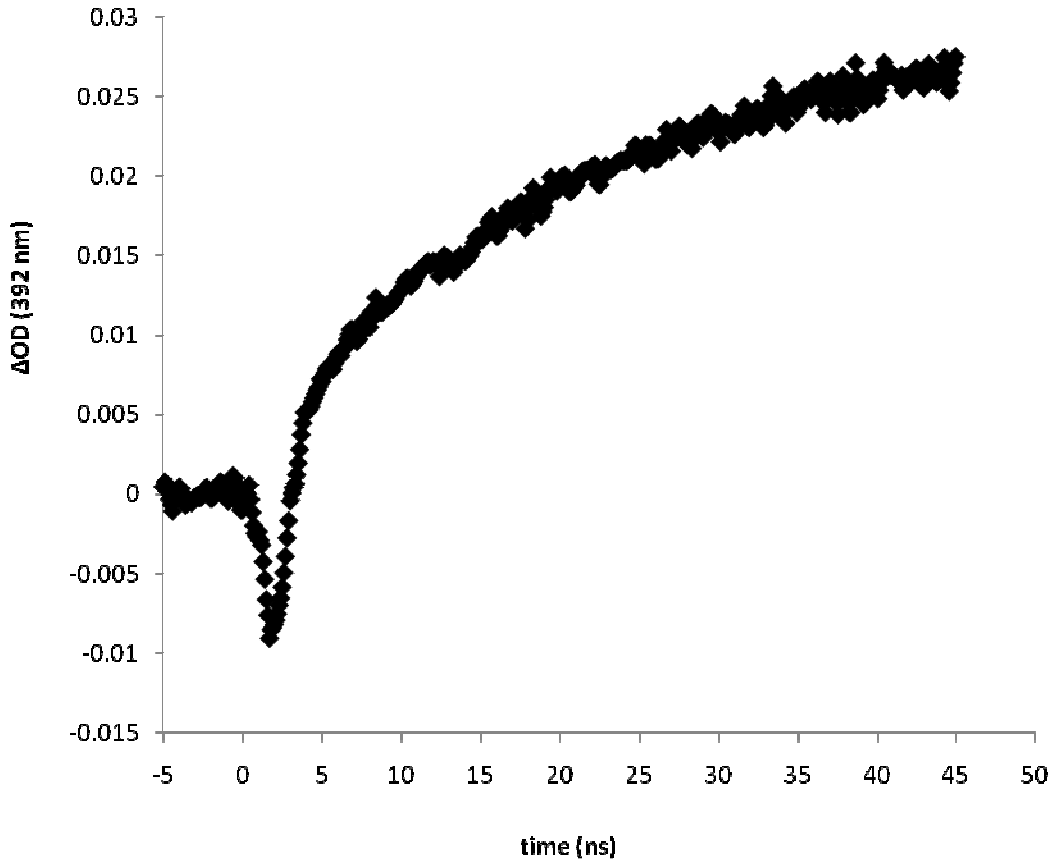

Figure 2-25. Transient signal for the buildup of **HO-TS•** at 392 nm in the presence of 0.045 M chloroform in acetonitrile generated by laser flash photolysis of 0.65 mM PSH.

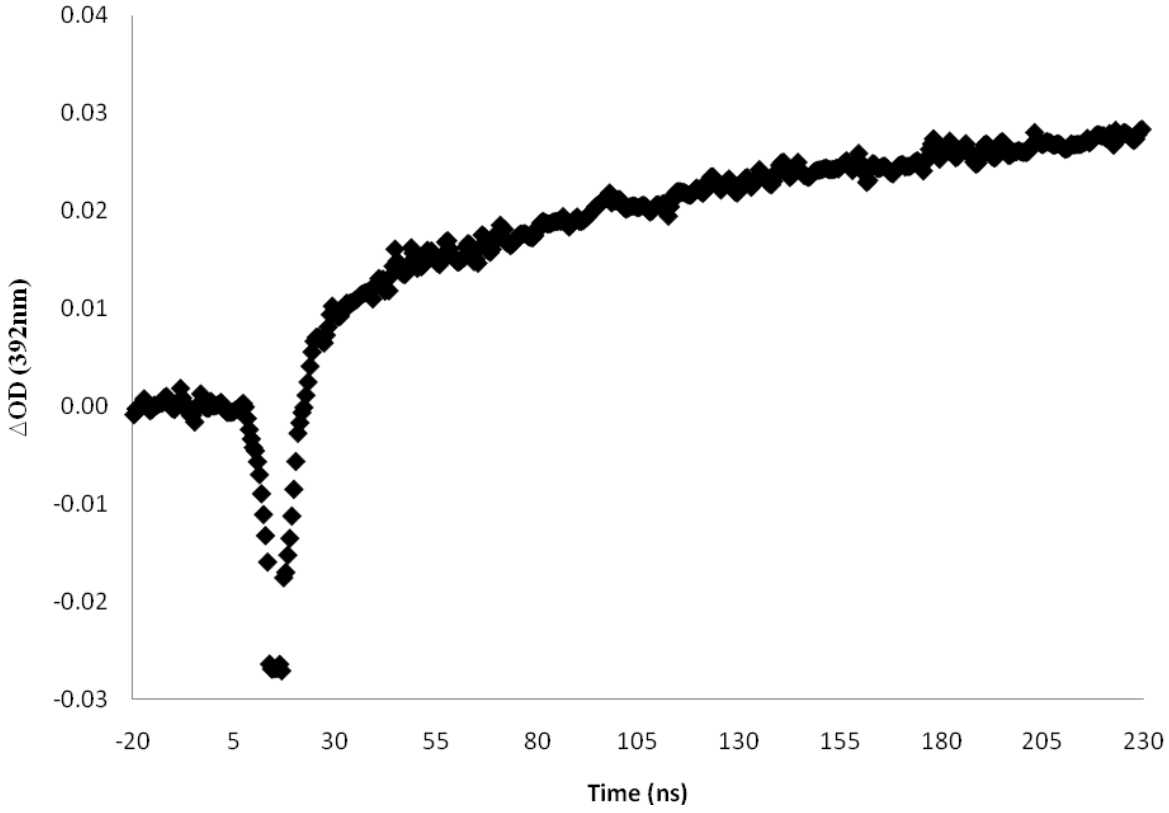

Figure 2-26. Transient signal for the buildup of **HO-TS•** at 392 nm in the presence of 0.110 M chloroacetic acid in acetonitrile generated by laser flash photolysis of 0.65 mM PSH.

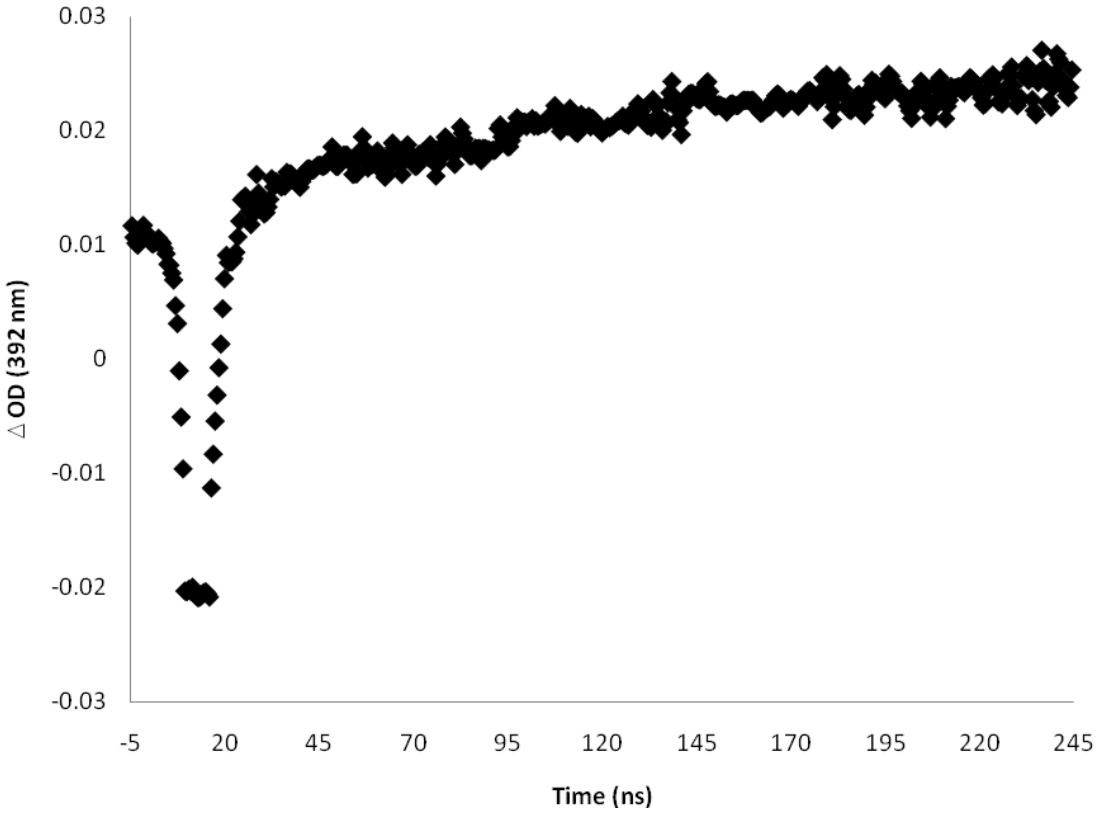

Figure 2-27. Concentration profile for the reaction of HO• with tetramethylbutane in acetonitrile in the presence of 1.5 mM trans-stilbene as a spectroscopic probe (monitoring the buildup of the 392 nm transient attributable to HO-TS•)

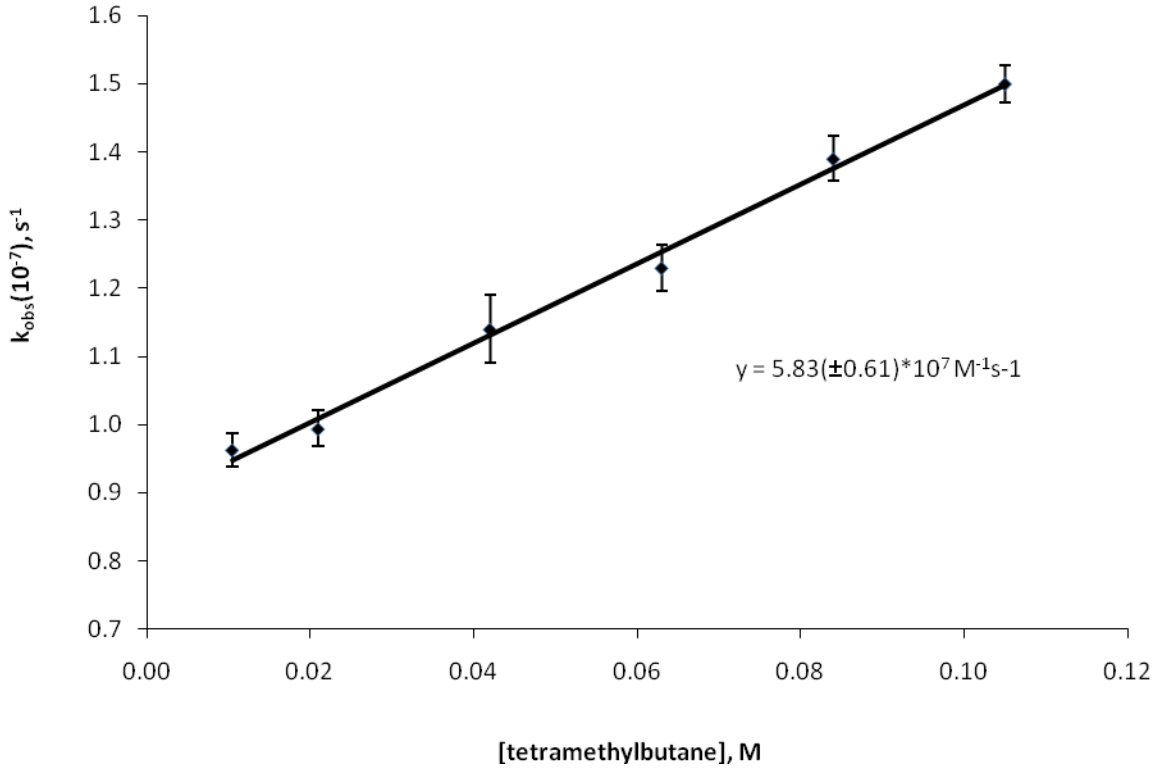

[tetramethylbutane], M	$k_{obs}(10^{-7})$, s^{-1}	Standard Deviation(10^{-7})
0.011	0.96	0.024
0.021	0.99	0.027
0.042	1.14	0.049
0.063	1.23	0.033
0.084	1.39	0.033
0.105	1.50	0.028

Figure 2-28. Concentration profile for the reaction of HO• with hexane in acetonitrile in the presence of 1.5 mM trans-stilbene as a spectroscopic probe (monitoring the buildup of the 392 nm transient attributable to **HO-TS•**)

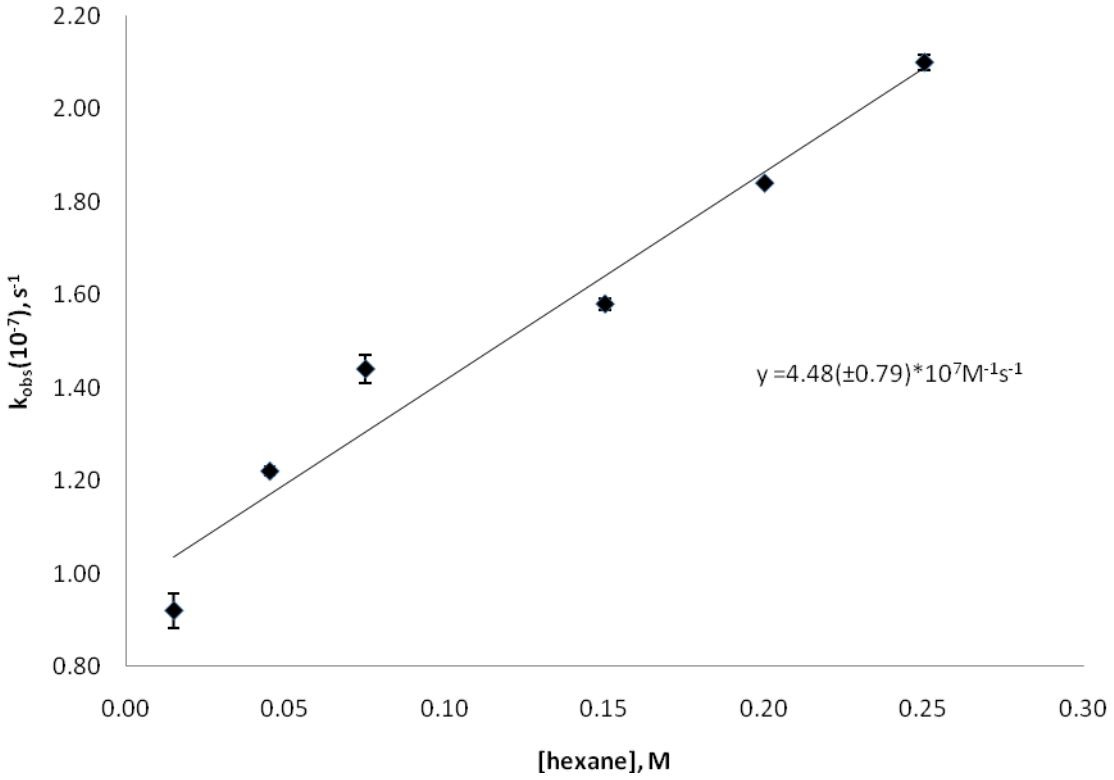

[hexane], M	$k_{obs}(10^{-7})$, s^{-1}	Standard Deviation (10^{-7})
0.015	0.92	0.037
0.045	1.22	0.010
0.075	1.44	0.030
0.150	1.58	0.013
0.200	1.84	0.005
0.250	2.10	0.016

Figure 2-29. Concentration profile for the reaction of HO• with heptane in acetonitrile in the presence of 1.5 mM trans-stilbene as a spectroscopic probe (monitoring the buildup of the 392 nm transient attributable to **HO-TS•**)

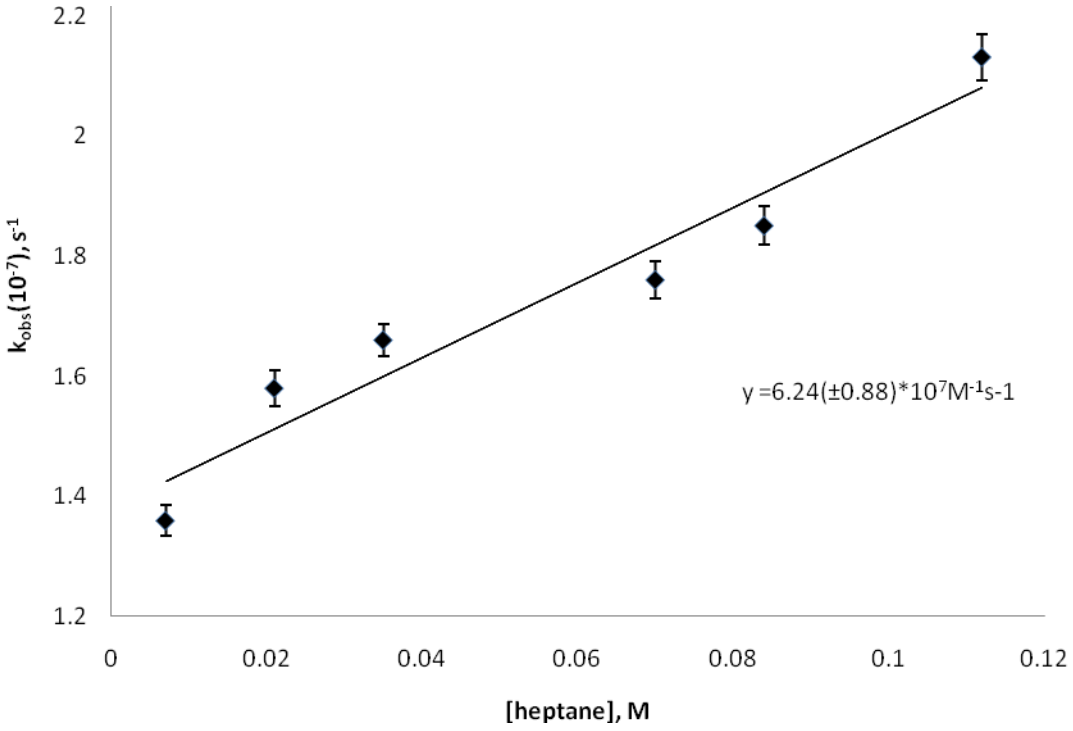

[heptane], M	$k_{obs}(10^{-7})$, s^{-1}	Standard Deviation(10^{-7})
0.007	1.36	0.026
0.021	1.58	0.030
0.035	1.66	0.026
0.070	1.76	0.030
0.084	1.85	0.032
0.112	2.13	0.038

Figure 2-30. Concentration profile for the reaction of HO• with methylcyclohexane in acetonitrile in the presence of 1.5 mM trans-stilbene as a spectroscopic probe (monitoring the buildup of the 392 nm transient attributable to **HO-TS•**)

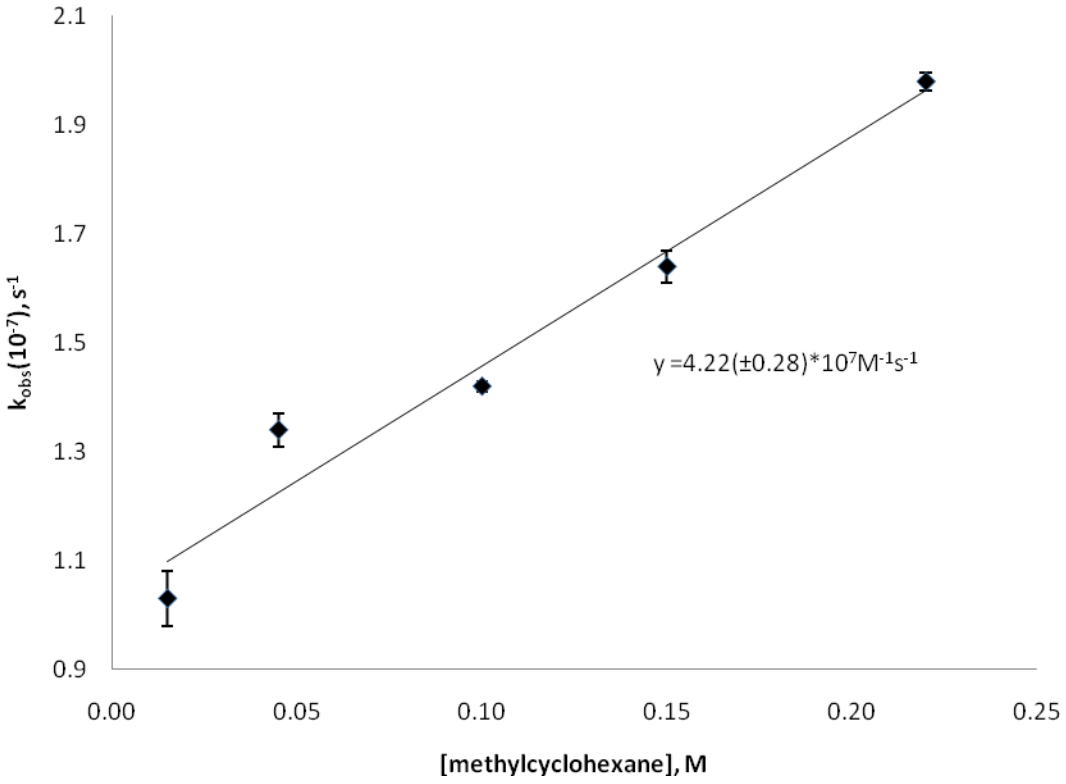

[methylcyclohexane], M	$k_{obs}(10^{-7})$, s^{-1}	Standard Deviation (10^{-7})
0.015	1.03	0.050
0.045	1.34	0.030
0.100	1.42	0.010
0.150	1.64	0.030
0.220	1.98	0.016

\

Figure 2-31. Concentration profile for the reaction of HO• with cyclohexane in acetonitrile in the presence of 1.5 mM trans-stilbene as a spectroscopic probe (monitoring the buildup of the 392 nm transient attributable to **HO-TS•**)

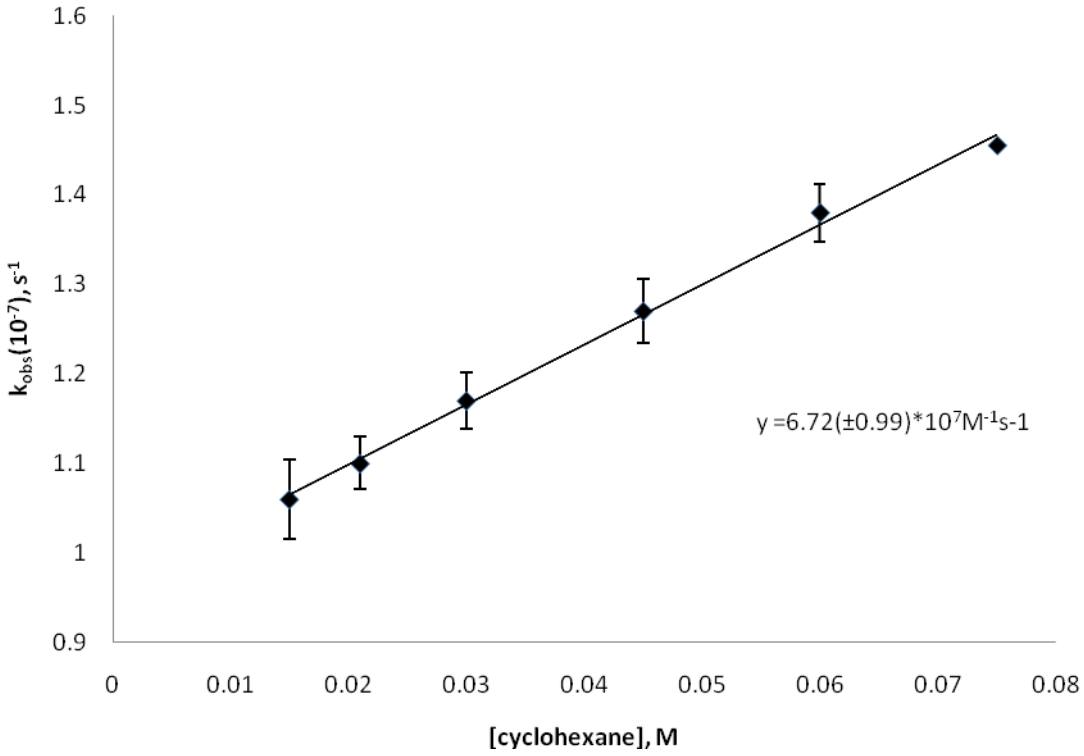

[cyclohexane], M	$k_{obs}(10^{-7})$, s^{-1}	Standard Deviation(10^{-7})
0.015	1.06	0.031
0.021	1.10	0.044
0.030	1.17	0.029
0.045	1.27	0.032
0.060	1.38	0.036
0.075	1.46	0.032

Figure 2-32. Concentration profile for the reaction of HO• with dimethylbutane in acetonitrile in the presence of 1.5 mM trans-stilbene as a spectroscopic probe (monitoring the buildup of the 392 nm transient attributable to **HO-TS•**)

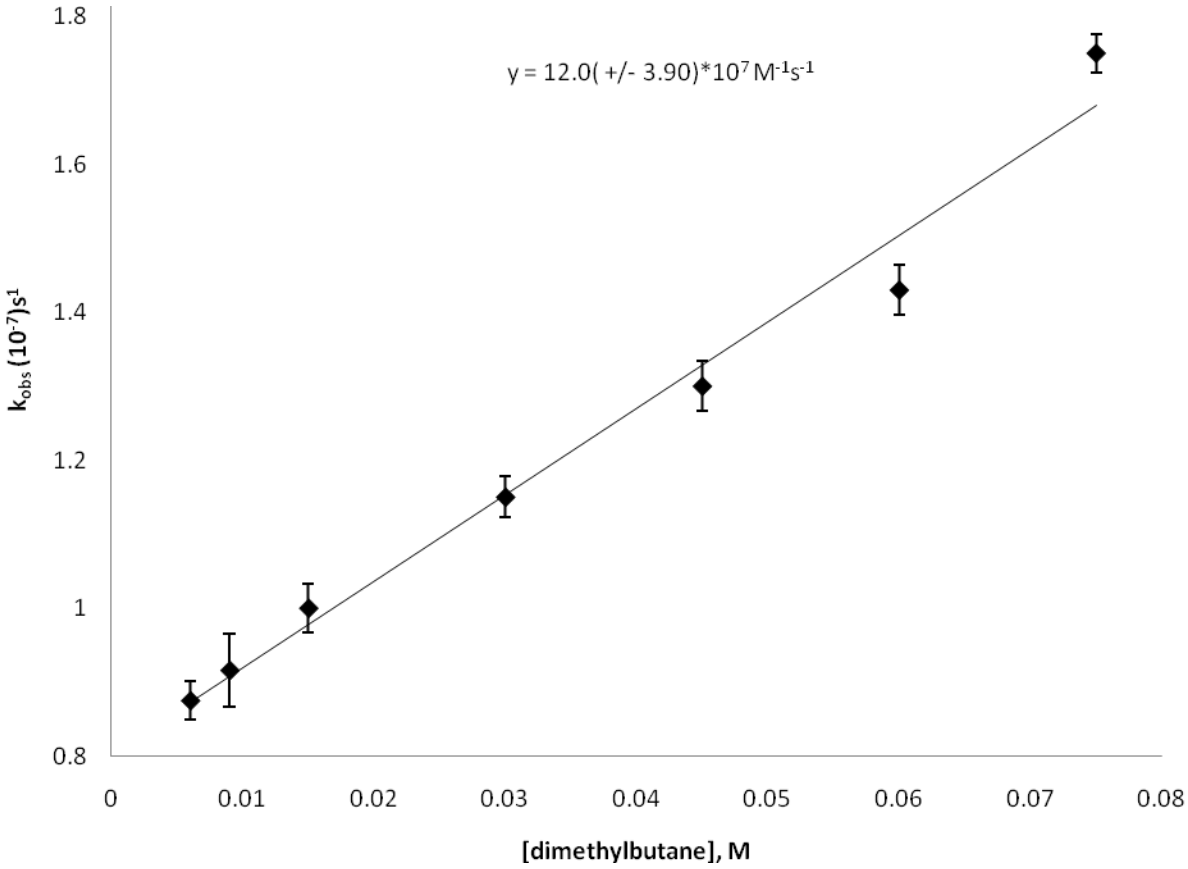

[dimethylbutane], M	$k_{obs}(10^{-7})$, s^{-1}	Standard Deviation (10^{-7})
0.006	0.88	0.026
0.009	0.92	0.049
0.015	1.00	0.033
0.030	1.15	0.033
0.045	1.30	0.028
0.060	1.43	0.033
0.075	1.75	0.033

Figure 2-33. Concentration profile for the reaction of HO• with 1-butanol in acetonitrile in the presence of 1.5 mM trans-stilbene as a spectroscopic probe (monitoring the buildup of the 392 nm transient attributable to **HO-TS•**)

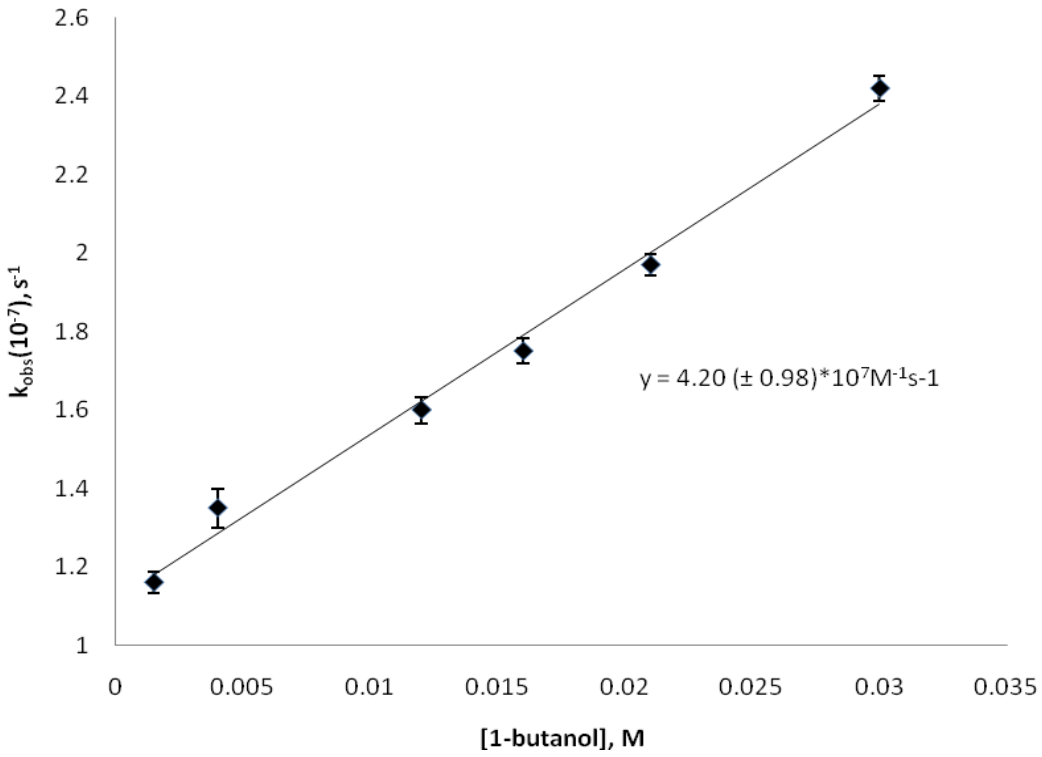

[1-butanol], M	$k_{obs}(10^{-7})$, s^{-1}	Standard Deviation(10^{-7})
0.002	1.16	0.026
0.004	1.35	0.049
0.012	1.60	0.033
0.016	1.75	0.033
0.021	1.97	0.028
0.030	2.42	0.033

Figure 2-34. Concentration profile for the reaction of HO• with ethanol in acetonitrile in the presence of 1.5 mM trans-stilbene as a spectroscopic probe (monitoring the buildup of the 392 nm transient attributable to **HO-TS•**)

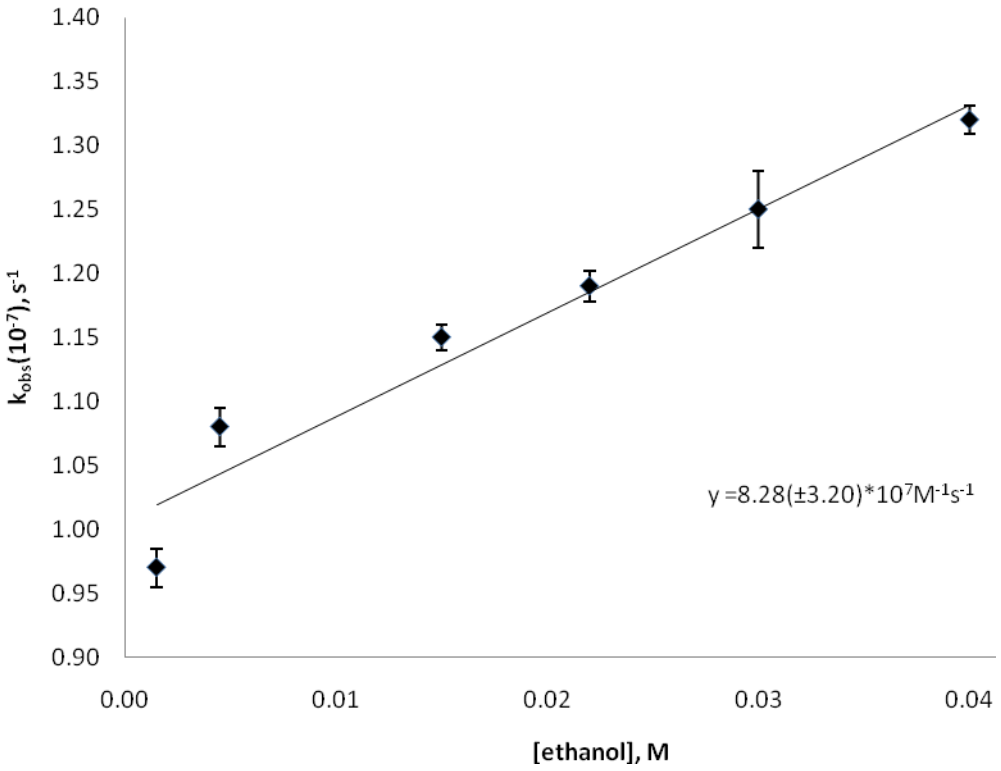

[ethanol], M	$k_{obs}(10^{-7})$, s^{-1}	Standard Deviation (10^{-7})
0.002	0.97	0.015
0.005	1.08	0.015
0.015	1.15	0.010
0.022	1.19	0.012
0.030	1.25	0.030
0.040	1.32	0.011

Figure 2-35. Concentration profile for the reaction of HO• with isopropanol in acetonitrile in the presence of 1.5 mM trans-stilbene as a spectroscopic probe (monitoring the buildup of the 392 nm transient attributable to **HO-TS•**)

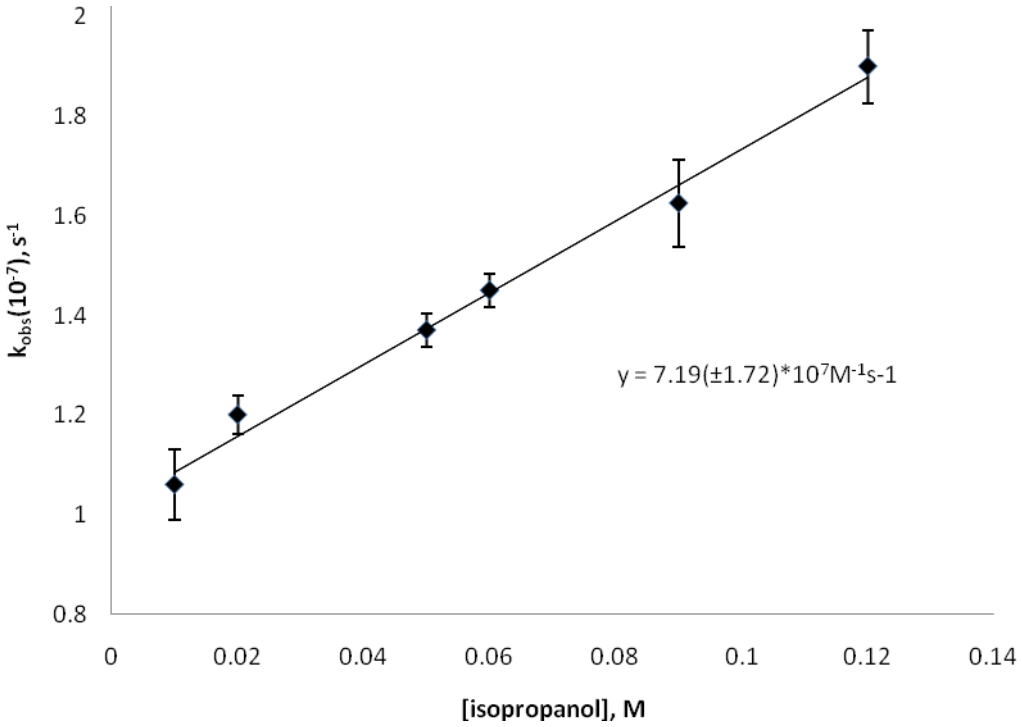

[iso-propanol], M	$k_{obs}(10^{-7})$, s^{-1}	Standard Deviation(10^{-7})
0.010	1.06	0.070
0.020	1.20	0.039
0.050	1.37	0.033
0.060	1.45	0.033
0.090	1.63	0.088
0.120	1.90	0.073

Figure 2-36. Concentration profile for the reaction of HO• with methanol in acetonitrile in the presence of 1.5 mM trans-stilbene as a spectroscopic probe (monitoring the buildup of the 392 nm transient attributable to **HO-TS•**)

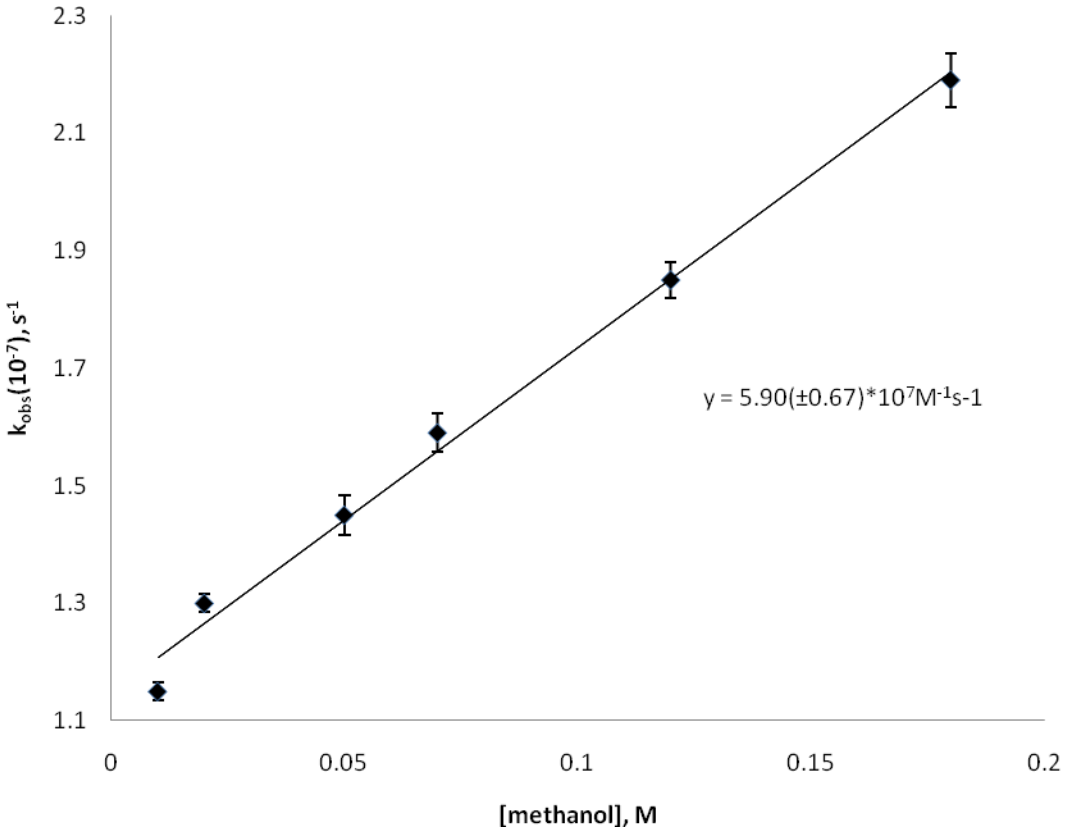

[methanol], M	$k_{obs}(10^{-7})$, s^{-1}	Standard Deviation(10^{-7})
0.010	1.15	0.015
0.020	1.30	0.015
0.050	1.45	0.033
0.070	1.59	0.033
0.120	1.85	0.030
0.180	2.19	0.045

Figure 2-37. Concentration profile for the reaction of HO• with tert-butanol in acetonitrile in the presence of 1.5 mM trans-stilbene as a spectroscopic probe (monitoring the buildup of the 392 nm transient attributable to **HO-TS•**)

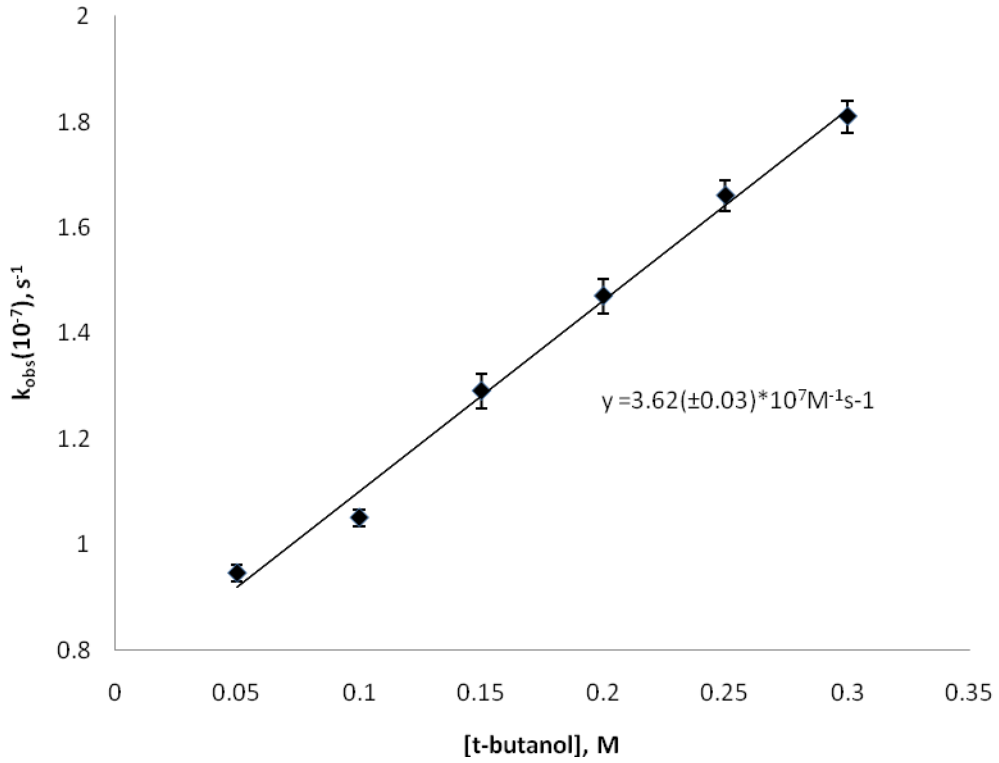

[t-butanol], M	$k_{obs}(10^{-7})$, s^{-1}	Standard Deviation(10^{-7})
0.050	0.95	0.015
0.100	1.05	0.015
0.150	1.29	0.033
0.200	1.47	0.033
0.250	1.66	0.030
0.300	1.81	0.030

Figure 2-38. Concentration profile for the reaction of HO• with diethyl ether in acetonitrile in the presence of 1.5 mM trans-stilbene as a spectroscopic probe (monitoring the buildup of the 392 nm transient attributable to **HO-TS•**)

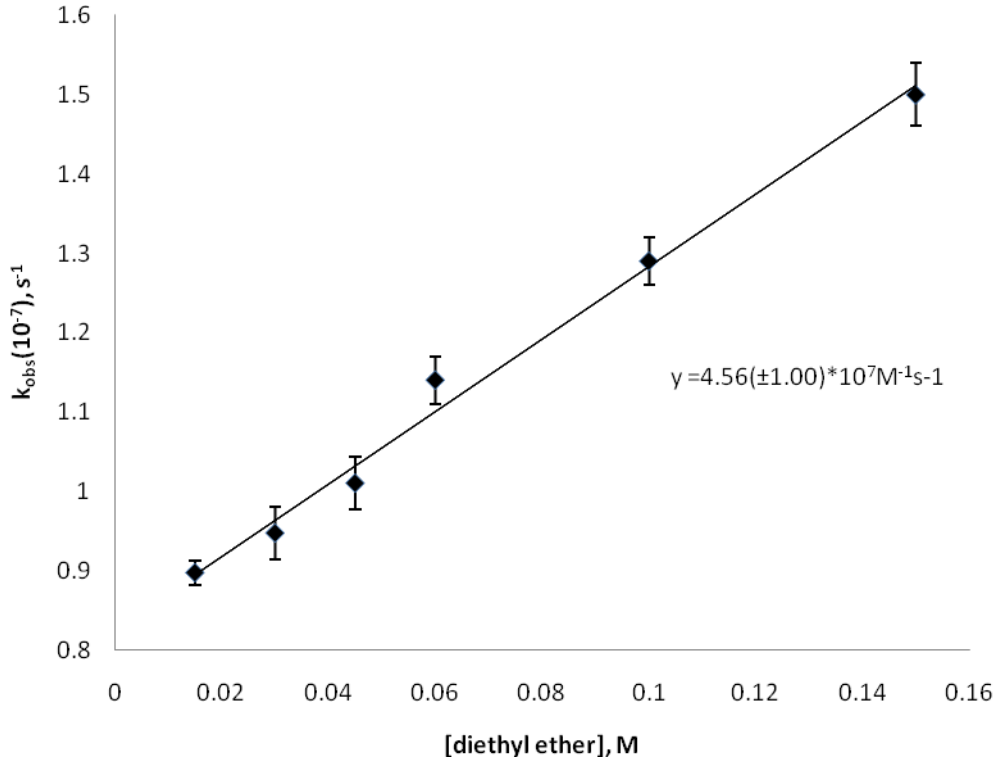

[diethyl ether], M	$k_{obs}(10^{-7})$, s^{-1}	Standard Deviation(10^{-7})
0.015	0.90	0.015
0.030	0.95	0.033
0.045	1.01	0.033
0.060	1.14	0.030
0.100	1.29	0.030
0.150	1.50	0.040

Figure 2-39. Concentration profile for the reaction of HO• with tert-butyl methyl ether in acetonitrile in the presence of 1.5 mM trans-stilbene as a spectroscopic probe (monitoring the buildup of the 392 nm transient attributable to **HO-TS•**)

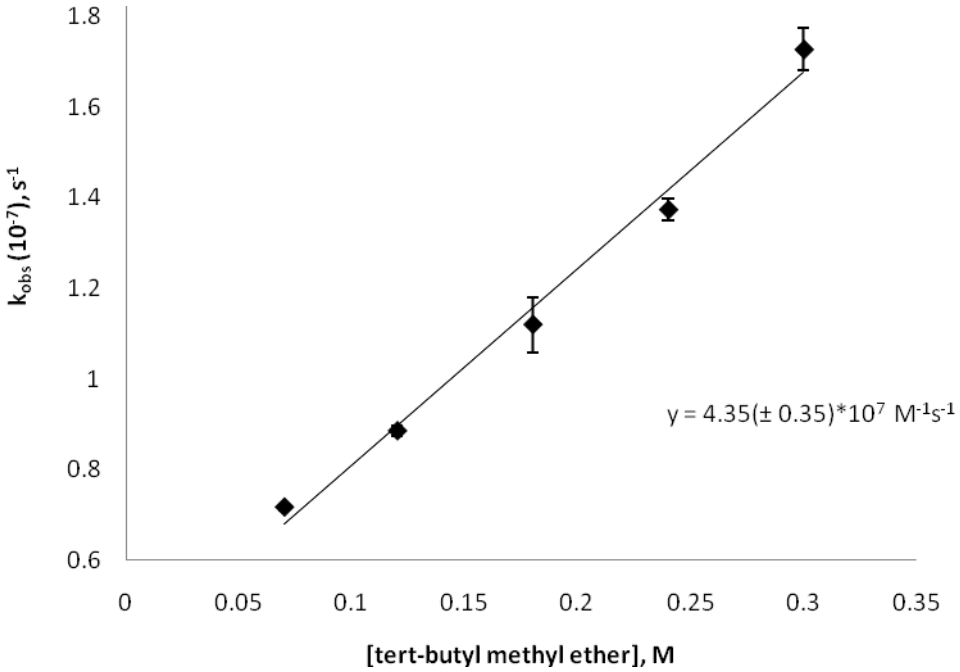

[t-butyl methyl ether], M	$k_{obs}(10^{-7})$, s^{-1}	Standard Deviation (10^{-7})
0.070	0.72	0.006
0.120	0.89	0.012
0.180	1.12	0.061
0.240	1.37	0.025
0.300	1.73	0.047

Figure 2-40. Concentration profile for the reaction of HO• with tert-butyl ethyl ether in acetonitrile in the presence of 1.5 mM trans-stilbene as a spectroscopic probe (monitoring the buildup of the 392 nm transient attributable to **HO-TS•**)

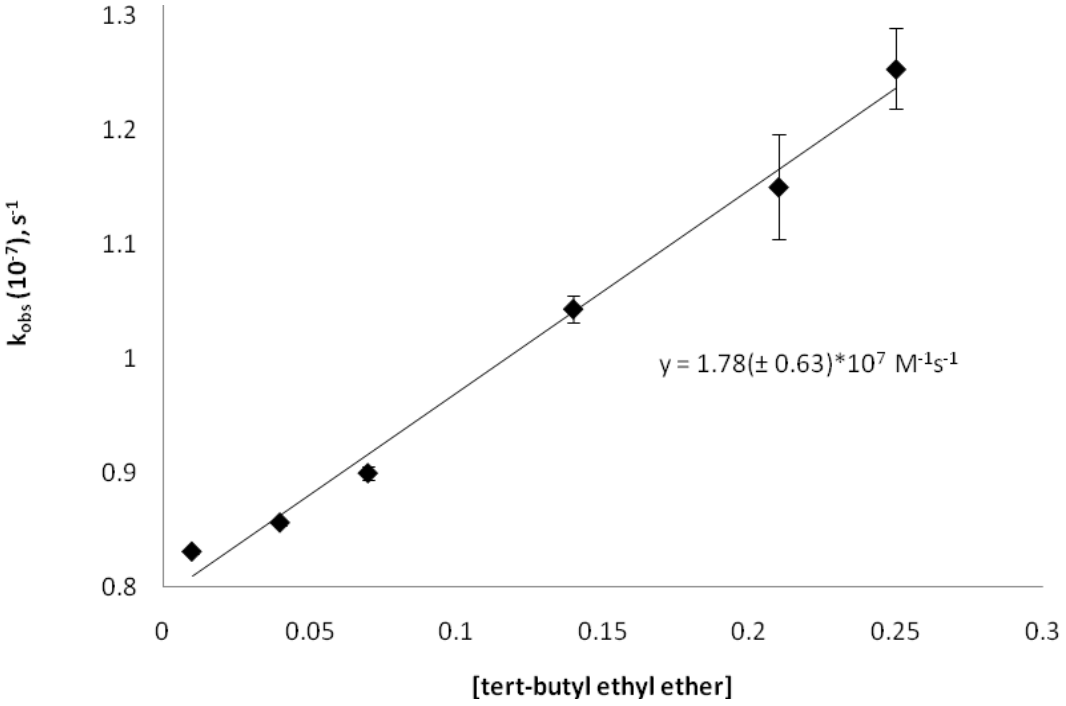

[t-butyl ethyl ether], M	k_{obs}(10^{-7}), s^{-1}	Standard Deviation (10^{-7})
0.010	0.83	0.002
0.040	0.86	0.003
0.070	0.90	0.006
0.140	1.04	0.012
0.210	1.15	0.046
0.250	1.25	0.035

Figure 2-41. Concentration profile for the reaction of HO• with tetrahydrofuran in acetonitrile in the presence of 1.5 mM trans-stilbene as a spectroscopic probe (monitoring the buildup of the 392 nm transient attributable to **HO-TS•**)

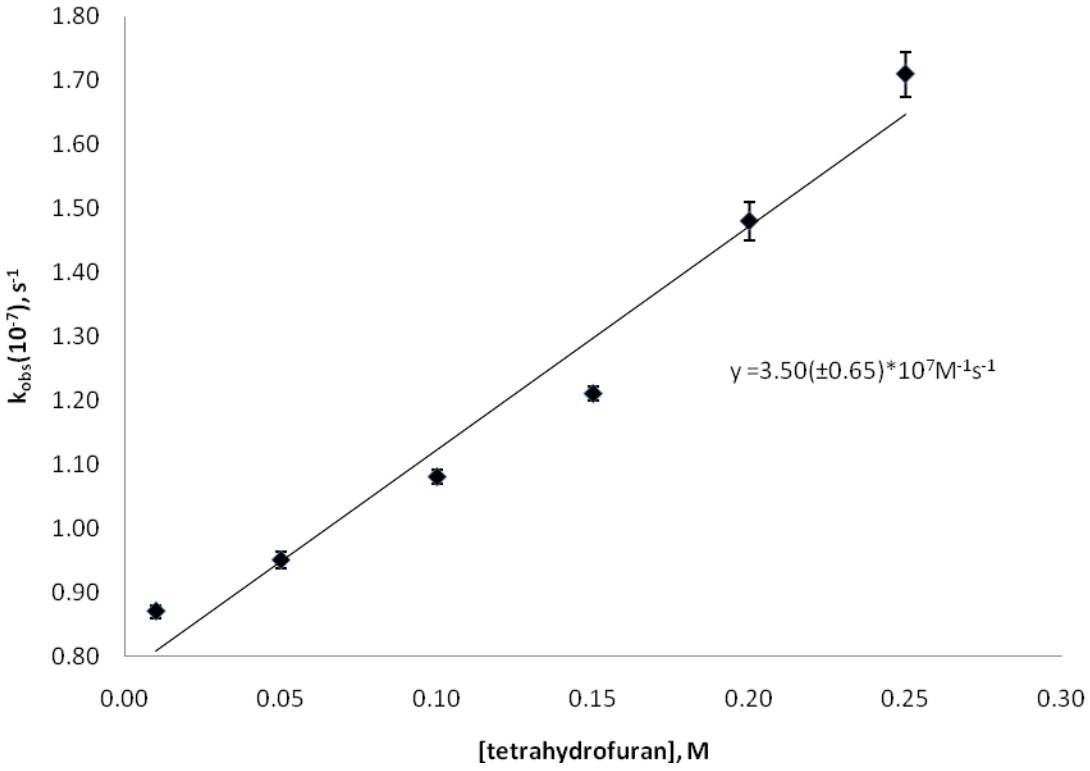

[tetrahydrofuran], M	$k_{obs}(10^{-7})$, s^{-1}	Standard Deviation (10^{-7})
0.010	0.87	0.010
0.050	0.95	0.013
0.100	1.08	0.011
0.150	1.21	0.011
0.200	1.48	0.030
0.250	1.71	0.035

Figure 2-42. Concentration profile for the reaction of HO• with methylene chloride in acetonitrile in the presence of 1.5 mM trans-stilbene as a spectroscopic probe (monitoring the buildup of the 392 nm transient attributable to **HO-TS•**)

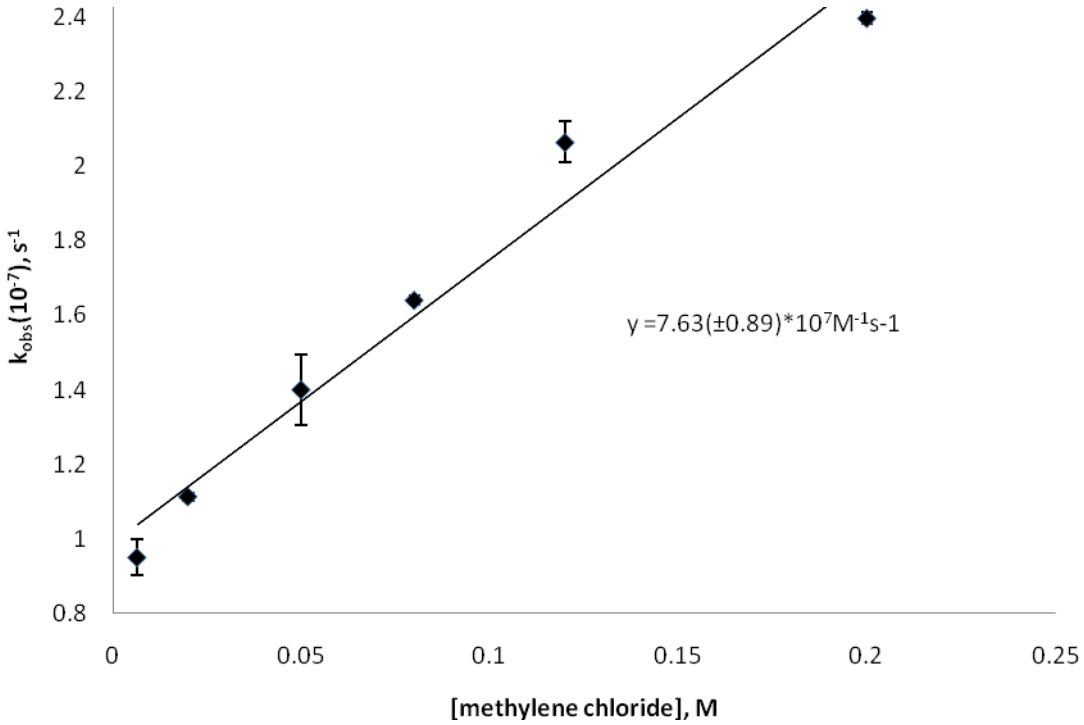

[methylene chloride], M	$k_{obs}(10^{-7})$, s^{-1}	Standard Deviation (10^{-7})
0.007	0.95	0.047
0.020	1.11	0.010
0.050	1.40	0.095
0.080	1.64	0.013
0.120	2.06	0.055
0.200	2.40	0.016

Figure 2-43. Concentration profile for the reaction of HO• with acetone in acetonitrile in the presence of 1.5 mM trans-stilbene as a spectroscopic probe (monitoring the buildup of the 392 nm transient attributable to **HO-TS•**)

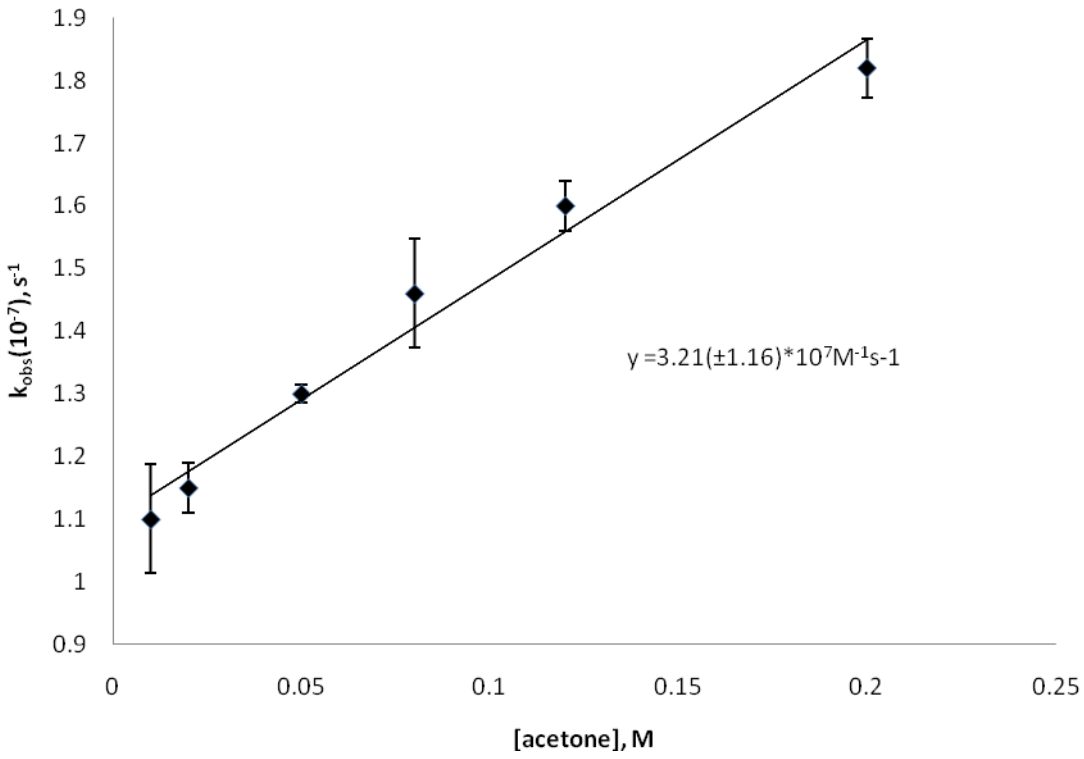

[acetone], M	$k_{obs}(10^{-7})$, s^{-1}	Standard Deviation(10^{-7})
0.010	1.10	0.087
0.020	1.15	0.040
0.050	1.30	0.015
0.080	1.46	0.087
0.120	1.60	0.040
0.200	1.82	0.047

Figure 2-44. Concentration profile for the reaction of HO• with bromoform in acetonitrile in the presence of 1.5 mM trans-stilbene as a spectroscopic probe (monitoring the buildup of the 392 nm transient attributable to **HO-TS•**)

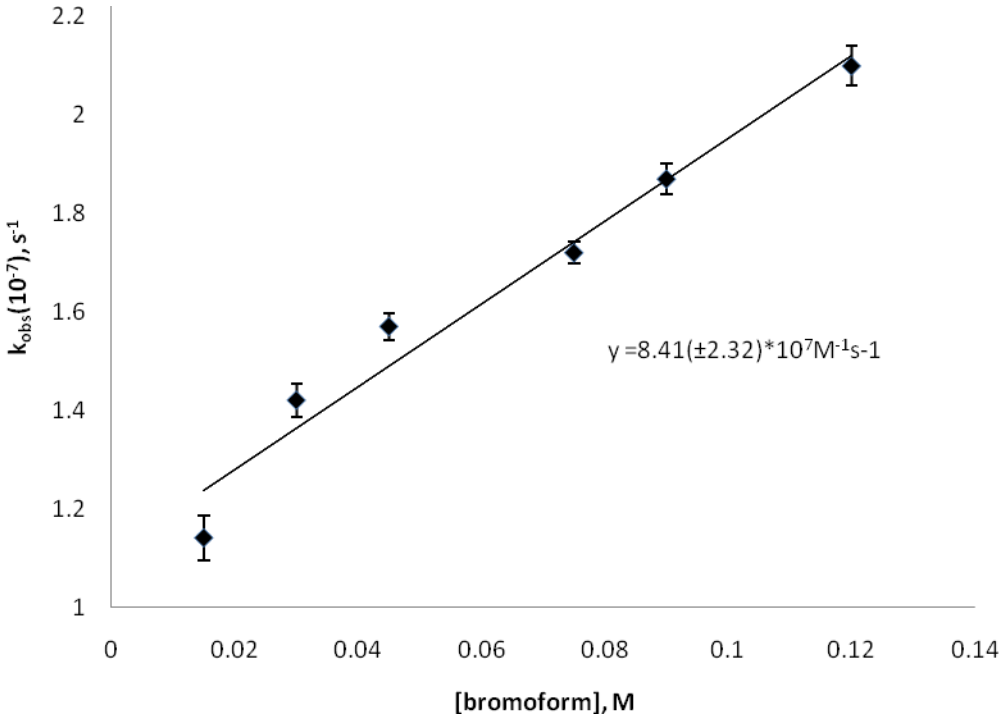

[bromoform], M	$k_{obs}(10^{-7})$, s^{-1}	Standard Deviation(10^{-7})
0.015	1.14	0.045
0.030	1.42	0.033
0.045	1.57	0.028
0.075	1.72	0.023
0.090	1.87	0.030
0.120	2.10	0.040

Figure 2-45. Concentration profile for the reaction of HO• with chloroform in acetonitrile in the presence of 1.5 mM trans-stilbene as a spectroscopic probe (monitoring the buildup of the 392 nm transient attributable to **HO-TS•**)

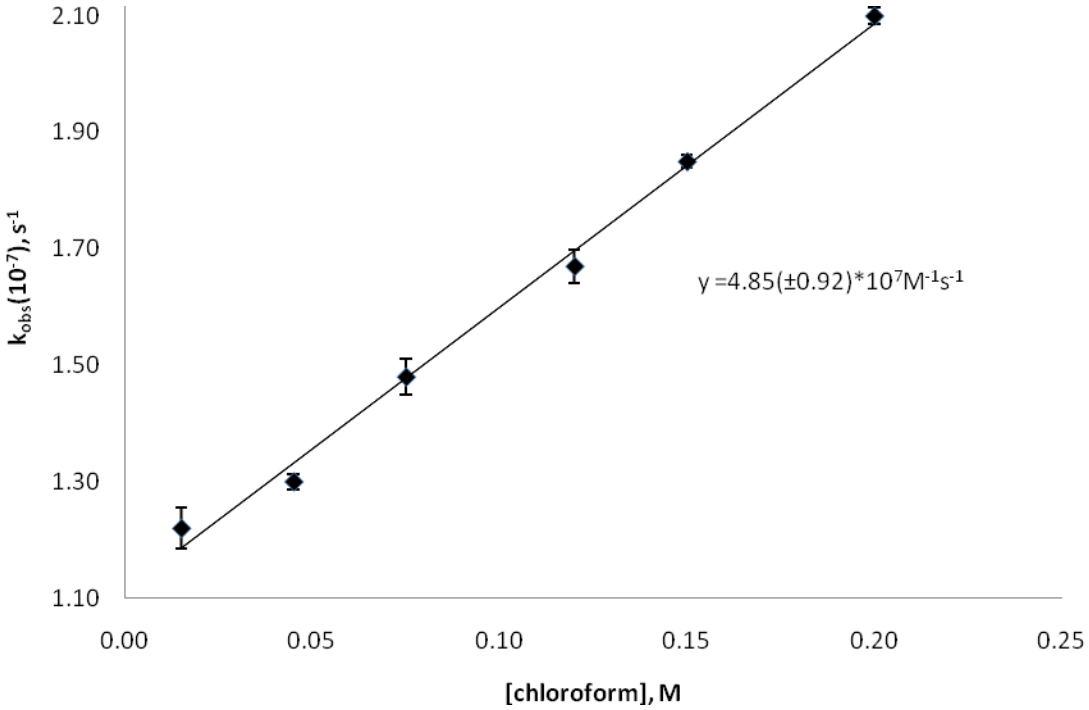

[chloroform], M	$k_{obs}(10^{-7})$, s^{-1}	Standard Deviation (10^{-7})
0.015	1.22	0.035
0.045	1.30	0.013
0.075	1.48	0.031
0.120	1.67	0.029
0.150	1.85	0.010
0.200	2.10	0.015

Figure 2-46. Concentration profile for the reaction of HO• with chloroacetic acid in acetonitrile in the presence of 1.5 mM trans-stilbene as a spectroscopic probe (monitoring the buildup of the 392 nm transient attributable to **HO-TS•**)

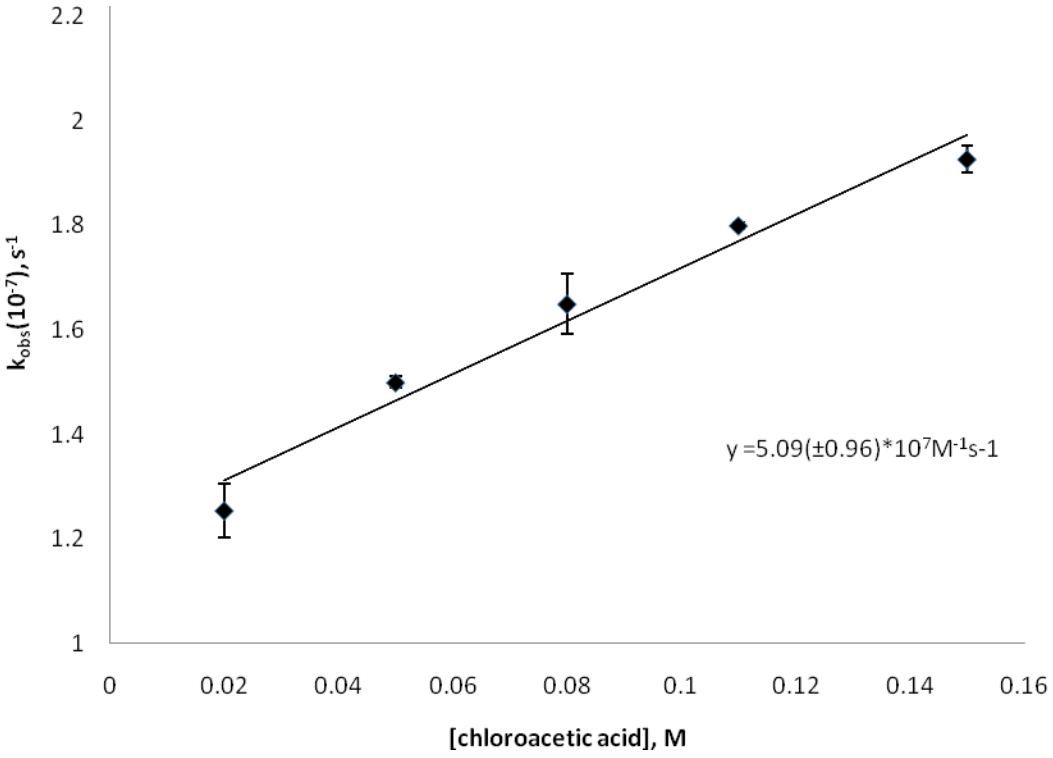

[chloroacetic acid], M	$k_{obs}(10^{-7})$, s^{-1}	Standard Deviation(10^{-7})
0.020	1.26	0.052
0.050	1.50	0.011
0.080	1.65	0.058
0.110	1.80	0.007
0.150	1.93	0.025

Figure 2-47. Transient signal for the buildup of **HO-TS•** at 392 nm in the presence of 0.040 M hexane in 10% water/ 90% acetonitrile generated by laser flash photolysis of 0.65 mM PSH.

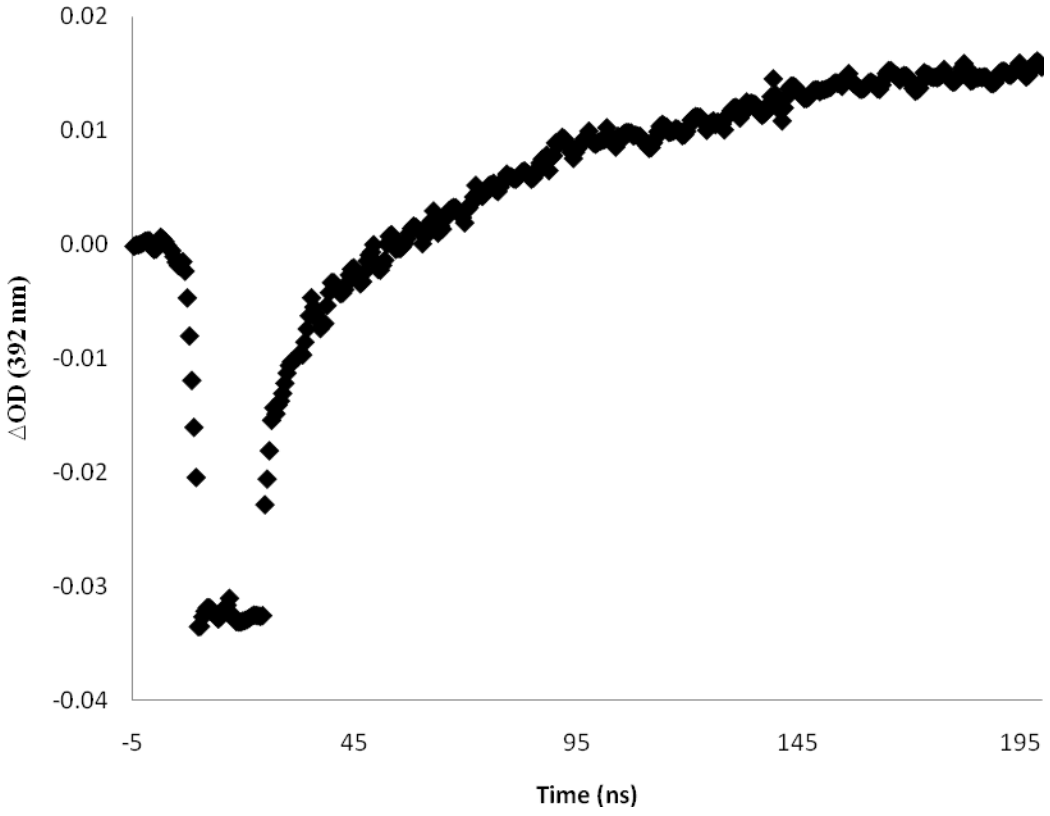

Figure 2-48. Transient signal for the buildup of **HO-TS•** at 392 nm in the presence of 0.045 M cyclohexane in 10% water/ 90% acetonitrile generated by laser flash photolysis of 0.65 mM PSH.

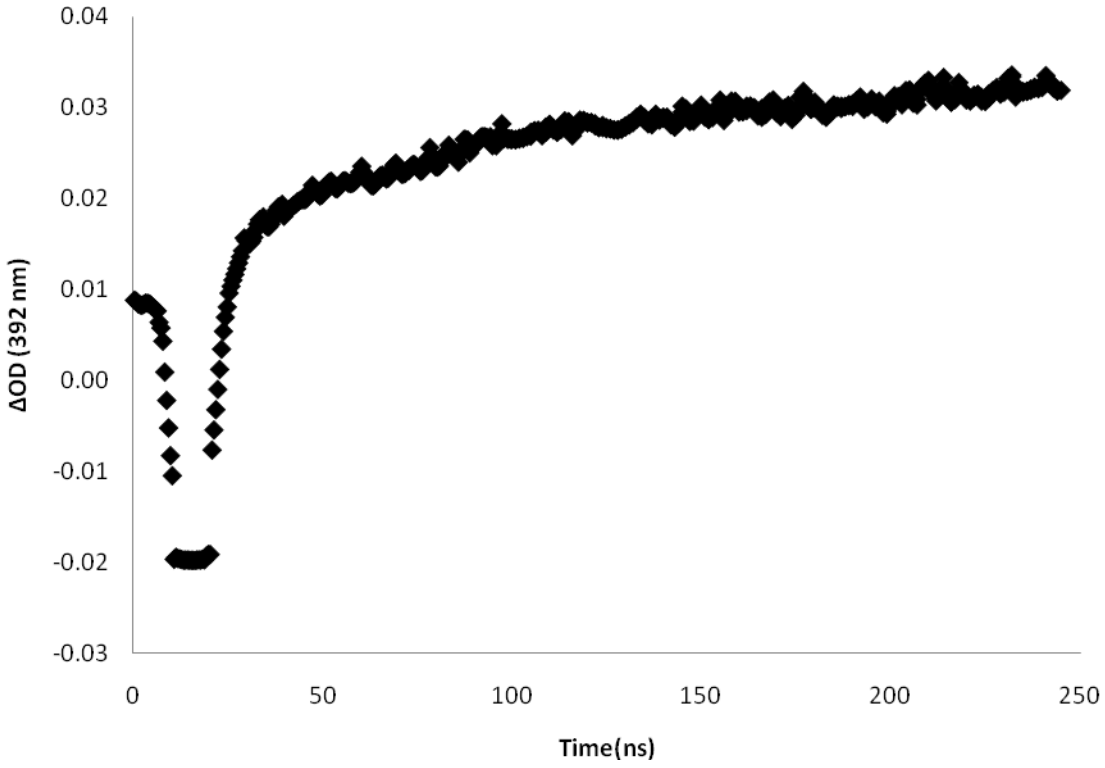

Figure 2-49. Transient signal for the buildup of **HO-TS•** at 392 nm in the presence of 0.045 M dimethylbutane in 10% water/ 90% acetonitrile generated by laser flash photolysis of 0.65 mM PSH.

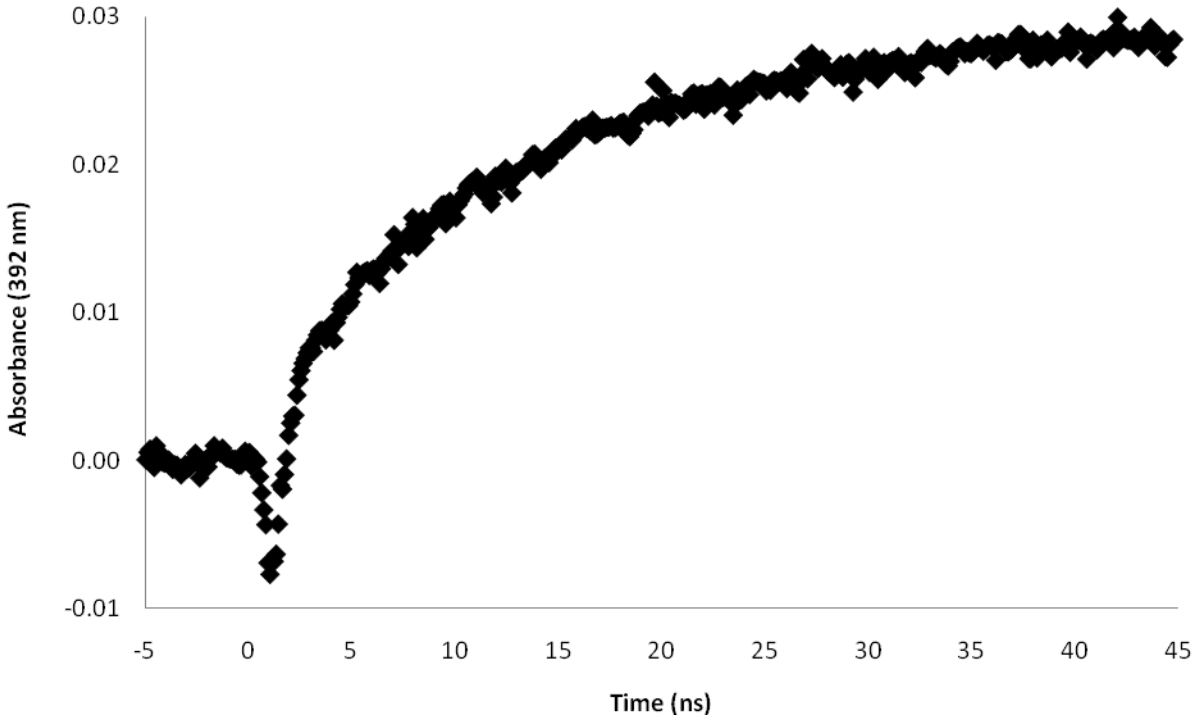

Figure 2-50. Transient signal for the buildup of **HO-TS•** at 392 nm in the presence of 0.045 M ethanol in 10% water/ 90% acetonitrile generated by laser flash photolysis of 0.65 mM PSH.

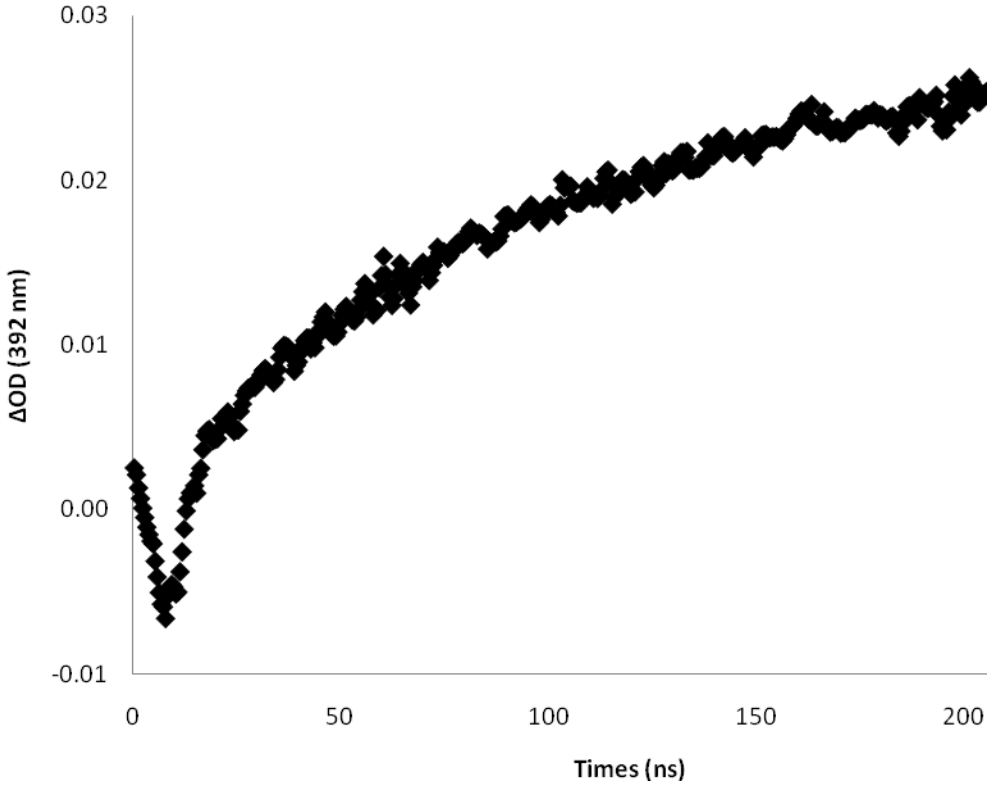

Figure 2-51. Transient signal for the buildup of HO-TS• at 392 nm in the presence of 0.045 M bromoform in 10% water/ 90% acetonitrile generated by laser flash photolysis of 0.65 mM PSH.

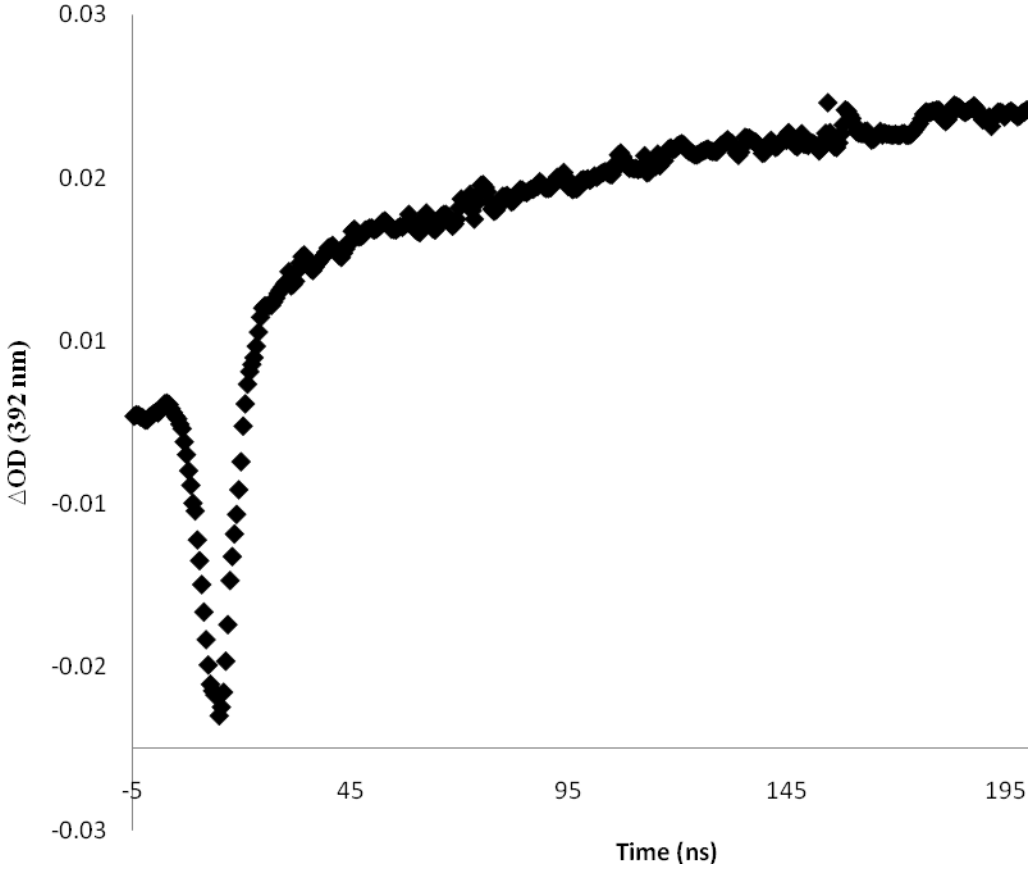

Figure 2-52. Transient signal for the buildup of **HO-TS•** at 392 nm in the presence of 0.040 M chloroform in 10% water/ 90% acetonitrile generated by laser flash photolysis of 0.65 mM PSH.

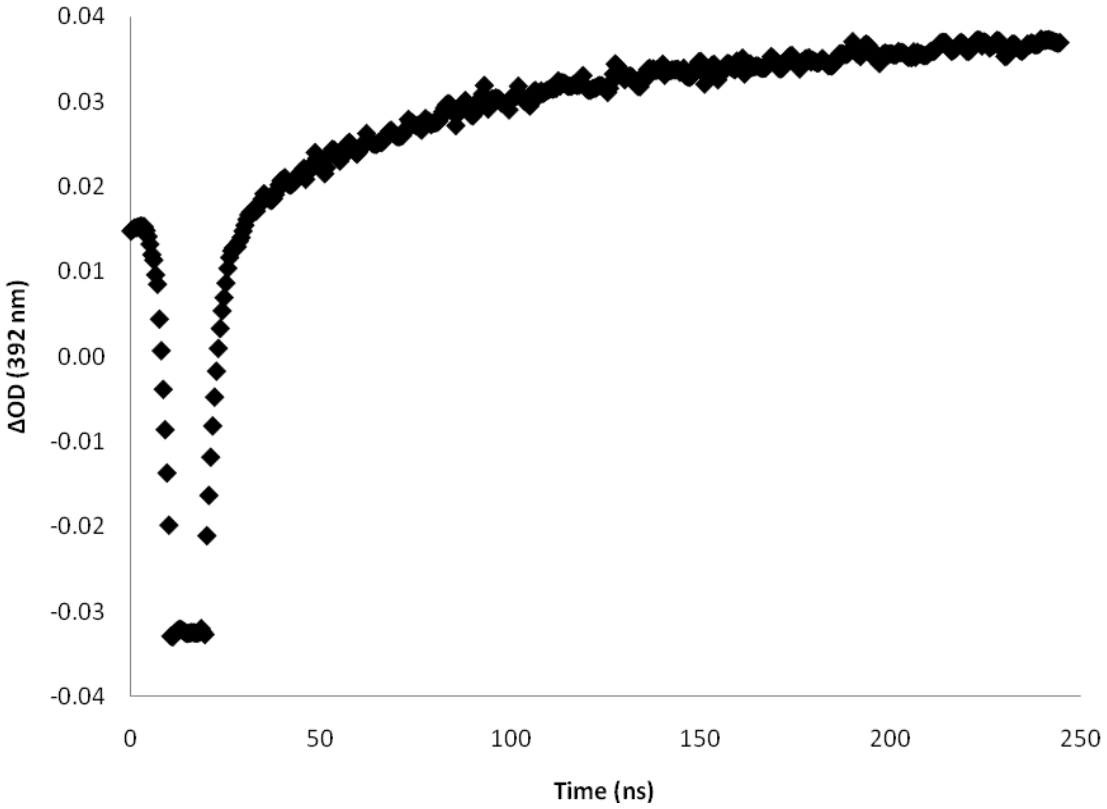

Figure 2-53. Concentration profile for the reaction of HO• with hexane in 10% water/90% acetonitrile in the presence of 1.5 mM trans-stilbene as a spectroscopic probe (monitoring the buildup of the 392 nm transient attributable to **HO-TS•**)

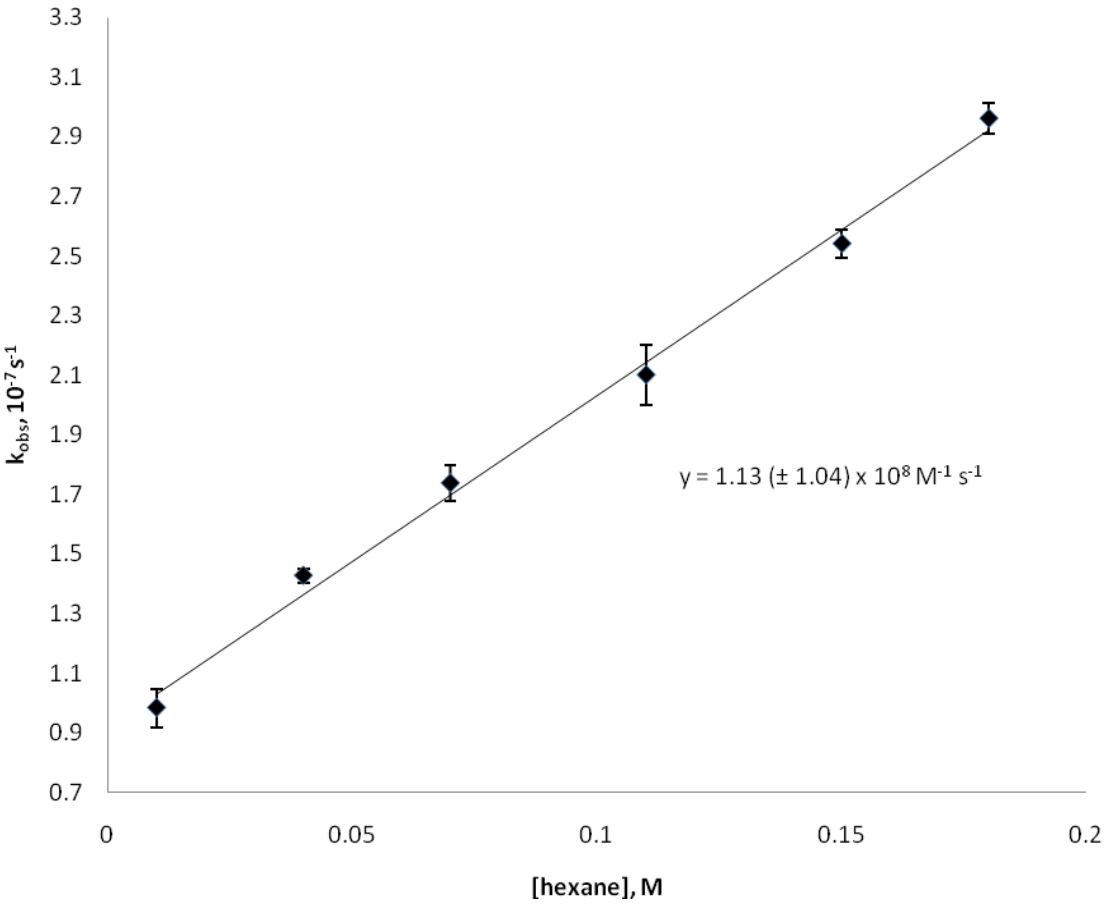

[hexane], M	$k_{obs}(10^{-7})$, s^{-1}	Standard Deviation (10^{-7})
0.010	0.98	0.065
0.040	1.43	0.025
0.070	1.74	0.060
0.110	2.10	0.100
0.150	2.54	0.046
0.180	2.96	0.052

Figure 2-54. Concentration profile for the reaction of HO• with cyclohexane in 10% water/90% acetonitrile in the presence of 1.5 mM trans-stilbene as a spectroscopic probe (monitoring the buildup of the 392 nm transient attributable to **HO-TS•**)

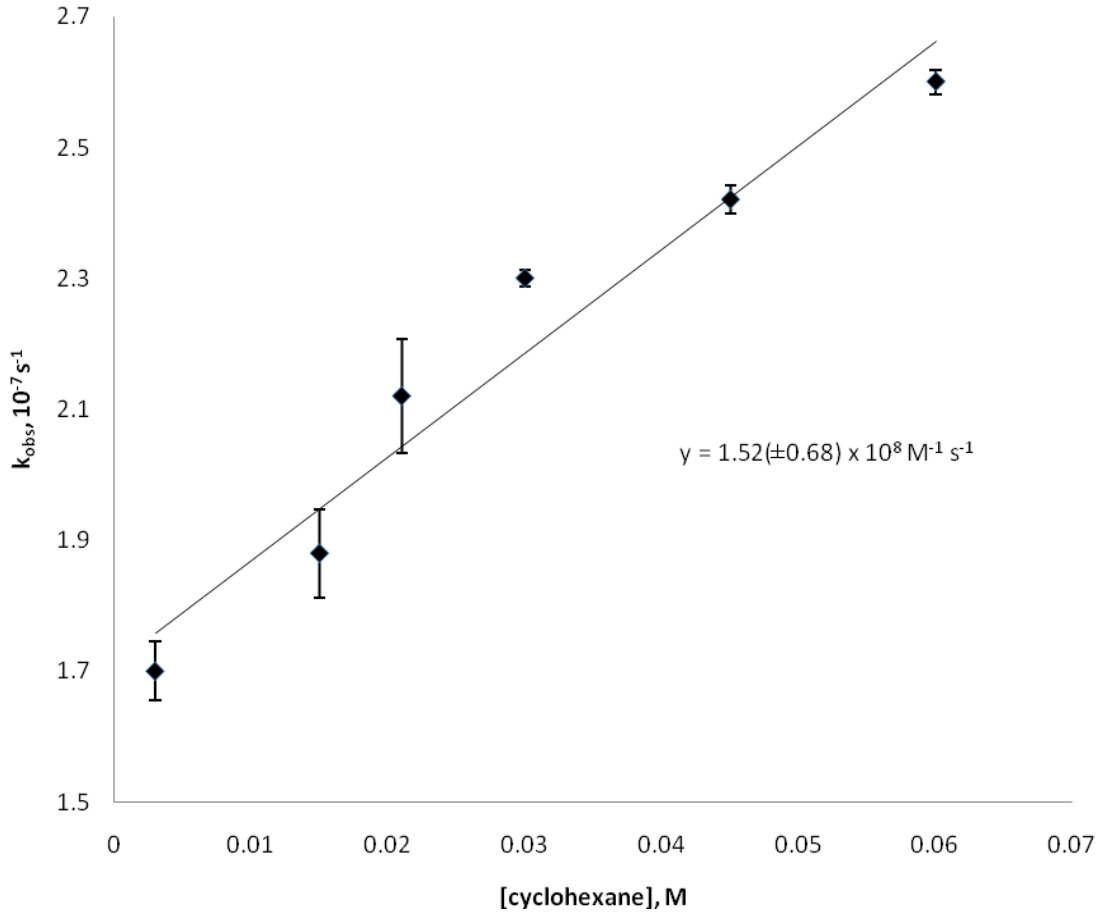

[cyclohexane], M	$k_{obs}(10^{-7})$, s^{-1}	Standard Deviation (10^{-7})
0.003	1.70	0.045
0.015	1.88	0.068
0.021	2.12	0.087
0.030	2.30	0.013
0.045	2.42	0.021
0.060	2.60	0.019

Figure 2-55. Concentration profile for the reaction of HO• with dimethylbutane in 10% water/90% acetonitrile in the presence of 1.5 mM trans-stilbene as a spectroscopic probe (monitoring the buildup of the 392 nm transient attributable to **HO-TS•**)

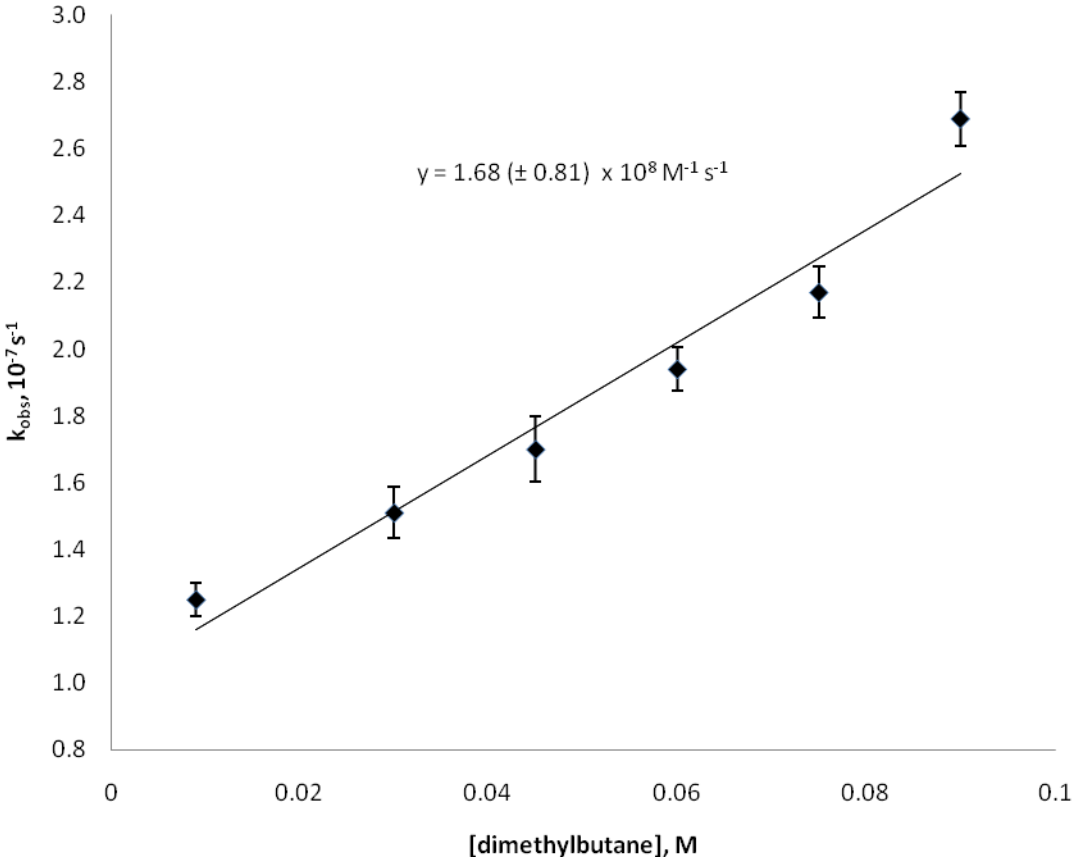

[dimethylbutane], M	$k_{obs}(10^{-7})$, s^{-1}	Standard Deviation (10^{-7})
0.009	1.25	0.05
0.030	1.51	0.08
0.045	1.70	0.10
0.060	1.94	0.06
0.075	2.17	0.08
0.090	2.69	0.08

Figure 2-56. Concentration profile for the reaction of HO• with ethanol in 10% water/90% acetonitrile in the presence of 1.5 mM trans-stilbene as a spectroscopic probe (monitoring the buildup of the 392 nm transient attributable to **HO-TS•**)

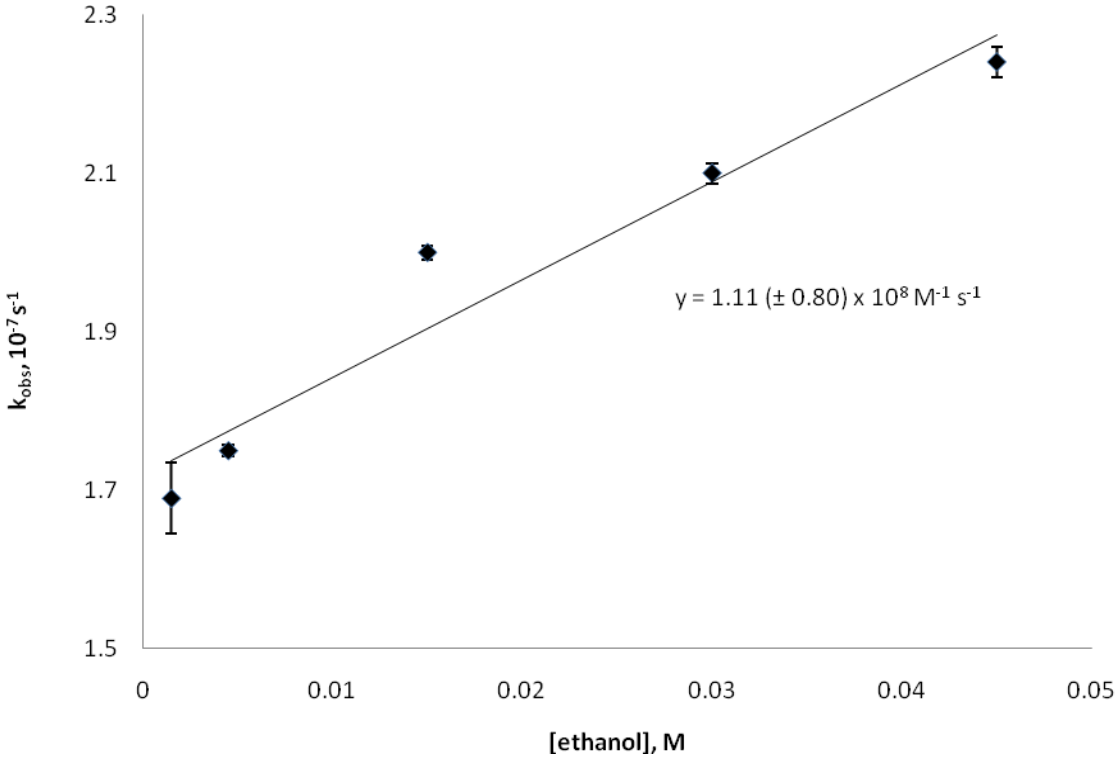

[ethanol], M	$k_{obs}(10^{-7})$, s^{-1}	Standard Deviation (10^{-7})
0.002	1.69	0.045
0.005	1.75	0.007
0.015	2.00	0.009
0.030	2.10	0.013
0.045	2.24	0.019

Figure 2-57. Concentration profile for the reaction of HO• with bromoform in 10% water/90% acetonitrile in the presence of 1.5 mM trans-stilbene as a spectroscopic probe (monitoring the buildup of the 392 nm transient attributable to **HO-TS•**)

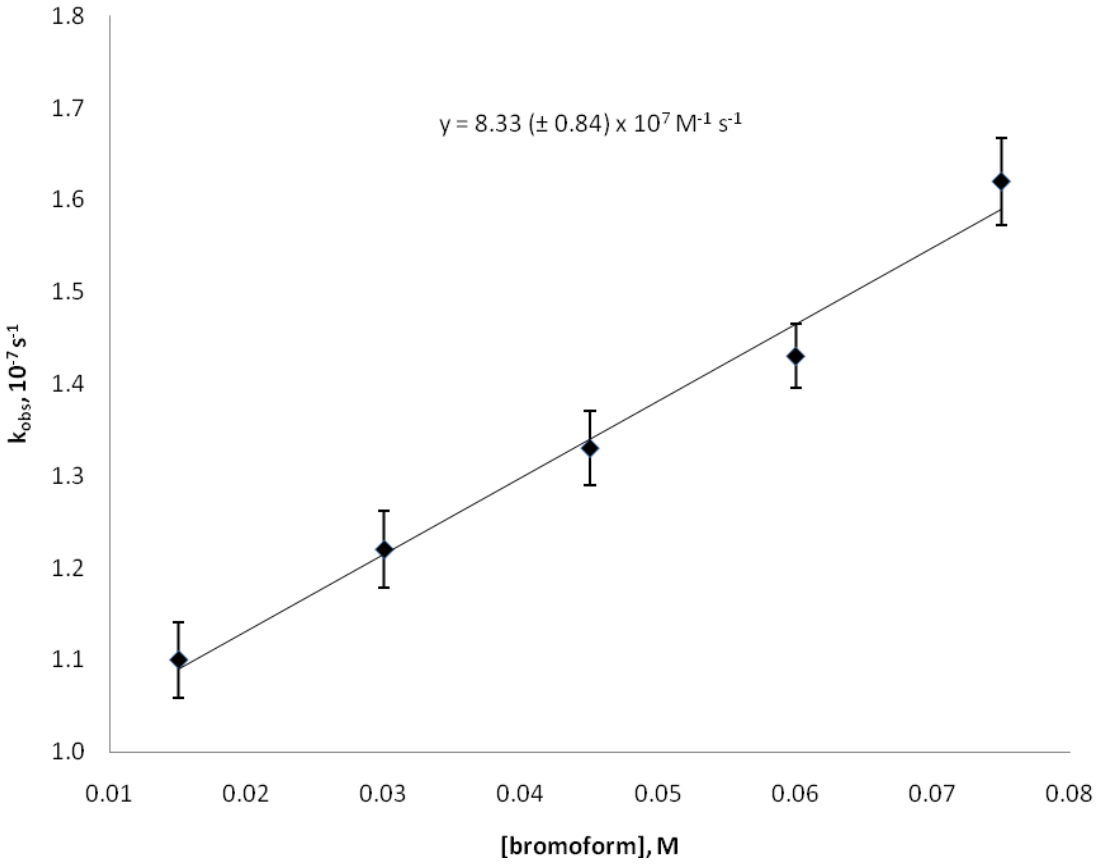

[bromoform], M	$k_{obs}(10^{-7})$, s^{-1}	Standard Deviation (10^{-7})
0.015	1.10	0.041
0.030	1.22	0.041
0.045	1.33	0.040
0.060	1.43	0.035
0.075	1.62	0.048

Figure 2-58. Concentration profile for the reaction of HO• with chloroform in 10% water/90% acetonitrile in the presence of 1.5 mM trans-stilbene as a spectroscopic probe (monitoring the buildup of the 392 nm transient attributable to **HO-TS•**)

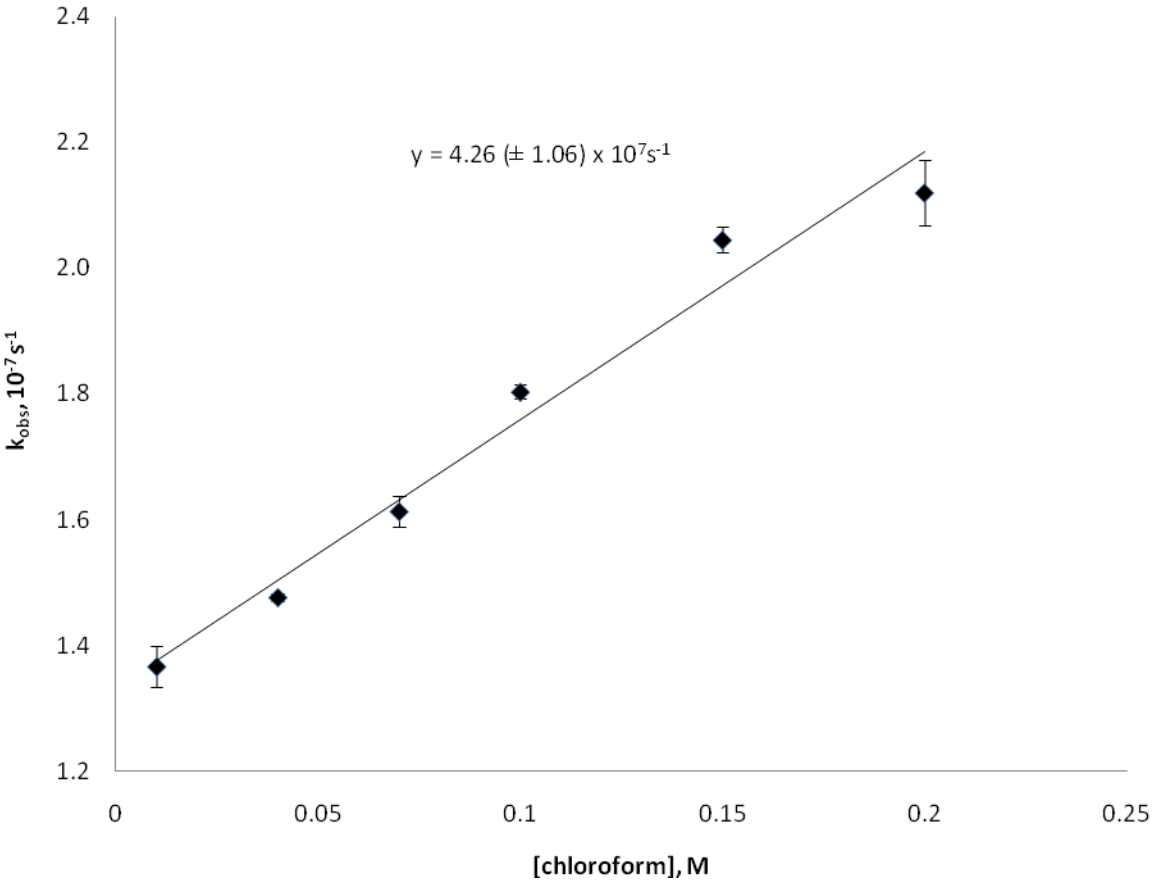

[chloroform], M	$k_{obs}(10^{-7})$, s^{-1}	Standard Deviation (10^{-7})
0.010	1.37	0.032
0.040	1.48	0.006
0.070	1.61	0.025
0.100	1.80	0.012
0.150	2.05	0.021
0.200	2.12	0.052

Figure 2-59. Transient signal for the buildup of **HO-TS•** at 412 nm in the presence of 0.030 M methanol in Freon-113 generated by laser flash photolysis of 0.65 mM PSH.

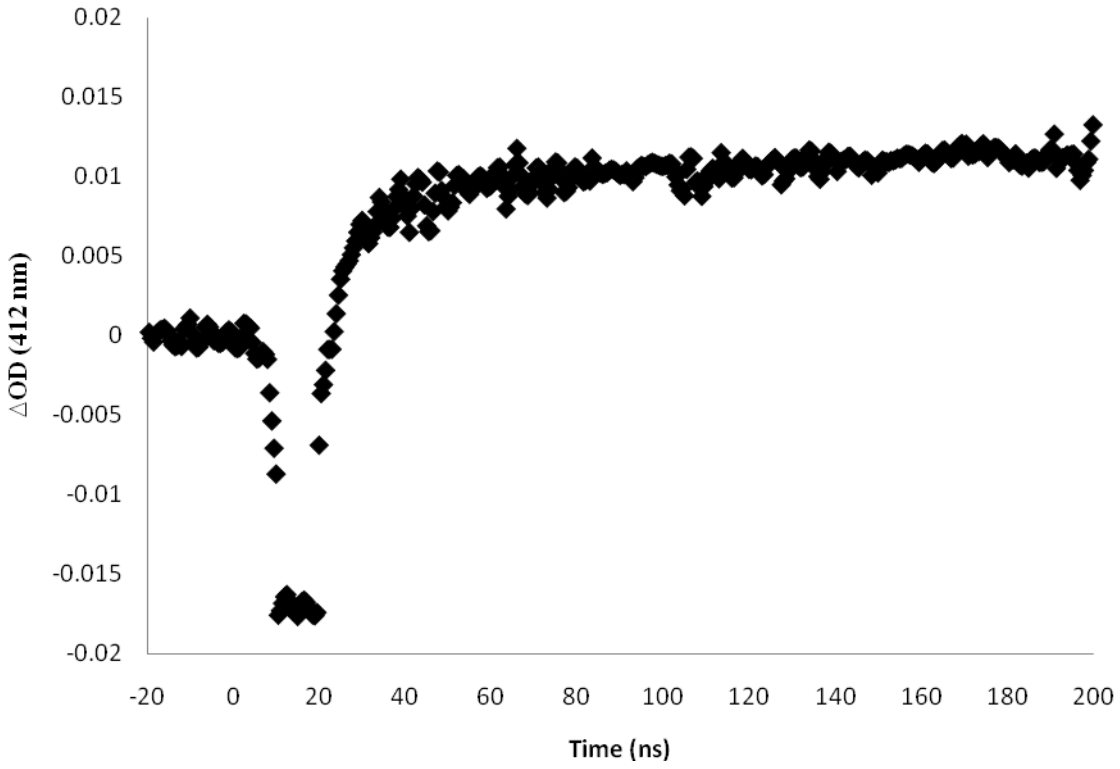

Figure 2-60. Transient signal for the buildup of **HO-TS•** at 412 nm in the presence of 0.045 M cyclohexane in Freon-113 generated by laser flash photolysis of 0.65 mM PSH.

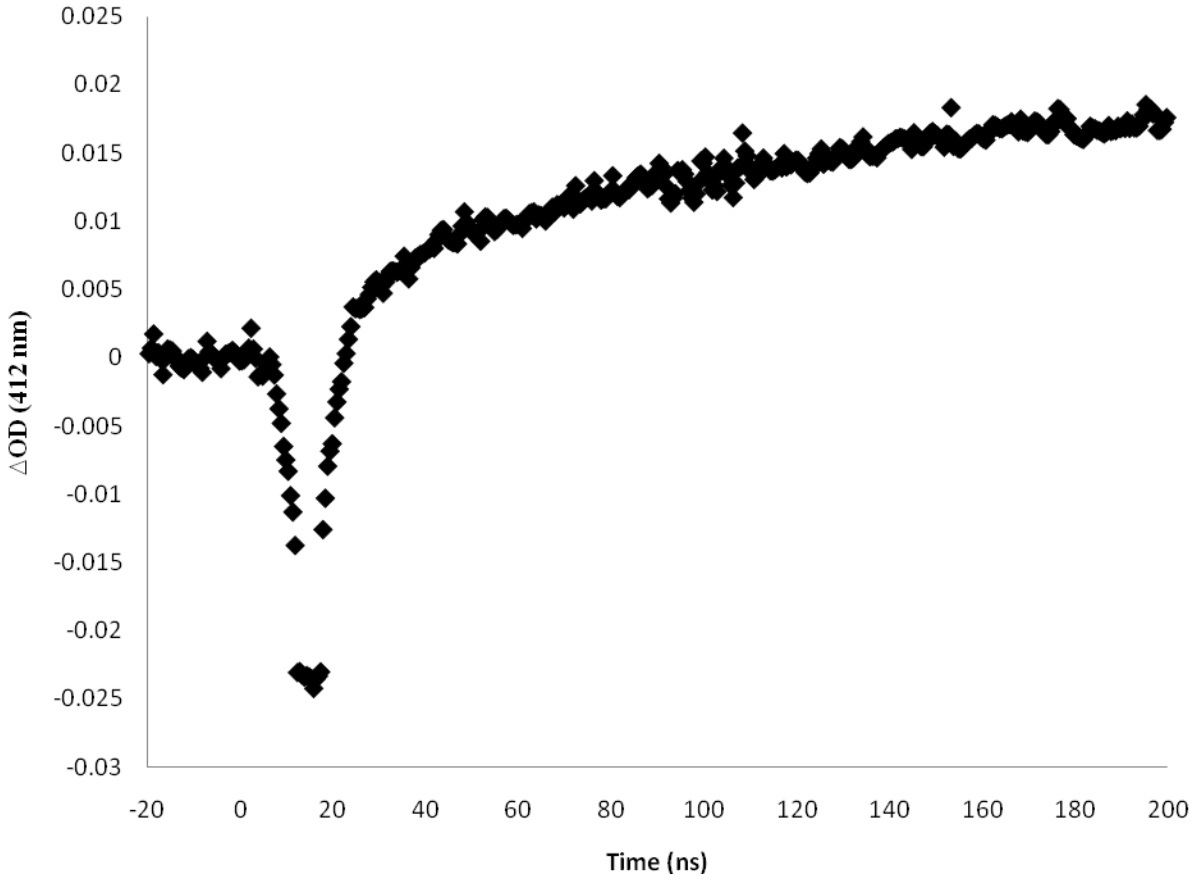

Figure 2-61. Concentration profile for the reaction of HO• with methanol in Freon-113 in the presence of 1.5 mM trans-stilbene as a spectroscopic probe (monitoring the buildup of the 412 nm transient attributable to **HO-TS•**)

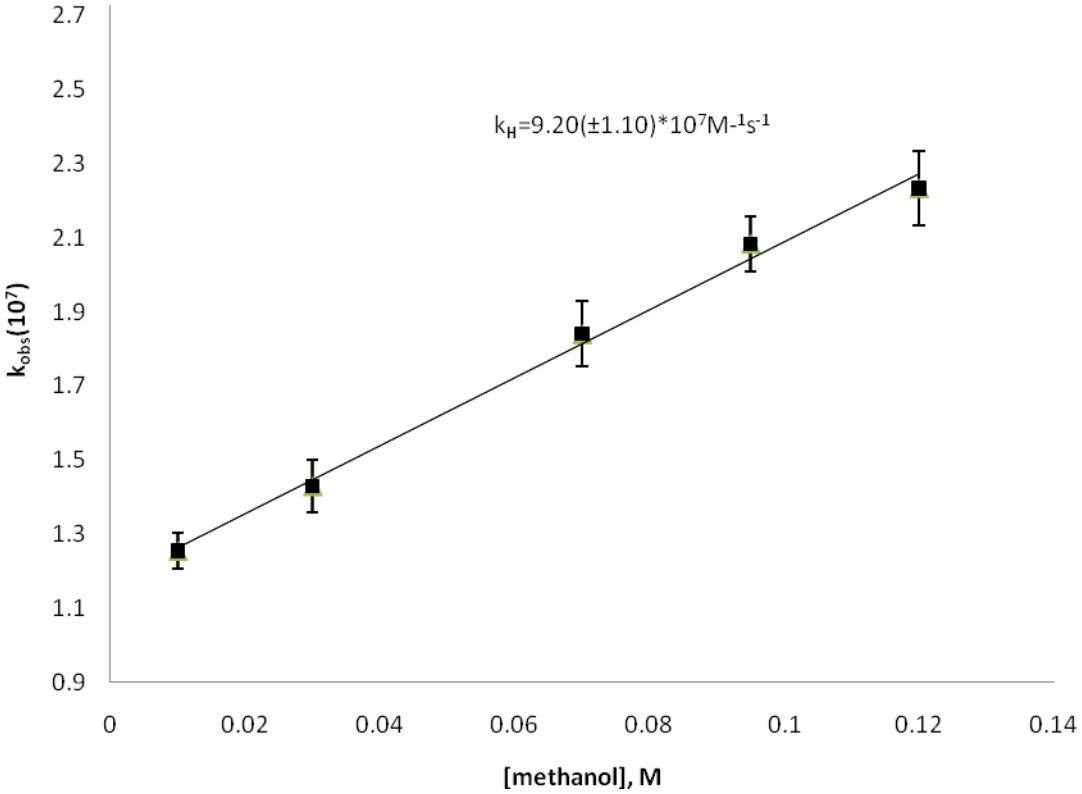

[methanol], M	$k_{obs}(10^{-7})$, s^{-1}	Standard Deviation (10^{-7})
0.010	1.26	0.049
0.030	1.43	0.071
0.070	1.84	0.089
0.095	2.08	0.074
0.120	2.23	0.099

Figure 2-62. Concentration profile for the reaction of HO• with cyclohexane in Freon-113 in the presence of 1.5 mM trans-stilbene as a spectroscopic probe (monitoring the buildup of the 412 nm transient attributable to **HO-TS•**)

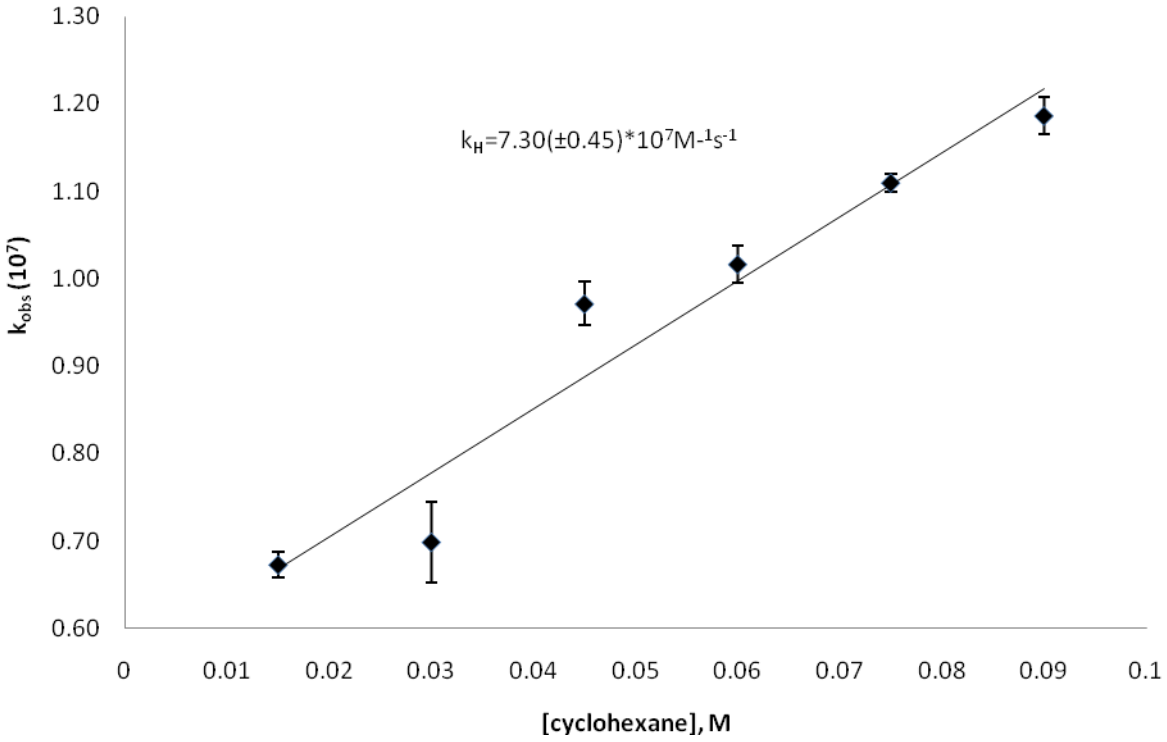

[cyclohexane], M	$k_{obs}(10^{-7})$, s^{-1}	Standard Deviation (10^{-7})
0.015	0.67	0.015
0.030	0.70	0.047
0.045	0.97	0.025
0.060	1.02	0.021
0.075	1.11	0.010
0.090	1.19	0.021

Absolute energies and optimized geometries for calculated structures

Table 2-7. Absolute energies and optimized geometries for calculated structures: HO•

Calculation Type SP
Calculation Method UMP2-FU
Basis Set Aug-CC-pVQZ
E(MP2) -75.67629933 a.u.

Center Number	Atomic Number	Atomic Type	Coordinates (Angstroms) X	Y	Z
1	1	0	0.000000	0.000000	-0.844410
2	8	0	0.000000	0.000000	0.105551

Table 2-8. Absolute energies and optimized geometries for calculated structures: Water

Calculation Type SP
Calculation Method RMP2-FU
Basis Set Aug-CC-pVQZ
E(MP2) -76.38200398 a.u.

Center Number	Atomic Number	Atomic Type	Coordinates (Angstroms) X	Y	Z
1	1	0	0.000000	0.757769	-0.444216
2	8	0	0.000000	-0.000000	0.111054
3	1	0	-0.000000	-0.757769	-0.444216

Table 2-9. Absolute energies and optimized geometries for calculated structures: Methane

Calculation Type SP
Calculation Method RMP2-FU
Basis Set Aug-CC-pVQZ
E(MP2) -40.45661379 a.u.

Center Number	Atomic Number	Atomic Type	Coordinates (Angstroms) X	Y	Z
1	1	0	0.625274	0.625274	0.625274
2	6	0	0.000000	0.000000	0.000000
3	1	0	-0.625274	-0.625274	0.625274
4	1	0	0.625274	-0.625274	-0.625274
5	1	0	-0.625274	0.625274	-0.625274

Table 2-10. Absolute energies and optimized geometries for calculated structures: Methane/HO•

transition state

Calculation Type SP
Calculation Method UMP2-FU
Basis Set Aug-CC-pVQZ
E(MP2) -116.12748772 a.u.

Center Number	Atomic Number	Atomic Type	Coordinates (Angstroms) X	Y	Z
1	1	0	1.459316	-0.823394	0.000000
2	8	0	1.282289	0.106233	0.000000
3	1	0	0.087252	0.119545	0.000090
4	6	0	-1.219303	-0.010955	0.000000
5	1	0	-1.464769	-0.545274	0.904189
6	1	0	-1.464497	-0.547435	-0.902984
7	1	0	-1.559799	1.012419	-0.001289

Table 2-11. Absolute energies and optimized geometries for calculated structures: Methyl

Calculation Type SP
Calculation Method UMP2-FU
Basis Set Aug-CC-pVQZ
E(MP2) -39.77804050

Center Number	Atomic Number	Atomic Type	Coordinates (Angstroms) X	Y	Z
1	1	0	-0.000000	0.000000	-1.072803
2	6	0	0.000000	-0.000000	0.000011
3	1	0	0.000000	0.929101	0.536370
4	1	0	-0.000000	-0.929101	0.536370

Table 2-12. Absolute energies and optimized geometries for calculated structures: Chloroform

Calculation Type SP
Calculation Method RMP2-FU
Basis Set Aug-CC-pVQZ
E(MP2) -1418.05187508 a.u.

Center Number	Atomic Number	Atomic Type	Coordinates (Angstroms) X	Y	Z
1	17	0	0.970715	1.375629	0.000000
2	6	0	-0.380457	0.241326	0.000000
3	17	0	-0.380457	-0.754356	1.456292
4	17	0	-0.380457	-0.754356	-1.456292
5	1	0	-1.283891	0.814443	0.000000

Table 2-13. Absolute energies and optimized geometries for calculated structures:

Chloroform/HO• transition state

Calculation Type SP
Calculation Method UMP2-FU
Basis Set Aug-CC-pVQZ
E(MP2) -1493.71826972 a.u.

Center Number	Atomic Number	Atomic Type	Coordinates (Angstroms) X	Y	Z
1	17	0	1.080367	-0.068699	-1.373960
2	6	0	-0.013260	0.000306	0.028048
3	17	0	-0.926484	1.511911	0.096877
4	1	0	0.671055	-0.014253	1.017924
5	17	0	-1.044046	-1.429963	0.149408
6	1	0	2.394205	0.031166	1.626187
7	8	0	1.518384	-0.030496	2.044760

Table 2-14. Absolute energies and optimized geometries for calculated structures: Cl_3C•

Calculation Type SP
Calculation Method UMP2-FU
Basis Set Aug-CC-pVQZ
E(MP2) -1417.38943784 a.u.

Center Number	Atomic Number	Atomic Type	Coordinates (Angstroms) X	Y	Z
1	17	0	-1.689693	-0.003763	-0.032288
2	6	0	-0.000309	-0.000001	0.274336
3	17	0	0.848161	-1.461250	-0.032268
4	17	0	0.841641	1.465013	-0.032268

Table 2-15. Absolute energies and optimized geometries for calculated structures: Methanol

Calculation Type SP
Calculation Method RMP2-FU
Basis Set Aug-CC-pVQZ
E(MP2) -115.62223681

Center Number	Atomic Number	Atomic Type	Coordinates (Angstroms) X	Y	Z
1	1	0	-0.440133	1.060518	0.883708
2	6	0	0.045662	0.654014	0.000000
3	1	0	-0.440133	1.060518	-0.883708
4	8	0	0.045662	-0.744180	0.000000
5	1	0	1.077480	0.974056	0.000000
6	1	0	-0.836482	-1.065732	0.000000

Table 2-16. Absolute energies and optimized geometries for calculated structures:

Methanol/HO• transition state

Calculation Type SP
Calculation Method UMP2-FU
Basis Set Aug-CC-pVQZ
E(MP2) -191.30373941 a.u.

Center Number	Atomic Number	Atomic Type	Coordinates (Angstroms) X	Y	Z
1	1	0	0.668647	0.333158	0.058495
2	6	0	-0.583616	0.637501	-0.007364
3	1	0	-0.735284	1.223755	0.890974
4	8	0	-1.338957	-0.501331	-0.086257
5	1	0	-0.696276	1.214671	-0.910020
6	1	0	-1.299824	-0.980835	0.721081
7	1	0	1.785542	-0.677875	-0.679730
8	8	0	1.811318	-0.115903	0.081681

Table 2-17. Absolute energies and optimized geometries for calculated structures: $HOCH_2$•

Calculation Type SP
Calculation Method UMP2-FU
Basis Set Aug-CC-pVQZ
E(MP2) -114.95730684 a.u.

Center Number	Atomic Number	Atomic Type	Coordinates (Angstroms) X	Y	Z
1	1	0	1.014128	1.135778	0.000000
2	6	0	0.049139	0.678000	0.000000
3	1	0	-0.875305	1.219882	0.000000
4	8	0	0.049139	-0.676324	0.000000
5	1	0	-0.826769	-1.013067	0.000000

Table 2-18. Absolute energies and optimized geometries for calculated structures: Methane

Calculation Type SP
Calculation Method CCSD(T)
Basis Set aug-cc-pVDZ
E(CCSD(T)) -0.40395771144D+02 a.u.

Center Number	Atomic Number	Atomic Type	Coordinates (Angstroms) X	Y	Z
1	6	0	-0.000000	0.000025	0.000000
2	1	0	0.754732	-0.797980	-0.000000
3	1	0	-1.003791	-0.445406	-0.000000
4	1	0	0.124530	0.621618	0.896702
5	1	0	0.124530	0.621618	-0.896702

Table 2-19. Absolute energies and optimized geometries for calculated structures: HO•

Calculation Type SP
Calculation Method CCSD(T)
Basis Set aug-cc-pVDZ
E(CCSD(T)) -0.75584062909D+02 a.u.

Center Number	Atomic Number	Atomic Type	Coordinates (Angstroms) X	Y	Z
1	8	0	0.000000	0.000000	0.108367

2	1	0	0.000000	0.000000	-0.866934

Table 2-20. Absolute energies and optimized geometries for calculated structures: HO-CH_4 transition state

Calculation Type SP
Calculation Method CCSD(T)
Basis Set aug-cc-pVDZ
E(CCSD(T)) -0.11596953231D+03 a.u.

Center Number	Atomic Number	Atomic Type	Coordinates (Angstroms) X	Y	Z
1	6	0	-0.048202	1.214767	0.000000
2	1	0	-0.137616	0.022705	0.000000
3	8	0	-0.048202	-1.313377	0.000000
4	1	0	0.924485	-1.369321	0.000000
5	1	0	-1.087360	1.564585	0.000000
6	1	0	0.487660	1.500222	0.912217
7	1	0	0.487660	1.500222	-0.912217

Table 2-21. Absolute energies and optimized geometries for calculated structures: HO•---H_2O (Hydrogen bond donor)

Calculation Type SP
Calculation Method CCSD(T)
Basis Set aug-cc-pVDZ
E(CCSD(T)) -0.15186400922D+03 a.u.

Center Number	Atomic Number	Atomic Type	Coordinates (Angstroms) X	Y	Z
1	8	0	1.546697	-0.111691	0.000000
2	8	0	-1.412787	0.118597	-0.000002
3	1	0	1.508164	0.864218	0.000013
4	1	0	-0.540363	-0.304132	-0.000035
5	1	0	-2.039079	-0.615331	0.000032

Table 2-22. Absolute energies and optimized geometries for calculated structures: CH_4-HO•---H_2O (Hydrogen bond donor) transition state

Calculation Type SP
Calculation Method CCSD(T)
Basis Set aug-cc-pVDZ
E(CCSD(T)) -0.19225315053D+03 a.u.

Center Number	Atomic Number	Atomic Type	Coordinates (Angstroms) X	Y	Z
1	6	0	1.506520	-0.891588	-0.001522
2	1	0	1.052339	0.187686	-0.165910
3	8	0	0.382448	1.396949	-0.104717
4	1	0	0.578867	1.576042	0.833610
5	1	0	1.930025	-1.162740	-0.975994
6	1	0	2.274108	-0.813896	0.777239
7	1	0	0.665721	-1.531456	0.287298
8	1	0	-1.243470	0.245558	-0.095314
9	8	0	-1.831119	-0.516453	0.047927
10	1	0	-2.707340	-0.195631	-0.197484

Table 2-23. Absolute energies and optimized geometries for calculated structures: HO•---H_2O (Hydrogen bond acceptor)

Calculation Type SP
Calculation Method CCSD(T)
Basis Set aug-cc-pVDZ
E(CCSD(T)) -0.15186732232D+03 a.u.

Center Number	Atomic Number	Atomic Type	Coordinates (Angstroms) X	Y	Z
1	8	0	0.036519	1.626401	0.000000
2	1	0	0.075360	0.645236	0.000000
3	8	0	0.036519	-1.272815	-0.000000
4	1	0	-0.329833	-1.736963	0.764176
5	1	0	-0.329833	-1.736963	-0.764176

Table 2-24. Absolute energies and optimized geometries for calculated structures: CH_4-HO•--- H_2O (Hydrogen bond acceptor) transition state

Calculation Type SP
Calculation Method CCSD(T)
Basis Set aug-cc-pVDZ
E(CCSD(T)) -0.19225182396D+03a.u.

Center Number	Atomic Number	Atomic Type	Coordinates (Angstroms) X	Y	Z
1	8	0	0.976849	0.909976	0.000000
2	1	0	1.239786	-0.381894	0.000000
3	6	0	1.252695	-1.584137	0.000000
4	1	0	-0.000000	0.827479	0.000000
5	1	0	1.787273	-1.873626	0.912267
6	1	0	1.787273	-1.873626	-0.912267
7	1	0	0.210965	-1.924736	0.000000
8	8	0	-1.949138	0.663997	0.000000
9	1	0	-2.381575	1.069723	0.763309
10	1	0	-2.381575	1.069723	-0.763309

Table 2-25. Absolute energies and optimized geometries for calculated structures: HO•---$(H_2O)_2$

(1 hydrogen bond donor, 1 hydrogen bond acceptor)

Calculation Type SP
Calculation Method CCSD(T)
Basis Set aug-cc-pVDZ
E(CCSD(T)) -0.22815656039D+03 a.u.

Center Number	Atomic Number	Atomic Type	Coordinates (Angstroms) X	Y	Z
1	8	0	-0.628449	1.630170	0.007521
2	1	0	-1.045389	0.733776	0.006950
3	8	0	-1.070637	-1.126478	-0.099112
4	1	0	-1.422413	-1.756719	0.541362
5	1	0	-0.098780	-1.195632	-0.027534
6	1	0	1.157231	0.601221	-0.005722
7	8	0	1.580136	-0.271661	0.087055
8	1	0	2.360957	-0.238896	-0.478767

Table 2-26. Absolute energies and optimized geometries for calculated structures: CH_4-HO•---$(H_2O)_2$ (1 hydrogen bond donor, 1 hydrogen bond acceptor) transition state

Calculation Type SP
Calculation Method CCSD(T)
Basis Set aug-cc-pVDZ
E(CCSD(T)) -0.26854382925D+03 a.u.

Center Number	Atomic Number	Atomic Type	Coordinates (Angstroms) X	Y	Z
1	6	0	2.142525	0.006192	-0.655151
2	8	0	0.585425	-0.254158	1.309713
3	8	0	-1.076793	1.501588	-0.198315
4	8	0	-1.511808	-1.255620	-0.314973
5	1	0	1.514531	-0.204961	0.337661
6	1	0	2.262586	-0.967923	-1.144297
7	1	0	1.560746	0.712245	-1.257910
8	1	0	3.096695	0.425830	-0.316423
9	1	0	0.115931	0.563666	1.023368
10	1	0	-1.822462	2.064625	0.043491
11	1	0	-1.476141	0.646835	-0.454963
12	1	0	-0.721545	-1.231462	0.261587
13	1	0	-1.360080	-1.980486	-0.933014

Table 2-27. Absolute energies and optimized geometries for calculated structures: HO•---$(H_2O)_2$

(2 hydrogen bond donors, 1 hydrogen bond acceptor)

Calculation Type SP
Calculation Method CCSD(T)
Basis Set aug-cc-pVDZ
E(CCSD(T)) -0.30443704440D+03 a.u.

Center Number	Atomic Number	Atomic Type	Coordinates (Angstroms) X	Y	Z
1	8	0	0.489581	-0.548456	-0.135892
2	1	0	0.036355	0.335432	-0.108107
3	8	0	-1.275458	1.544101	-0.104271
4	1	0	-1.401671	2.228813	0.564216
5	1	0	-1.993206	0.897141	0.036690
6	1	0	-1.543074	-1.295688	-0.033947
7	8	0	-2.441265	-0.972819	0.149768
8	1	0	-3.027273	-1.551029	-0.353911
9	1	0	2.492122	-0.251041	-0.018195
10	8	0	3.416602	0.030457	0.077467
11	1	0	3.921070	-0.789891	0.016673

Table 2-28. Absolute energies and optimized geometries for calculated structures: CH_4-HO•---$(H_2O)_3$ (2 hydrogen bond donor, 1 hydrogen bond acceptor) transition state

Calculation Type SP
Calculation Method CCSD(T)
Basis Set aug-cc-pVDZ
E(CCSD(T)) -0.34482750014D+03 a.u.

Center Number	Atomic Number	Atomic Type	Coordinates (Angstroms) X	Y	Z
1	6	0	0.856052	1.611531	0.869782
2	8	0	0.279488	-0.325968	-0.680640
3	8	0	-1.649771	-1.023608	1.210223
4	8	0	-2.487565	0.363294	-1.061683
5	8	0	3.168442	-0.570383	-0.304515
6	1	0	0.602134	0.813882	0.036188
7	1	0	-0.200812	-0.755820	0.069841
8	1	0	0.660517	2.588707	0.411404
9	1	0	1.915652	1.455335	1.100461
10	1	0	0.197603	1.405472	1.721159
11	1	0	-2.062072	-1.869958	1.423115
12	1	0	-2.261000	-0.587271	0.584275
13	1	0	-1.526675	0.357256	-1.231016
14	1	0	-2.776752	1.262627	-1.258230
15	1	0	2.228668	-0.635561	-0.548804
16	1	0	3.601686	-1.250532	-0.834162

The complete Gaussian ’03 citation:

Frisch, M. J.; Trucks, G. W.; Schlegel, H. B.; Scuseria, G. E.; Robb, M. A.; Cheeseman, J. R.; Montgomery, J., J. A.; Vreven, T.; Kudin, K. N.; Burant, J. C.; Millam, J. M.; Iyengar, S. S.; Tomasi, J.; Barone, V.; Mennucci, B.; Cossi, M.; Scalmani, G.; Rega, N.; Petersson, G. A.; Nakatsuji, H.; Hada, M.; Ehara, M.; Toyota, K.; Fukuda, R.; Hasegawa, J.; Ishida, M.; Nakajima, T.; Honda, Y.; Kitao, O.; Nakai, H.; Klene, M.; Li, X.; Knox, J. E.; Hratchian, H. P.; Cross, J. B.; Bakken, V.; Adamo, C.; Jaramillo, J.; Gomperts, R.; Stratmann, R. E.; Yazyev, O.; Austin, A. J.; Cammi, R.; Pomelli, C.; Ochterski, J. W.; Ayala, P. Y.; Morokuma, K.; Voth, G. A.; Salvador, P.; Dannenberg, J. J.; Zakrzewski, V. G.; Dapprich, S.; Daniels, A. D.; Strain, M. C.; Farkas, O.; Malick, D. K.; Rabuck, A. D.; Raghavachari, K.; Foresman, J. B.; Ortiz, J. V.; Cui, Q.; Baboul, A. G.; Clifford, S.; Cioslowski, J.; Stefanov, B. B.; Liu, G.; Liashenko, A.; Piskorz, P.; Komaromi, I.; Martin, R. L.; Fox, D. J.; Keith, T.; Al-Laham, M. A.; Peng, C. Y.; Nanayakkara, A.; Challacombe, M.; Gill, P. M. W.; Johnson, B.; Chen, W.; Wong, M. W.; Gonzalez, C.; Pople, J. A. *Gaussian 03, Revision C.02*, Gaussian, Inc.: Wallingford CT, 2004.

Appendix B: Supporting Material for Chapter 3 Mechanistic Degradation of High Density Polyethylene Potable Water Materials

The following represents the supporting information for Chapter 3, and includes representative IR spectra from aged HDPE pipe and aged HDPE resin samples, with reported relative intensities of relevant peaks.

Figure 3-7. IR of HDPE pipe sample prior to initiation of accelerated aging (0 h).

C—H stretch: 2916 cm^{-1} ,2848 cm^{-1} CH_2 ; C—H bend: 1473 cm^{-1}, 1462 cm^{-1}; CH_2rock: 731 cm^{-1}, 719 cm^{-1}

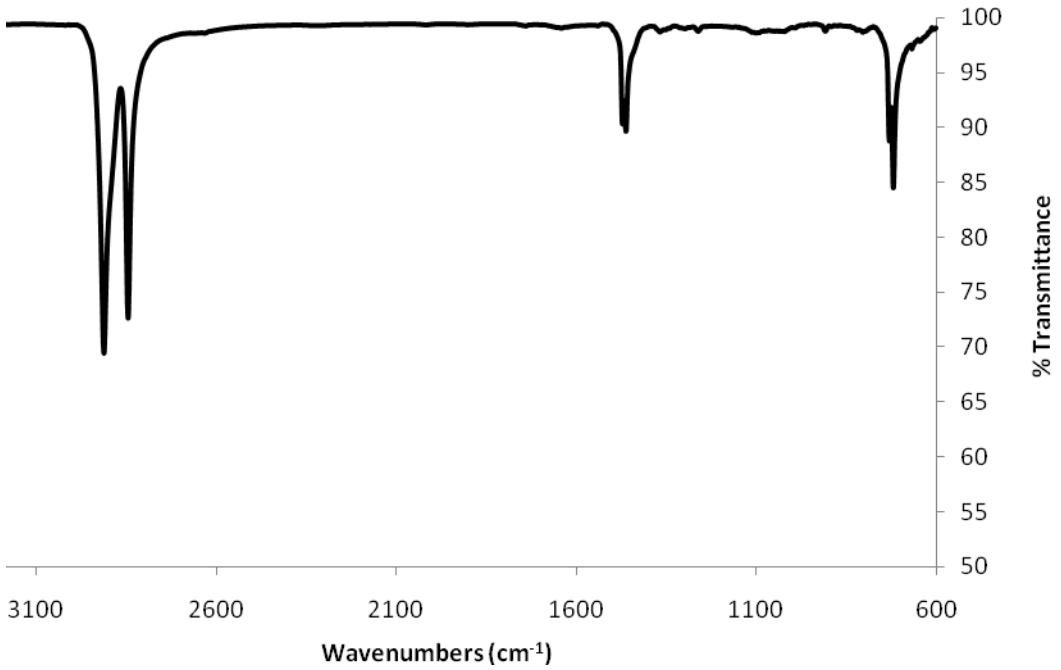

Figure 3-8. IR of HDPE pipe sample after 45 days (1080 h) of accelerated aging at 50 mg/L Cl_2.

CO stretch (aldehyde): 1742 cm^{-1}; CO stretch (keytone): 1715 cm^{-1};
1742 cm^{-1}:17.2% (relative to 1462 cm^{-1}); 1715 cm^{-1}: 18.1% (relative to 1462 cm^{-1})

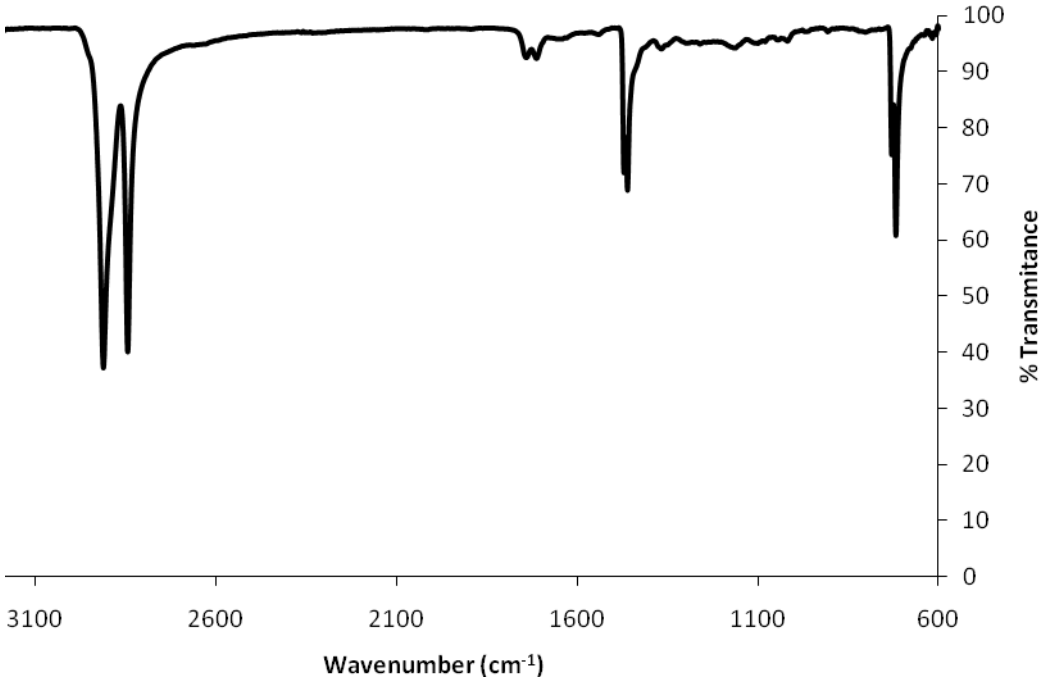

Figure 3-9. IR of HDPE pipe sample after 90 days (2160 h) of accelerated aging at 50 mg/L Cl_2.

CO stretch (aldehyde): 1742 cm^{-1}; CO stretch (keytone): 1715 cm^{-1};
1742 cm^{-1}:13.8% (relative to 1462 cm^{-1}); 1715 cm^{-1}: 22.3% (relative to 1462 cm^{-1})

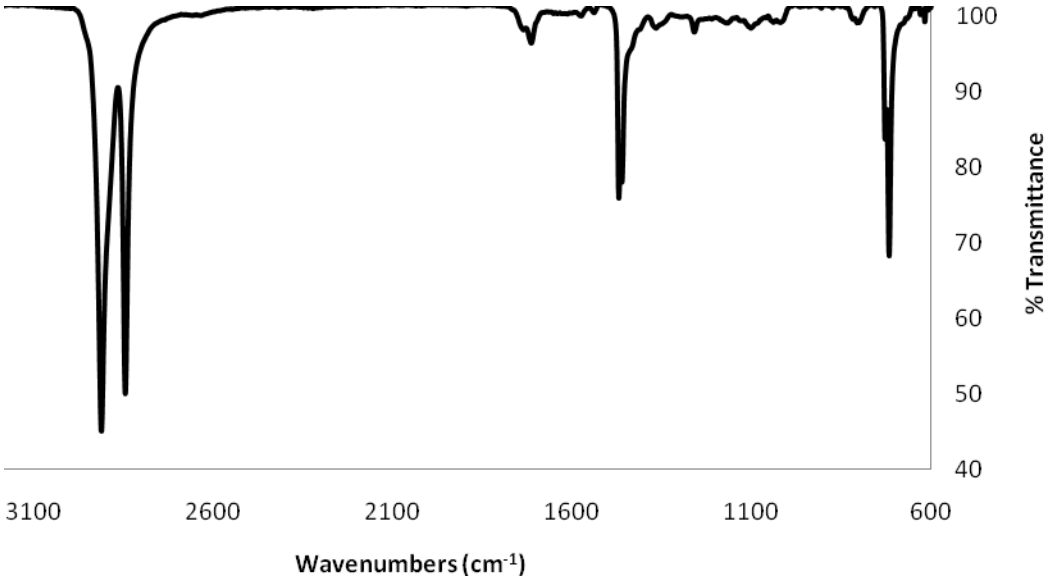

Figure 3-10. IR of HDPE pipe sample after 190 days (4560 h) of accelerated aging at 500 mg/L Cl_2.

CO stretch (aldehyde): 1742 cm^{-1}; CO stretch (keytone): 1715 cm^{-1}; C—O—OH stretch ($^{16}O_2$): 1113 cm^{-1}; 1742 cm^{-1}: 34.7% (relative to 1462 cm^{-1}); 1715 cm^{-1}:36.5% (relative to 1462 cm^{-1}); 1113 cm^{-1}; 25.4% (relative to 1462 cm^{-1})

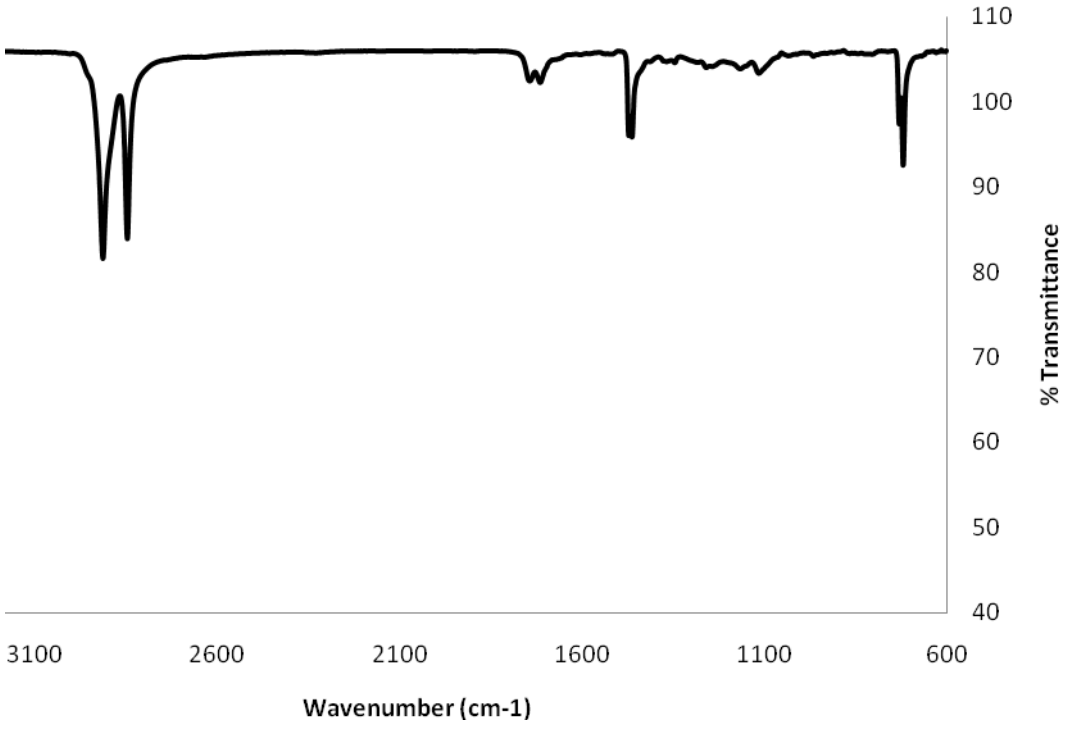

Figure 3-11. IR of HDPE pipe sample after 45 days (1080 h) of accelerated aging at 500 mg/L Cl_2.

CO stretch (aldehyde): 1742 cm^{-1}; CO stretch (keytone): 1715 cm^{-1}; 1742 cm^{-1}: 17.6% (relative to 1462 cm^{-1}); 1715 cm^{-1}: 22.3% (relative to 1462 cm^{-1})

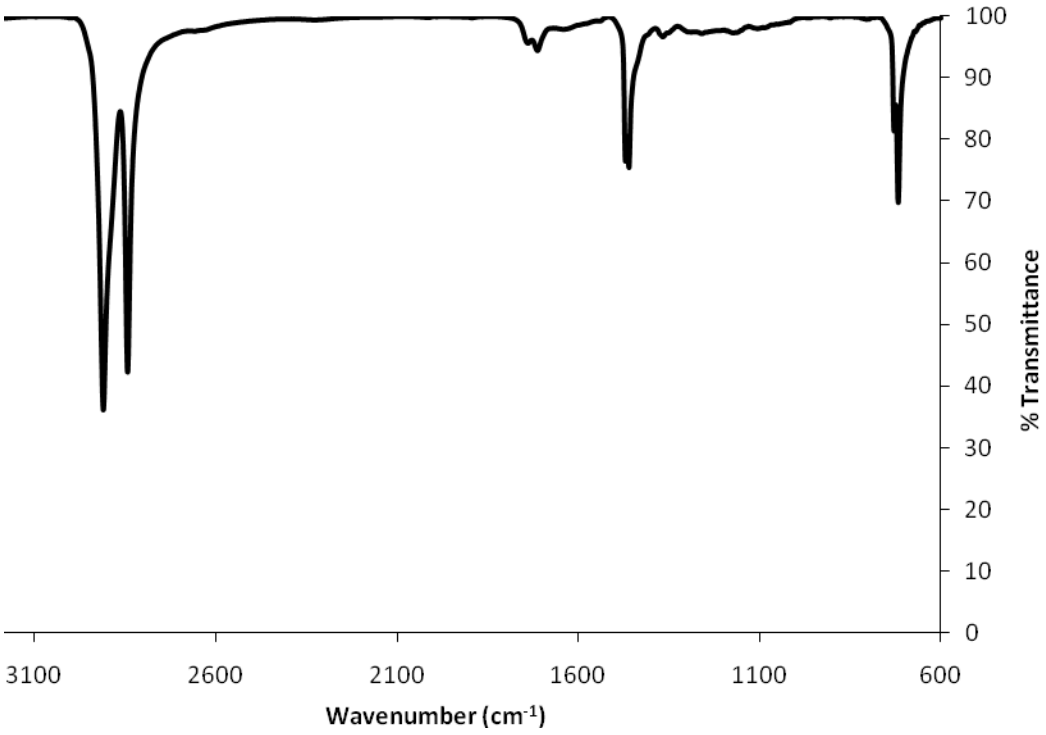

Figure 3-12. IR of HDPE pipe sample after 90 days (2160 h) of accelerated aging at 500 mg/L Cl_2.

CO stretch (aldehyde): 1742 cm^{-1}; CO stretch (keytone): 1715 cm^{-1};
1742 cm^{-1}: 16.0% (relative to 1462 cm^{-1}); 1715 cm^{-1}: 23.0% (relative to 1462 cm^{-1})

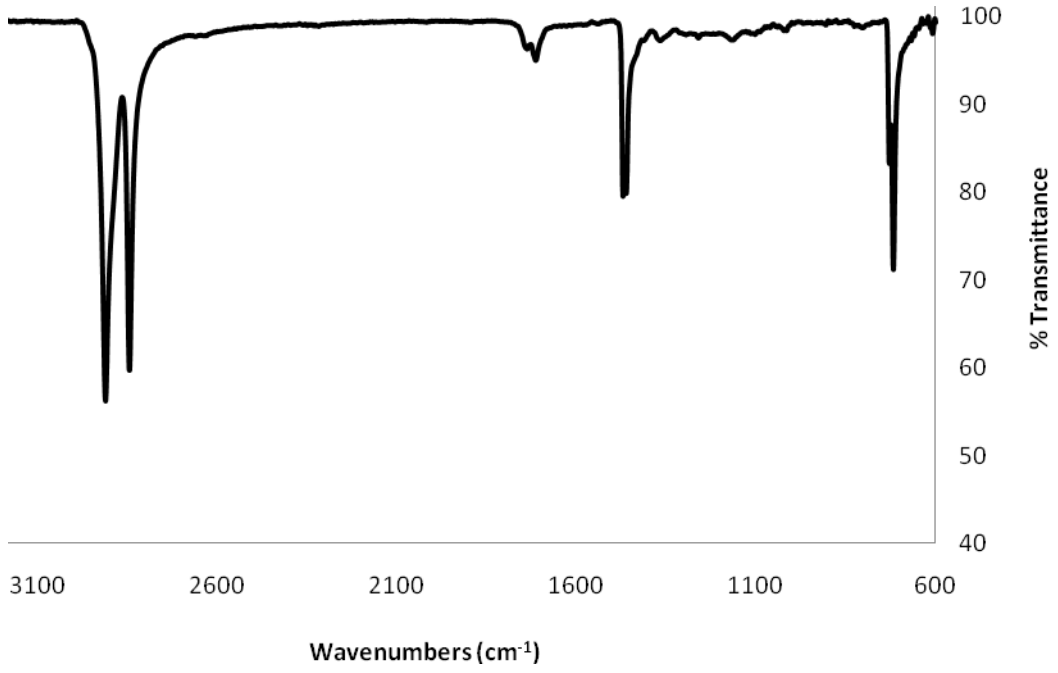

Figure 3-13. IR of HDPE pipe sample after 190 days (4560 h) of accelerated aging at 500 mg/L Cl_2.

CO stretch (aldehyde): 1742 cm^{-1}; CO stretch (keytone): 1715 cm^{-1}; C—O—OH stretch ($^{16}O_2$): 1113 cm^{-1}; 1742 cm^{-1}: 23.5% (relative to 1462 cm^{-1}); 1715 cm^{-1}:40.2% (relative to 1462 cm^{-1}); 1113 cm^{-1}; 18.1% (relative to 1462 cm^{-1})

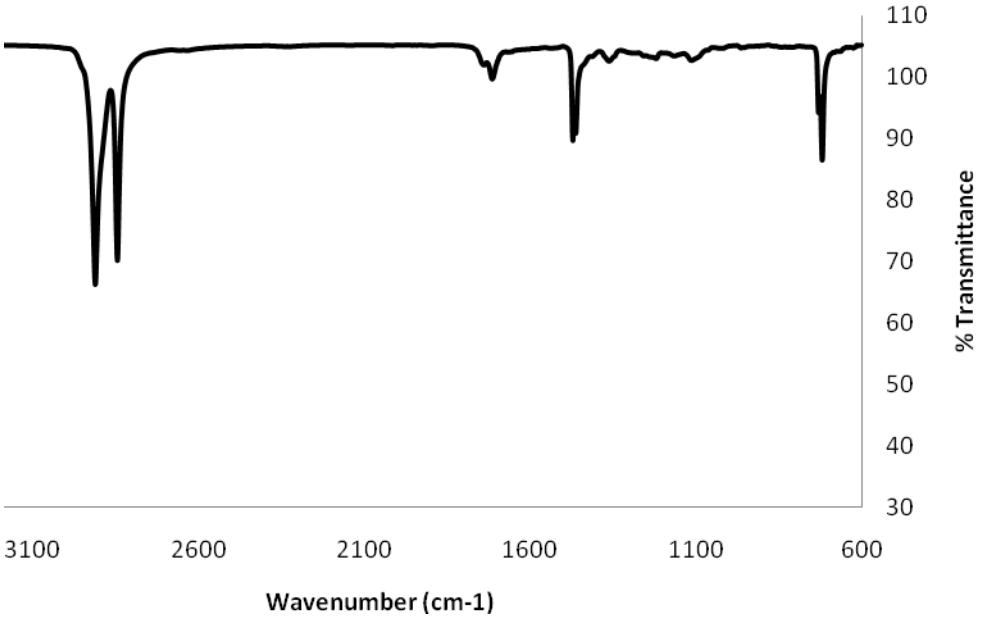

Figure 3-14. IR of HDPE resin sample prior to initiation of accelerated aging (0 h).

C—H stretch: 2916 cm^{-1} ,2848 cm^{-1} CH_2 ; C—H bend: 1473 cm^{-1}, 1462 cm^{-1}; CH_2rock: 731 cm^{-1}, 719 cm^{-1}

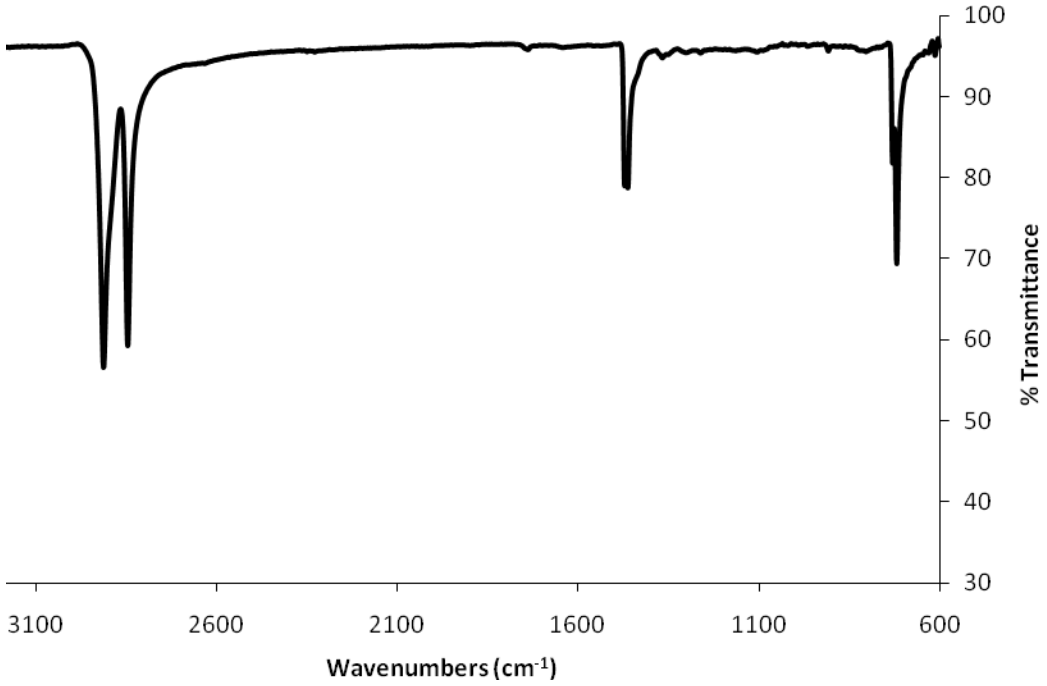

Figure 3-15. IR of HDPE resin sample after 21 days (504 h) of accelerated aging at 50 mg/L Cl_2.

CO stretch (aldehyde): 1742 cm^{-1}; 1742 cm^{-1}:10.1% (relative to 1462 cm^{-1});

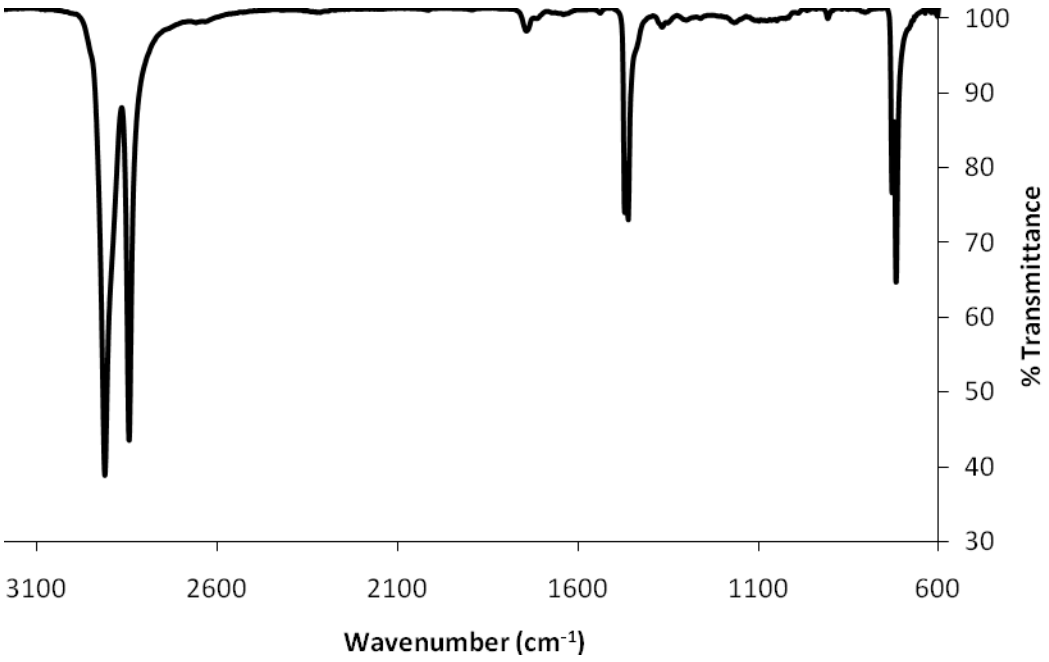

Figure 3-16. IR of HDPE resin sample after 90 days (2160 h) of accelerated aging at 50 mg/L Cl_2.

CO stretch (aldehyde): 1742 cm^{-1}; CO stretch (keytone): 1715 cm^{-1}; 1742 cm^{-1}: 8.0% (relative to 1462 cm^{-1}); 1715 cm^{-1}:6.0% (relative to 1462 cm^{-1});

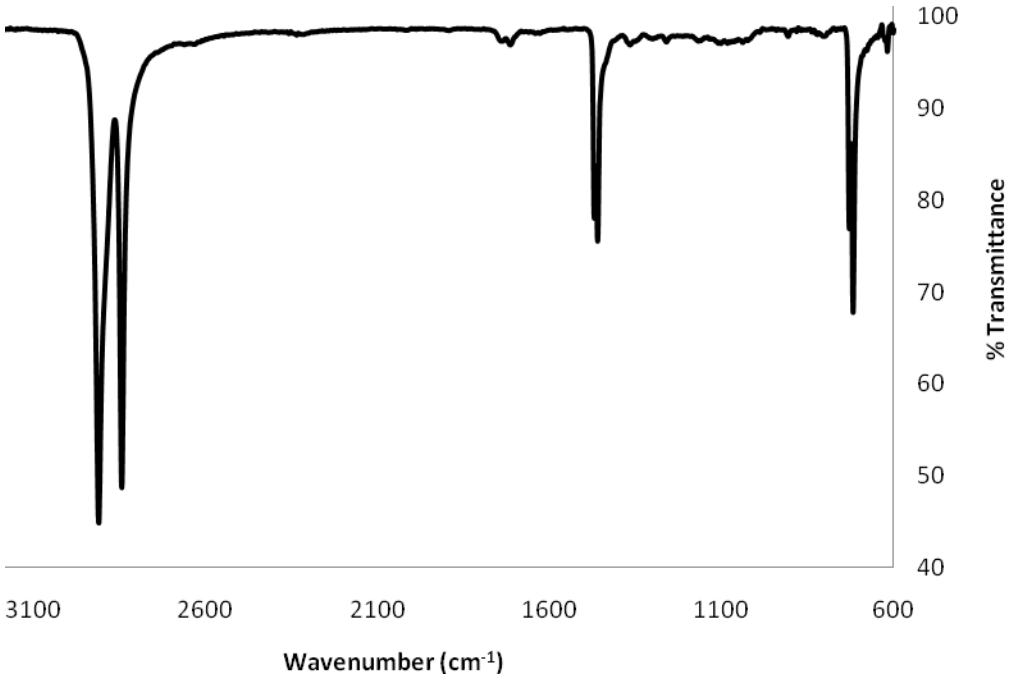

Figure 3-17. IR of HDPE resin sample after 160 days (3840 h) of accelerated aging at 50 mg/L Cl_2.

CO stretch (aldehyde): 1742 cm^{-1}; CO stretch (keytone): 1715 cm^{-1}; C—O—OH stretch ($^{16}O_2$): 1113 cm^{-1}; 1742 cm^{-1}: 34.7% (relative to 1462 cm^{-1}); 1715 cm^{-1}:36.6% (relative to 1462 cm^{-1}); 1113 cm^{-1}; 25.4% (relative to 1462 cm^{-1})

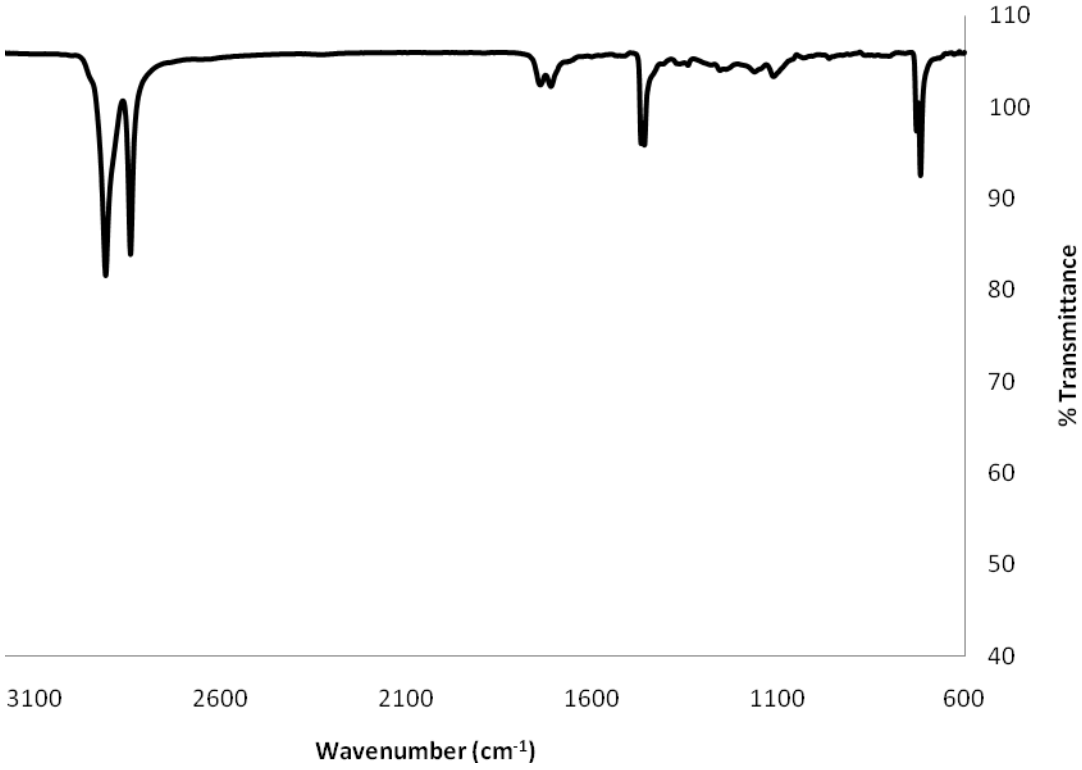

Figure 3-18. IR of HDPE resin sample after 21 days (504 h) of accelerated aging at 250 mg/L Cl_2.

CO stretch (aldehyde): 1742 cm^{-1} 1742 cm^{-1}:18.0% (relative to 1462 cm^{-1});

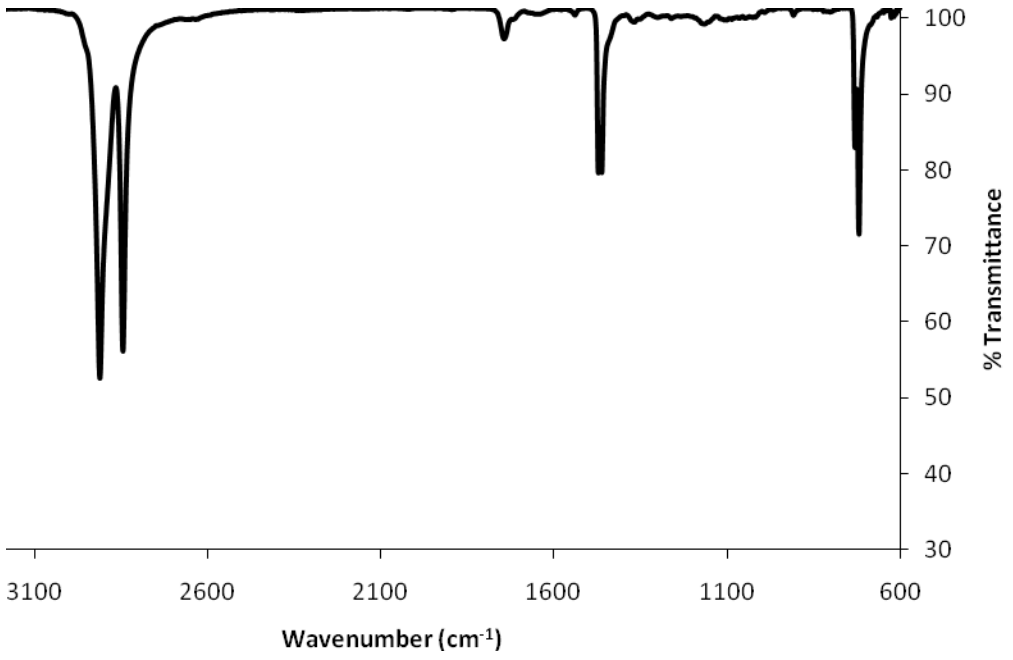

Figure 3-19. IR of HDPE resin sample after 90 days (2160 h) of accelerated aging at 250 mg/L Cl_2.

CO stretch (aldehyde): 1742 cm^{-1}; CO stretch (keytone): 1715 cm^{-1}; 1742 cm^{-1}: 9.4% (relative to 1462 cm^{-1}); 1715 cm^{-1}:12.0% (relative to 1462 cm^{-1});

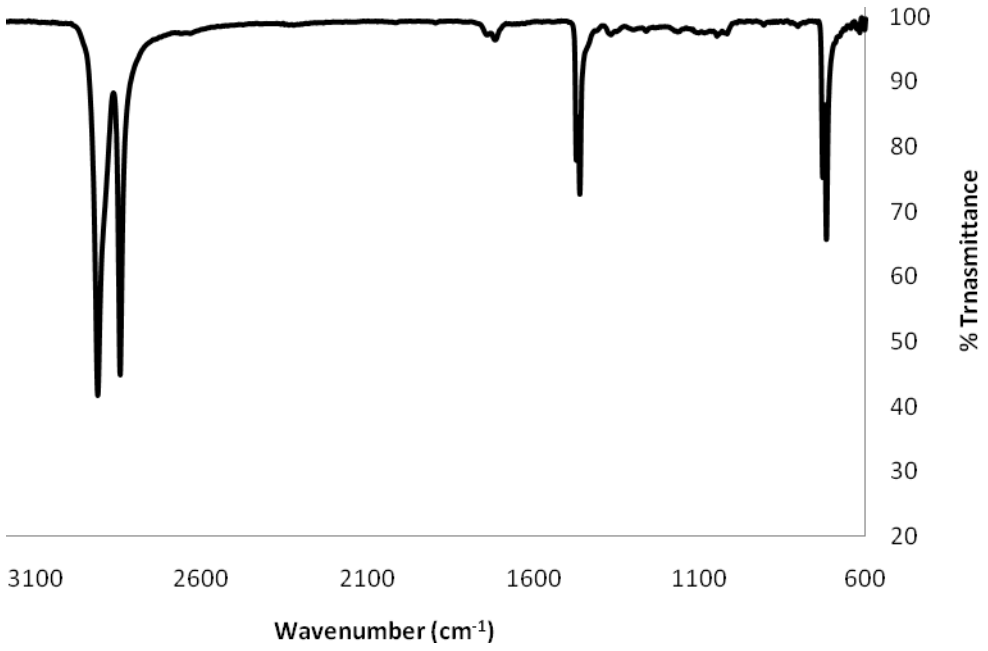

Figure 3-20. IR of HDPE resin sample after 160 days (3840 h) of accelerated aging at 250 mg/L Cl_2.

CO stretch (aldehyde): 1742 cm^{-1}; CO stretch (keytone): 1715 cm^{-1}; C—O—OH stretch ($^{16}O_2$): 1113 cm^{-1}; 1742 cm^{-1}: 18.7% (relative to 1462 cm^{-1}); 1715 cm^{-1}:24.2% (relative to 1462 cm^{-1}); 1113 cm^{-1}; 24.1% (relative to 1462 cm^{-1})

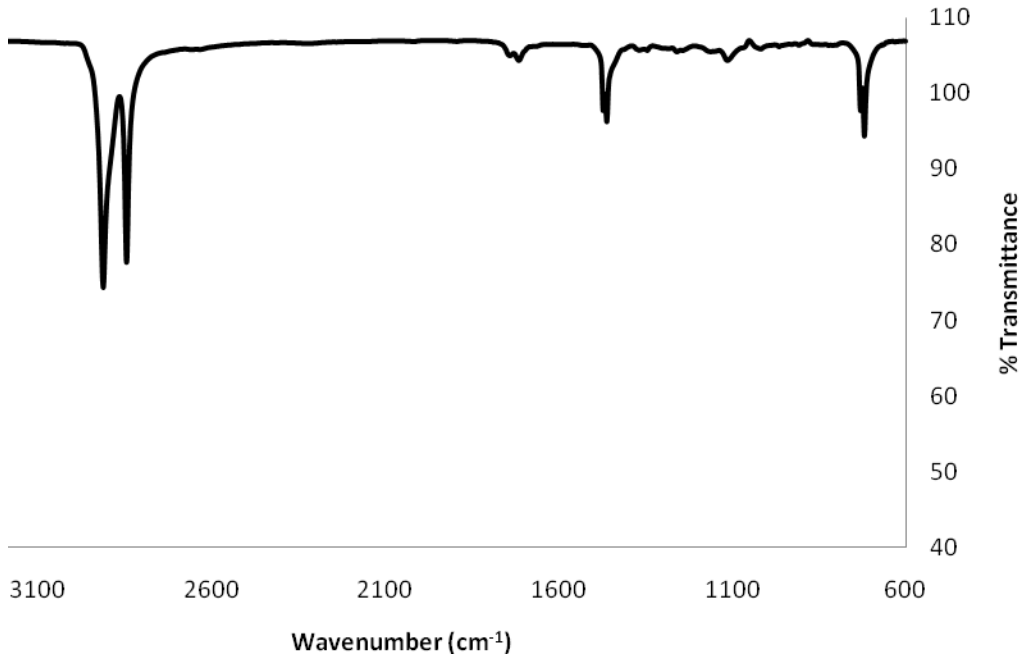

Figure 3-21. IR of HDPE resin sample after 21 days (504 h) of accelerated aging at 250 mg/L Cl_2 in the presence of $^{18}O_2$ (water not changed).

$C^{16}O$ stretch (keytone): 1715 cm^{-1}; $C^{18}O$ stretch (keytone): 1648 cm^{-1}. C—^{16}O—^{16}OH stretch: 1113 cm^{-1}; C—^{18}O—^{18}OH stretch: 1063 cm^{-1}; 1263 cm^{-1}, 820 cm^{-1}
1715 cm^{-1}: 6.8% (relative to 1462 cm^{-1}); 1648 cm^{-1}: 5.9% (relative to 1462 cm^{-1})

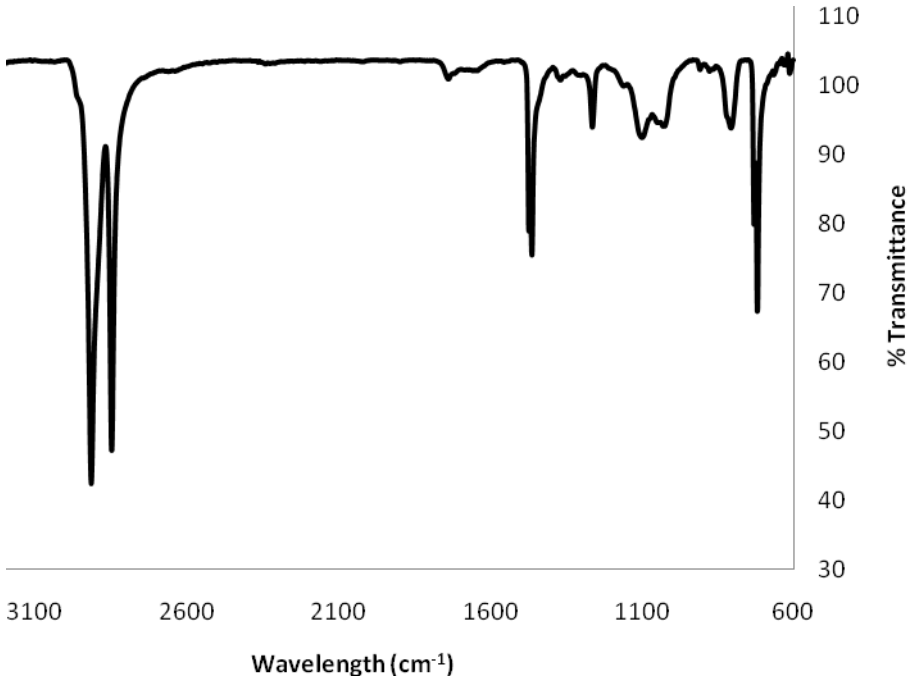

Figure 3-23. IR of HDPE resin sample after 21 days (504 h) of accelerated aging at 250 mg/L. C—^{16}O—^{16}OH stretch: 1106 cm^{-1}; 1263 cm^{-1}, 820 cm^{-1}